

DISSERTATION

FLOW RESISTANCE PREDICTION
IN HIGH-GRADIENT STREAMS

Submitted by

Steven E. Yochum

Department of Civil and Environmental Engineering

In partial fulfillment of the requirements

For the Degree of Doctor of Philosophy

Colorado State University

Fort Collins, Colorado

Fall 2010

COLORADO STATE UNIVERSITY

July 30, 2010

WE HEREBY RECOMMEND THAT THE DISSERTATION PREPARED UNDER OUR SUPERVISION BY STEVEN E. YOCHUM ENTITLED PREDICTION OF FLOW RESISTANCE AND VELOCITY IN HIGH-GRADIENT STREAMS BE ACCEPTED AS FULFILLING IN PART REQUIREMENTS FOR THE DEGREE OF DOCTOR OF PHILOSOPHY.

Committee on Graduate Work

Sara L. Rathburn

Chester C. Watson

Ellen E. Wohl

Advisor: Brian P. Bledsoe

Department Head: Luis A. Garcia

ABSTRACT OF DISSERTATION
FLOW RESISTANCE PREDICTION
IN HIGH-GRADIENT STREAMS

Flow resistance measurements were collected on high-gradient streams in the Fraser Experimental Forest, Colorado, for bankfull through low flows using Rhodamine WT dye tracing, ground-based LiDAR scans, and laser theodolite surveying of longitudinal profiles and below-water features. A dataset of 59 resistance measurements was collected on fifteen reaches with instream wood present in varying densities. Values of Manning's n ranged from 0.05 to 0.52, and Darcy-Weisbach f varied from 0.28 to 56. All measurements indicated subcritical reach-average conditions, with Froude numbers ranging from 0.15 to 0.78. Relative grain submergence (R/D_{84}) was a poor predictor of flow resistance while relative bedform submergence, defined as the ratio of depth or hydraulic radius to the standard deviation of the residuals of a bed profile regression (h_m/σ_z , R/σ_z), explained up to 76 and 80 percent of the variance of n and f , respectively. Both clasts and instream wood contribute to bed variability; steps are heightened by wood lodging among the clast steps. Hence relative bedform submergence captures the combined influence of wood and clasts, which contribute both form and spill resistance. Relative bedform submergence is less effective for prediction in reaches with substantial non-step-forming instream wood and in steep channels. In the steepest reaches, with slopes over about 18 percent, the data indicate a shift towards a skimming regime with a

partial submergence of bedforms and a threshold reduction in flow resistance. Three-dimensional measures of geometric variability were explored, to assess the correlation of flow resistance with higher-order spatial variation due to composite effects of bedforms, large clasts, and instream wood. With the exclusion of bank effects, a normalized variable (h_{a3}/σ_{z3}) explained 77 and 81 percent of the variance of n and f , respectively. Multivariate regression models with variables describing bedforms, bankforms, and instream wood explained 87 percent of the variance of n and f . On average, flow resistance due to bedforms (form and spill) are the greatest contributor to overall flow resistance in these high-gradient streams, followed by form resistance generated by bankforms, and lastly, by form resistance induced by non-step instream wood.

Steven E. Yochum
Department of Civil and Environmental Engineering
Colorado State University
Fort Collins, CO 80523
Fall 2010

ACKNOWLEDGMENTS

Appreciation is expressed for my research partner Gabrielle David and to the principal investigators for the project, Brian Bledsoe and Ellen Wohl. Brian Bledsoe is also thanked for his role as advisor on my dissertation as is Ellen Wohl for sitting on my research committee and providing thoughtful advice throughout the project. Additional committee members Sara Rathburn and Chester Watson are also valued for their time and guidance. Importantly, appreciation is expressed to the National Science Foundation for funding (Grant Number EAR0608918), to the U. S. Department of Agriculture Forest Service Rocky Mountain Research Station for hosting the research on the Fraser Experimental Forest, to the U. S. Department of Agriculture Natural Resources Conservation Service for additional funding, and to our field assistants Mark Hussey, Dan Dolan, and Lina Polvi. Dan Dolan is especially valued for the difficult job of helping to transport and repeatedly setup the LiDAR equipment in the rugged terrain of the research area. Finally, the datasets provided by Francesco Comiti and Andre Zimmermann are appreciated.

TABLE OF CONTENTS

ABSTRACT OF DISSERTATION	iii
ACKNOWLEDGMENTS	v
LIST OF FIGURES	viii
LIST OF TABLES	xiii
LIST OF SYMBOLS, VARIABLES, AND ABBREVIATIONS	xiv
CHAPTER 1 INTRODUCTION	1
1.1 Objectives	3
1.2 Organization	3
CHAPTER 2 BACKGROUND	4
2.1 Resistance Coefficient Prediction.....	10
CHAPTER 3 METHODS	18
3.1 Field Methodology	18
3.1.1 Study Area	18
3.1.2 Geometry.....	22
3.1.3 Velocity.....	28
3.2 Geometric Data Extraction	34
3.2.1 Cross Sections.....	34
3.2.2 Two-dimensional Characteristics.....	35
3.2.3 Three-dimensional Spatial Characteristics	39
3.3 Statistical Analyses.....	43
CHAPTER 4 VELOCITY AND RESISTANCE MEASUREMENTS	46
4.1 Measured Flow Paths	47
4.2 Shortest Potential Flow Paths	53
4.3 Photographic Guidance for Resistance Coefficients	57
CHAPTER 5 RESULTS AND DISCUSSION	73
5.1 Data Collection and Post Processing.....	73
5.2 Resistance Prediction Using Simple Linear Regressions.....	76
5.2.1 Bed Material and Slope.....	76
5.2.2 Bed Variability.....	78
5.2.3 Bank Variability.....	94
5.2.4 Instream Wood.....	97

5.3	Performance of Prior Prediction Methodologies	101
5.4	Resistance Prediction Using 3-D Spatial Analysis.....	106
5.5	Multivariate Regression with Bedform, Bankform, and Instream Wood	113
5.6	Velocity Prediction.....	121
5.7	Flow Path Influence on Resistance Estimates and Prediction.....	124
5.8	Future Research	128
CHAPTER 6 SUMMARY AND CONCLUSIONS.....		131
REFERENCES.....		135
APPENDIX A 2007 AND 2008 DAILY DISCHARGE DATA		146
APPENDIX B LOG-PEARSON FREQUENCY ANALYSIS SPREADSHEETS		150
APPENDIX C BED AND BANK DATA		160
APPENDIX D DEPTH VARIABILITY GRIDS		167

LIST OF FIGURES

Figure 3-1: Research watersheds and stream reaches, Fraser Experimental Forest, Colorado.	19
Figure 3-2: Low-flow photographs of selected research reaches, Fraser Experimental Forest, Colorado.	20
Figure 3-3: LiDAR equipment.	24
Figure 3-4: LiDAR point cloud for reach ESL-9, with accompanying photograph of near-bankfull flow.	25
Figure 3-5: Raw and cleaned LiDAR point clouds, reach ESL-9.	27
Figure 3-6: 2-D flow depth with flow paths for all four ESL-7 resistance measurements. This image provides depth data for the entire wetted width for the July 2007 measurements, with a 5-cm pixel size.	28
Figure 3-7: Rhodamine WT dye injection by field assistant Mark Hussey.	29
Figure 3-8: Example dye tracing dataset illustrating peak, harmonic, and centroid travel times.	32
Figure 3-9: Extracted cross sections for reach ESL-7, with bankfull modeled water surface.	35
Figure 3-10: Bed residual computation, ESL-1 at ~bankfull flow.	38
Figure 3-11: Water surface model development, ESL-4, bankfull flow.	42
Figure 3-12: Bed model development, ESL-4, bankfull flow.	42
Figure 3-13: Depth model computation, ESL-4, bankfull flow.	43
Figure 4-1: Flow path types.	47
Figure 4-2: Manning’s n and Darcy-Weisbach f as a function of friction slope.	49
Figure 4-3: Darcy-Weisbach f as a function of friction slope, with variability induced due to measured versus shortest potential flow paths.	54
Figure 4-4: East Saint Louis Creek, reach ESL-6 (plane bed).	58
Figure 4-5: Fool Creek, reach FC-1 (transitional between plane bed and step pool).	59
Figure 4-6: Fool Creek, reach FC-2 (step pool).	60
Figure 4-7: East Saint Louis Creek, reach ESL-3 (cascade).	61
Figure 4-8: East Saint Louis Creek, reach ESL-7 (cascade).	62

Figure 4-9: Fool Creek, reach FC-6 (cascade).....	63
Figure 4-10: Fool Creek, reach FC-5 (cascade).....	64
Figure 4-11: East Saint Louis Creek, reach ESL-8 (step pool).....	65
Figure 4-12: East Saint Louis Creek, reach ESL-1 (step pool).....	66
Figure 4-13: East Saint Louis Creek, reach ESL-2 (step pool).....	67
Figure 4-14: Fool Creek, reach FC-3 (step pool).....	68
Figure 4-15: East Saint Louis Creek, reach ESL-9 (step pool).....	69
Figure 4-16: Fool Creek, reach FC-4 (step pool).....	70
Figure 4-17: East Saint Louis Creek, reach ESL-4 (step pool).....	71
Figure 4-17: East Saint Louis Creek, reach ESL-5 (cascade).....	71
Figure 5-1: Harmonic versus peak and centroid velocity comparisons.	75
Figure 5-2: Resistance coefficients prediction with R/D_{84} and S_f	77
Figure 5-3: Selected longitudinal profiles, with bed and water surface elevations.	79
Figure 5-4: Resistance coefficients prediction with A/SDA , R/SDR , and h_m/SDh_m	81
Figure 5-5: Resistance coefficients prediction with median, average, and maximum bed residual.....	82
Figure 5-6: Resistance coefficients prediction with relative submergence, using maximum bed residual and both hydraulic radius and maximum depth.	83
Figure 5-7: Resistance coefficients prediction with the standard deviation of a bed profile regression and relative submergence, using the standard deviation of the residuals of a bed profile regression and both hydraulic radius and maximum depth.....	84
Figure 5-8: Cross-validation results, h_m/σ_z	87
Figure 5-9: Student residuals of n versus h_m/σ_z , in natural logarithm space with reach ID labels and outlying reach descriptions..	91
Figure 5-10: Bankfull flow in reach FC-6.	93
Figure 5-11: Resistance coefficients prediction with bank variability variables K_b , K_{bh} , and σ_y	95
Figure 5-12: Resistance coefficients prediction with bank variability variables TW/σ_y , R/σ_y , and h_m/σ_y	96
Figure 5-13: Resistance coefficients prediction with instream wood variables V_w/V and V_{wb}/V	98
Figure 5-14: Resistance coefficients prediction with instream wood variables V_{wd}/V and V_{wp}/V	99

Figure 5-15: Resistance coefficients prediction with instream wood variables V_{wdp}/V , V_{wpd}/V , and V_{wbpd}/V	100
Figure 5-16: Flow resistance coefficients prediction testing, using Fraser database.....	103
Figure 5-17: Depth variability for bankfull flow, reach ESL-1. Pixel size is 5 cm, for a total of 32,300 geo-referenced points.....	108
Figure 5-18: Resistance coefficients prediction with 3-D variables h_{a3}/σ_{h3} , h_{a3}/σ_{z3} , and h_{m3}/σ_{z3} , for the entire channel width.....	109
Figure 5-19: Resistance coefficients prediction with 3-D variables h_a/σ_{h3} , h_{a3}/σ_{z3} , and h_{m3}/σ_{z3} , for the center 50 percent of the channel width.....	110
Figure 5-20: Correlation of relative bedform submergence with 3-D depth variability.....	111
Figure 5-21: Student residuals of n versus h_{m3}/σ_{z3} , in natural logarithm space with reach ID labels and outlying reach descriptions.....	112
Figure 5-22: Correlation of relative bedform submergence with bank sinuosity.....	115
Figure 5-23: Measured versus predicted resistance coefficients, with predictors describing bedform and bankform.....	115
Figure 5-24: Correlation of predictors describing bedform, bankform, and instream wood ratios.....	118
Figure 5-25: Measured versus predicted resistance coefficients, with predictors describing bedform, bankform, and instream wood.....	119
Figure 5-26: Most effective exponents of R and S	123
Figure 5-27: Comparison of Darcy-Weisbach f , shortest potential (S) versus measured (M) flow paths.....	126
Figure 5-28: Prediction of n and f using relative bedform submergence, with shortest potential flow paths.....	127
Figure A-1: East Saint Louis Creek average daily streamflow, 2007.....	147
Figure A-2: East Saint Louis Creek average daily streamflow, 2008.....	147
Figure A-3: Lower Fool Creek average daily streamflow, 2007.....	148
Figure A-4: Lower Fool Creek average daily streamflow, 2008.....	148
Figure A-5: Upper Fool Creek average daily streamflow, 2008.....	149
Figure B-1: East Saint Louis Log-Pearson Frequency Analysis Spreadsheet.....	151
Figure B-2: Lower Fool Creek Log-Pearson Frequency Analysis Spreadsheet.....	154
Figure B-3: Upper Fool Creek Log-Pearson Frequency Analysis Spreadsheet.....	157
Figure D-1: Depth variability for ~bankfull flow, reach ESL-1 (6/10/2008).....	168
Figure D-2: Depth variability for mid flow, reach ESL-1 (7/22/2008).....	169

Figure D-3: Depth variability for mid flow, reach ESL-2 (7/9/2007).	170
Figure D-4: Depth variability for ~bankfull flow, reach ESL-2 (6/6/2008).	171
Figure D-5: Depth variability for mid flow, reach ESL-2 (7/15/2008).	172
Figure D-6: Depth variability for mid flow, reach ESL-3 (7/10/2007).	173
Figure D-7: Depth variability for ~bankfull flow, reach ESL-3 (6/7/2008).	174
Figure D-8: Depth variability for mid flow, reach ESL-3 (7/15/2008).	175
Figure D-9: Depth variability for mid flow, reach ESL-4 (7/10/2007).	176
Figure D-10: Depth variability for ~bankfull flow, reach ESL-4 (6/7/2008).	177
Figure D-11: Depth variability for mid flow, reach ESL-4 (7/14/2008).	178
Figure D-12: Depth variability for mid flow, reach ESL-5 (7/12/2007).	179
Figure D-13: Depth variability for ~bankfull flow, reach ESL-5 (6/9/2008).	180
Figure D-14: Depth variability for mid flow, reach ESL-5 (7/14/2008).	181
Figure D-15: Depth variability for mid flow, reach ESL-6 (7/13/2007).	182
Figure D-16: Depth variability for ~bankfull flow, reach ESL-6 (6/9/2008).	183
Figure D-17: Depth variability for mid flow, reach ESL-6 (7/14/2008).	184
Figure D-18: Depth variability for mid flow, reach ESL-7 (7/12/2007).	185
Figure D-19: Depth variability for ~bankfull flow, reach ESL-7 (6/8/2008).	186
Figure D-20: Depth variability for mid flow, reach ESL-7 (7/15/2008).	187
Figure D-21: Depth variability for mid flow, reach ESL-8 (7/11/2007).	188
Figure D-22: Depth variability for ~bankfull flow, reach ESL-8 (6/9/2008).	189
Figure D-23: Depth variability for mid flow, reach ESL-8 (7/16/2008).	190
Figure D-24: Depth variability for mid flow, reach ESL-9 (7/11/2007).	191
Figure D-25: Depth variability for ~bankfull flow, reach ESL-9 (6/8/2008).	192
Figure D-26: Depth variability for mid flow, reach ESL-9 (7/16/2008).	193
Figure D-27: Depth variability for mid flow, reach FC-1 (7/5/2007).	194
Figure D-28: Depth variability for ~bankfull flow, reach FC-1 (6/11/2008).	195
Figure D-29: Depth variability for mid flow, reach FC-1 (7/23/2008).	196
Figure D-30: Depth variability for mid flow, reach FC-2 (7/7/2007).	197
Figure D-31: Depth variability for ~bankfull flow, reach FC-2 (6/11/2008).	198
Figure D-32: Depth variability for mid flow, reach FC-2 (7/23/2008).	199
Figure D-33: Depth variability for mid flow, reach FC-3 (7/16/2007).	200
Figure D-34: Depth variability for ~bankfull flow, reach FC-3 (6/12/2008).	201
Figure D-35: Depth variability for mid flow, reach FC-3 (7/22/2008).	202

Figure D-36: Depth variability for mid flow, reach FC-4 (7/7/2007).....	203
Figure D-37: Depth variability for ~bankfull flow, reach FC-4 (6/12/2008).	204
Figure D-38: Depth variability for mid flow, reach FC-4 (7/21/2008).....	205
Figure D-39: Depth variability for mid flow, reach FC-5 (7/8/2007).....	206
Figure D-40: Depth variability for ~bankfull flow, reach FC-5 (6/25/2008).	207
Figure D-41: Depth variability for mid flow, reach FC-5 (7/17/2008).....	208
Figure D-42: Depth variability for mid flow, reach FC-6 (7/8/2007).....	209
Figure D-43: Depth variability for ~bankfull flow, reach FC-8 (6/25/2008).	210
Figure D-44: Depth variability for mid flow, reach FC-6 (7/17/2008).....	211

LIST OF TABLES

Table 2-1: Data characteristics of potentially-applicable flow resistance prediction equations.	13
Table 4-1: Measured reach resistance coefficients, average velocities, and Froude numbers.	48
Table 4-2: Travel time and velocity measurements (measured flow paths).	50
Table 4-3: Flow resistance and associated measurements (measured flow paths).	52
Table 4-4: Flow resistance and associated measurements (shortest potential flow paths).	55
Table 5-1: Most relevant explanatory variables, with all data used for models 1 through 8 and only bankfull data for model 9.	85
Table 5-2 : Log-transformation bias corrections.	88
Table 5-3: Longitudinal spacing sensitivity analysis.	90
Table 5-4: Error analysis of tested resistance relationships, by slope.	102
Table 5-5: Multivariate regression results with entire database (n = 59), using variables describing bedform and bankform. Predictors significant with $\alpha = 0.01$	114
Table 5-6: Multivariate regression results for Manning's n with exclusion of low-flow data (n = 44), using variables describing bedform, bankform, and instream wood. Predictors significant with $\alpha = 0.05$	117
Table 5-7: Multivariate regression results for Darcy-Weisbach f with exclusion of low-flow data (n = 44), using variables describing bedform, bankform, and instream wood. Predictors significant with $\alpha = 0.10$	117
Table 5-8: Multivariate regression results for Darcy-Weisbach f with exclusion of low-flow data (n = 44), using variables describing 3-D bedform and instream wood. Predictors significant with $\alpha = 0.05$	119
Table C-1: Bed data.	161
Table C-2: Bank data.	163
Table C-3: Instream wood data.	165
Table C-4: Three-dimensional spatial variability data.	166

LIST OF SYMBOLS, VARIABLES, AND ABBREVIATIONS

Symbols

A	=	cross-sectional area (m^2)
A	=	average of the area measurements computed at each cross section
A/SDA	=	area/standard deviation of the area
$c(x,t)$	=	tracer concentration
C	=	Chezy coefficient
CF	=	correction factor
C_p	=	peak concentration desired ($\mu\text{g/L}$)
D_{50}	=	median bed-material size
D_{84}	=	84 th percentile of the bed-material size (m)
D_{84}/D_{50}	=	ratio of the 84 th percentile of the bed-material size to the median bed-material size
e	=	average percentage error of the prediction (measured – predicted)
f	=	Darcy-Weisbach friction factor
Fr	=	Froude number
g	=	acceleration due to gravity
\bar{h}	=	mean depth
\bar{h}/D_{84}	=	ratio of the average depth to the 84 th percentile of the bed-material size.
h_{a3}	=	3-D variable – average depth
h_{a3}/σ_{z3}	=	3-D relative resistance element submergence term
h_{a3}/σ_{h3}	=	3-D depth variability term, normalized by average depth
h_c/z	=	critical flow depth / average step height ratio

h_m	=	average of the maximum depth computed at each cross section
h_m/SDh_m	=	maximum depth variability
h_m/δ_m	=	relative submergence version of the maximum residual
h_m/σ_z	=	relative bedform submergence
h_{m3}	=	3-D variable – maximum depth
h_{m3}/σ_{z3}	=	3-D depth variability term, normalized by maximum depth
i	=	initial time of the censored tracer concentration, just above the limit of the data noise
I_x	=	sum of concentration over time at a fixed point x
j	=	trailing time of the same censored concentration
K	=	Ripley's function
K_b	=	average of left and right bank sinuosity (bank length / profile length)
K_{bh}	=	horizontal projection of average of left and right bank sinuosity
L	=	stream distance of interest (m)
M	=	measured flow paths
n	=	sample size
n	=	Manning's boundary roughness
$p_x(t)$	=	temporal probability density function
P_w	=	wetted perimeter (m)
P_w	=	average of the wetted perimeter measurements computed at each cross section
q	=	unit discharge
q^*	=	dimensionless flow rate

Q	=	reach discharge (m^3/s)
R	=	hydraulic radius (m)
R/D_{84}	=	relative submergence
R/SDR	=	hydraulic radius variability
R/δ_m	=	relative submergence version of the maximum residual
R/σ_z	=	relative bedform submergence
s^2	=	mean square error of the regression
S	=	shortest potential flow paths
S	=	slope exponent
S_f	=	friction slope (m/m)
S_o	=	bed slope (m/m)
SDA	=	standard deviation of the area measurements
SDh_m	=	standard deviation of the maximum depth measurements
SDP_w	=	standard deviation of the wetted perimeter
SDR	=	standard deviation of the hydraulic radius
t	=	tracer travel time from the injection point
t_{HM}	=	harmonic mean travel time
TW	=	average of the top width measurements at each cross section
TW/h_a	=	width-depth ratio
$TW/SDTW$	=	ratio of top width to the standard deviation of the top width
v	=	average reach velocity (m/s)
v	=	mean velocity (m/s)
v	=	harmonic average reach velocity

V	=	overall flow volume
V	=	volume of dye (mL)
V	=	flow volume
V_w	=	instream wood volume
V_w/V	=	regressions of resistance coefficients versus volume ratios
V_w	=	instream wood volume
V_{wb}	=	branched instream wood volume
V_{wb}/V	=	regressions of resistance coefficients versus volume ratios
V_{wb}	=	branched instream wood volume
V_{wbd}	=	branched, thalweg-distance reduced instream wood volume
V_{wbdp}	=	branched, thalweg-distance reduced, projected instream wood volume
V_{wbpd}/V	=	regressions of resistance coefficients versus volume ratios
V_{wbp}	=	branched, projected instream wood volume
V_{wd}	=	thalweg-distance reduced instream wood volume
V_{wd}/V	=	regressions of resistance coefficients versus volume ratios
V_{wdd}/V	=	regressions of resistance coefficients versus volume ratios
V_{wdp}/V	=	regressions of resistance coefficients versus volume ratios
V_{wp}	=	projected instream wood volume
V_{wp}	=	projected instream wood volume
V_{wp}/V	=	regressions of resistance coefficients versus volume ratios
x	=	explanatory variable
x, y, z	=	axes
β_0	=	regression-defined intercept and exponent term

β_1	=	regression-defined slope
δ	=	bed residual
δ_a	=	average bed residual
$\delta_{average}$	=	average bed residual
δ_m	=	maximum bed residual (absolute)
δ_{median}	=	median bed residual
Δt	=	time step of the measurements
λ or e	=	roughness concentration factor, where e is defined as the cumulative step height divided by the reach length
σ_{h3}	=	3-D variable – detrended standard deviation of depth
σ_y	=	standard deviation of the residuals of a bank profile regression
σ_z	=	standard deviation of the residuals of a bed profile regression, a detrended bed irregularity index
σ_{z3}	=	3-D variable – detrended standard deviation of bed elevations

Abbreviations

®	registered
1-D	one-dimensional
2-D	two-dimensional
3-D	three-dimensional
.dbf	dbase file extension
ESL	East Saint Louis
FC	Fool Creek
FESWMS-2DH	Finite Element Surface-Water Modeling System: Two-Dimensional Flow in a Horizontal Plane
GPS	Global Positioning System
HEC-RAS	Hydrologic Engineering Centers River Analysis System
ID	identification
LFC	lower Fool Creek
LiDAR	Light Detection and Ranging
Max.	maximum
Min.	minimum
NAD	North American Datum
NAVD	North American Vertical Datum
NOAA	National Oceanic and Atmospheric Administration
OPUS	Online Positioning User Service
PRISM	Parameter-elevation Regressions on Independent Slopes Model
Pts.	points

RMS	root mean square
TDS	Tripod Data Systems
TIN	triangulated irregular network
UFC	upper Fool Creek
UTM	Universal Transverse Mercator
Vel.	velocity measurement technique
WT	Water Tracing

CHAPTER 1

INTRODUCTION

Methods for predicting Manning's n and the Darcy Weisbach friction factor (f) in high-gradient mountain streams are essential for many practical applications, including hydraulic modeling, stream restoration, geomorphic analysis, and quantification of ecological habitat characteristics. Approaches that provide an effective method for estimating flow resistance from simply-measured channel characteristics are the most useful in application but are also the most elusive to obtain, especially for a full range of instream flows.

Flow resistance in open channels is composed of three fundamental components (Leopold *et al.* 1960): (1) skin or boundary resistance, which can be expressed as a force per unit boundary area; (2) internal distortion or form resistance, from a deflection that causes super elevated and depressed water surfaces, resulting in secondary currents and eddying; and (3) impact or spill resistance, resulting from sudden flow deceleration from supercritical flow, such as at the base of a waterfall. In lower-gradient, gravel-bed streams boundary resistance is typically dominant, hence the effectiveness of relative grain submergence as a resistance-prediction tool. In cascade and step-pool streams, form resistance has many sources, including bed and bank variability, boulders that project through the flow field, and instream wood. Spill resistance is identified by jets, drops, and

standing waves, indicating sub-reach supercritical to subcritical flow transitions (hydraulic jumps). Step resistance, due to bedforms in step-pool and cascade channels, consists of both form and spill resistance. In high-gradient streams ($> \sim 2\%$) a large proportion of the resistance often results from spill, where rapid flow and waterfalls impact on standing water, resulting in a high degree of turbulence. In step-pool and cascade streams, spill resistance is typically dominant (Curran and Wohl 2003; MacFarlane and Wohl 2003; Wilcox *et al.* 2006). In a flume-based study, Wilcox *et al.* (2006) attributed 68 and 92 percent of the total resistance to spill, while grain resistance was found to contribute only 8 to 32 percent of the total. As discharge and slope increase, the mechanism of flow resistance can shift from resistance being dominated by a nappe regime, where flow alternates between supercritical at step treads to subcritical in well-defined, unsubmerged pools just below the step, to a process approaching a skimming regime, where the bedforms are submerged and the flow becomes entirely critical or supercritical (Comiti *et al.* 2009).

Despite the complex sources of resistance in steep mountain streams, and the resulting non-uniform flow conditions that define these stream types, there may likely be consistency in the spatial form of the roughness components at the reach scale that allow for reasonable estimates of reach-scale velocity (Lee and Ferguson 2002). Defining geometric characteristics of these stream types that can predict average reach velocity and resistance coefficients is both a practical exercise, to provide practitioners tools for predicting flow velocity, as well as a research tool for identifying underlying processes of flow resistance.

1.1 Objectives

The primary objectives of this dissertation were to:

- conduct flow resistance measurements in cascade, step-pool, and plane-bed stream reaches, to add to the database provided in the literature;
- document field measurement and analysis techniques used to develop the dataset;
- present photographic guidance for general resistance coefficient estimation in high-gradient channels;
- develop simple linear and multivariate regression models for estimating flow resistance coefficients and velocity in cascade, step-pool, and plane-bed stream reaches; and
- compare model performance with other prediction methodologies.

1.2 Organization

Although this dissertation contains multiple research themes that will ultimately be submitted as individual manuscripts, composited presentations of background, methods, results, and discussion are provided. The following presentation sequence was adopted: background; methods for field methodology, data extraction, and statistical analyses; and measurements, including photographic guidance. Additionally, a chapter with all results and discussion is presented, with sections focusing upon resistance prediction using simple linear regression, the performance of other prediction methodologies, three-dimensional (3-D) spatial analysis, resistance prediction using multivariate regression, velocity prediction, and the impact of flow path measurements. Finally, a future research section and a summary / conclusions chapter is provided.

CHAPTER 2

BACKGROUND

The two primary flow resistance coefficients are Manning's n and the Darcy-Weisbach f . The Manning's coefficient is defined as:

$$n = \frac{R^{2/3} S_f^{1/2}}{v} \quad (2-1)$$

where the hydraulic radius (m), R , is expressed as:

$$R = \frac{A}{P_w} \quad (2-2)$$

and v is the average reach velocity (m/s); S_f is the friction slope (m/m); A is the cross-sectional area (m^2); and P_w is the wetted perimeter (m). For a reach-averaged n value, all other terms must also be reach-averaged values.

Manning's n was developed as a measure of boundary roughness given steady, uniform flow but is often used as a measure of all sources of energy loss in a stream system. Its development is linked to the Chezy equation, which was developed by the French engineer Chezy in about 1768 for the practical application of a canal design for the Paris water supply system. The Chezy equation is:

$$v = C\sqrt{RS} \quad (2-3)$$

where C is the Chezy coefficient. As discussed in Henderson (1966) and Daugherty *et al.* (1985), the Manning's equation was developed to fit existing data of the time to C , to simplify data compiled and fitted by Ganguillet and Kutter (1869) using a somewhat complicated equation. Reportedly, Gauckler (1868) and Hagen (1881) independently concluded that C could be simply expressed as:

$$C = \frac{R^{1/6}}{n} \quad (2-4)$$

This conclusion has been incorrectly attributed to Manning, who published in 1890. This formulation is also referred to as the Strickler equation. Although the Manning coefficient has the unsatisfying dimensions of $time \cdot length^{-1/3}$, practicing professionals typically use Manning's n for estimating stream resistance.

The Darcy-Weisbach friction factor, originally developed for pipes flowing full, is expressed as:

$$f = \frac{8gRS_f}{v^2} \quad (2-5)$$

where g is the acceleration due to gravity. The friction factor has the substantial advantage of being dimensionless and has been argued to be the more appropriate roughness coefficient for general use in open-channel hydraulics (Hey 1979). The friction factor can be translated to n using the equation:

$$n = R^{1/6} \sqrt{\frac{f}{8g}} \quad (2-6)$$

A comprehensive discussion of flow resistance approaches and equations is provided in Ferguson (2007).

As an alternative to the exponents used in the Chezy, Manning, and Darcy-Weisbach equations, it has been proposed that a hydraulic radius exponent greater than $2/3$ and a slope exponent closer to $1/4$ or $1/3$ than $1/2$ provide a better fit to available data in gravel-bed and mountain stream types (Lopez *et al.* 2007; Bjerklie *et al.* 2005). Other researchers have developed alternative forms of the resistance equations with varying S and R exponents, either directly or indirectly (Golubtsov 1969; Williams 1978; Bray 1979; Jarrett 1984; Dingman and Sharma 1997). Indirectly refers to predictions of a roughness coefficient using R and S , such as in Jarrett (1984). Golubtsov (1969) argued that flow dependence on slope varies with the power $1/2$ in streams with gradients less than 0.001, and the power $1/6$ in streams with gradients over 0.004. Adjusting exponents in the Darcy-Weisbach equation makes f dimensional and negates a perceived advantage of this coefficient for resistance prediction.

2.1 Flow Resistance

Numerous researchers have found that resistance in high-gradient streams varies substantially with flow (Limerinos 1970; Bathurst 1985; Lee and Ferguson 2002; Wilcox and Wohl 2006), with resistance decreasing as flow increases. Steep streams are typically characterized by low relative submergence, defined as the ratio of R to some characteristic roughness element size, such as grain size. While lower gradient streams have velocity profiles that are logarithmic, velocity profiles measured in steep streams with low relative grain submergence are typically not logarithmic, but instead are

inflected with a form more similar to an “S” shape (Jarrett 1991; Marchand *et al.* 1984) in response to large roughness elements. Recking *et al.* (2008) discussed approximating the S-shape profile with a modified logarithmic function. Katul *et al.* (2002) developed a mixing layer theory for flow resistance in flows with low relative submergence, using a hyperbolic tangent function. An analogy was drawn with forest canopy turbulence, where the structure of the flow is similar to a mixing layer, with an inflection near the mean roughness height.

In high-gradient streams, researchers have found that bed-material size is a poor predictor of overall resistance (Curran and Wohl 2003; MacFarlane and Wohl 2003). Wilcox *et al.* (2006) attributed only 8 to 32 percent of total resistance to grain. MacFarlane and Wohl (2003) compared the characteristics of twenty step-pool streams with wood and twenty without wood. During low-flow conditions, they found that grain resistance was negligible for both groups and form resistance due to variable channel shape and non-step forming instream wood contributed more towards total resistance. In comparing step-pool, plane-bed, and pool-riffle streams, Wohl and Merritt (2008) assembled an extensive dataset that indicated a similar range in friction factors among the channel types despite varying relative submergence. They conclude from this that sources of resistance other than grain, such as bedforms, adjust to maintain a similar range in roughness. However, Orlandini *et al.* (2006) found that there was good correlation between grain size and reach velocity in a high-gradient alpine watershed.

Wilcox and Wohl (2006) investigated flow resistance dynamics in a fixed-bed flume, where they manipulated characteristics that contribute to resistance. The presence or absence of steps was found to strongly influence flow resistance, with steps having a

stronger effect at low flows. More closely-spaced treads increased resistance compared to wider-spaced treads, with this effect being most substantial at lower flows. A measure of bed variability, the standard deviation of bed elevations, has been well-correlated with flow resistance from longitudinal profiles in the laboratory (Aberle and Smart 2003) but is an unproven technique in the field. Additionally, the standard deviations of three-dimensional bed elevations in a sand-bedded river has been correlated with discharge and may be a more effective measure of bed roughness than bedform height (Aberle *et al.* 2010). A method for developing estimates of form drag due to bank and bed features has been developed by Kean and Smith (2006a), in relation to their work to develop theoretical rating curves for stage-discharge relationships (Kean and Smith 2005). The approach models regular form elements using Gaussian shapes, which are defined by a protrusion height, a longitudinal length scale, and a wavelength. This work was extended in Kean and Smith (2006b) to model irregular form elements.

It has been suggested that bedform dynamics, with resulting shifts in form and spill resistance, typically prevent the occurrence of supercritical flow at the reach scale (Leopold *et al.* 1960). Grant (1997) hypothesized that bedform dynamics prevent the occurrence of supercritical flow for more than short distances and brief time periods in most alluvial rivers, with supporting data collected in a steep, sand-bedded coastal stream.

Predicting resistance in streams is complicated by the influence of instream wood. In a spring-dominated, gravel-bed stream, Manga and Kirchner (2000) found that, as debris was added to the stream, total shear stress increased due to deeper flows, while bed shear stress decreased as a greater proportion of the shear stress was borne by the debris.

During low-flow conditions streams without wood may have significantly shallower flows, lower steps, shorter step spacing, a greater proportion of the water surface drop due to steps, larger grain sizes, and lower friction factors (MacFarlane and Wohl 2003). In old growth forests of the Southern Andes, reaches with substantial instream wood were found to have finer sediments, taller steps, and higher flow resistance than non-wood reaches, with up to an order of magnitude increase in resistance from instream wood dams (Comiti *et al.* 2008). Wilcox and Wohl (2006) found that instream wood density affected resistance more than other wood variables, while slope mediated the density effect with decreasing slope reducing the density effect. The effect of density diminished at higher densities, due to wake influences. Wood orientation effects were nearly as substantial as density. Wood length and arrangement effect interacted strongly with discharge, with stacked pieces causing the highest friction factors measured, possibly due to considerable ponding forced by this arrangement. Instream wood jams did not create substantially-different roughness than evenly-spaced single pieces, though these jams were substantially simplified in comparison to natural jams. Clustering of instream wood near step lips created substantially higher roughness than instream wood positioned further up the step tread. Significantly, there was a synergistic effect among roughness components in that the cumulative resistance of all interacting components was greater than the sum of the individual components (Wilcox and Wohl 2006).

In addition to instream wood, live vegetation can substantially affect instream resistance during bankfull or near-bankfull flows (Jarrett 1984). The degree of influence on flow resistance is dependent upon spacing, density, extent, height, and stiffness (Masterman and Thorne 1994). Substantial vegetation may result in smaller bed-material

grain sizes (Buffington and Montgomery 1999) due to increased roughness as well as channel narrowing through increased bank strength. Masterman and Thorne (1994) developed a theoretical method for including the influence of vegetated banks in flow resistance. They assert that typical bank vegetation tends to substantially influence flow resistance at width/depth ratios less than 16. A physically-based model was developed by Nepf (1999) for describing the drag, turbulence, and diffusion of flow through wetland vegetation. Nepf introduced the concept of mechanical diffusion to vegetated flows. Through an analogy with forest canopies, Ghisalberti and Nepf (2002) applied mixing layer theory to flow through submerged aquatic vegetation, with application to a laboratory model using scaled sea grass. Kean and Smith (2005) have incorporated vegetation effects into their methodology for developing theoretical rating curves for stage-discharge relationships.

From the multiple sources and complex interactions contributing to flow resistance, coefficients are used as aggregate variables to define the overall flow resistance. Techniques for prediction of these coefficients is incomplete due to the complex processes involved.

2.1 Resistance Coefficient Prediction

Flow resistance has been characterized in lower-gradient streams in many studies; however, less work has been performed on higher-gradient streams. Commonly-cited references for estimating n typically underestimate the resistance in steeper streams. For example, the Hydrologic Engineering Centers – River Analysis System (HEC-RAS) *Hydraulic Reference Manual* (Brunner 2008) makes recommendations based upon Chow

(1959), with a maximum n of 0.07 suggested for “*mountain streams, no vegetation in channel, banks usually steep, with trees and brush on banks submerged, cobbles and large boulders.*” This research and others (Reid and Hickin 2008; Comiti *et al.* 2007; Lee and Ferguson 2002) indicate substantially higher expected resistance values in steep mountain streams with such a description, with n commonly falling between 0.1 to 0.3 for bankfull flows and flow resistance increasing with decreasing discharge. Other commonly-used references for estimating n , such as the use of base and additive values (Cowan 1956; Arcement and Schneider 1989) can also be misleading in steep streams. Photographic guides for visual comparison (Barnes 1967; Aldridge and Garrett 1973; Arcement and Schneider 1989; Hicks and Mason 1999) provide guidance for lower-gradient streams and Yochum and Bledsoe (2010) provide visual guidance in the stream reaches quantified in this research; however photo guides are not a substitute for quantitative methodologies but are instead a helpful initial step in a selection process. The underestimation of Manning’s n can lead to substantially-overestimated flow velocities, underestimated travel times, the miscategorization of flow regime (subcritical versus supercritical flow), and computational instability in common applications such as steady and unsteady 1-D and two-dimensional (2-D) computational models (*e.g.*, HEC-RAS and Finite Element Surface-Water Modeling System: Two-Dimensional Flow in a Horizontal Plane (FESWMS-2DH)).

There are various quantitative methods developed in the field and potentially applicable for estimating resistance coefficients in cascade, plane-bed, and step-pool channels (Table 2-1). Some of these techniques have been developed primarily in plane-bed and pool-riffle stream types (Montgomery and Buffington 1997). In twenty-one

high-gradient Colorado streams (slopes less than 3.4 percent), Jarrett (1984) made seventy-five current-meter measurements of discharge and used three to five surveyed cross sections per reach with marked water surface elevations at each section to compute Manning's n values. From these data, the multivariate regression model:

$$n = 0.32S_f^{0.38}R^{-0.16} \quad (2-7)$$

was computed. Marcus *et al.* (1992) evaluated eleven techniques for estimating Manning's n in a glacial stream and found that Jarrett (1984) performed best, though it did overpredict n at the relatively-steep slopes tested, compared to Jarrett's dataset. Soto and Madrid-Aris (1994) evaluated available prediction equations for flow resistance coefficients using a dataset of sixty-two measurements in nineteen reaches of mountain streams in Chile and found that the Jarrett formula had an average error of 19 percent. At three sections immediately adjacent to stream gages, Bathurst (1985) used the discharge estimates at the gages combined with the detailed sections to compute average section velocities and friction factors for streams less than 5 percent slope. He fit a regression model to these forty-four data points, specifically:

$$\sqrt{\frac{8}{f}} = 5.62 \log\left(\frac{\bar{h}}{D_{84}}\right) + 4 \quad (2-8)$$

where \bar{h} is the mean depth and D_{84} is the 84th percentile of the bed-material size. Soto and Madrid-Aris (1994) found that the Bathurst formula had average errors of 22 percent for their dataset.

Table 2-1: Data characteristics of potentially-applicable flow resistance prediction equations.

Method	Data Pts.	Slope		Discharge (cms)		n		f		Vel.
		Min.	Max.	Min.	Max.	Min.	Max.	Min.	Max.	
Jarrett (1984)	75	0.002	0.034	0.34	130	0.028	0.16	0.16	6.7	(a)
Bathurst (1985)	44	0.004	0.037	0.14	200	0.027	0.19	0.060	5.5	(a)
Mussetter (1988)	178	0.005	0.17	0.0048	18.7	0.026	2.8	0.14	2600	(a)
Soto and Madrid-Aris (1994), $0 < R/D_{84} < 1$	119	0.002	0.037	0.14	200	0.027	0.19	0.060	6.7	(a)
Soto and Madrid-Aris (1994), $1 < R/D_{84} < 12.5$	62	----	----	2.7	370	----	----	----	----	----
Lee and Ferguson (2002)	81	0.030	0.18	0.0018	0.53	----	----	----	----	(b)
Aberle and Smart (2003)	94	0.020	0.10	----	----	----	----	----	----	(b)
Comiti <i>et al.</i> (2007)	44	0.080	0.21	0.080	1.86	----	----	1.8	28	(b)
Comiti <i>et al.</i> (2007)	177	0.020	0.21	----	----	----	----	----	----	(b)

Abbreviations: Max. = Maximum; Min. = Minimum; Pts. = points; and Vel. = velocity measurement technique.

Notes: The velocity measurement techniques used in each analysis were: ^(a) use of current meter and stream-gaging techniques for estimating discharge and using this discharge and the section area to compute velocity; ^(b) use of a tracer to measure average reach velocity; and --- denotes insufficient data available.

Using a heavily-parameterized approach, Soto and Madrid-Aris (1994) developed two equations for predicting Manning n using the Froude number (Fr), friction slope, relative submergence (R/D_{84}), and the bed-material grain size (D_{84} , in m). Using the dataset of Jarrett (1984) and Bathurst (1985), they present the equation:

$$n = \left[0.183 + \ln \left(\frac{1.75 S_f^{0.158}}{Fr^{0.263}} \right) \right] \frac{(D_{84})^{1/6}}{\sqrt{g}} \quad (2-9)$$

for relative grain submergence less than 1. For relative grain submergence between 1 and 12.5 (intermediate-scale roughness elements), n is predicted using the Chilean dataset of sixty-two measurements, specifically:

$$n = \left[0.183 + \ln \left(\frac{1.30 S_f^{0.0785} \left(\frac{R}{D_{84}} \right)^{0.0211}}{Fr^{0.171}} \right) \right] \frac{(D_{84})^{1/6}}{\sqrt{g}} \quad (2-10)$$

The use of the Froude number makes Equations 2-9 and 2-10 of limited use for prediction.

In higher-gradient streams that have step-pool and cascade forms, several equations have been developed for predicting flow resistance coefficients. Mussetter (1988) measured flow resistance at multiple discharges in fifty-three Colorado streams, for a total of 178 measurements. With slopes ranging from 0.008 to 0.17, these reaches were in riffle-pool, plane-bed, step-pool, and cascade streams. He developed the equation:

$$\sqrt{\frac{8}{f}} = 1.11 \left(\frac{\bar{h}}{D_{84}} \right)^{0.46} \left(\frac{D_{84}}{D_{50}} \right)^{-0.85} (S_f)^{-0.39} \quad (2-11)$$

where D_{50} is the median bed-material size. This equation explained 82 percent of the variance in his dataset. Based upon both field and flume data, Lee and Ferguson (2002) developed a friction factor equation based on relative grain submergence for self-formed clast-stepped channels. From a dataset of eighty-one points, they developed the equation:

$$\sqrt{\frac{1}{f}} = 1.48 \left(\frac{R}{D_{84}} \right)^{1.80} \quad (2-12)$$

Aberle and Smart (2003) developed an equation based upon mobile-bed flume data:

$$\sqrt{\frac{8}{f}} = 0.91 \frac{\bar{h}}{\sigma_z} \quad (2-13)$$

where σ_z is the standard deviation of the residuals of a bed profile regression, a detrended bed irregularity index. This relationship explained 92 percent of the variance in the dataset. They argue that morphology of steeply-sloped streams cannot be sufficiently described by a characteristic grain size and that σ_z can be used as a characteristic roughness length to represent bedforms. The variable σ_z was first presented by Aberle *et al.* (1999). In a field setting, Comiti *et al.* (2007) used salt tracers to measure flow velocity and three cross sections per reach to characterize the geometry for less-than-bankfull flows in step-pool and cascade channels of the Rio Cordon. They found that velocity and flow resistance are best described, in order of decreasing influence, by the dimensionless unit discharge, channel slope, and the ratio of step height to step length. Relative grain submergence was found to be a poor predictor of flow resistance. From the Rio Cordon data, they presented the flow resistance prediction equation:

$$f = 87.1q^{*-0.50}S_f^{1.83} \quad (2-14)$$

where q^* is the dimensionless flow rate:

$$q^* = \frac{q}{\sqrt{gD_{84}^3}} \quad (2-15)$$

and q is the unit discharge. This equation explained 78 percent of the variance in the dataset. Additionally, Comiti *et al.* (2007) combined the Rio Cordon data with data collected by Lee and Ferguson (2002), MacFarlane and Wohl (2003), Curran and Wohl (2003), and Wohl and Wilcox (2005) to obtain:

$$f = 10.47q^{*-1.13}S_f^{1.12} \quad (2-16)$$

which explained 61 percent of the variance.

Additional parameters that have been investigated for their potential in explaining resistance include the roughness concentration factor, λ or e (Rouse 1965; Wohl *et al.* 1997), with e defined as the cumulative step height divided by the reach length as well as the relative form submergence factor (R/H), where H is the bedform amplitude (Wohl and Merritt 2008). Another parameter that has been used as a descriptor of step-pool form is the vertical sinuosity index, which refers to the bedforms of step-pool channels (Chin and Phillips 2007). This value is computed as the ratio of the vertical sinuous bed distance divided by the straight-line distance.

Slope can substantially influence resistance (Golubtsov 1969; Aldridge and Garrett 1973; Jarrett 1984; Wohl *et al.* 2004) and reach velocity prediction (Orlandini *et al.* 2006; Zimmermann 2009), with an increase in resistance as slope increases (Pagliara and Chiavaccini 2006). The explanatory power of slope in resistance estimation is supported by related studies indicating that slope is the most important parameter for predicting stream type in mountain settings (Wohl and Merritt 2005). In flume and field tests of steep riprap channels, Abt *et al.* (1988) and Rice *et al.* (1998) found that the gradient, in addition to mean clast diameter or relative submergence, were the best predictors of resistance coefficients. Wilcox and Wohl (2006) found that f increased with slope, though slope was less influential than other tested variables.

In summary, the literature indicates that coefficient prediction using a variable describing bedform is likely to be effective in predicting flow resistance in steep mountain streams. Of particular interest is the use of the standard deviation of bed

elevations (σ_z), due to its relative simplicity and potential descriptive power. Slope is an additional variable that may be helpful in predictive models. Instream wood, other vegetation, and influences such as bank variability all have the potential to increase flow resistance in high-gradient streams.

CHAPTER 3

METHODS

The study sites, data-collection methodologies, data-extraction techniques, and statistical methods are discussed in this chapter. Data extraction refers to the methods used to extract geometric data from ground-based Light Detection and Ranging (LiDAR) scans.

3.1 Field Methodology

3.1.1 Study Area

Data collection was performed in the Fraser Experimental Forest, on East Saint Louis and Fool Creeks (Figure 3-1). The Fraser Experimental Forest is located in the Fraser River Watershed, in the Upper Colorado Basin west of the town of Fraser, approximately 115 km west of Denver, Colorado, USA. The upper watershed boundary of East Saint Louis Creek is the Continental Divide. All research reaches are just upstream of gaging stations monitored by the U. S. Forest Service using sharp-crested weirs. Data were collected on five cascade, eight step-pool, one plane-bed, and one transitional (between step-pool and plane-bed) stream reaches. Instream wood was present in all of the reaches, with many of the steps formed by clasts anchoring debris

material. Photographs illustrating the channel characteristics of selected reaches are provided in Figure 3-2.

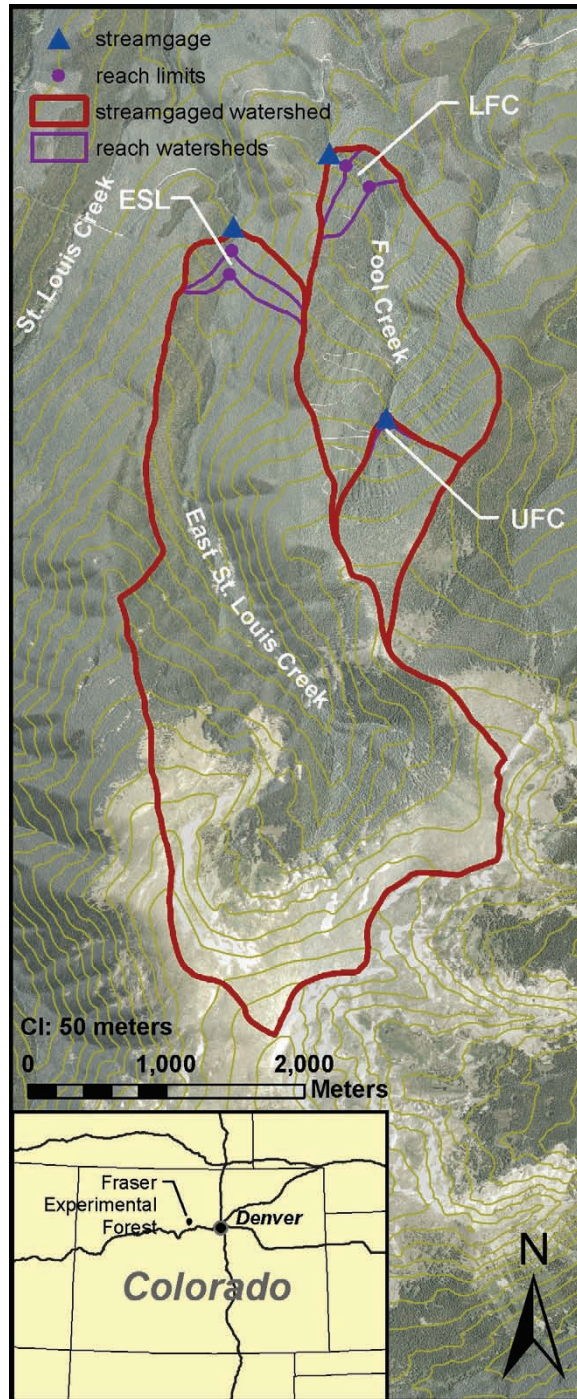


Figure 3-1: Research watersheds and stream reaches, Fraser Experimental Forest, Colorado.



Figure 3-2: Low-flow photographs of selected research reaches, Fraser Experimental Forest, Colorado.

The East Saint Louis (ESL) watershed ranges in elevation from 2895 m to 3850 m. Average precipitation in the watershed, from 1961 to 1990 Parameter-elevation

Regressions on Independent Slopes Model (PRISM) estimates (Daly *et al.* 1994), ranges from about 68 cm at the lower limit of the watershed to 89 cm at the upper limit, primarily in the form of snow. At the stream gage, the watershed area is 8.7 km². The study reaches range in elevation from 2915 to 2935 m. The lower limit of the study reaches drains 97.9 percent of the gaged watershed, while the upper limit drains 96.5 percent of the gaged watershed. The watersheds are illustrated in Figure 3-1.

The Fool Creek (FC) watershed ranges in elevation from 2910 m to 3525 m. Average precipitation of the watershed ranges from about 64 cm to 79 cm, also primarily in the form of snow. At the lower and upper stream gages, the watershed area is 3.0 km² and 0.69 km², respectively. The lower limit of the lower research reaches (LFC) drains 97.9 percent of the gaged watershed, while the upper limit drains 92.9 percent of the gaged watershed. The study reaches range in elevation from 2924 to 2943 m in the lower segment to 3212 to 3217 m in the upper segment. The upper study reaches (UFC) drain 100 percent of the gaged watershed at their lower limit and 98.0 percent at their upper limit.

In both East Saint Louis and Fool Creeks peak snowmelt typically occurs in early June. Lower and drier portions of the watershed are dominated by lodgepole pine forest, with Engelmann spruce and subalpine fir dominating at higher elevations. The upper portions of the watersheds are alpine tundra. There is only a small portion of tundra in the Fool Creek watershed but roughly 30 percent of the East Saint Louis Creek watershed is tundra. There are no significant alpine lakes present. The lodgepole pine forest is heavily infested by beetle, with high tree mortality rates; substantial additional quantities of instream wood will be recruited during the next few years. Soils of the watersheds

contain angular gravel, with low percentages of silt and clay; they are primarily derived from gneiss and schist at lower elevations and sandstone at higher elevations. The soils are quite permeable – substantial infiltration can occur during snowmelt and summer rains. The subsequent interflow and baseflow can make up a substantial proportion of annual streamflow. Riparian corridors have an alluvial fill composed of a mixture of glacial till, glacial outwash, and recent valley fill (Retzer 1962).

Data collection is composed of numerous longitudinal water surface profiles, at high, medium, and low flows; bed, bank, and floodplain surveying; bed-material characterization; and average reach velocity measurements. The data were collected by the author and his research partner Gabrielle David, with the help of field assistants. The collection methodology is described in the following sections.

3.1.2 Geometry

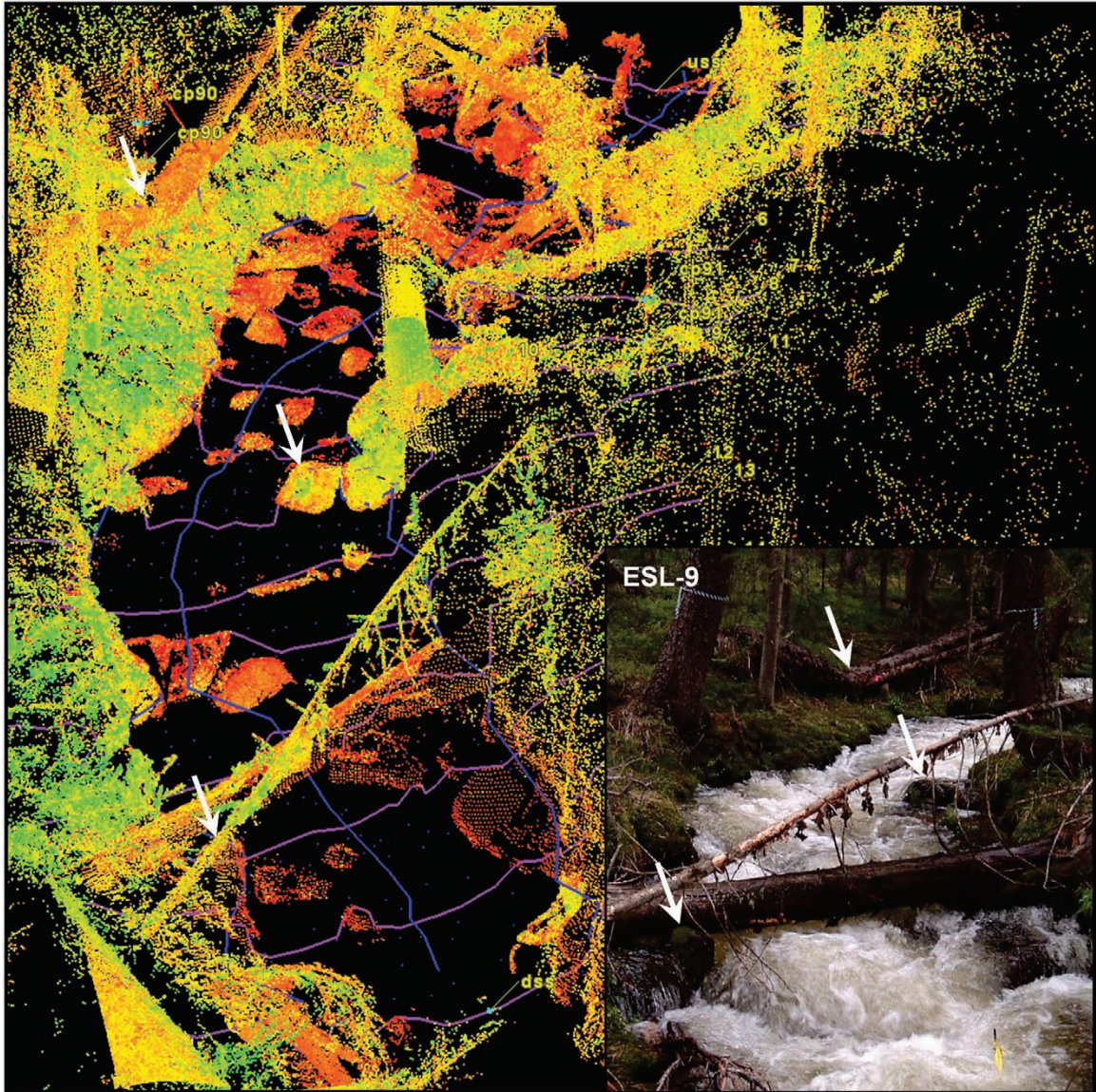
Reach surveying was performed through the use of a tripod-mounted LiDAR scanner for above-water surface features and a gridded laser theodolite survey for below-water features. Additionally, a laser theodolite was used for measuring longitudinal profiles of the bed and water surface during each resistance measurement. Longitudinal reach lengths varied from 6.2 to 35 m, with widths from 0.7 to 4.0 m. The profile point spacing was uniform, with an average spacing of 0.29 m; this scale well-defines the bed feature variation. The longitudinal profiles were collected at the thalweg, and left and right edges of water. Bed gradation was measured using a 300-point, spatially-referenced pebble count.

The Leica HDS Scanstation scanning system was used for collecting the LiDAR data. Each of the fifteen reaches was scanned from multiple directions to minimize shadow. Targets were set up over at least two, preferably three, control points to provide a consistent coordinate system. The LiDAR scanning equipment used in this research cannot penetrate water; below water features were surveyed using a sub-meter scale feature-based gridded laser theodolite survey, at a necessarily lower resolution than the scanned data. The LiDAR equipment is shown in Figure 3-3, while an example screenshot of a LiDAR point cloud is provided in Figure 3-4. A key advantage of using LiDAR is that this surveying technique allows a virtual revisit and resurvey of morphologic characteristics at any time. For example, detailed cross sections, instream wood characteristics, and 3-D bed geometry can be extracted from the dataset in the office, reducing overall field time and allowing the extraction of geometric characteristics without *a priori* identification.



A: LiDAR scanner, set up on reach ESL-9
B: field assistant Dan Dolan setting up a target used for merging and georeferencing the point clouds
C: field equipment, including laptop, generator, fuel, extension cords, data cables, tripod, targets, and scanner
D: author scanning reach ESL-9

Figure 3-3: LiDAR equipment.



Legend

Blue lines indicate high-flow water surface profiles

Violet lines indicate cross sections

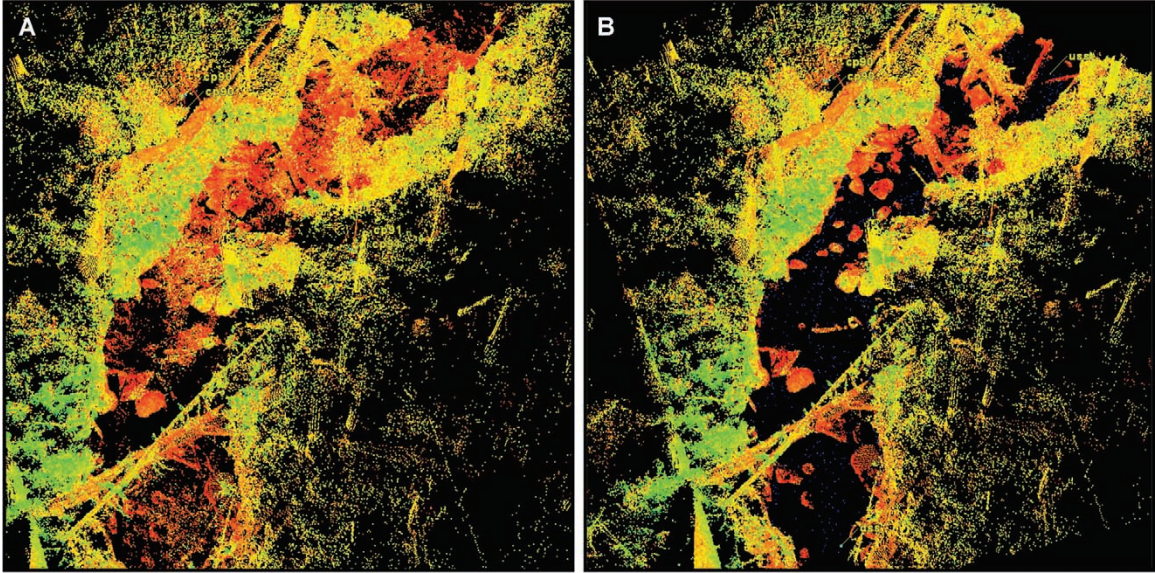
White arrows indicate common points between the point cloud and photograph

Figure 3-4: LiDAR point cloud for reach ESL-9, with accompanying photograph of near-bankfull flow.

When collecting geometric information using multiple methods, it is essential to establish a common coordinate system so that data from different sources will be compatible. In this study, all data were collected in the Universal Transverse Mercator (UTM) coordinate system. A survey-grade Trimble 5800 Global Positioning System

(GPS) unit was set up over benchmark pairs and the National Oceanic and Atmospheric Administration (NOAA) Online Positioning User Service (OPUS) system was used to fix the location of the benchmarks. The chosen coordinate system was UTM-13, NAD-83 (North American Datum), orthogonal height (Geoid03, NAVD 88 (North American Vertical Datum)). According to the OPUS solution, the total root mean square (RMS) errors associated with these benchmarks ranged from 0.017 to 0.025 m. From these benchmarks, a laser theodolite survey was traversed to the research reaches, where control points were set with defined UTM coordinates. These control points were used as reference points in the LiDAR scanning and total station surveying to automatically register the data into common coordinates. This system yielded minimized and consistent errors in all survey data collected for the study.

Within the Leica Cyclone software (Version 6.0), the individual LiDAR scanworlds of portions of the study reaches were merged into a common georeferenced scanworld and total station surveys of the bed and multiple profile surveys were added to create a continuous, minimally-shadowed point cloud. All scanned points were unified to create a more stable model. Layers were used with different features on different layers to aid in interpretation. The merged scanworlds were cleaned, *i.e.*, non-flow impacting vegetation in these highly-vegetated reaches and artificial features such as the water surface and turbulence were removed from the point clouds (Figure 3-5). All features at or below the water surface are unreliable and were deleted except when verified by total station data. In a few cases where the scanner's laser was at a steep angle ($> \sim 35$ degrees) with respect to a smooth water surface, the scanned data were found to accurately measure the form of the bed.



A: before cleaning

B: cleaned point cloud

Figure 3-5: Raw and cleaned LiDAR point clouds, reach ESL-9.

The slope of the water surface was assumed to be equivalent to the friction slope (S_f) and was computed using the upstream and downstream water surface elevations and the length of the thalweg longitudinal profile. This thalweg length, instead of being simply defined by the deepest portion of the channel, instead followed the path of the estimated center of mass of the flow, which is identical to the traditionally-observed thalweg path in reaches with triangular sections. This approach was implemented in response to field observations that a single deepest portion of the stream was not always readily identifiable due to rectangular cross section geometry, that the velocity varied substantially across each section, and that the locations of highest section velocity varied by stage, especially in the vicinity of the instream wood steps. As illustrated by the flow depth grid provided in Figure 3-6, this flow path follows the deepest portion of the channel in areas with triangular sections but varies in rectangular sections and in the vicinity of wood steps where a single maximum depth is not observed. In these areas,

large clasts and instream wood divert the flow in a complex manner that varies by discharge. Surveying the longitudinal profiles along the observed flow paths, which is readily identifiable by experienced hydrologists by sight and feel and is repeatable during any particular resistance measurement, has the advantage of providing the most hydraulically-representative reach lengths for a specific flow while defining what specific resistance elements are in high- and low-velocity zones within the stream channel. A disadvantage is that this flow path cannot be known until the discharge of interest is observed.

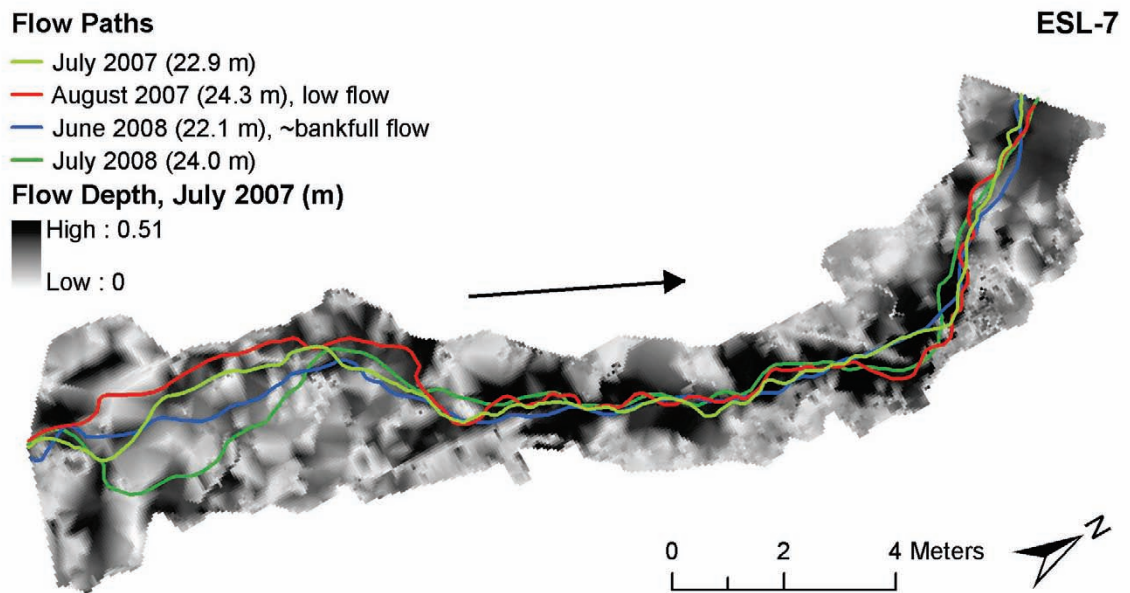


Figure 3-6: 2-D flow depth with flow paths for all four ESL-7 resistance measurements. This image provides depth data for the entire wetted width for the July 2007 measurements, with a 5-cm pixel size.

3.1.3 Velocity

Average reach velocities were characterized using Rhodamine WT dye (20-percent solution), with replicates of four to five injections per resistance measurement.

The Rhodamine WT was measured at a 1-sec time step using two Turner Designs Cyclops 7 fluorometers linked with two synchronized Campbell Scientific CR10X dataloggers. Multi-gain software written by Turner designs for the CR10X datalogger was used within a Tripod Data Systems (TDS) Recon Pocket PC, which also doubled as a total station data logger. The instrument output is in millivolts (mV). Initial calibrations were performed for the instruments, to relate voltage output with concentration. This relationship is dependent upon temperature, but typically 10 $\mu\text{g/L}$ corresponded to about 36 to 42 mV output in our field conditions. The fluorometers were mounted to rebar in the center of mass of the flow, to assure consistency in tracer pulse peak measurement. The dye was released as a slug in midstream (Figure 3-7).

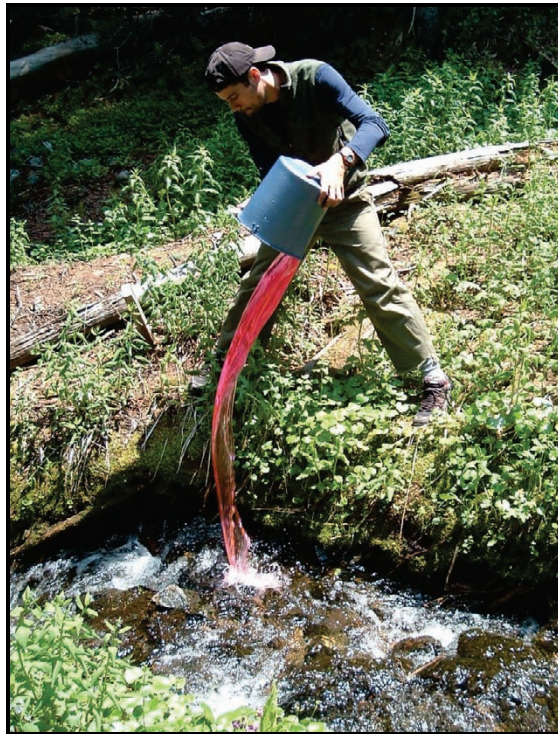


Figure 3-7: Rhodamine WT dye injection by field assistant Mark Hussey.

Both sunlight and aeration can be problematic when using fluorometers in the field. Sunlight masks the fluorescence of the Rhodamine WT. Highly-aerated flow can cause excessive data noise. Typically, the impact of direct sun is countered by the use of a shade cap but the bubbles in highly-aerated flow can block the holes in the cap, inhibiting water flow and dye pulse detection. To address sunlight and noise due to turbulence, the fluorometer was placed at a level in the water column that has the least amount of aerated flow (but still in the velocity field), the sensor was shaded with a tarp, and sufficient dye was injected to provide a return that substantially exceeded the data noise.

Rhodamine WT was recommended by the U.S. Forest Service as the tracer of choice for this specific study on their experimental forest. A salt tracer was undesired due to potential contamination of a long-term major-ion study. The U. S. Environmental Protection Agency (*Federal Register*, 1998, Volume 63, Number 40) indicates that Rhodamine WT is safe if used in low concentrations, with a maximum concentration of 10 µg/L for water entering a water treatment plant and 0.1 µg/L in drinking water. However, it should be noted that Rhodamine WT has not been recommended for use in tracer studies by at least one group of researchers, due to potential genotoxic properties (Behrens *et al.* 2001), based upon a salmonella/microsome test (gene mutation) and cytogenetic analysis. Other research has shown that Rhodamine WT is acutely toxic at concentrations above 320000 to 20000 µg/L for periods greater than 48 to 96 hrs (Field *et al.* 1995). In this study, detectable levels of the dye (~0.5 µg/L) persisted for only a few minutes and attenuated substantially (20 to 40 percent) within these relatively short (< 40 m) reaches. Skin adsorption potential is considered to be minimal for Rhodamine WT

(Field *et al.* 1995), however, the use of gloves when working with 20-percent dye solution is recommended.

Given a target concentration of dye in the stream, the volume of 20-percent Rhodamine WT to be injected was initially estimated using a relationship developed by Kilpatrick (1970):

$$V = 0.0892 \left[\frac{QL}{v} \right]^{0.93} C_p \quad (3-1)$$

where V is the volume of dye (mL); Q is the reach discharge (m^3/s); L is the stream distance of interest (m); v is the mean velocity (m/s); and C_p is the peak concentration desired ($\mu\text{g}/\text{L}$). It was found that this equation substantially overestimated the injection volume (by an order of magnitude) for the relatively small (< 40-m long, < 3-m wide) reaches investigated. On East Saint Louis Creek, bankfull flows typically required 1.5 mL of 20-percent dye solution (at 0.6 cms) and mid-flows typically required 0.8 mL of dye solution (at 0.25 cms). On lower Fool Creek, bankfull flows typically required 0.8 mL of 20-percent dye solution (at 0.25 cms) and mid to low flows typically required 0.1 mL of dye solution (at 0.05 cms).

To obtain average reach velocities, travel time is typically computed using either time between peaks, time between centroids, or a spatial harmonic mean travel time (Figure 3-8). Abrahams *et al.* (1995), Curran and Wohl (2003), and Wilcox and Wohl (2006) used a difference between peaks, while Kratzer and Biagtan (1997) preferred a difference between centroids approach. Lee (1995) used the time between the leading edge, peak, centroid, and trailing edge and implemented logarithmic plots to determine

the most appropriate estimates. Walden (2004) asserts that average reach velocity under steady-flow conditions is best computed using a spatial harmonic mean travel time.

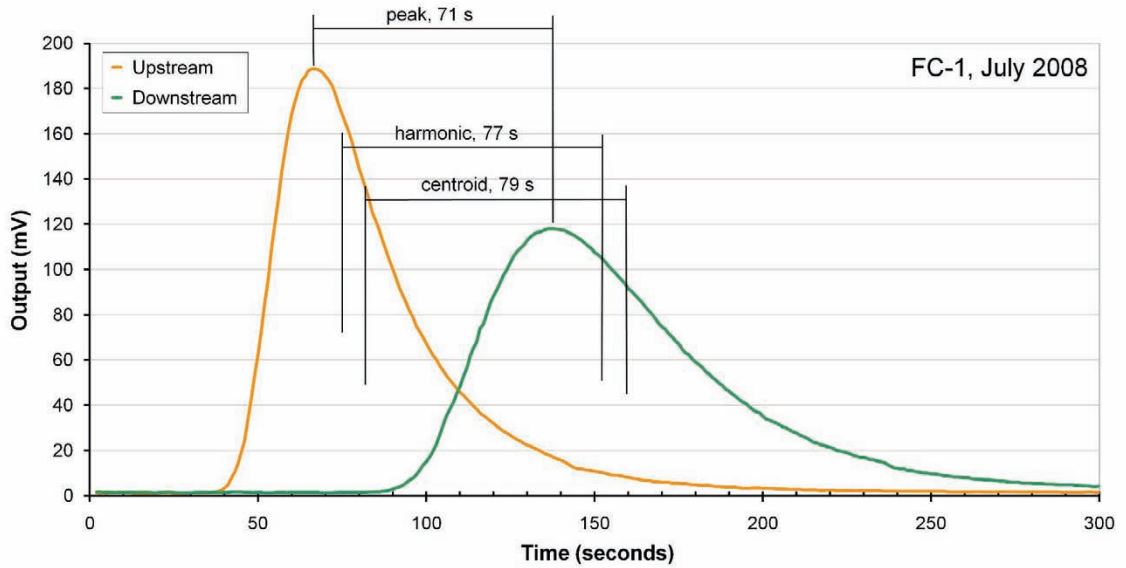


Figure 3-8: Example dye tracing dataset illustrating peak, harmonic, and centroid travel times.

To address the variability due to data noise, a single-pass 3-point median smoothing methodology was applied to the Rhodamine WT data. Median smoothing, suggested by Tukey (1974), tends to preserve sharp signal edges while filtering out impulses (Gallagher and Wise 1981; Ataman *et al.* 1981). Signal impulses frequently result from sunlight and aeration effects in high-gradient streams.

The smoothed data facilitate the use of the spatial harmonic mean travel time in the average reach velocity computations. As derived from Walden (2004), in differential form the harmonic mean travel time (t_{HM}) for a tracer passing a fixed point is:

$$t_{HM} = \frac{1}{\sum_{t=i}^j \left[\frac{1}{t} p_x(t) \Delta t \right]} \quad (3-2)$$

where t is the tracer travel time from the injection point; i is the initial time of the censored tracer concentration, just above the limit of the data noise; j is the trailing time of the same censored concentration; Δt is the time step of the measurements; and $p_x(t)$ is the temporal probability density function, defined as:

$$p_x(t) = \frac{1}{I_x} c(x, t) \quad (3-3)$$

and $c(x, t)$ is the tracer concentration. I_x is defined as the sum of concentration over time at a fixed point x :

$$I_x = \sum_{t=i}^j [c(x, t) \Delta t] \quad (3-4)$$

Censored concentration limits need to be identical for both the upstream and downstream tracer pulse curves for each individual travel time computation. Differential times between the temporal centroids of the tracer pulses at the upstream and downstream limits of each reach were computed for each injection, with these travel times combined with the thalweg reach length to obtain the average reach velocity for each flow resistance measurement.

This work is closely associated with the research presented in David (2010), however, velocity and the resultant flow resistance values differ due to dataset refinement. Specifically, this work employs the use of a dataset resulting from the elimination of replicate outlying travel times, the use of smoothed tracer data to reduce the influence of excessive noise from aeration and sunlight interactions with the fluorometers, and the use of harmonic as opposed to centroid travel times. Additionally, David (2010) used a regression to compute the reach friction slopes, while this research

computed S_f using the slope of the water surface as defined by the limits and the measured flow lengths.

3.2 Geometric Data Extraction

Data extracted from the LiDAR scans included cross section, bankform, instream wood and bedform characteristics. These methods were often complex, requiring interaction between numerous software including Leica Cyclone, Microsoft Excel[®] and Access[®], Notepad, and ArcGIS. Details are provided in this section for the benefit of other researchers. Additionally, the development of bed characteristics directly from the longitudinal profiles is also described.

3.2.1 Cross Sections

Cross sections were developed from the cleaned point-cloud data at an interval of 0.75 to 1.50 m over the 6- to 35-m reach lengths, for a total of nine to twenty-seven sections for each reach. Figure 3-9 illustrates the extracted cross sections for reach ESL-7. The methodology consisted of using an automated Cyclone function to cut rough automated cross sections at the chosen spacing from the cleaned point clouds using a smooth horizontal profile line and using the resulting jagged section as orientation for creating pick points that made up each section and were exported into an Excel[®] spreadsheet. The initial sections were jagged and unusable since they were generated from a triangulated irregular network (TIN) created from highly-vegetated point clouds. Overhanging banks were measured by the LiDAR scanner in some locations – these overhangs were incorporated into the area and wetted perimeter measurements through the use of an Excel[®] spreadsheet that was designed to account for this characteristic. The

substantial numbers of sections in each reach were deemed necessary to account for the geometric variability in the average reach values. Generally, the cross-section wetted perimeters include the largest clasts and large instream wood sitting on the bed but ignores smaller clasts and all other instream wood.

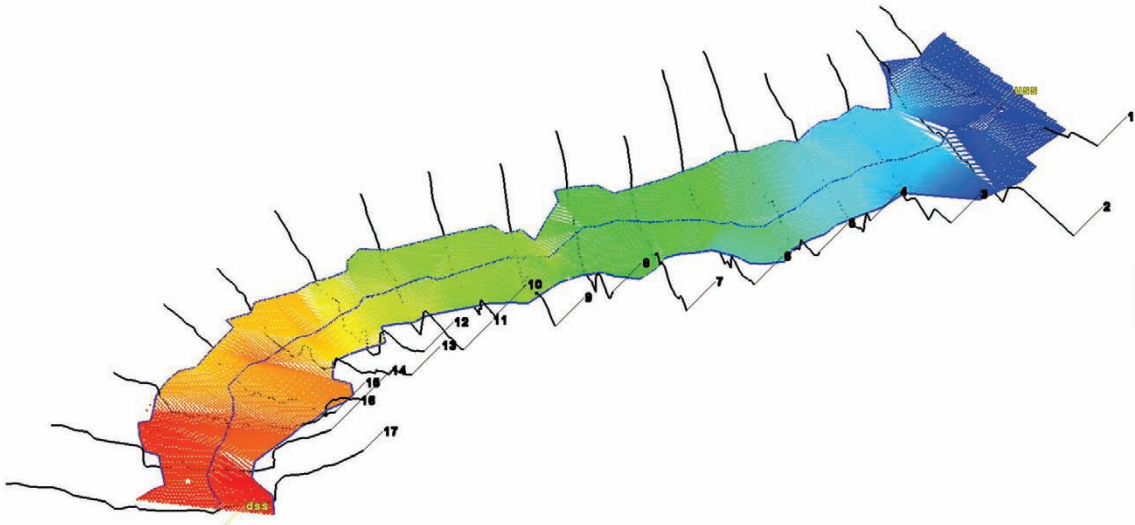


Figure 3-9: Extracted cross sections for reach ESL-7, with bankfull modeled water surface.

3.2.2 Two-dimensional Characteristics

A substantial number of 2-D characteristics were investigated for their potential as predictors of flow resistance. This section provides definition of the investigated variables, with details on how they were computed. The variables are:

- **A**: average of the area measurements computed at each cross section; **SDA**: standard deviation of the area measurements.
- **D_{84}** : material size at which 84 percent of the material is finer, as determined by a 300-point pebble count.

- δ_a : average bed residual, with the residuals computed from simple linear regressions of elevation versus the measured longitudinal distance. This method is illustrated in Figure 3-10. This variable tested for correlation with average bed variability, both alone and as the roughness variable in a relative submergence term.
- δ_m : maximum bed residual (absolute), with the residuals computed as discussed above. This variable tested for correlation with maximum bed variability, both alone and as the roughness variable in a relative submergence term.
- δ_{median} : median bed residual, with the residuals computed as discussed above.
- h_m : average of the maximum depth computed at each cross section. This variable is used for normalization in relative submergence; SDh_m : standard deviation of the maximum depth measurements.
- K_b : average of left and right bank sinuosity (bank length / profile length), measured using the edge-of-water longitudinal profiles.
- K_{bh} : horizontal projection of average of left and right bank sinuosity, measured using the edge-of-water longitudinal profiles and with the length parameter corrected for slope.
- P_w : average of the wetted perimeter measurements computed at each cross section; SDP_w : standard deviation of the wetted perimeter.
- R : average of the hydraulic radius measurements at each cross section; SDR : standard deviation of the hydraulic radius.

- σ_y : standard deviation of the residuals of a bank profile regression. This variable was computed using the edge-of-water longitudinal profiles by defining a vertical reference plane connecting the first and last thalweg points. A simple linear regression was computed of y-distance (perpendicular to stream axis, in a horizontal plane) versus the longitudinal distance; from this regression, the standard deviation of the regression residuals for each flow resistance measurement was computed to define a bank variability predictor.
- σ_z : detrended standard deviation of bed elevations. This variable is computed from the longitudinal profiles by performing a simple linear regression of elevation versus the longitudinal distance for each flow resistance measurement and computing the standard deviation of the regression residuals (Figure 3-10). This variable tests correlation with a detrended bed variability term, both alone and as the roughness variable for relative bedform submergence ($h_m/\sigma_z, R/\sigma_z$).
- $h_m/\sigma_z, R/\sigma_z$: relative bedform submergence.
- S_f : friction slope of the resistance measurement, assumed equal to the water surface slope.
- TW : average of the top width measurements at each cross section.
- TW/h_a : width-depth ratio, computed from average reach cross-section properties.
- V : flow volume, computed using cross-sectional data.
- V_w : instream wood volume.

- V_{wb} : branched instream wood volume, computed by multiplying the instream wood diameter by a correction to estimate the effect of attached branches acting as strainers.
- V_{wd} : thalweg-distance reduced instream wood volume, computed by reducing the effective volume of the instream wood by a factor based upon its distance from the measured flow path.
- V_{wp} : projected instream wood volume, computed by multiplying V_w by the sine of the attack angle.
- V_{wbp} : branched, projected instream wood volume.
- V_{wbd} : branched, thalweg-distance reduced instream wood volume.
- V_{wbdp} : branched, thalweg-distance reduced, projected instream wood volume.

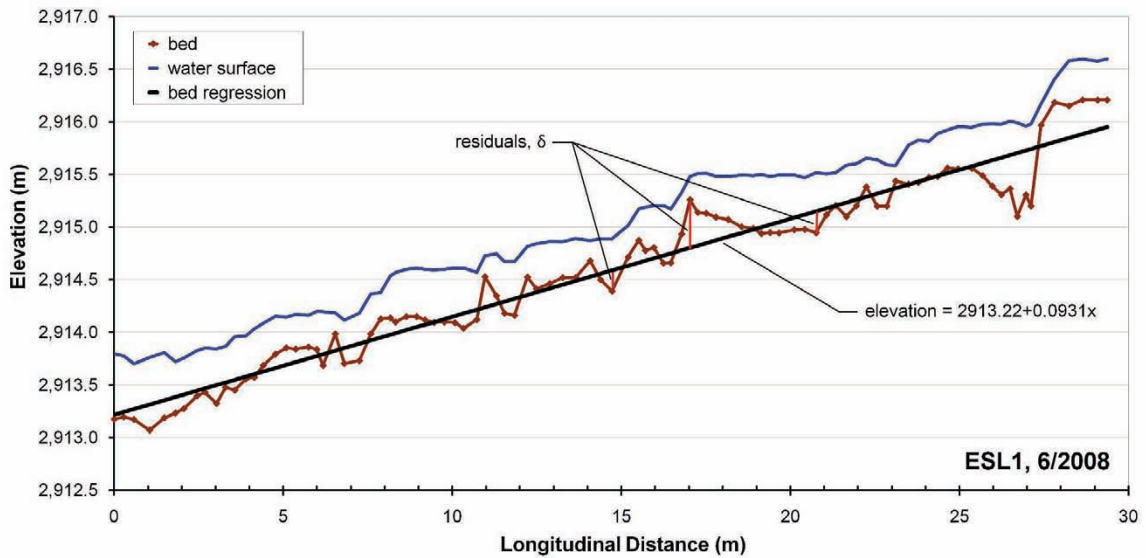


Figure 3-10: Bed residual computation, ESL-1 at ~bankfull flow.

3.2.3 Three-dimensional Spatial Characteristics

More complex, 3-D characteristics were also investigated for their potential to explain flow resistance variability in the Fraser dataset. Information on the extraction of these data from the LiDAR point clouds is provided below. The variables are:

- h_{a3} : average depth, computed from a grid of the wetted channel.
- h_{m3} : maximum depth, from a grid of the wetted channel.
- σ_{h3} : detrended standard deviation of depth, computed from a grid of the wetted channel.
- σ_{z3} : detrended standard deviation of bed elevations, computed from a grid of the wetted channel.

For each resistance measurement, the 3-D data were extracted from cleaned LiDAR point clouds using the following process. 3-D representations were only developed for the non-low flow resistance measurements, providing forty-four data points for analysis:

1. From each set of the longitudinal profile surveys (Figure 3-11A), collected for each resistance measurement, TIN mesh models of the water surface were created in Cyclone (Figure 3-11B).
2. Gridded data, at a resolution of 5 cm, were sampled from the water surface TIN models (Figure 3-11C).
3. These gridded water surface data were exported as a text file and converted to a .dbf file (using Microsoft Access[®]) for import into ArcGIS.

4. All bed survey points (from the bed survey and the four longitudinal profile surveys) were imported into Cyclone and unified with the bed/bank LiDAR point cloud (Figure 3-12B).
5. For each resistance measurement, the bed point cloud was cleaned to remove all points outside of the flow volume (Figure 3-12C), as defined by the water surface TIN and the LiDAR points that make up the banks. All points inside the flow volume were retained. Hence, features retained within this resistance element point-cloud representation include bed features, large clasts, and instream wood; these point clouds include the primary sources of flow resistance in these streams.
6. Breaklines were created from the surveyed bed points to force a truer representation of the bedform (Figure 3-12D).
7. TINs were created from the resistance element point cloud and breaklines, for each resistance measurement (Figure 3-12E).
8. Gridded data, at a resolution of 5 cm, were sampled from the bed TIN models (Figure 3-12F).
9. These gridded bed data were exported as a text file and converted to a .dbf file for import into ArcGIS.
10. Using the thalweg regressions used to compute the 2-D σ_z , a reference plane was created in Cyclone with the origin set to the upstream-most point of each measured flow length and the x-axis aligned with the regressed points. The coordinate system was set from this reference plane. In this orientation, the z-axis represents the residual between the actual bed point and the

regression plane. Points outside the water surface extent were deleted and the locally-referenced gridded bed data were exported to a text file.

11. The detrended bed data were imported into Microsoft Excel[®], where detrended standard deviation of the bed elevations (σ_{z3}) was computed.
12. To compute depth variability during each flow resistance measurement, the gridded data representing the resistance elements and water surface were both imported into ArcGIS in the UTM coordinate system.
13. In ArcGIS, TINs were created from both the water surface and resistance element gridded data (Figures 3-13A and 3-13B).
14. These TINs were converted to raster datasets, using a 5-cm cell size (Figures 3-13C and 3-13D).
15. Using the raster calculator function and an analysis mask that limited computations to the flow extents, the bed raster was subtracted from the water surface raster to create a depth raster (Figure 3-13E). Depths less than 0 were eliminated.
16. Using an analysis mask that limited computations to 50% flow extents (about the thalweg), the bed raster was subtracted from the water surface raster to create a depth raster (Figure 3-13F). Depths less than 0 were eliminated.
17. Statistics of flow depth maximum, mean, and standard deviation were recorded.

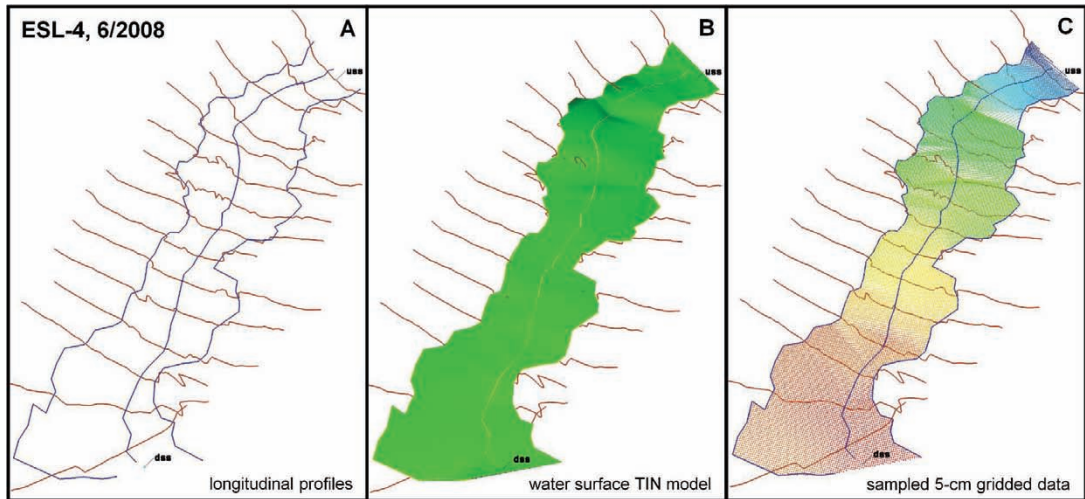


Figure 3-11: Water surface model development, ESL-4, bankfull flow.

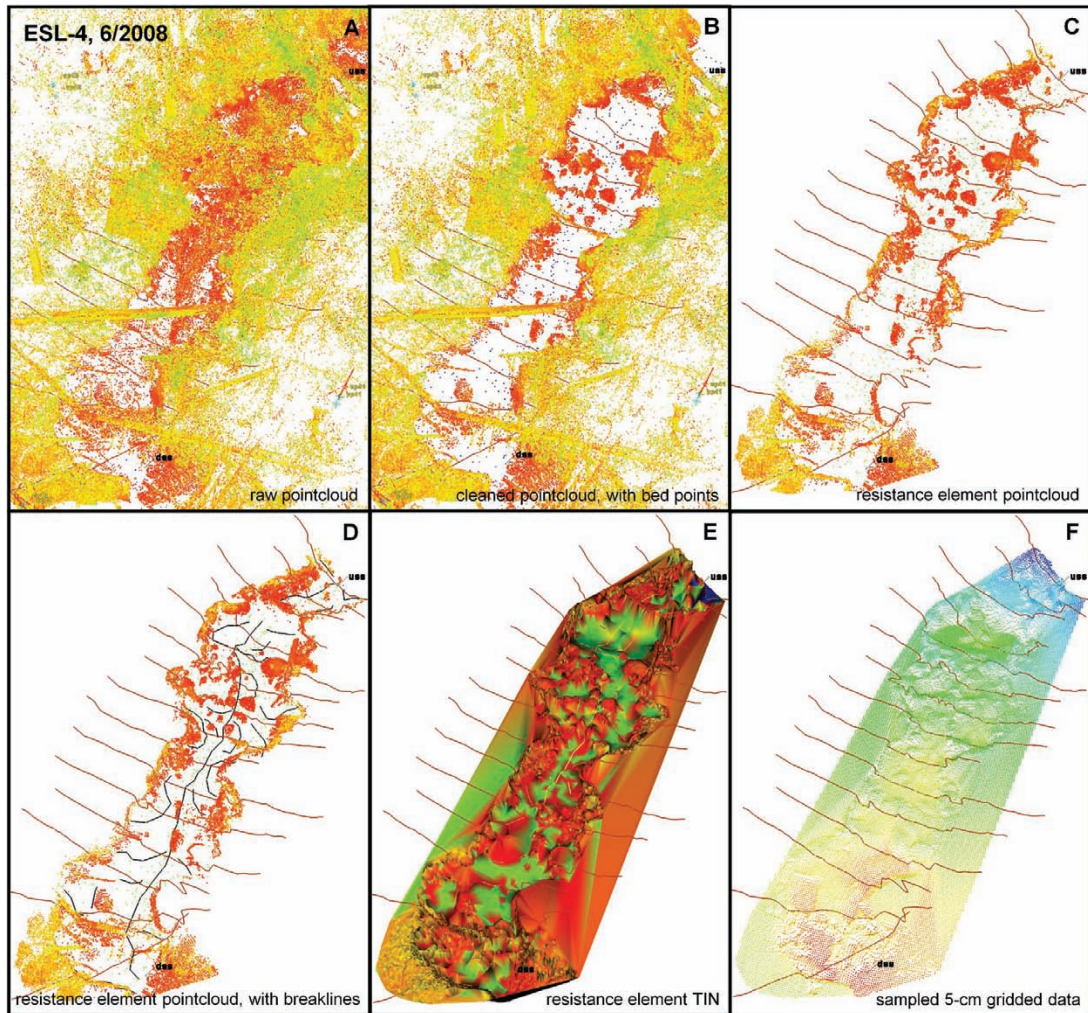


Figure 3-12: Bed model development, ESL-4, bankfull flow.

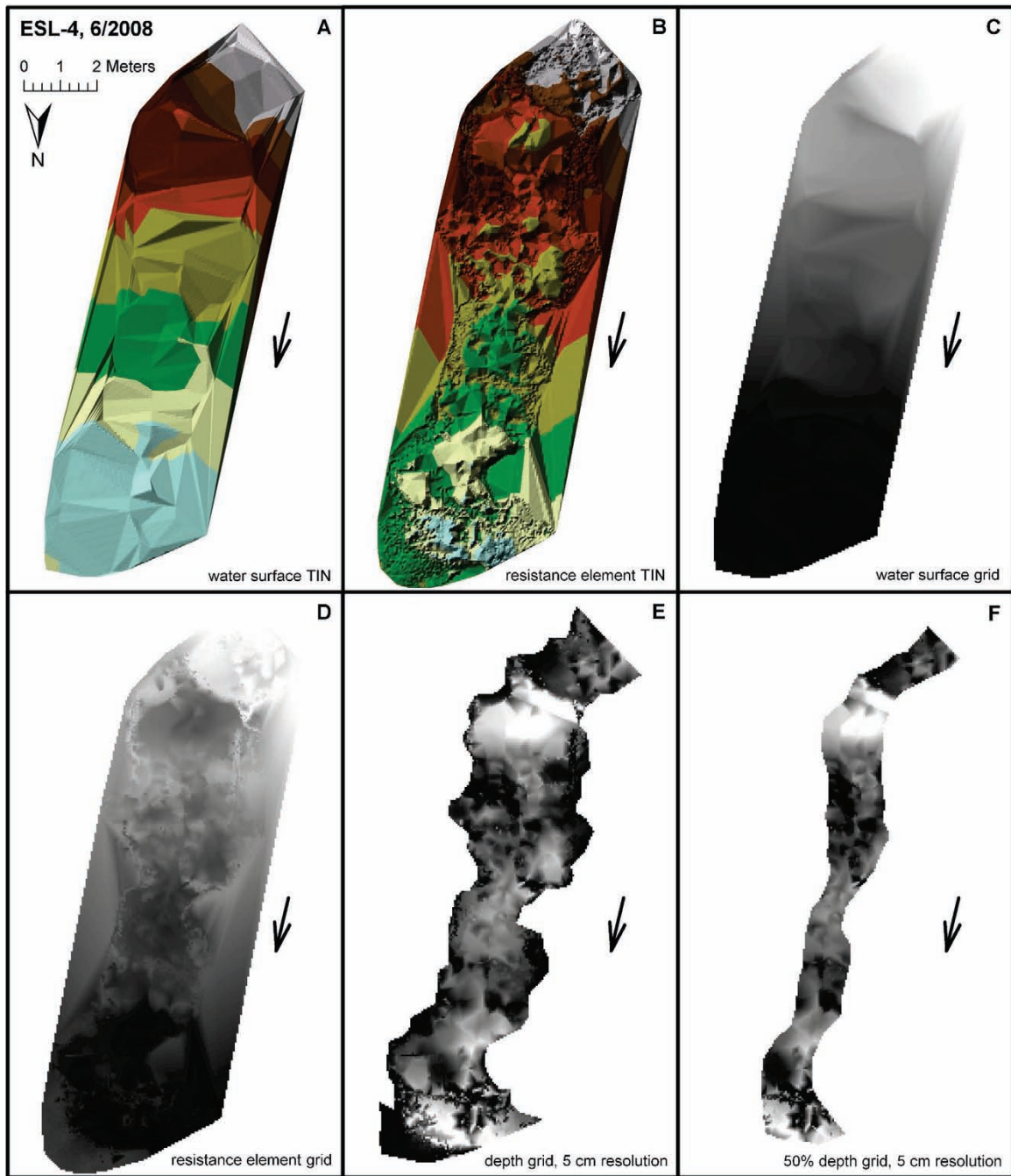


Figure 3-13: Depth model computation, ESL-4, bankfull flow.

3.3 Statistical Analyses

Simple-linear and multivariate regressions were performed on the assembled dataset, to search for effective explanatory variables for predicting flow resistance and for

illuminating flow resistance processes. Statistical analyses were performed in SAS (Version 9.2). Tested explanatory variables described the physical characteristics of bed material, slope, bed and bank variability, and instream wood. Natural logarithmic transformations were applied, which typically provided good adherence to the regression assumptions of linearity, homoscedasticity, and independent and normally-distributed residuals. A cross-validation analysis was also performed on relative bedform submergence using two approaches: (1) data splitting (random sample) and (2) jackknife (one-at-a-time). The data-splitting method randomly withheld nineteen of the fifty-nine data points, with the regression of the forty remaining points used to predict the resistance for the nineteen withheld measurements. The jackknife approach used fifty-nine separate regressions, each withholding one datapoint and estimating the resistance coefficient for that point based upon the remaining fifty-eight points. With an understanding of the explained variance using these single variables, the variables were combined in multiple regression analyses using variables that were found to explain substantial variance for differing resistance processes, such as bed variability, bank variability, and instream wood volume. The variables were combined using a best-subsets analysis to determine the most effective multivariate regressions.

Because the single variables that explain the greatest variance in the dataset are dependent upon the resolution of the longitudinal profile, a sensitivity analysis of the profile spacing was performed to assess the impact of spacing variability upon the predictions, with $\frac{3}{4}$, $\frac{1}{2}$, and $\frac{1}{4}$ of the longitudinal points used to predict n and f .

Log-transformations of predicted variables were required to honor the regression assumptions. However, the log-transformation induces a systematic bias in predictions,

which requires correction (Beauchamp and Olson 1973; Sprugel 1983; Ferguson 1987; Newman 1993). Typically, procedures correct the intercept term, while it has been suggested by McCuen *et al.* (1990) that a numerical approach is most appropriate since it adjusts both the intercept and slope terms. The approach presented in Sprugel (1983), Ferguson (1987), and Newman (1993) was used to correct bias in the intercept term. Specifically, the correction factor (CF) for natural log-transformed data is:

$$CF = e^{(s^2/2)} \quad (3-5)$$

where s^2 is the mean square error of the regression.

CHAPTER 4

VELOCITY AND RESISTANCE MEASUREMENTS

This chapter provides measurements and calculations of flow characteristics of the fifteen reaches on East Saint Louis and Fool Creeks of the Fraser Experimental Forest, Colorado. Significantly, results vary depending on whether measured flow paths versus shortest potential flow paths are used in the computations of slope, velocity, and flow resistance coefficients. The shortest potential flow paths refer to a smooth curve in the stream centerline that represents the shortest potential flow length (Figure 4-1), which can be similar to results obtained using field techniques that rely upon laser level and tape. Since the measured flow paths are the most hydraulically representative for a specific flow, defining what specific resistance elements are in high- and low-velocity zones within the stream channel, results based upon these values are typically the most appropriate for analysis. However, the use of shortest potential flow paths may be useful when comparing this dataset to those assembled by other researchers, who often have performed single surveys of thalweg profiles for use with multiple discharges, with varying levels of detail measured. This single reach length may be approximated by the shortest potential flow path, to provide a uniform length for all flows as some researchers would expect. The use of shortest potential flow path is also helpful for the practical application of prediction, where flow paths are typically not known beforehand and need

to be assumed in rectangular channels where single maximum depth is not clearly identified. In this dissertation, it is only explicitly stated what method was used when the shortest potential flow paths were used in the computation.

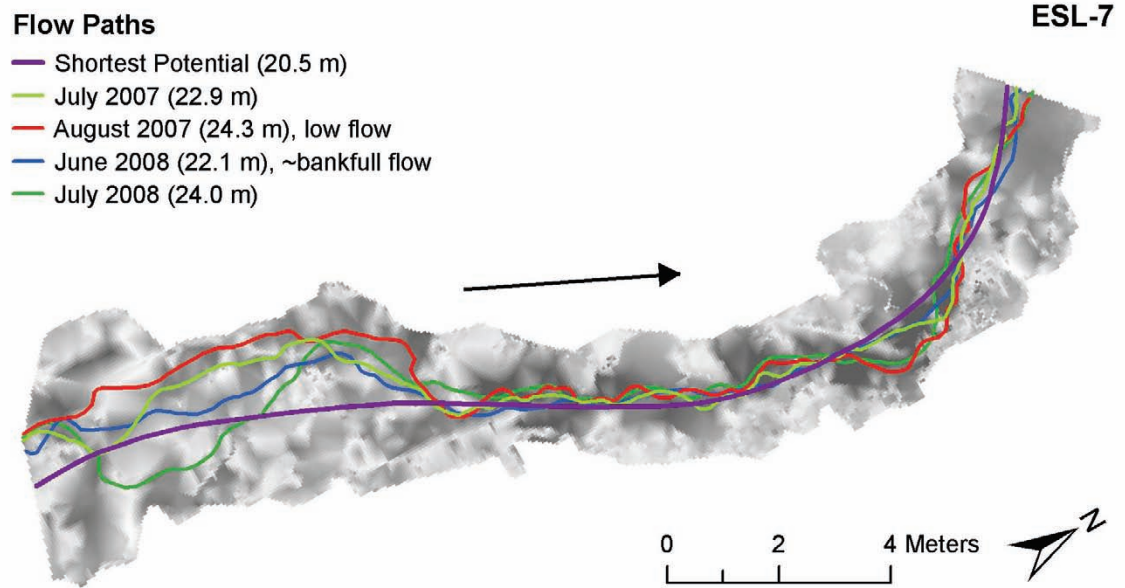


Figure 4-1: Flow path types.

4.1 Measured Flow Paths

A summary of reach resistance coefficients, average reach velocities, and Froude numbers is provided in Table 4-1. The magnitude of the measured n and f values were higher than values typically recommended by commonly-used references for mountain streams. Manning’s n computed from this dataset of fifty-nine measurements in cascade, step-pool, a transitional, and a plane-bed reach ranged from 0.05 to 0.30 for near-bankfull conditions, 0.08 to 0.40 for mid-flow measurements, and 0.10 to 0.52 for low-flow measurements. The Darcy-Weisbach friction factor (f) varied from 0.28 to 11.1 for near-bankfull conditions, 0.67 to 26.3 for mid-flow measurements, and 1.4 to 55.6 for low-

flow measurements. All measurements indicated subcritical reach-average conditions, with Froude numbers varying from 0.15 to 0.78. In the step-pool and cascade stream reaches (excluding plane-bed ESL-6 and transitional FC-1), Manning’s n varied from 0.13 to 0.52, while the friction factor varied from 2.2 to 56. As mentioned in the methods chapter, these results differ from those presented in David (2010) due to velocity dataset refinement, specifically in regard to the elimination of outlying replicate travel times, the use of smoothed tracer data, and the use of harmonic travel times. Figure 4-2 illustrates the resistance coefficients as a function of friction slope; measurements based upon measured flow paths are provided in Tables 4-2 and 4-3.

Table 4-1: Measured reach resistance coefficients, average velocities, and Froude numbers. Low flow: <100% of the median flow; mid flow: 150% to 260% of median; ~bankfull flow: > 360% of median, 1.1- to 2.1-year return intervals.

A: plane-bed, step-pool, and cascade reaches (S_f : 1.5 – 20 %)				
	Manning's n	Darcy-Weisbach f	Velocity (m/s)	Froude number Fr
~bankfull flow	0.05 – 0.30	0.28 – 11	0.51 – 1.3	0.30 – 0.77
mid flow	0.08 – 0.40	0.67 – 26	0.18 – 0.61	0.15 – 0.38
low flow	0.10 – 0.52	1.4 – 56	0.11 – 0.40	0.13 – 0.31
B: step-pool and cascade reaches (S_f : 5.7 – 20 %)				
	Manning's n	Darcy-Weisbach f	Velocity (m/s)	Froude number Fr
~bankfull flow	0.95 – 0.30	1.3 – 11	0.51 – 0.79	0.30 – 0.58
mid flow	0.13 – 0.40	3.0 – 26	0.18 – 0.59	0.15 – 0.38
low flow	0.20 – 0.52	6.0 – 56	0.11 – 0.40	0.13 – 0.31

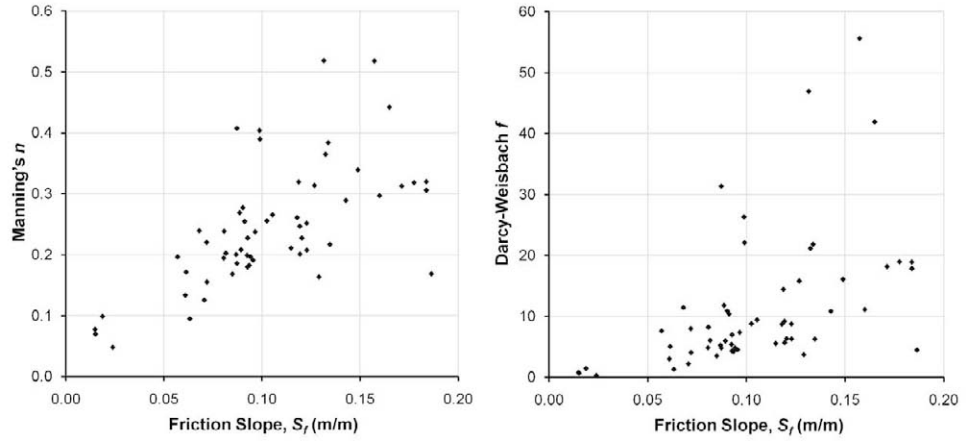


Figure 4-2: Manning's n and Darcy-Weisbach f as a function of friction slope.

Table 4-2: Travel time and velocity measurements (measured flow paths).

Reach ID	Date	Travel Time (s)			Velocity (m/s)			Stream Length (m)
		Centroid	Peak	Harmonic	Centroid	Peak	Harmonic	
ESL-1	2-Aug-07	113.0	110.0	111.0	0.28	0.29	0.28	31.4
	10-Jun-08	46.7	41.3	45.7	0.63	0.75	0.65	29.4
	22-Jul-08	61.2	65.0	64.8	0.45	0.42	0.42	27.3
ESL-2	9-Jul-07	30.5	29.8	30.8	0.46	0.47	0.45	13.9
	9-Aug-07	59.0	57.0	58.0	0.23	0.24	0.24	13.6
	6-Jun-08	24.7	21.3	22.3	0.56	0.64	0.61	13.7
	15-Jul-08	25.3	23.0	23.8	0.55	0.62	0.59	14.0
ESL-3	10-Jul-07	23.3	18.0	22.0	0.46	0.60	0.49	10.7
	9-Aug-07	27.0	14.0	30.0	0.42	0.81	0.38	11.3
	7-Jun-08	13.5	15.3	14.5	0.76	0.68	0.71	10.2
	15-Jul-08	20.5	23.0	20.0	0.52	0.47	0.54	10.7
ESL-4	10-Jul-07	37.3	27.8	35.0	0.42	0.57	0.45	15.8
	6-Aug-07	51.3	44.0	49.8	0.32	0.38	0.33	16.5
	7-Jun-08	25.0	25.0	25.0	0.63	0.62	0.63	15.6
	14-Jul-08	35.0	26.0	32.0	0.45	0.62	0.50	15.9
ESL-5	12-Jul-07	40.3	30.7	37.7	0.34	0.44	0.36	13.5
	8-Aug-07	58.5	50.5	56.5	0.26	0.30	0.27	15.1
	9-Jun-08	27.7	19.3	24.0	0.45	0.65	0.52	12.5
	14-Jul-08	30.0	25.0	29.0	0.46	0.56	0.48	13.9
ESL-6	13-Jul-07	11.0	11.2	11.4	0.60	0.59	0.58	6.5
	8-Aug-07	16.0	15.3	16.0	0.39	0.52	0.39	6.2
	9-Jun-08	6.3	3.7	5.0	1.28	1.78	1.32	6.4
	14-Jul-08	12.0	7.0	10.5	0.55	0.92	0.61	6.4
ESL-7	12-Jul-07	49.4	41.2	45.8	0.46	0.56	0.50	22.9
	4-Aug-07	62.5	58.0	61.0	0.39	0.42	0.40	24.3
	8-Jun-08	29.8	34.5	32.0	0.74	0.64	0.69	22.1
	15-Jul-08	45.8	40.0	44.0	0.53	0.60	0.55	24.0
ESL-8	11-Jul-07	70.6	61.8	67.8	0.45	0.51	0.46	31.4
	5-Aug-07	100.5	98.5	101.0	0.35	0.36	0.35	35.5
	9-Jun-08	51.0	40.3	48.3	0.60	0.76	0.64	30.7
	16-Jul-08	67.8	47.3	62.3	0.48	0.70	0.53	32.6
ESL-9	11-Jul-07	39.0	33.5	38.0	0.42	0.49	0.43	16.2
	6-Aug-07	57.5	54.5	56.3	0.32	0.34	0.33	18.6
	8-Jun-08	29.0	23.0	25.6	0.57	0.71	0.64	16.3
	16-Jul-08	36.5	31.3	35.0	0.45	0.53	0.47	16.5
FC-1	5-Jul-07	61.5	54.0	59.8	0.39	0.44	0.40	23.7
	12-Aug-07	132.0	123.8	130.3	0.19	0.20	0.19	25.1
	11-Jun-08	31.0	27.7	29.3	0.75	0.84	0.79	23.1
	23-Jul-08	78.8	70.8	76.6	0.29	0.33	0.30	23.2
FC-2	7-Jul-07	40.8	39.0	40.8	0.37	0.39	0.37	15.1
	12-Aug-07	92.5	86.5	89.0	0.16	0.17	0.17	14.9
	11-Jun-08	22.3	21.3	21.7	0.64	0.68	0.66	14.4
	23-Jul-08	55.4	49.2	51.4	0.26	0.29	0.28	14.2

Table 4-2 (continued): Travel time and velocity measurements (measured flow paths).

Reach ID	Date	Travel Time (s)			Velocity (m/s)			Stream Length (m)
		Centroid	Peak	Harmonic	Centroid	Peak	Harmonic	
FC-3	6-Jul-07	59.5	55.3	58.0	0.25	0.27	0.26	14.9
	11-Aug-07	124.0	109.8	119.0	0.12	0.14	0.12	14.9
	12-Jun-08	28.3	24.0	26.7	0.48	0.57	0.51	13.5
	22-Jul-08	70.5	62.0	66.5	0.17	0.20	0.18	12.2
FC-4	7-Jul-07	79.7	77.3	78.7	0.24	0.25	0.24	19.0
	11-Aug-07	134.0	125.5	136.0	0.14	0.15	0.14	19.2
	12-Jun-08	32.0	28.0	32.0	0.59	0.67	0.59	18.9
	21-Jul-08	74.5	70.3	73.0	0.27	0.28	0.27	19.8
FC-5	8-Jul-07	56.0	53.3	55.3	0.23	0.25	0.24	13.1
	10-Aug-07	131.5	121.5	130.0	0.11	0.12	0.11	14.2
	25-Jun-08	20.6	14.4	18.6	0.59	0.83	0.64	11.9
	17-Jul-08	51.3	40.8	49.0	0.23	0.29	0.24	11.9
FC-6	8-Jul-07	83.0	76.3	83.8	0.24	0.26	0.24	19.8
	10-Aug-07	180.5	171.0	179.5	0.12	0.13	0.12	22.1
	25-Jun-08	30.8	31.5	31.0	0.62	0.61	0.62	19.1
	17-Jul-08	95.5	81.0	88.0	0.22	0.25	0.23	20.6

Abbreviation: ID = identification.

Table 4-3: Flow resistance and associated measurements (measured flow paths).

Reach ID	Date	Discharge (cms)	Percent of Average	Return Interval (yr)	Slope (m/m)	Top Width (m)	Froude Number	<i>n</i>	<i>f</i>
ESL-1	2-Aug-07	0.11	46	----	0.091	2.0	0.24	0.25	10.4
	10-Jun-08	0.56	243	1.2	0.095	2.9	0.35	0.19	4.5
	22-Jul-08	0.24	102	----	0.105	2.6	0.26	0.27	9.4
ESL-2	9-Jul-07	0.22	95	----	0.093	2.9	0.30	0.23	7.0
	9-Aug-07	0.09	41	----	0.099	2.6	0.18	0.39	22.1
	6-Jun-08	0.53	230	1.2	0.094	3.2	0.35	0.20	4.8
	15-Jul-08	0.31	134	----	0.093	3.0	0.38	0.18	4.3
ESL-3	10-Jul-07	0.22	94	----	0.123	3.0	0.35	0.21	6.3
	9-Aug-07	0.09	39	----	0.119	2.4	0.29	0.25	9.2
	7-Jun-08	0.46	201	1.1	0.129	3.6	0.46	0.16	3.7
	15-Jul-08	0.30	132	----	0.119	3.5	0.36	0.20	5.7
ESL-4	10-Jul-07	0.21	89	----	0.123	2.5	0.30	0.25	8.7
	6-Aug-07	0.12	51	----	0.119	2.3	0.23	0.32	14.4
	7-Jun-08	0.61	264	1.2	0.120	2.9	0.34	0.23	6.3
	14-Jul-08	0.32	138	----	0.118	2.7	0.29	0.26	8.7
ESL-5	12-Jul-07	0.19	82	----	0.149	3.6	0.25	0.34	16.1
	8-Aug-07	0.10	45	----	0.134	3.3	0.20	0.38	21.8
	9-Jun-08	0.50	218	1.1	0.160	4.0	0.30	0.30	11.1
	14-Jul-08	0.33	143	----	0.143	4.0	0.29	0.29	10.8
ESL-6	13-Jul-07	0.19	82	----	0.015	2.7	0.40	0.07	0.7
	8-Aug-07	0.10	43	----	0.019	2.7	0.31	0.10	1.4
	9-Jun-08	0.52	226	1.2	0.024	3.0	0.77	0.05	0.3
	14-Jul-08	0.32	140	----	0.015	2.9	0.37	0.08	0.8
ESL-7	12-Jul-07	0.20	85	----	0.087	2.7	0.35	0.19	4.8
	4-Aug-07	0.10	45	----	0.082	2.5	0.31	0.20	6.0
	8-Jun-08	0.52	224	1.2	0.085	3.0	0.39	0.17	3.5
	15-Jul-08	0.30	130	----	0.081	2.9	0.32	0.19	4.8
ESL-8	11-Jul-07	0.21	89	----	0.089	2.7	0.32	0.21	6.0
	5-Aug-07	0.10	44	----	0.081	2.6	0.26	0.24	8.2
	9-Jun-08	0.46	202	1.1	0.094	3.2	0.38	0.18	4.2
	16-Jul-08	0.29	126	----	0.087	3.0	0.33	0.20	5.3
ESL-9	11-Jul-07	0.20	87	----	0.103	2.6	0.27	0.26	8.8
	6-Aug-07	0.11	47	----	0.090	2.3	0.23	0.28	10.9
	8-Jun-08	0.57	247	1.1	0.115	2.8	0.36	0.21	5.5
	16-Jul-08	0.28	124	----	0.097	2.6	0.29	0.24	7.4
FC-1	5-Jul-07	0.05	88	----	0.061	1.6	0.38	0.13	3.0
	12-Aug-07	0.01	25	----	0.057	1.3	0.23	0.20	7.6
	11-Jun-08	0.23	419	1.6	0.063	2.0	0.58	0.09	1.3
	23-Jul-08	0.04	67	----	0.061	1.6	0.29	0.17	5.0
FC-2	7-Jul-07	0.04	78	----	0.072	1.4	0.34	0.16	4.1
	12-Aug-07	0.01	24	----	0.068	1.1	0.20	0.24	11.4
	11-Jun-08	0.24	439	1.7	0.071	1.6	0.44	0.13	2.2
	23-Jul-08	0.04	69	----	0.072	1.4	0.24	0.22	8.0

Table 4-3 (continued): Flow resistance and associated measurements (measured flow paths).

Reach ID	Date	Discharge (cms)	Percent of Average	Return Interval (yr)	Slope (m/m)	Top Width (m)	Froude Number	<i>n</i>	<i>f</i>
FC-3	6-Jul-07	0.04	81	----	0.089	1.6	0.22	0.27	11.8
	11-Aug-07	0.01	23	----	0.087	1.4	0.13	0.41	31.4
	12-Jun-08	0.22	389	1.5	0.092	2.1	0.32	0.20	5.4
	22-Jul-08	0.04	70	----	0.099	1.7	0.15	0.40	26.3
FC-4	7-Jul-07	0.04	75	----	0.132	1.4	0.20	0.36	21.1
	11-Aug-07	0.01	25	----	0.132	1.2	0.13	0.52	46.9
	12-Jun-08	0.22	390	1.5	0.135	1.6	0.34	0.22	6.3
	21-Jul-08	0.05	81	----	0.127	1.4	0.22	0.31	15.8
FC-5	8-Jul-07	0.01	56	----	0.171	0.9	0.24	0.31	18.2
	10-Aug-07	0.01	26	----	0.157	0.8	0.13	0.52	55.6
	25-Jun-08	0.15	568	2.1	0.186	1.1	0.49	0.17	4.5
	17-Jul-08	0.02	65	----	0.184	0.9	0.24	0.32	18.9
FC-6	8-Jul-07	0.01	54	----	0.184	0.9	0.25	0.31	17.8
	10-Aug-07	0.01	26	----	0.165	0.7	0.15	0.44	41.9
	25-Jun-08	0.14	543	1.9	0.200	1.1	0.50	0.17	4.8
	17-Jul-08	0.02	65	----	0.178	0.9	0.24	0.32	18.9

Measurements were collected during flows ranging from 23 to 570 percent of the average mean daily flow, based upon the available gage records (East Saint Louis: 1943-2006; Lower Fool Creek: 1940-2006; and Upper Fool Creek: 1986-2006). Near-bankfull measurements were made at flows equivalent to the 1.1- to 2.1-yr return period, as defined by log-Pearson Type III frequency analyses of the gage records. Daily discharge data for 2007 and 2008 are shown in Appendix A, while flow-frequency computations are provided in Appendix B.

4.2 Shortest Potential Flow Paths

As discussed above, shortest potential flow paths refer to a smooth curve that represents the shortest potential flow length in each stream reach. Although these paths are not the most hydraulically representative, velocity and flow resistance coefficient

values computed using these reach lengths may be more appropriate in certain circumstances. Results are shown with the measured flow path data in Figure 4-3. The use of shortest potential flow paths tends to increase flow resistance, due to the shorter paths having a combined effect of increasing slopes and decreasing velocities (given identical measured travel times). Results computed using shortest potential flow paths are provided in Table 4-4, with an additional comparison in Table 5-27.

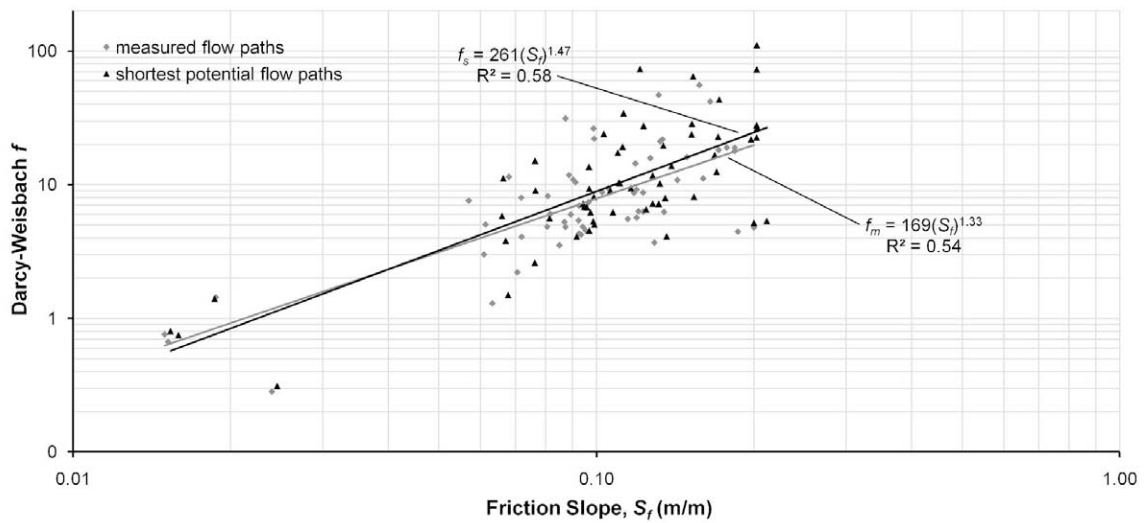


Figure 4-3: Darcy-Weisbach f as a function of friction slope, with variability induced due to measured versus shortest potential flow paths.

Table 4-4: Flow resistance and associated measurements (shortest potential flow paths).

Reach ID	Date	Stream Length (m)	Velocity (m/s)	Slope (m/m)	Froude Number	<i>n</i>	<i>f</i>
ESL-1	2-Aug-07	26.1	0.23	0.110	0.20	0.33	17.4
	10-Jun-08	26.1	0.57	0.108	0.31	0.22	6.2
	22-Jul-08	26.1	0.40	0.110	0.25	0.28	10.4
ESL-2	9-Jul-07	13.1	0.43	0.099	0.27	0.25	8.1
	9-Aug-07	13.1	0.23	0.103	0.16	0.41	24.0
	6-Jun-08	13.1	0.59	0.099	0.33	0.21	5.3
	15-Jul-08	13.1	0.55	0.099	0.34	0.19	5.0
ESL-3	10-Jul-07	9.7	0.44	0.135	0.32	0.23	8.0
	9-Aug-07	9.7	0.32	0.139	0.24	0.30	13.8
	7-Jun-08	9.7	0.67	0.136	0.44	0.17	4.1
	15-Jul-08	9.7	0.49	0.132	0.33	0.23	7.2
ESL-4	10-Jul-07	14.6	0.42	0.132	0.28	0.27	10.2
	6-Aug-07	14.6	0.29	0.134	0.21	0.37	19.7
	7-Jun-08	14.6	0.59	0.128	0.32	0.24	7.3
	14-Jul-08	14.6	0.46	0.128	0.25	0.31	11.7
ESL-5	12-Jul-07	11.8	0.31	0.171	0.21	0.40	22.9
	8-Aug-07	11.8	0.21	0.172	0.16	0.54	43.5
	9-Jun-08	11.8	0.49	0.170	0.29	0.31	12.5
	14-Jul-08	11.8	0.41	0.168	0.25	0.36	16.7
ESL-6	13-Jul-07	6.3	0.55	0.016	0.38	0.07	0.8
	8-Aug-07	6.3	0.39	0.019	0.31	0.10	1.4
	9-Jun-08	6.3	1.25	0.025	0.73	0.05	0.3
	14-Jul-08	6.3	0.60	0.015	0.36	0.08	0.8
ESL-7	12-Jul-07	20.5	0.45	0.097	0.30	0.21	6.2
	4-Aug-07	20.5	0.34	0.097	0.25	0.25	9.4
	8-Jun-08	20.5	0.64	0.092	0.36	0.18	4.1
	15-Jul-08	20.5	0.47	0.094	0.28	0.24	7.2
ESL-8	11-Jul-07	29.6	0.44	0.095	0.29	0.22	6.9
	5-Aug-07	29.6	0.29	0.097	0.21	0.31	13.7
	9-Jun-08	29.6	0.61	0.097	0.36	0.19	4.5
	16-Jul-08	29.6	0.48	0.096	0.29	0.23	6.9
ESL-9	11-Jul-07	15.0	0.39	0.111	0.25	0.28	10.3
	6-Aug-07	15.0	0.27	0.112	0.19	0.37	19.3
	8-Jun-08	15.0	0.59	0.124	0.33	0.23	6.6
	16-Jul-08	15.0	0.43	0.106	0.26	0.26	9.1
FC-1	5-Jul-07	21.6	0.36	0.067	0.34	0.15	3.8
	12-Aug-07	21.6	0.17	0.066	0.20	0.24	11.2
	11-Jun-08	21.6	0.74	0.068	0.54	0.10	1.5
	23-Jul-08	21.6	0.28	0.066	0.27	0.18	5.8
FC-2	7-Jul-07	13.3	0.33	0.081	0.30	0.18	5.6
	12-Aug-07	13.3	0.15	0.076	0.18	0.28	15.2
	11-Jun-08	13.3	0.61	0.076	0.40	0.14	2.6
	23-Jul-08	13.3	0.26	0.076	0.23	0.23	9.1

Table 4-4 (continued): Flow resistance and associated measurements (shortest potential flow paths).

Reach ID	Date	Stream Length (m)	Velocity (m/s)	Slope (m/m)	Froude Number	<i>n</i>	<i>f</i>
FC-3	6-Jul-07	10.7	0.18	0.123	0.16	0.41	27.7
	11-Aug-07	10.7	0.09	0.121	0.10	0.62	73.6
	12-Jun-08	10.7	0.40	0.116	0.25	0.26	9.4
	22-Jul-08	10.7	0.16	0.113	0.13	0.46	34.3
FC-4	7-Jul-07	16.5	0.21	0.152	0.17	0.42	28.7
	11-Aug-07	16.5	0.12	0.153	0.12	0.61	64.8
	12-Jun-08	16.5	0.52	0.154	0.30	0.25	8.1
	21-Jul-08	16.5	0.23	0.152	0.19	0.39	23.9
FC-5	8-Jul-07	11.1	0.20	0.202	0.20	0.39	28.0
	10-Aug-07	11.1	0.09	0.202	0.11	0.73	111.0
	25-Jun-08	11.1	0.59	0.200	0.44	0.18	5.2
	17-Jul-08	11.1	0.23	0.198	0.22	0.34	21.9
FC-6	8-Jul-07	18.0	0.22	0.202	0.23	0.34	22.6
	10-Aug-07	18.0	0.10	0.202	0.13	0.58	73.2
	25-Jun-08	18.0	0.58	0.212	0.46	0.18	5.4
	17-Jul-08	18.0	0.20	0.203	0.21	0.38	26.8

4.3 Photographic Guidance for Resistance Coefficients

In this section, figures are presented for each of the research reaches, illustrating stream reach characteristics and providing Manning's n and Darcy-Weisbach f given for low, mid, and ~bankfull flows. Photographs of the reaches from multiple perspectives and flow magnitudes are provided. Profile plots are also included, to depict the bed and water surface during bankfull flow. The figures are ordered from the lowest to highest bankfull n values.

In these cascade, step-pool, and plane-bed stream reaches, computed Manning's n values were substantially higher than those suggested by commonly-cited references, although they are comparable to values measured by other researchers in similar stream types. These figures collectively provide a photographic tool that is helpful for general resistance coefficient selection in high-gradient streams; however, caution is warranted when judging the wisdom of extrapolating these results to larger streams or reaches where the flow interacts more substantially with non-step-forming instream wood.

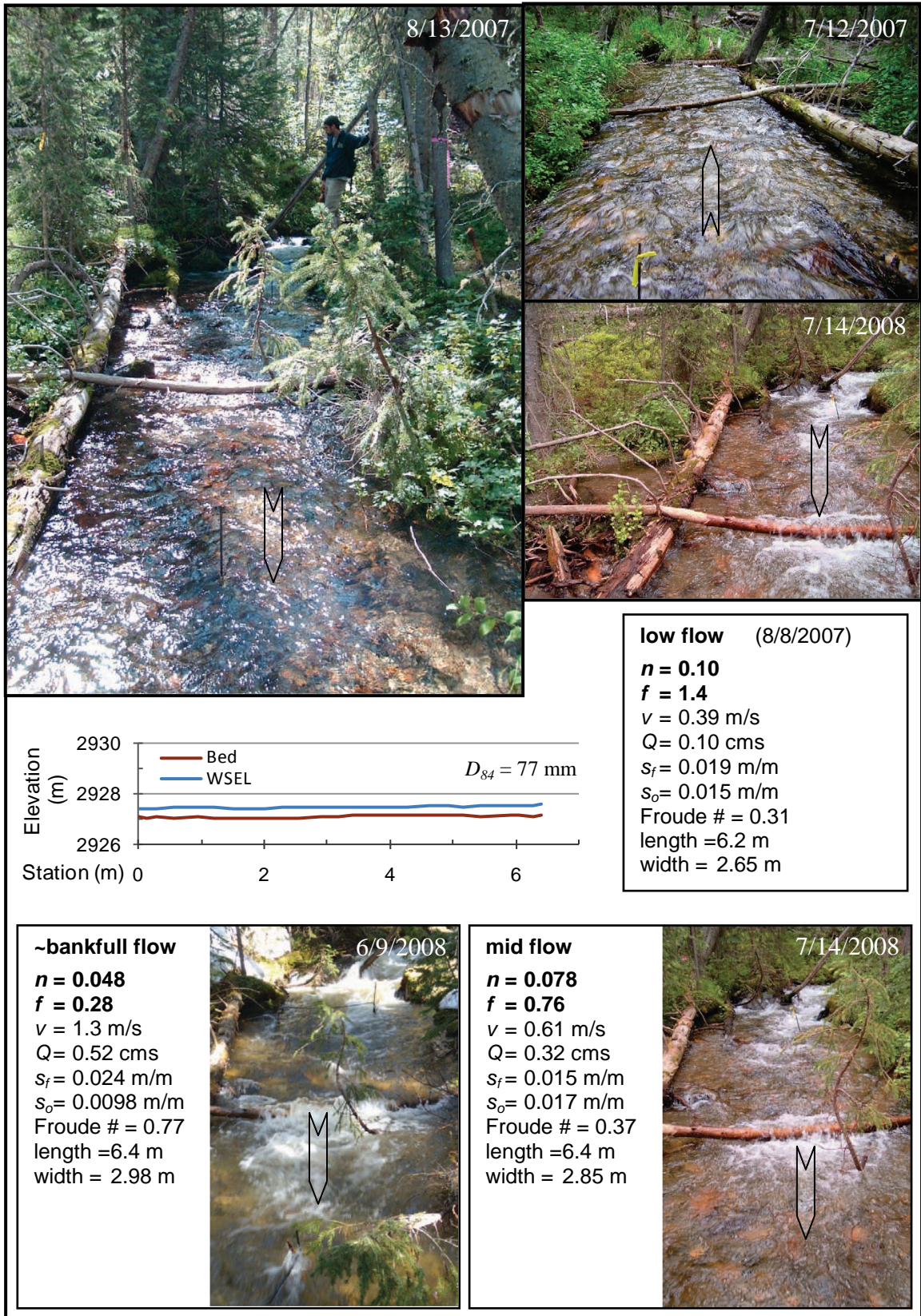


Figure 4-4: East Saint Louis Creek, reach ESL-6 (plane bed).

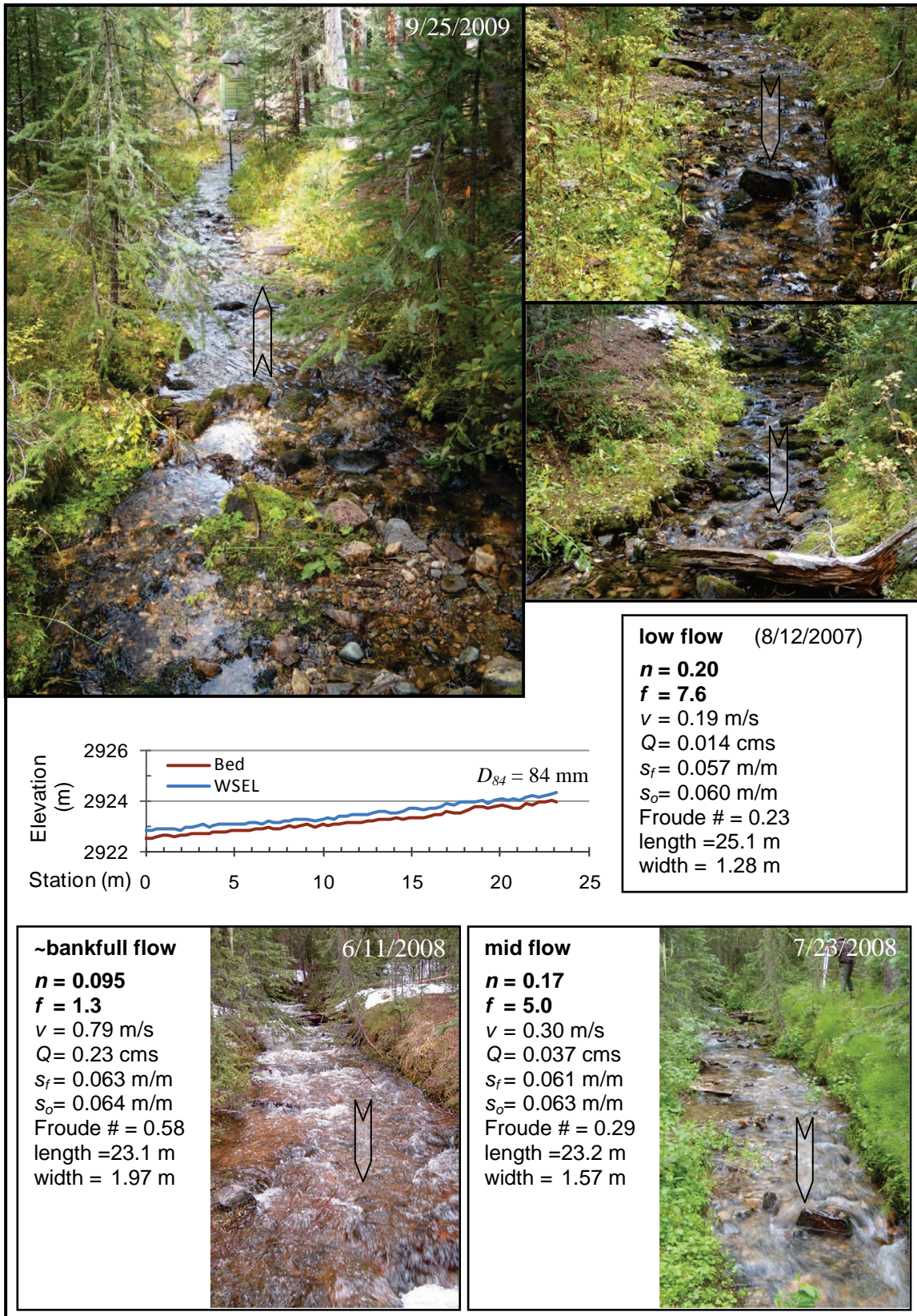


Figure 4-5: Fool Creek, reach FC-1 (transitional between plane bed and step pool).

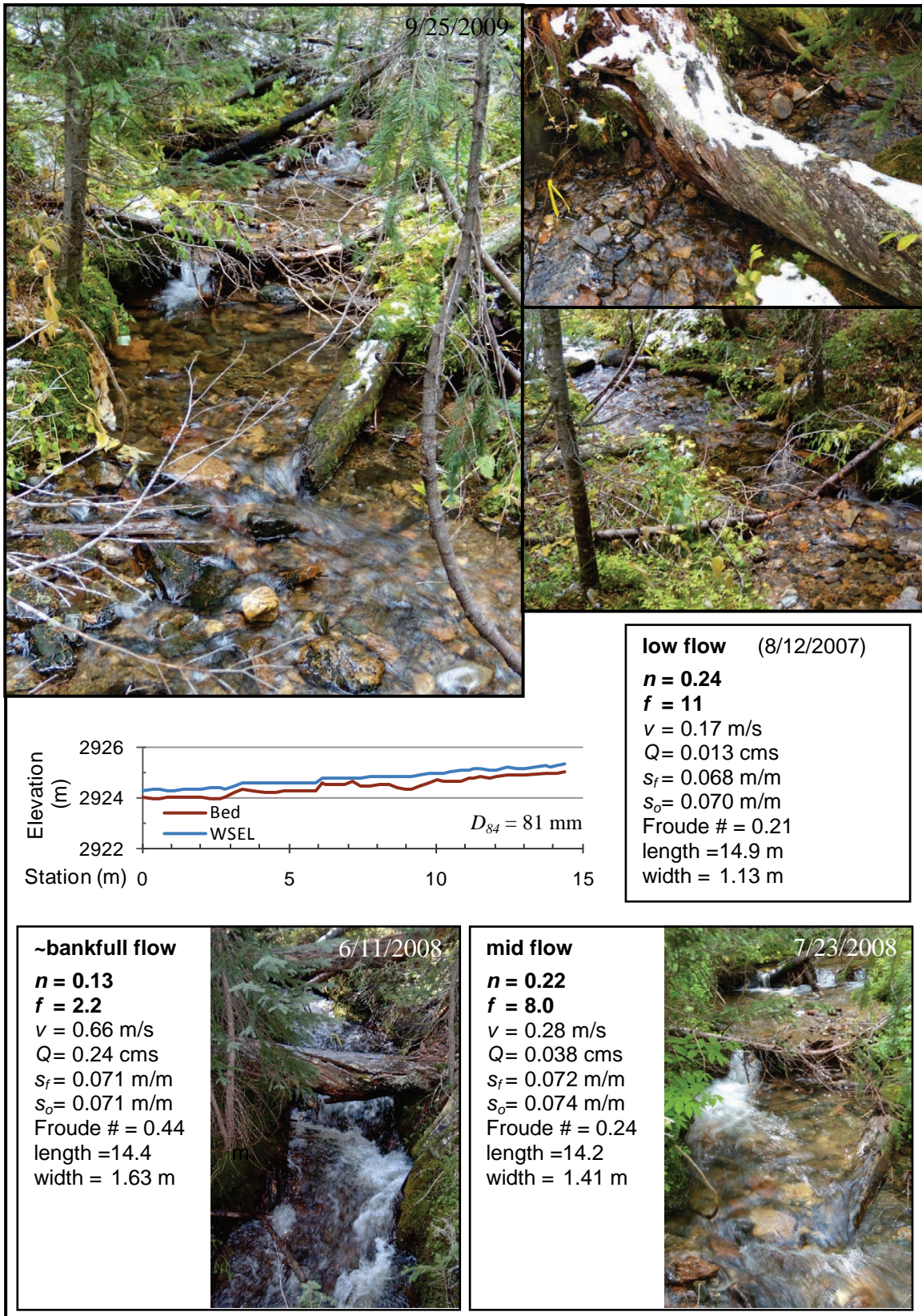


Figure 4-6: Fool Creek, reach FC-2 (step pool).

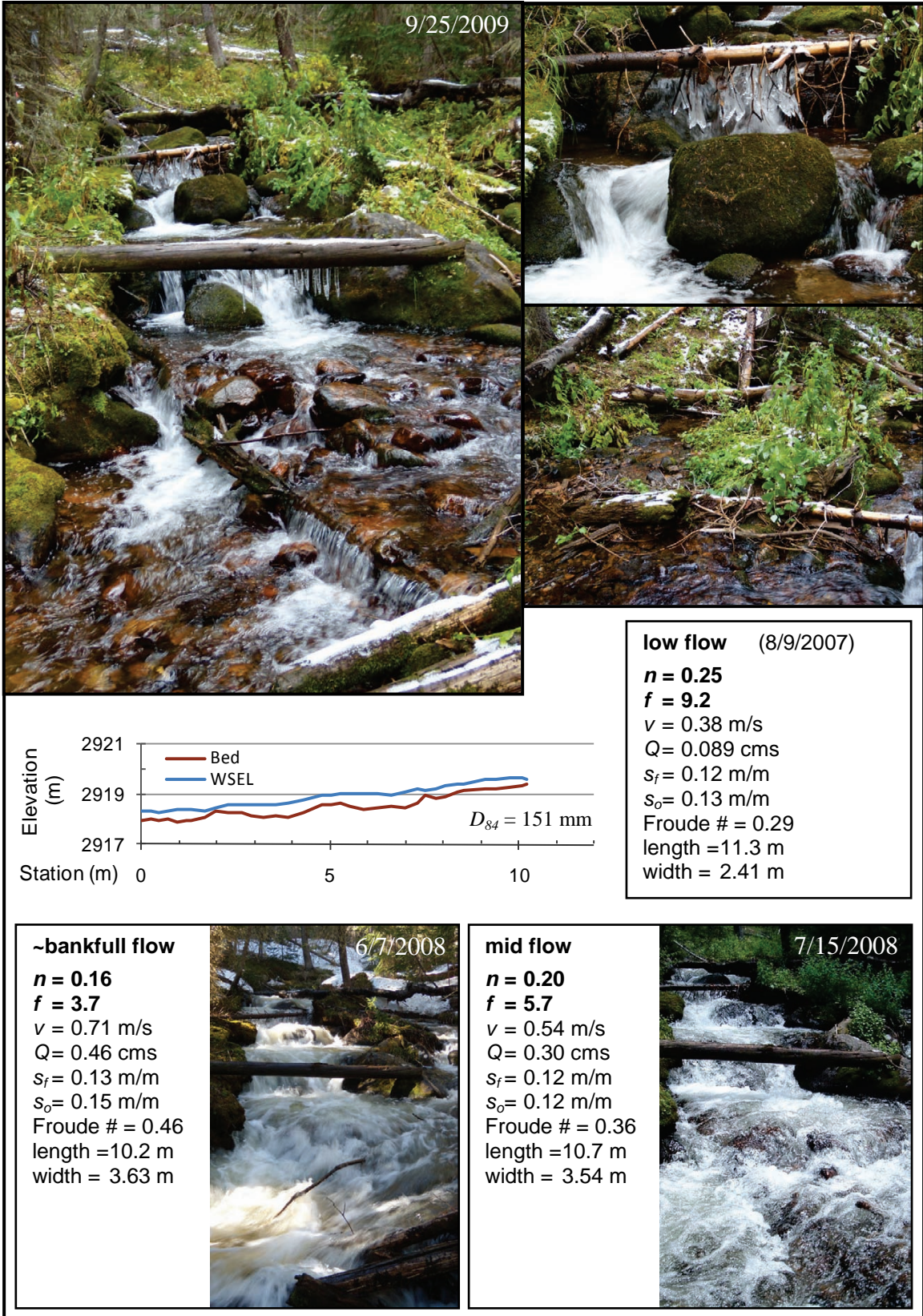


Figure 4-7: East Saint Louis Creek, reach ESL-3 (cascade).

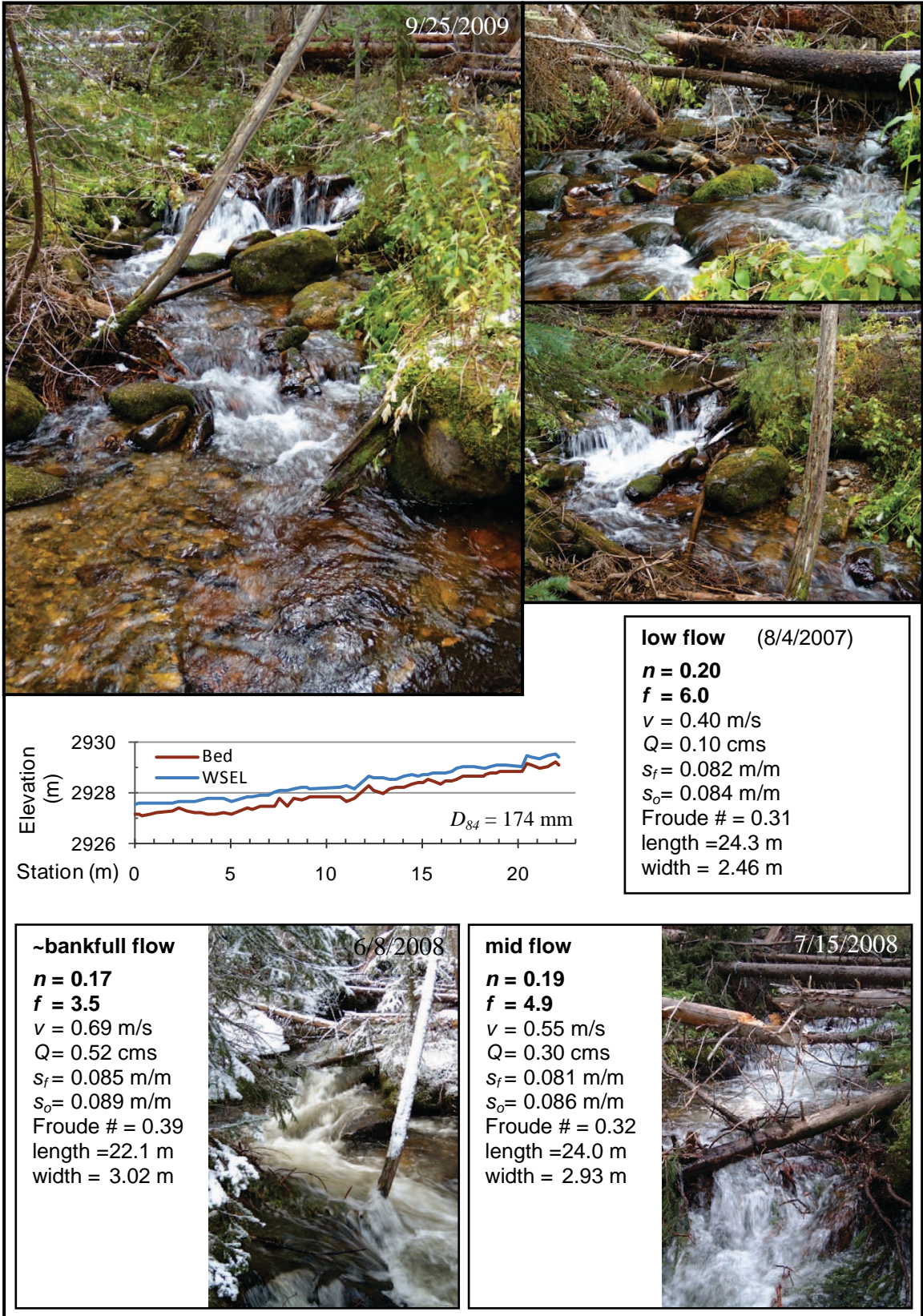


Figure 4-8: East Saint Louis Creek, reach ESL-7 (cascade).

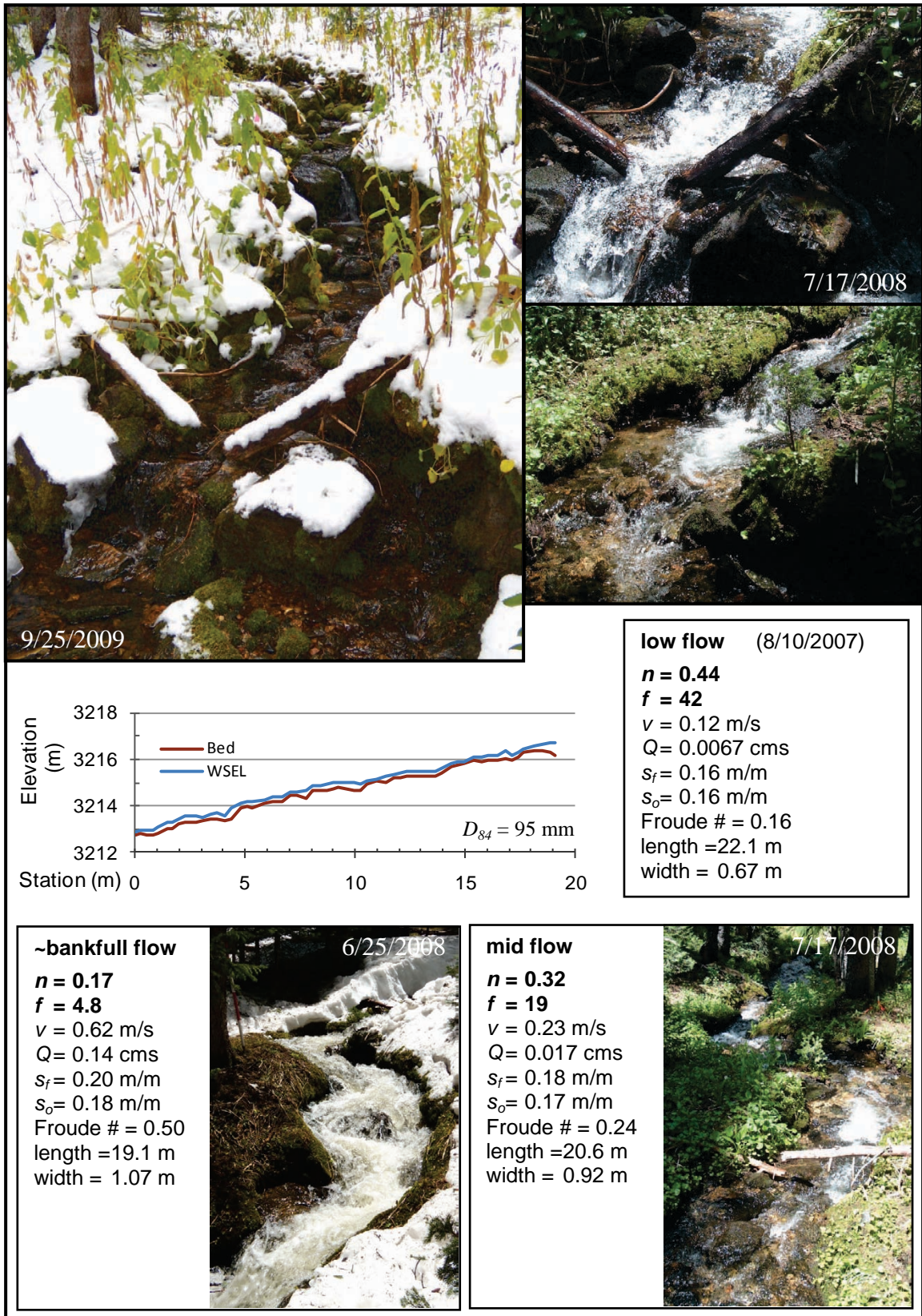


Figure 4-9: Fool Creek, reach FC-6 (cascade).

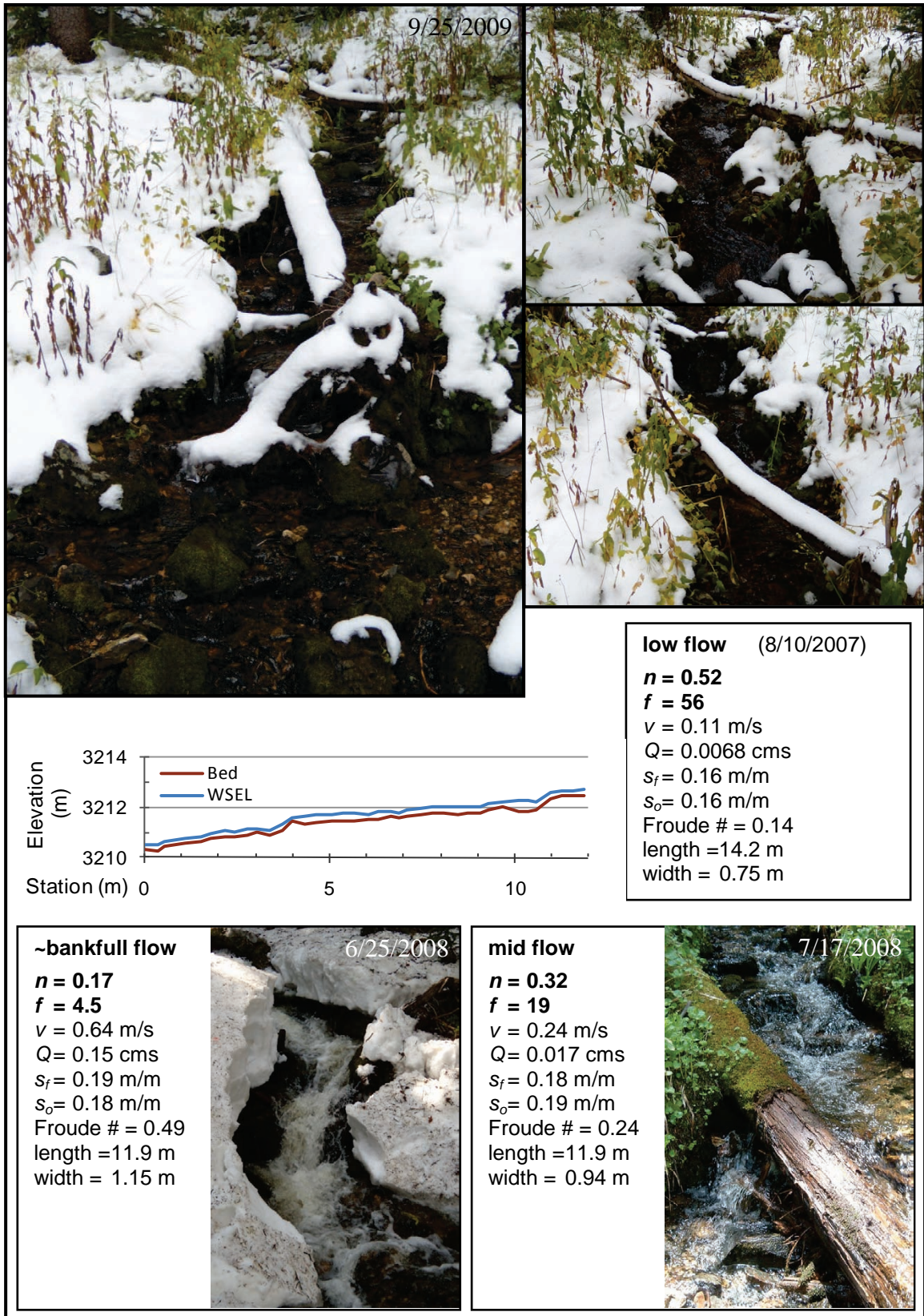


Figure 4-10: Fool Creek, reach FC-5 (cascade).

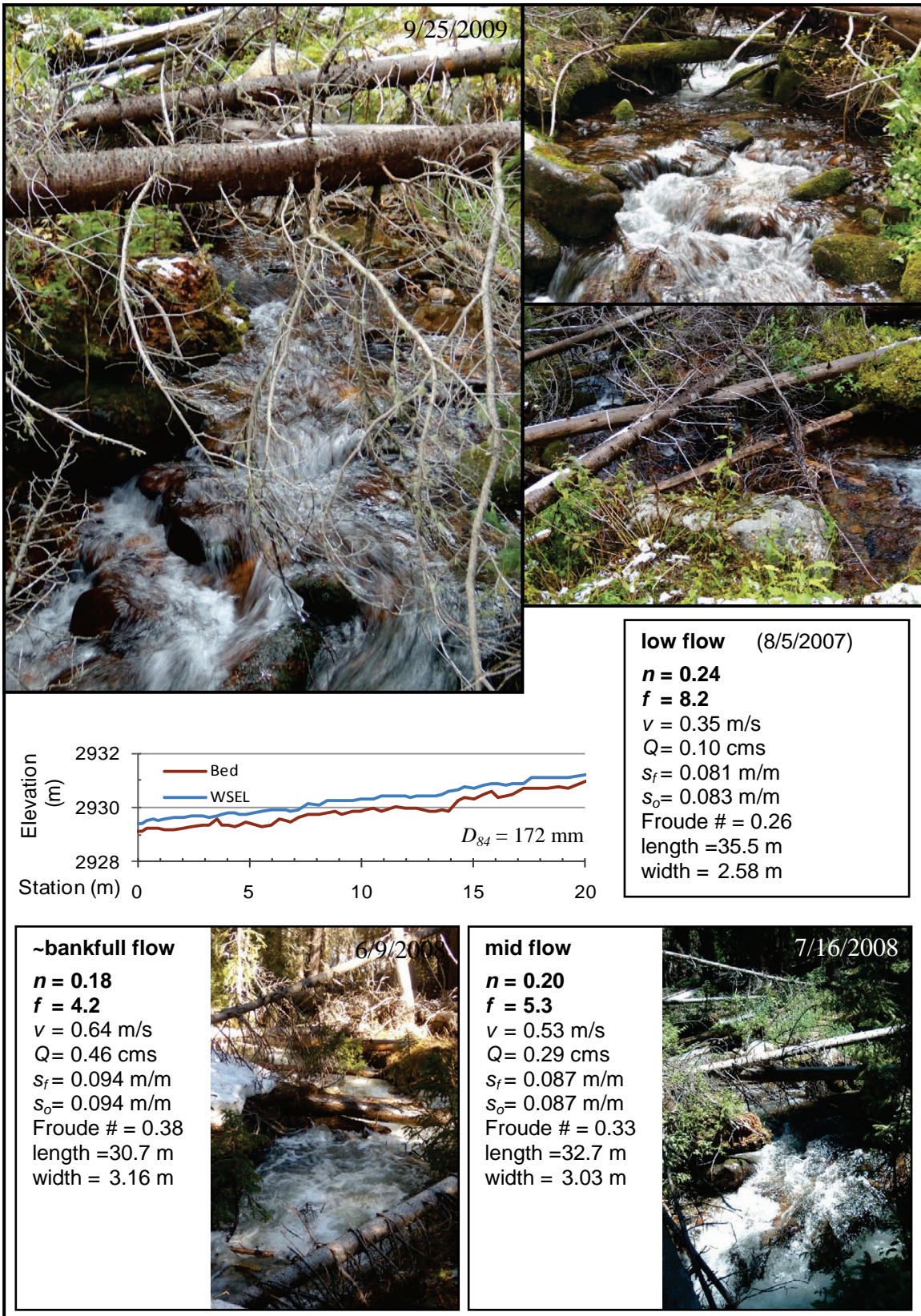
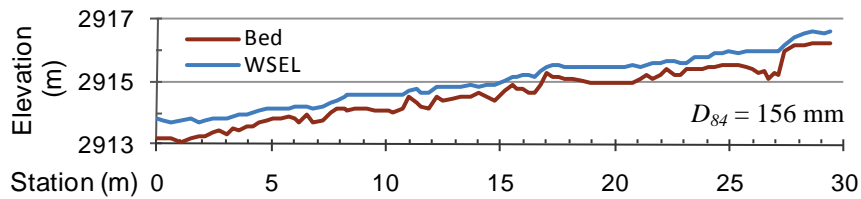


Figure 4-11: East Saint Louis Creek, reach ESL-8 (step pool).



<p>~bankfull flow</p> <p>$n = 0.19$ $f = 4.5$ $v = 0.65$ m/s $Q = 0.56$ cms $s_f = 0.095$ m/m $s_o = 0.10$ m/m Froude # = 0.35 length = 29.4 m width = 2.92 m</p>	<p>6/10/2008</p>	<p>mid flow</p> <p>$n = 0.27$ $f = 9.4$ $v = 0.42$ m/s $Q = 0.24$ cms $s_f = 0.11$ m/m $s_o = 0.11$ m/m Froude # = 0.26 length = 27.3 m width = 2.60 m</p>	<p>7/22/2008</p>
--	------------------	---	------------------

Figure 4-12: East Saint Louis Creek, reach ESL-1 (step pool).

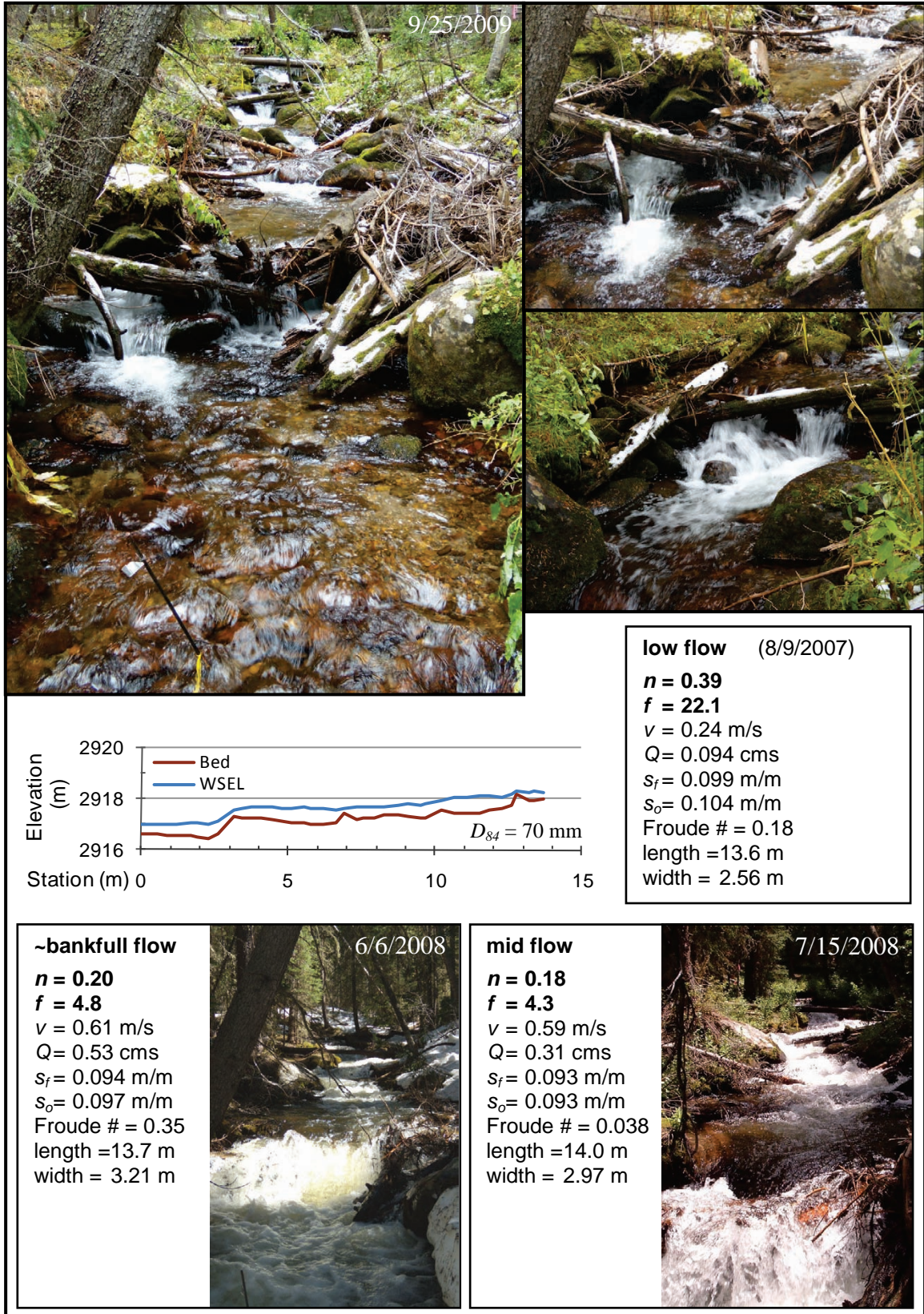


Figure 4-13: East Saint Louis Creek, reach ESL-2 (step pool).

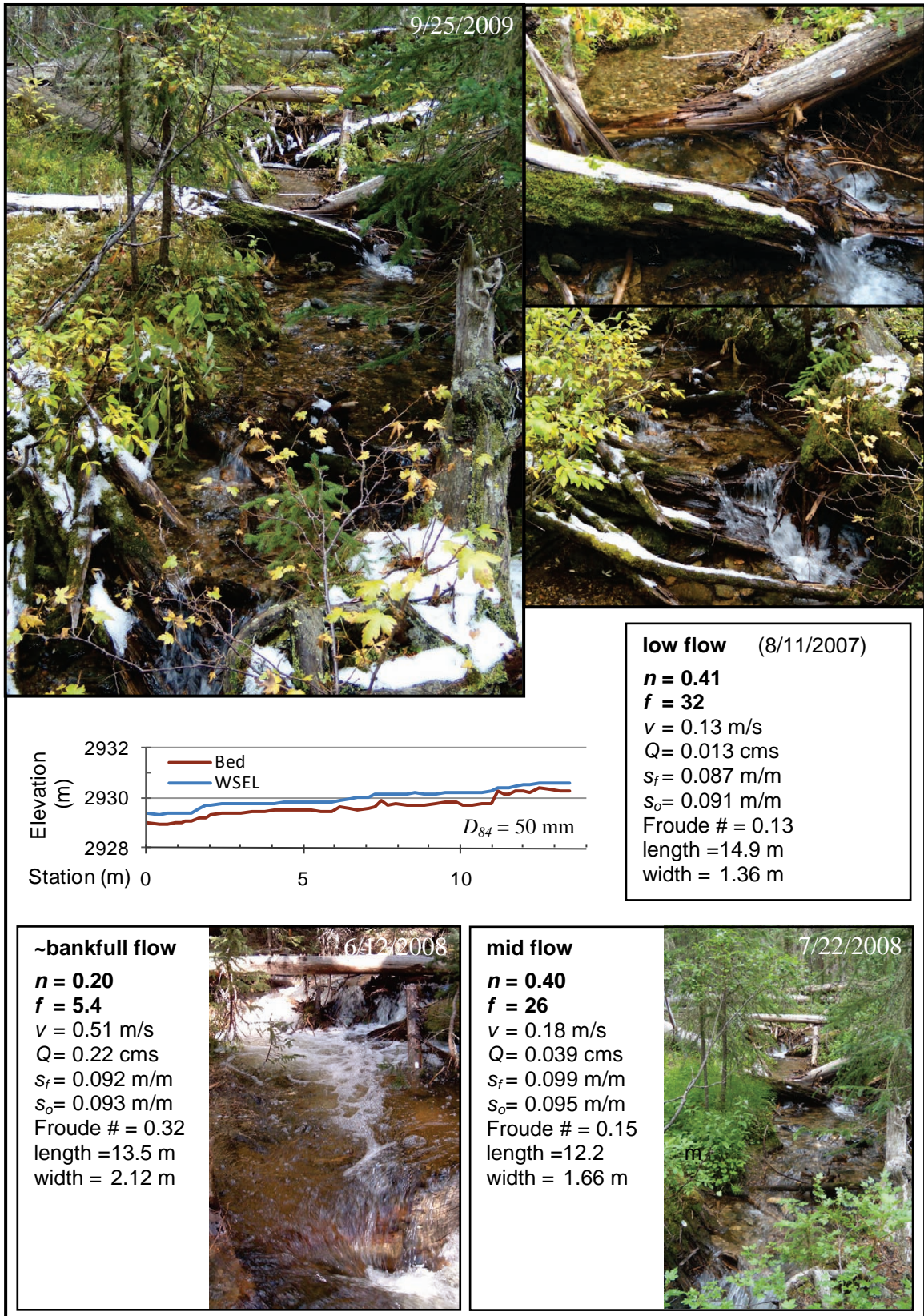


Figure 4-14: Fool Creek, reach FC-3 (step pool).

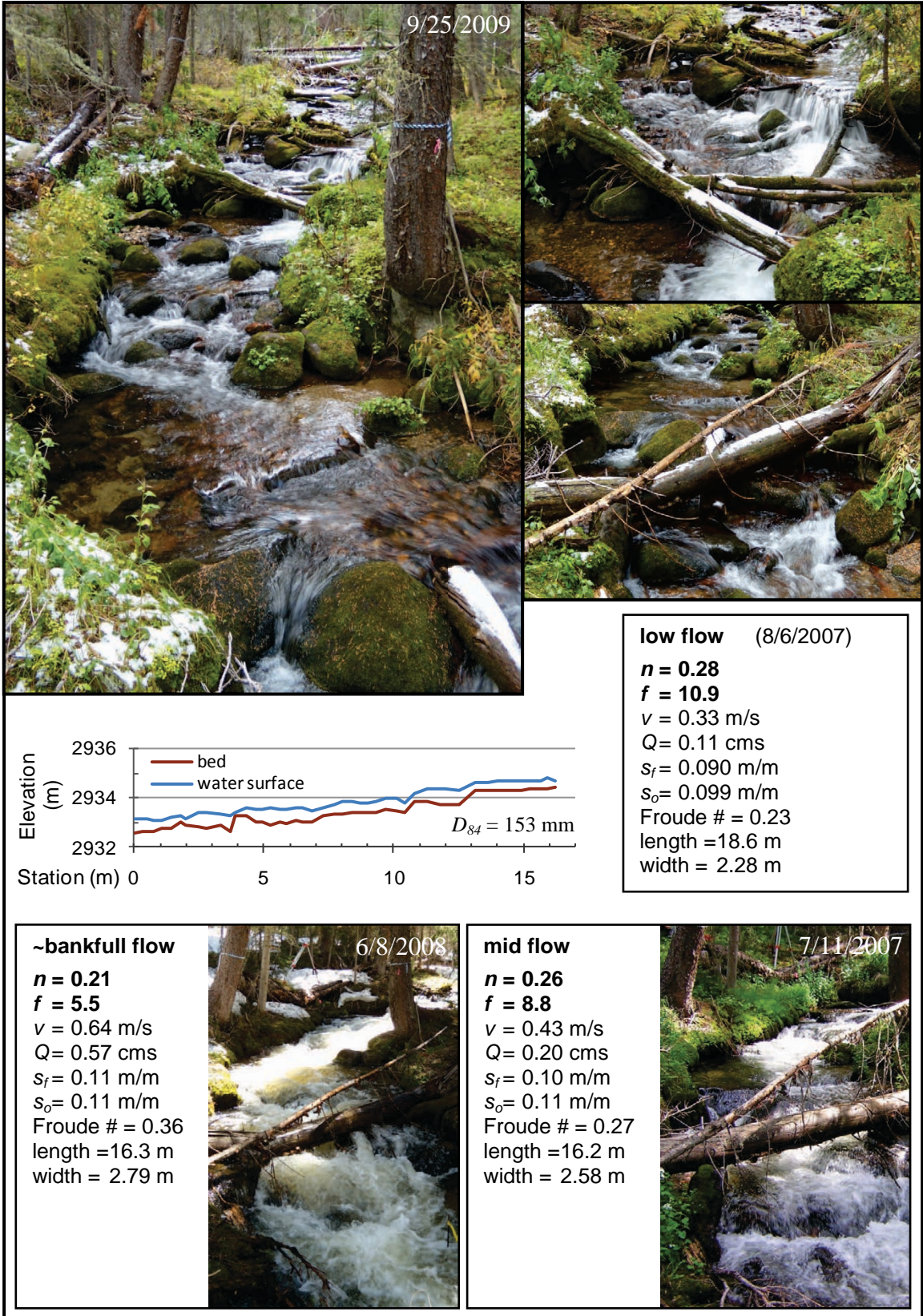


Figure 4-15: East Saint Louis Creek, reach ESL-9 (step pool).

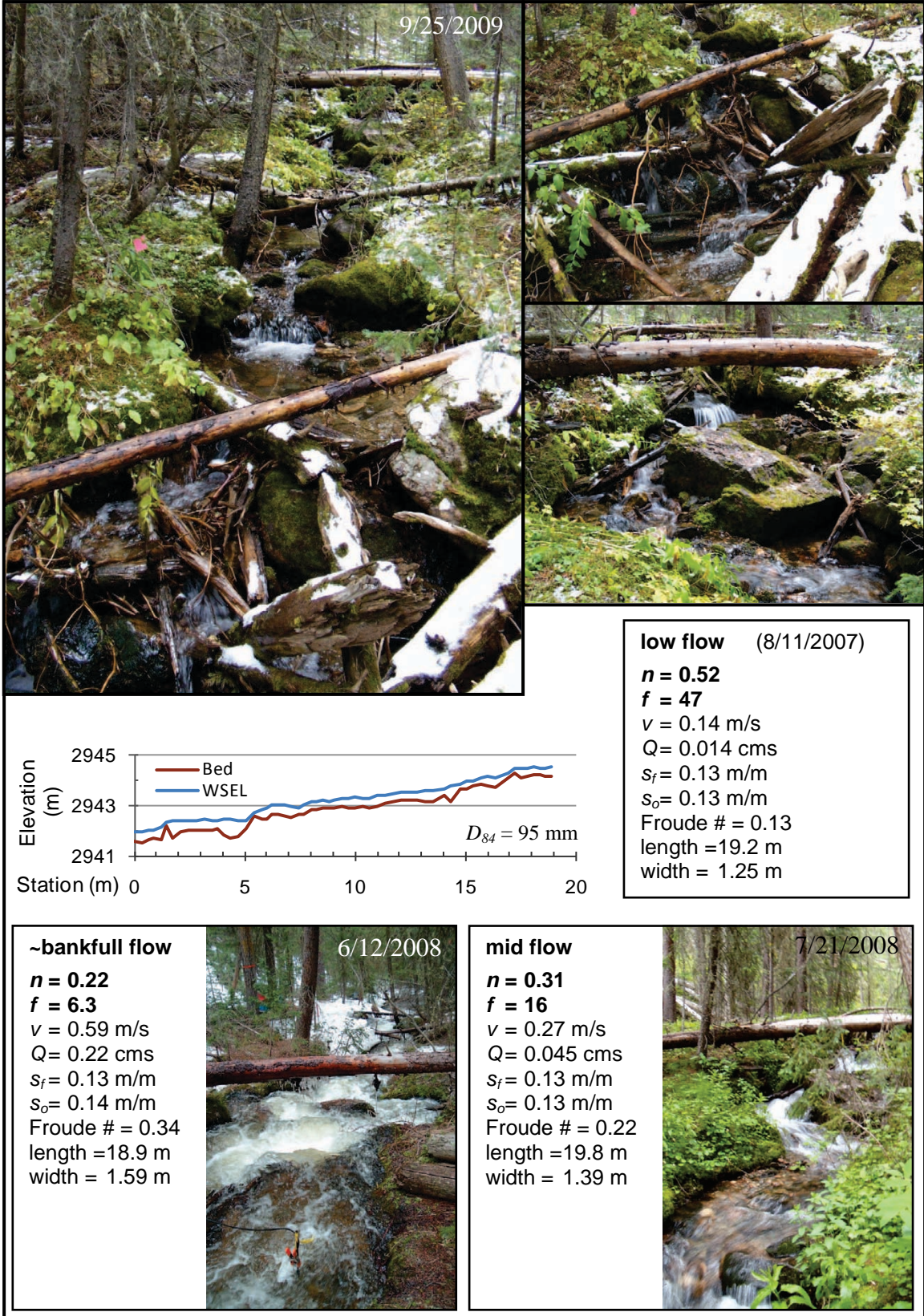


Figure 4-16: Fool Creek, reach FC-4 (step pool).

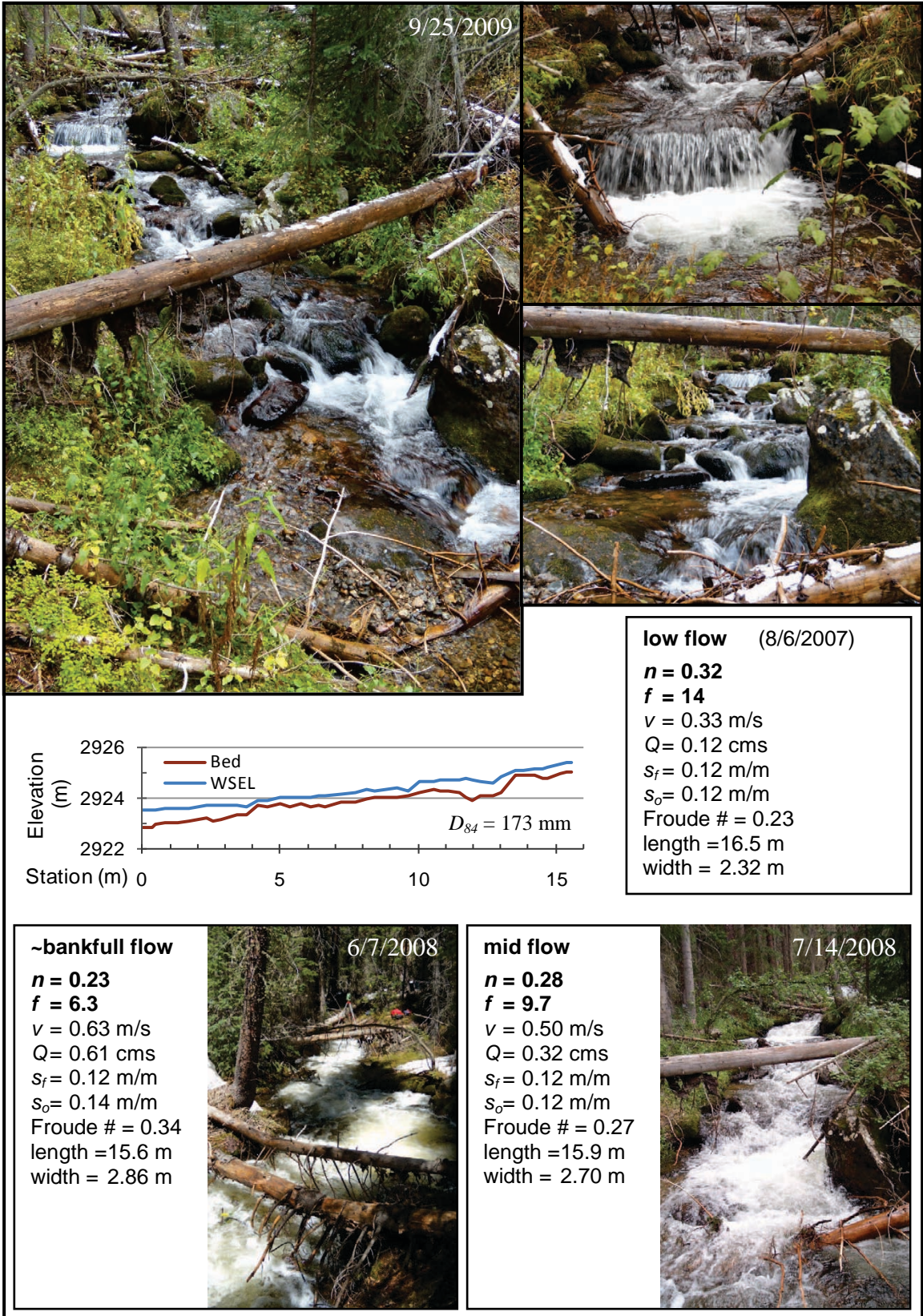


Figure 4-17: East Saint Louis Creek, reach ESL-4 (step pool).

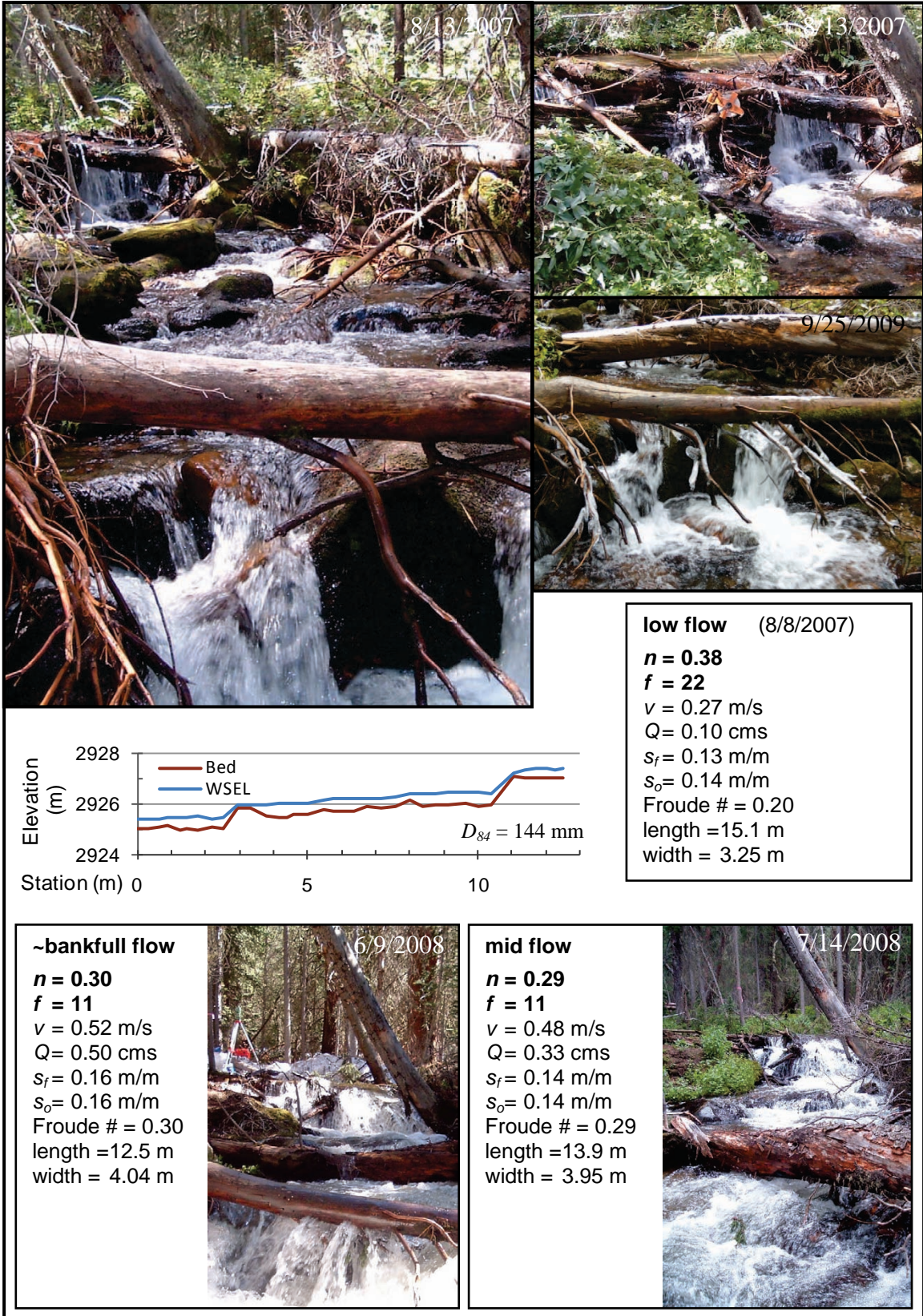


Figure 4-18: East Saint Louis Creek, reach ESL-5 (cascade).

CHAPTER 5

RESULTS AND DISCUSSION

Flow resistance in these high-gradient streams has been found to be higher in magnitude than many references indicate. There was as much variation in resistance between discharges as between reaches, with lower resistance coefficients at higher flow. Effective methods for resistance prediction were found using relative bedform submergence alone and in combination with variables that describe bank sinuosity and instream wood density. The presentation and discussion of results are presented below with sections focusing on data collection and post processing; resistance prediction using simple linear regression; the performance of prior prediction methodologies; resistance prediction using 3-D spatial analysis; multivariate regression using predictors describing bedform, bankform, and instream wood; velocity prediction; and flow path influence upon resistance measurements and prediction. Future research needs and opportunities are also discussed.

5.1 Data Collection and Post Processing

The use of ground-based LiDAR surveying, though cumbersome in the field, allows 3-D analysis of resistance characteristics. Additionally, this method facilitates quantifying instream wood volume and the substantial number of sections needed to

describe these highly-variable reaches, though these data could have been surveyed using a laser theodolite in the field. Water-penetrating LiDAR would have enhanced the dataset, but its impact would have likely been limited due to flow aeration effects on visibility.

Tracers provide a simple and effective method for measuring travel times and reach-average velocities. The most commonly-used tracer for such studies is salt, with measurements collected using conductivity probes. The use of Rhodamine WT and fluorometers in this research added additional costs and potential error to the results, due to impacts of aeration and sunlight in the shallow, turbulent water. These problems, as well as potential toxicity issues, were mitigated by field techniques and data-smoothing algorithms but salt tracers are preferred when possible. With the implemented tracer being Rhodamine WT, the use of a smoothing technique proved to be valuable for enhancing the quality of the tracer data used in the reach velocity computations. The use of a single-pass, 3-point median method minimized the chance of masking signals, while the use of a 5-point median filter or multiple passes of a 3-point median filter may have provided additional beneficial smoothing.

From the smoothed tracer values, the average reach velocity was computed using a spatial harmonic mean travel time and compared to the peak and centroid travel times (Figure 5-1). Peak velocities differed from harmonic by an average of 12.4 percent (range of -13 to 114 percent), while centroid velocities differed by -2.8 percent (range of -13 to 11 percent). Differences between peak methods tend to overpredict velocities, while differences between centroids tend to slightly underpredict velocities. Travel time estimates computed using centroid values are similar to the harmonic, while those

computed using tracer peaks were found to induce a bias to the flow velocity and resistance estimates. The average standard deviation of the harmonic, peak, and centroid velocity computations were 0.021, 0.043, and 0.036 m/s, respectively. Hence it appears that harmonic velocities are not only the most appropriate (Walden 2004), but are also the most accurately computed when compared to values obtained from both peak and centroid methodologies, using an identical dataset. With an average 12-percent difference in reach velocities between time between peaks and the harmonic average, this difference may be significant when performing statistical analyses. Additionally, the lesser standard deviation of the harmonic average computations measurements compared to the peaks and centroid methodologies, using the identical dataset, indicate greater stability in the harmonic computations.

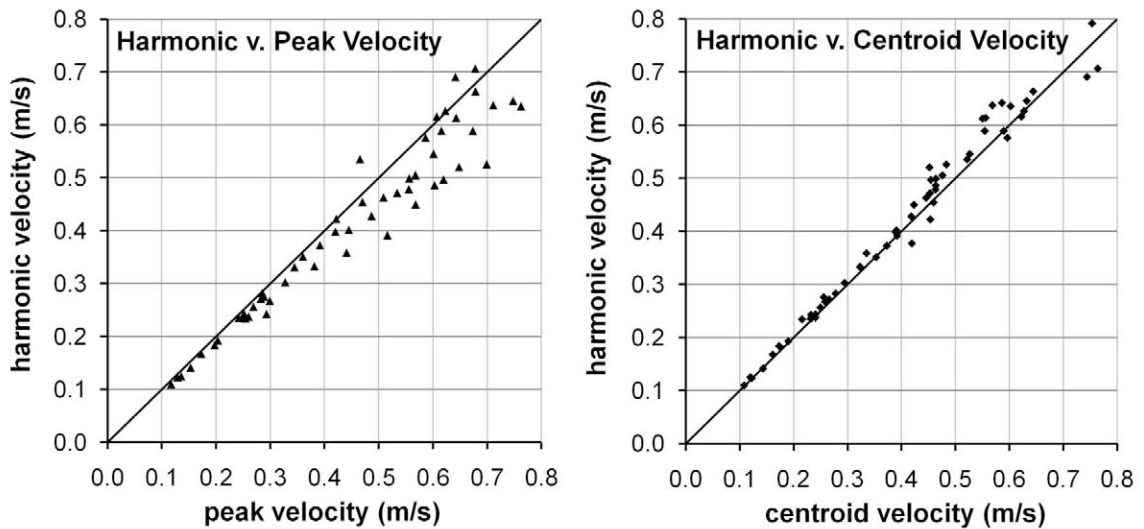


Figure 5-1: Harmonic versus peak and centroid velocity comparisons.

5.2 Resistance Prediction Using Simple Linear Regressions

Univariate regression models for predicting both Manning's n and Darcy-Weisbach f were developed using single predictor variables that quantified longitudinal and cross-sectional bedform, bankform, bed-material gradation, and instream wood (Section 3.2.2). Analyses were performed using both n and f to reflect the differing preferences of applied and academic workers. Good adherence to the assumptions of linearity, homoscedasticity, and independent and normally-distributed residuals was obtained through the use of the natural logarithmic transformations.

5.2.1 Bed Material and Slope

The simply-measured and traditionally-used variables of relative grain submergence (R/D_{84}) and slope (S_f) were tested for their predictive capability with this dataset. The regressions are illustrated in Figure 5-2, while the data for R/D_{84} are provided in Table C-1. Relative grain submergence explained 25 and 30 percent of the variance of n and f , respectively. Slope explained 57 and 54 percent of the variance of n and f , respectively. Excluding the plane-bed data reduced the explained variance to 27 and 25 percent. Using only bankfull data with slope increased the explained variance to 68 and 76 percent.

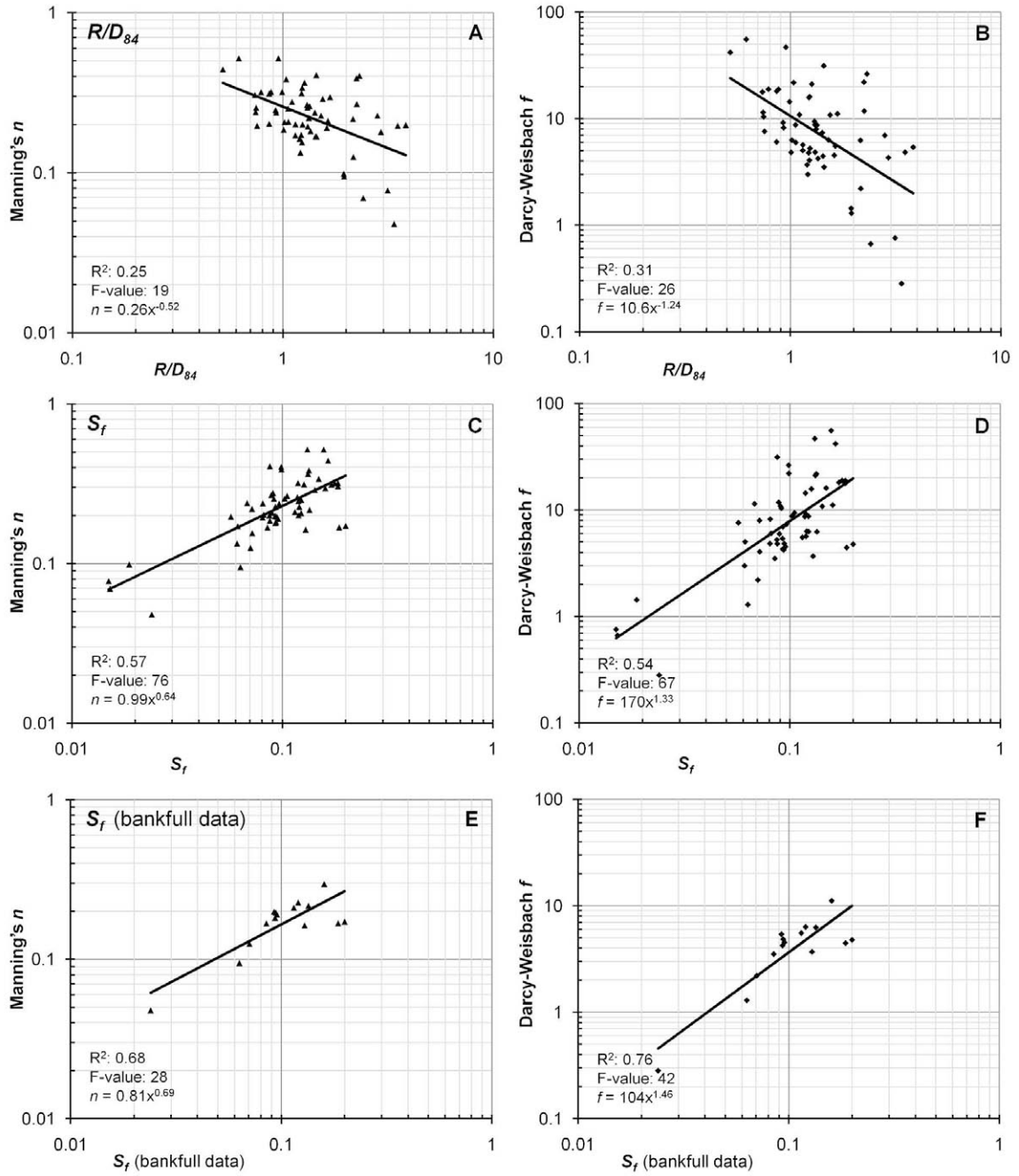


Figure 5-2: Resistance coefficients prediction with R/D_{84} and S_f .

Hence, boundary resistance as defined by D_{84} is a relatively-low contributor to overall flow resistance in these stream reaches. Slope explained more variance. The finding that relative grain submergence is a poor predictor of total resistance in high-gradient streams is consistent with the findings of other researchers (Curran and Wohl 2003; MacFarlane and Wohl 2003; Wohl and Merritt 2008; David et al. 2010). Wilcox *et al.* (2006) attributed 8 to 32 percent of the total resistance to grain while MacFarlane and Wohl (2003), under low flow conditions, found that grain resistance was negligible for both groups and form resistance due to variable channel shape and non-step forming instream wood contributed more towards total resistance. Hence, variables that quantify bed variability may explain greater variability in the data.

5.2.2 Bed Variability

Bed variability was defined using several variables, including the cross-sectional flow area, hydraulic radius, average and maximum cross-sectional depth, and variability in bed residuals (δ) from longitudinal profile regressions. Measured values of these variables are provided in Table C-1. The most effective predictors were constructed as dimensionless ratios of relative submergence, with a normalization term divided by a variability term. The cross-sectional flow area and hydraulic radius ratios are composite variables that includes both bed and bank variability. Of specific interest was the standard deviation of the bed profile regression (σ_z) derived from thalweg longitudinal profiles, which has been previously found to explain flow resistance in laboratory data (Aberle and Smart 2003). Increasing bed variation is associated with increases in flow resistance (Figure 5-3). Application of these variables for prediction varies in complexity, with area

and hydraulic radius variability requiring the measurement of numerous cross sections, while other measures require only two longitudinal profiles. Additionally, prediction using these bed variability descriptors can only be applied in situations where the actual flow of interest is occurring or where the water surface can be approximated, such as bankfull flow.

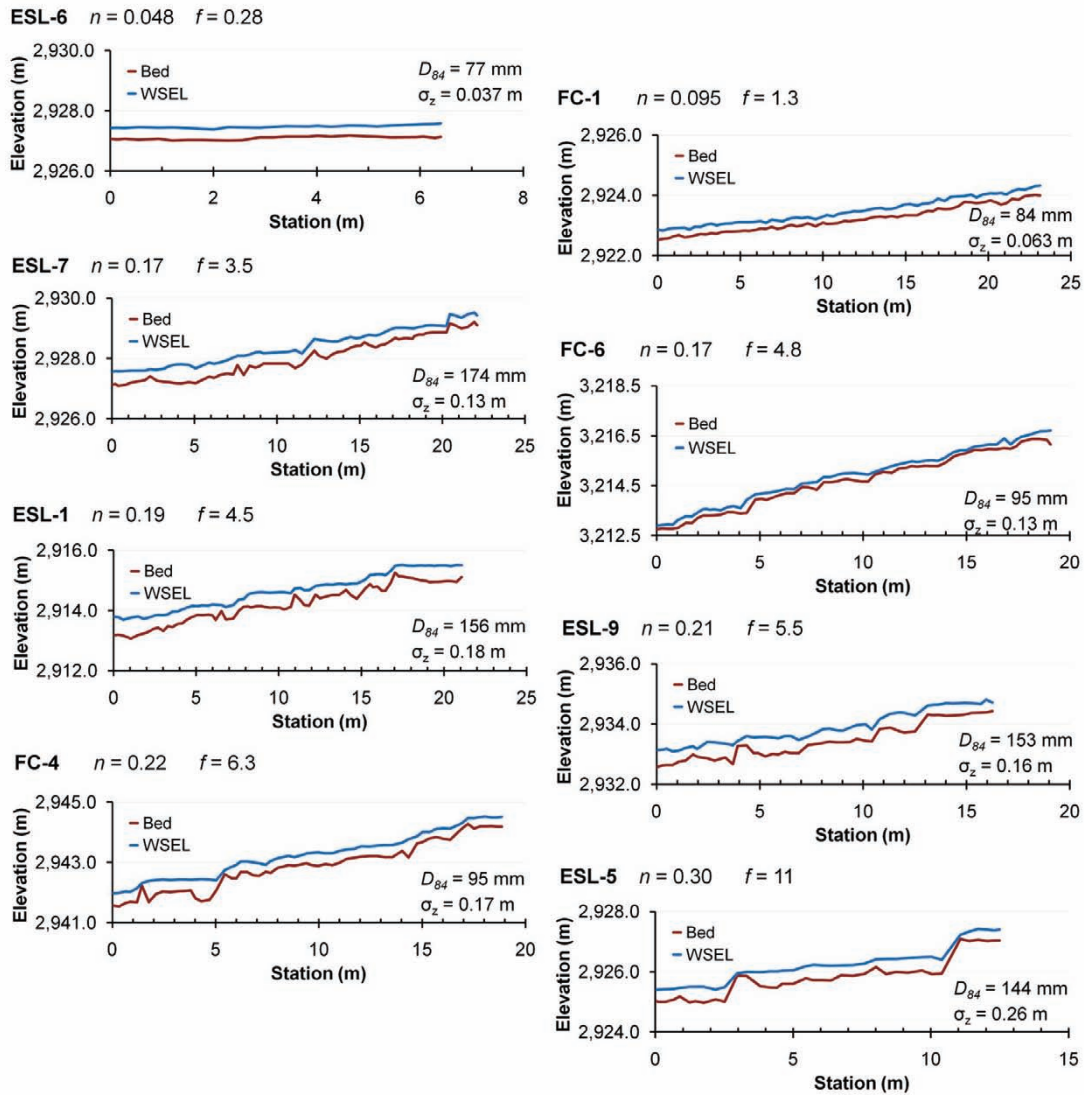


Figure 5-3: Selected bankfull longitudinal profiles, with bed and water surface elevations.

Results of the bed variability regression analyses are shown in Figures 5-4 through 5-7, for both Manning's n and the Darcy-Weisbach f , with a summary of the key variables provided in Table 5-1. The results obtained using both n and f are similar; for simplicity in the discussion, the friction factor is focused upon. Area variability, in the form of area/standard deviation of the area (A/SDA), explained 74 percent of the variability of f in the dataset (Figure 5-4B). This variable explained 58 percent of variance with the plane-bed data excluded. Hydraulic radius variability (R/SDR) explained 61 percent of the variance (Figure 5-4D), while maximum depth variability (h_m/SDh_m) explained 65 percent of the variance (Figure 5-4F). The use of non-relative bed profile regression residuals reduced predictive accuracy (Figure 5-5), with the median residual (δ_{median}) explaining 32 percent of the variance in f , average residual ($\delta_{average}$) explaining 33 percent of the variance, maximum residual (δ_m) explaining 38 percent of the variance, and the standard deviation of the residuals (σ_z) explaining 33 percent of the variance (Figure 5-7B). The use of relative submergence versions of the maximum residual provided a better fit, with R/δ_m explaining 79 percent of the variance in f (Figure 5-6B) and h_m/δ_m explaining 78 percent of the variance (Figure 5-6D). Relative submergence versions of the standard deviation of the bed profile regressions provided the best fit to these 2-D data, with both R/σ_z and h_m/σ_z explaining 80 percent of the variation in f . These variables (R/σ_z and h_m/σ_z) explained 76 and 75 percent of the variation in n , respectively (Figure 5-7). Excluding plane-bed data, R/σ_z and h_m/σ_z explained 66 percent of the variation in f . For the purposes of this dissertation, relative bedform submergence is defined as both h_m/σ_z and R/σ_z .

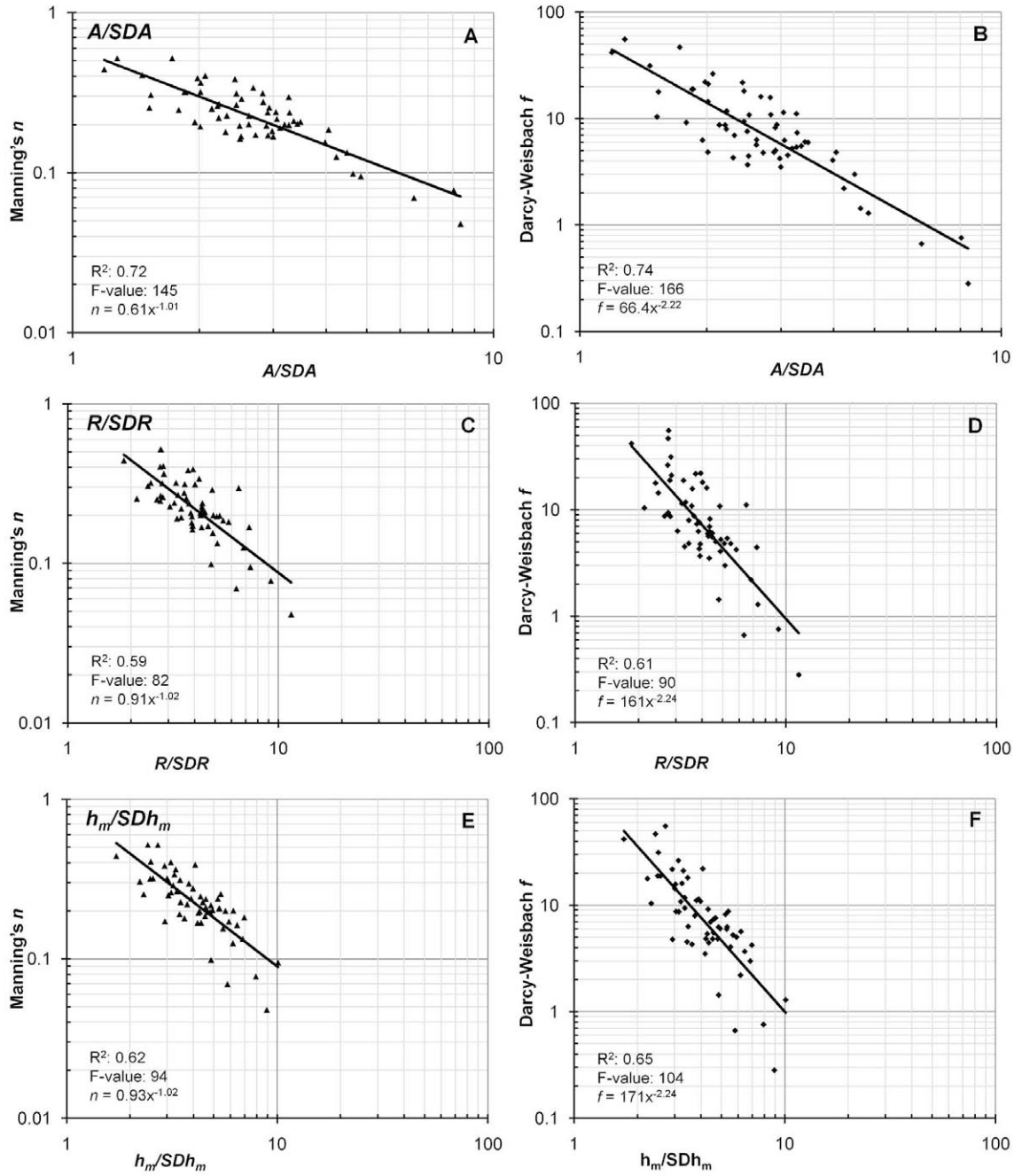


Figure 5-4: Resistance coefficients prediction with A/SDA , R/SDR , and h_m/SDh_m .

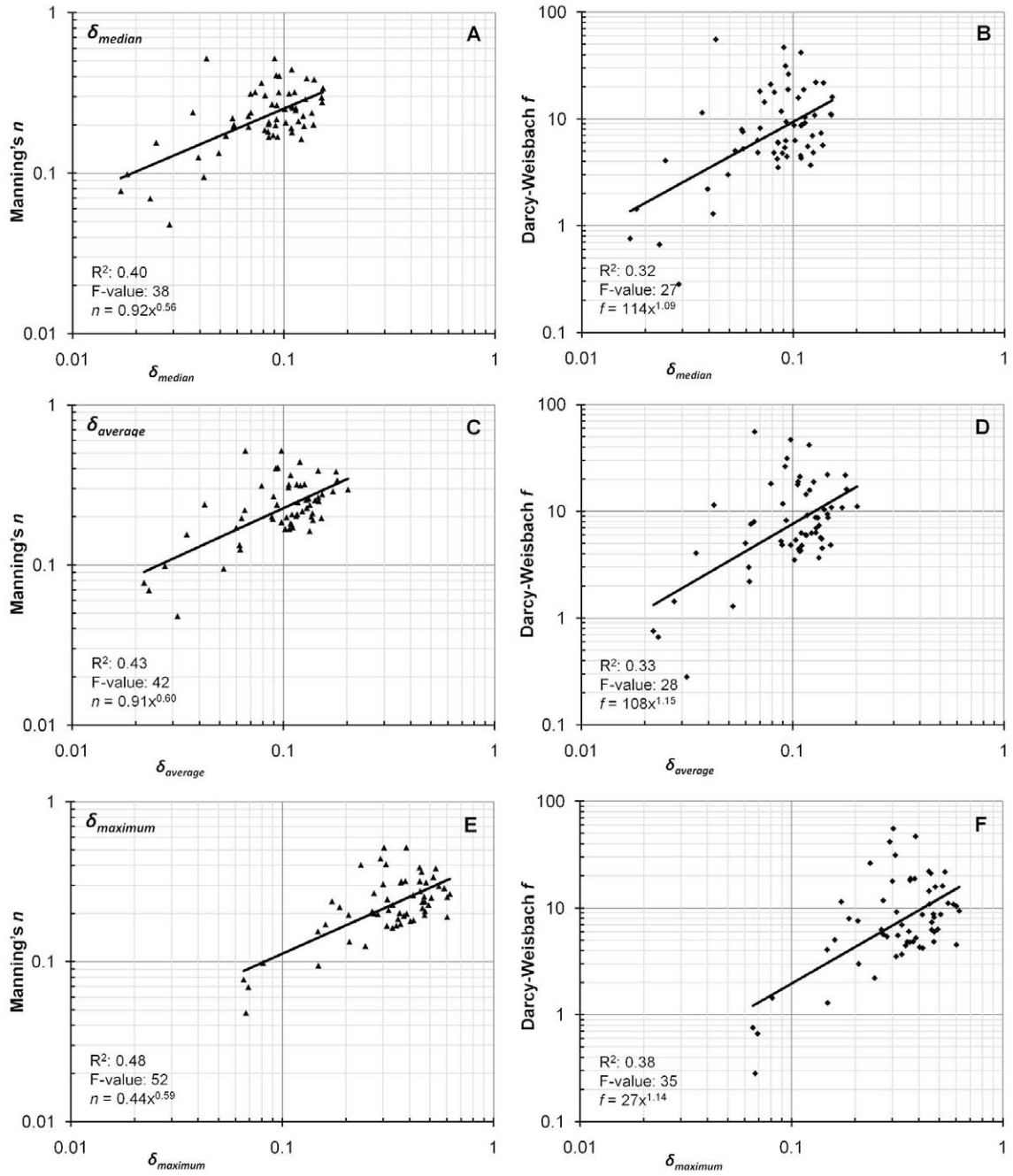


Figure 5-5: Resistance coefficients prediction with median, average, and maximum bed residual.

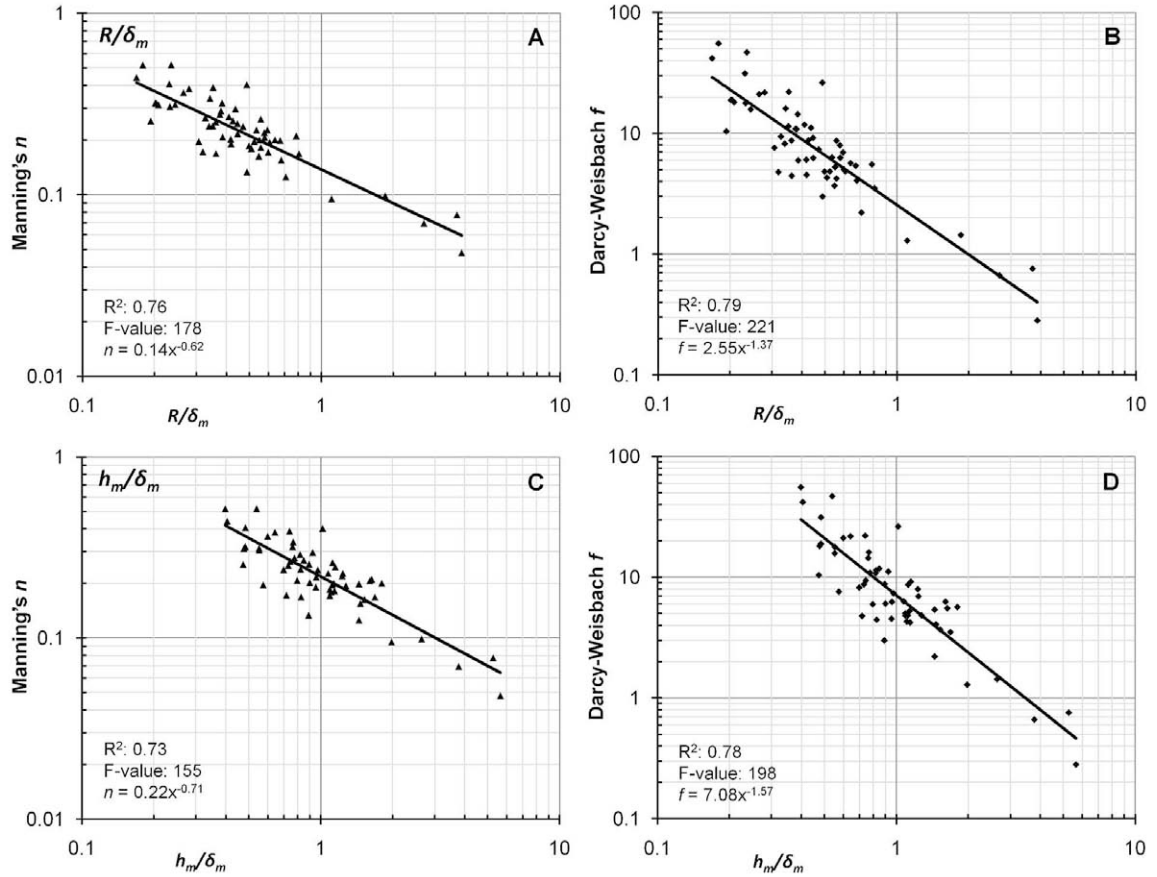


Figure 5-6: Resistance coefficients prediction with relative submergence, using maximum bed residual and both hydraulic radius and maximum depth.

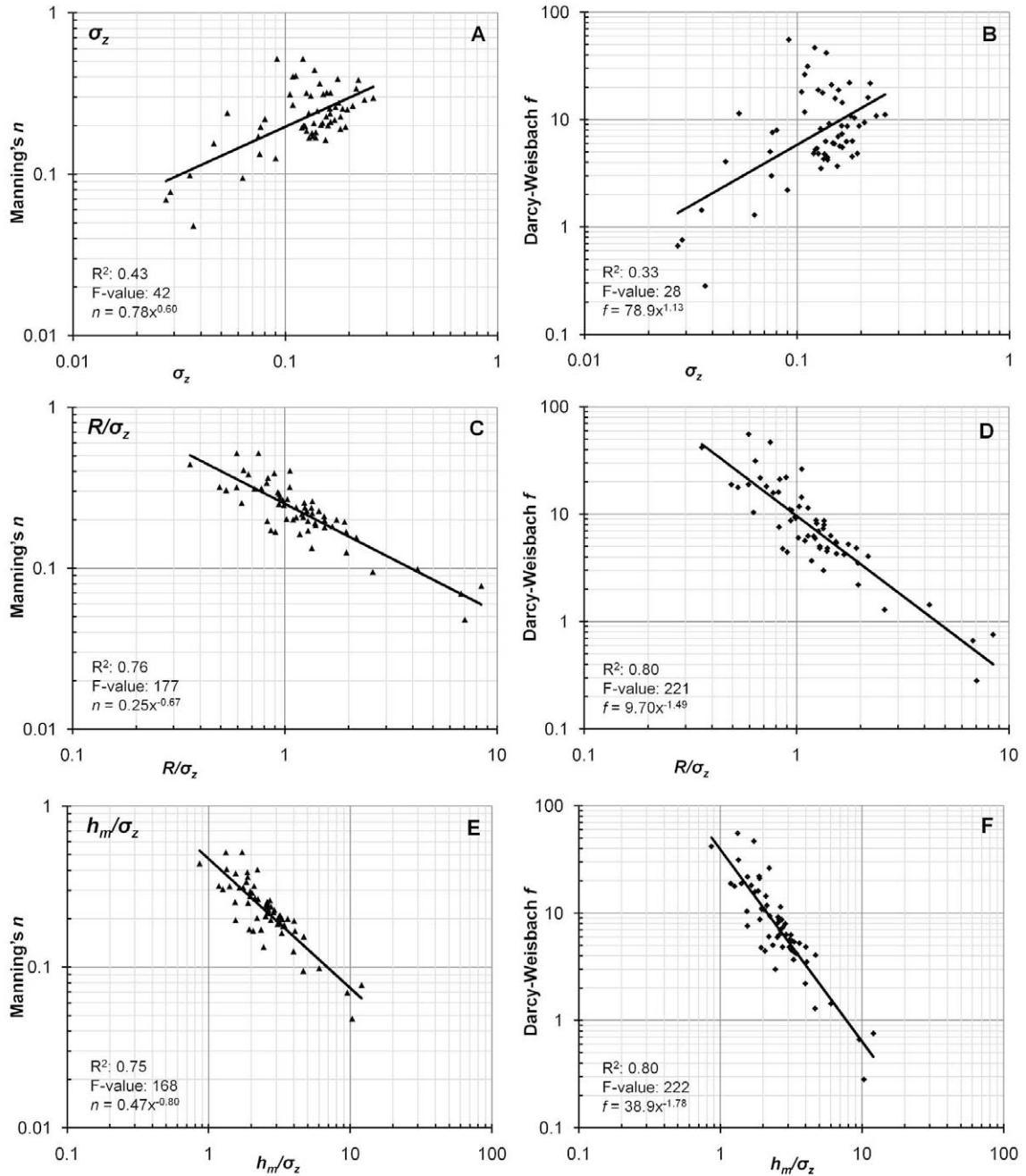


Figure 5-7: Resistance coefficients prediction with the standard deviation of a bed profile regression and relative submergence, using the standard deviation of the residuals of a bed profile regression and both hydraulic radius and maximum depth.

Table 5-1: Most relevant explanatory variables, with all data used for models 1 through 8 and only bankfull data for model 9.

Model	Explanatory variable, x	R^2		F-value		Equation ^(a)	
		n	f	n	f	n	f
1	R/σ_z	0.76	0.80	177	221	$n = 0.252(x)^{-0.673}$	$f = 9.70(x)^{-1.49}$
2	$h_m/\sigma_z^{(b)}$	0.75	0.80	168	222	$n = 0.470(x)^{-0.799}$	$f = 38.9(x)^{-1.78}$
3	A/SDA	0.72	0.74	145	166	$n = 0.606(x)^{-1.01}$	$f = 66.4(x)^{-2.22}$
4	$h_m/SDh_m^{(b)}$	0.62	0.65	94	104	$n = 0.932(x)^{-1.02}$	$f = 171(x)^{-2.24}$
5	R/SDR	0.59	0.61	82	90	$n = 0.906(x)^{-1.02}$	$f = 161(x)^{-2.24}$
6	$S_f^{(b)}$	0.57	0.54	76	67	$n = 0.993(x)^{0.635}$	$f = 170(x)^{1.33}$
7	$TW/SDTW^{(b)}$	0.35	0.36	30	32	$n = 0.651(x)^{-0.809}$	$f = 78.0(x)^{-1.78}$
8	R/D_{84}	0.25	0.31	19	26	$n = 0.259(x)^{-0.516}$	$f = 10.6(x)^{-1.24}$
9	S_f (only bankfull data) ^(b)	0.68	0.76	28	42	$n = 0.811(x)^{0.697}$	$f = 104(x)^{1.46}$

Statistical analysis terms: F-value = fit statistic; and R^2 = coefficient of determination.

Notes: ^(a) equations have not been corrected for log-transformation biases (see Table 5-2) and ^(b) bold variables are considered simpler to measure in the field. All p are $< 10^{-4}$.

A substantial amount of the variance in both Manning's n and Darcy-Weisbach f was explained using bedform descriptors. The use of relative submergence, with hydraulic radius or flow depth, was necessary to account for resistance varying as much between stages as between reaches. The standard deviation of bed profile regression residuals has been previously investigated as a potential parameter for predicting flow resistance in high-gradient channels (Aberle *et al.* 1999; Aberle and Smart 2003; Comiti *et al.* 2007), though previous work was in the laboratory was found to have poor correlation (Comiti *et al.* 2007). Since the maximum, average, and median bed residuals are, in sequence, less powerful in predicting both n and f , the analysis indicates that extremes in bed variability (*e.g.*, the largest drops in a reach) tend to be disproportionately influential. This bed variability is caused by both clasts and instream wood as steps are heightened by wood lodging among the clast steps. Hence, bed variability predictors capture the combined influence of wood and clasts. Most of the hydraulically-effective instream wood contributes to resistance in such a manner, though there is a variable influence of non-step-forming wood present in the fifteen reaches.

The inclusion of plane-bed data substantially alters the explained variance of these simple linear regressions. Only one of the fifteen reaches was plane bed in form though another of the reaches was transitional between plane bed and step pool. I decided to not consider the plane-bed data as outliers in the regressions because these data fall into the same log-space trend for not only h_m/σ_z but all explanatory variables and, hence, appear to be all part of the same population. The variable h_m/SDh_m , due to the nature of its computation, indicates minimal spread between the plane-bed data and the step-pool and cascade data, with the R^2 for f varying from 0.65 to 0.63 for inclusion versus exclusion of the plane-bed data, respectively. This characteristic supports inclusion of the plane-bed data in the overall analysis. Additionally, there is a physical argument for including the plane-bed data in that this stream type is in the natural progression of “roughness configurations” from cascade to step pool to plane bed, as described by the classification scheme of Montgomery and Buffington (1997).

A cross-validation analysis was performed of h_m/σ_z for both n and f . Both the data-splitting and jackknife methods were used, to develop a less-optimistic view of the predictive power of the regressions when extrapolated beyond the Fraser Experimental Forest (Figure 5-8). The data-splitting approach provided regressions of the observed versus estimated n and f with R^2 of 0.68 and 0.55, respectively. The jackknife approach provided resulting regressions of the observed versus estimated n and f with R^2 of 0.59 and 0.52, respectively. With R^2 of the observed versus estimated resistance coefficients varying from 0.52 to 0.68, results indicate substantially less prediction accuracy should be expected if the models are applied outside this dataset. The highest resistance coefficients were predicted with the least accuracy, indicating that higher resistance

values are composed of more resistance components than what is explained by variation in the relative bedform submergence. However, the high explained variance that relative bedform submergence provides with this dataset indicates that this variable is likely to be relevant for explaining flow resistance in other high-gradient streams.

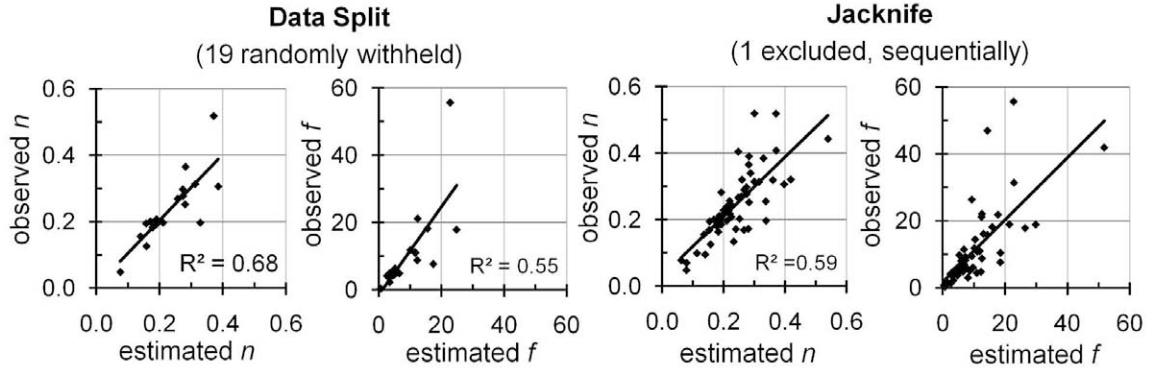


Figure 5-8: Cross-validation results, h_m/σ_z .

Predictions made from these simple linear regressions are affected by a log-transformation bias. To minimize this bias, a correction factor (CF) is implemented in the form:

$$Y = CF * \hat{\beta}_0 X^{\beta_1} \quad (5-1)$$

where the CF is as presented in Equation 3-5 and the β s are the regression-defined intercept and exponent terms (Table 5-2). Correction factors ranged from 2.8 to 10.8 percent adjustments for n and f , respectively, for h_m/σ_z and 8.5 to 42 percent adjustments for n and f , respectively, for R/D_{84} .

Table 5-2 : Log-transformation bias corrections.

Explanatory variable, x	Correction factors, CF	
	n	f
R/σ_z	1.027	1.109
h_m/σ_z ^(a)	1.028	1.108
A/SDA	1.031	1.138
h_m/SDh_m ^(a)	1.042	1.195
R/SDR	1.045	1.216
S_f ^(a)	1.047	1.260
$TW/SDTW$ ^(a)	1.073	1.379
R/D_{84}	1.085	1.416
S_f (only bankfull data) ^(a)	1.032	1.098

Note: ^(a) bold variables are considered simpler to measure in the field

I unsuccessfully endeavored to include other data to assess the effectiveness of relative bedform submergence in a combined dataset. Only two datasets that provided longitudinal profiles and sufficient data for calculating resistance coefficients were found to have sufficient information for comparison: Comiti *et al.* (2007) and Zimmermann and Church (2001). Some of the data from Comiti *et al.* (2007) plotted within the bounds of the Fraser dataset but the majority of their data generally plotted below the range of resistance coefficients measured in the Fraser Experimental Forest, especially at higher σ_z . This disparity may be explained in part by substantial differences in data collection and computational methods including a 5-sec time step for tracer travel time measurements, difference in tracer peaks used for velocities instead of a harmonic average, and differences in how slopes and flow lengths were measured. Most substantially, these reaches have less-developed bedforms, likely due to the long term practice of instream wood removal; this may account for the differing results, with different populations potentially represented. The Zimmermann and Church (2001) dataset provided sufficient data for only two observations of flow resistance, that did plot within the bounds of the Fraser data albeit lower than the overall trend of the Fraser data.

There were also substantially different data-collection and analysis techniques used including relatively few cross sections, water surface elevation measurements at locations not matching the section locations, difference in tracer peaks used for velocities instead of a harmonic average, and differences in how slopes and flow lengths were measured, with bed slopes used instead of water surface. These methodological differences among studies precluded an assessment of the efficacy of models based on relative bedform submergence using data from other regions.

Two key characteristics of the surveyed thalweg longitudinal profiles are the: (1) scale (spacing magnitude) and (2) spacing variability. A question that arises regarding the use of longitudinal profiles is what spacing magnitude is necessary to retain a high level of explained variance? Spacing can be described using a dimensionless channel width/spacing ratio, where the flow width is divided by the average spacing of the thalweg longitudinal profile. Results of a sensitivity analysis performed to assess the impact of spacing variability upon h_m/σ_z prediction equations are provided in Table 5-3. Using $\frac{3}{4}$, $\frac{1}{2}$, and $\frac{1}{4}$ of the longitudinal points varied the point density from an average of 0.28 to 1.05 m, with the average width/spacing ratio ranging from 7.9 to 2.2. Reducing the point density by 25 and 50 percent had a small but detectable effect on the predictions. Point density reductions of 75 percent ($\frac{1}{4}$ points) had a more substantial negative influence upon the predictions. The nature of the 25-percent reduction test (models 2 and 8) involved creating non-uniform point spacing; these models being slightly weaker than the 50%-reduction test (models 3 and 9) likely indicates the negative consequence of non-uniform point spacing. Additionally, low width/spacing ratio values were eliminated to examine whether lower point densities in the original dataset

negatively influence the prediction equations. Models were created eliminating data points with ratios <4 (models 5 and 11) and <5 (models 6 and 12). These models indicate that point density is a substantial influence upon the original models, with explained variance of 82 percent in n and 84 percent for f . However, other processes are occurring which may account for this disparity including a shift towards a skimming flow regime in the highest gradient reaches. Hence it was found that average point density could have been potentially reduced from an average width/spacing ratio of 7.9 to 4.1 with a small but detectable negative influence upon the predictions. Incorporation of any measurements with low ratios can have negative influences upon predictive models. Ultimately, longitudinal profiles should be measured with uniform spacing at sufficient scale for quantifying bed variability. In this study streams surveyed with average ratios >6 provided sufficient resolution to define the bed variability.

Table 5-3: Longitudinal spacing sensitivity analysis.

Longitudinal points	Model	Average spacing (m)	Average width/spacing	Resistance coefficient	Number of observations	R^2	F-value	β_0	β_1
All	1	0.28	7.9	n	59	0.75	168	0.470	-0.799
$\frac{3}{4}$	2	0.38	6.0	n	59	0.73	155	0.468	-0.791
$\frac{1}{2}$	3	0.55	4.1	n	59	0.73	156	0.460	-0.768
$\frac{1}{4}$	4	1.05	2.2	n	59	0.68	124	0.431	-0.713
All	5	0.286	8.4	n	53	0.79	190	0.530	-0.886
All	6	0.288	9.0	n	46	0.82	205	0.558	-0.920
All	7	0.28	7.9	f	59	0.80	222	38.9	-1.78
$\frac{3}{4}$	8	0.38	6.0	f	59	0.78	205	38.7	-1.77
$\frac{1}{2}$	9	0.55	4.1	f	59	0.79	209	37.3	-1.72
$\frac{1}{4}$	10	1.05	2.2	f	59	0.74	162	32.4	-1.60
All	11	0.286	8.4	f	53	0.82	227	47.1	-1.92
All	12	0.288	9.0	f	46	0.84	224	48.1	-1.93

Notes: β_0 and β_1 refer to the intercept and slope, respectively.

The inspection of residuals is a helpful tool for understanding the underlying processes of flow resistance generation as well as providing some insight into the applicability of a regression for prediction. Student residuals of the regression of n versus relative bedform submergence, h_m/σ_z , were plotted with reach descriptions provided for

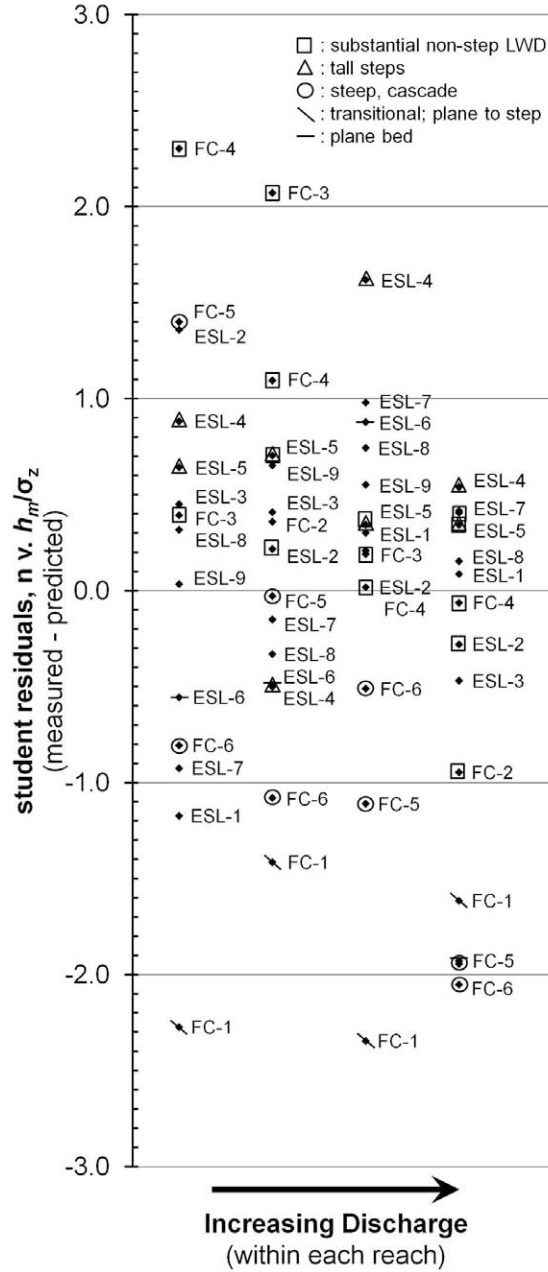


Figure 5-9: Student residuals of n versus h_m/σ_z , in natural logarithm space with reach ID labels and outlying reach descriptions.

outlying points (Figure 5-9). As discharge increases for a particular reach (up to bankfull discharge), the strength of the prediction using h_m/σ_z increases, with an exception being for the steepest reaches ($> \sim 18$ percent). In general, h_m/σ_z was found to underpredict n at lower flows, accurately predict n at higher flows in reaches with substantial non-step-forming instream wood and underpredict n in reaches with tall steps. Flow principally flowed over the step-forming instream wood during higher discharges; however, during low flow much of the discharge passed through the wood jams, complicating the flow characterization and contributing to resistance underprediction. Additionally, h_m/σ_z substantially overpredicts n at higher flows in reaches that are the most steep and narrow, consistently overpredicts n in the reach that displays a transitional bedform between step pool and plane bed, and tends to overpredict n in the plane-bed reach. Hence, it appears that relative bedform submergence is less effective for prediction in streams with substantial non-step-forming instream wood during lower flows, in the steepest channels, and in the transitional channel.

In the steepest reaches (FC-5 and FC-6) at the higher flows (Figure 5-10), relative bedform submergence overpredicted resistance. As discharge increases towards bankfull and the reach slope is greater than approximately 18 percent, these data indicate a possible shift towards a skimming regime, with a partial submergence of bedforms and a threshold reduction in flow resistance. In a full skimming regime, hydraulic jumps and aeration are eliminated and the flow becomes completely critical or supercritical (Comiti *et al.* 2009), instead of alternating between supercritical and subcritical flow in the nappe regime typical in these stream reaches. With reach-average Froude numbers of about 0.50 and only partial submergence of the bedforms (Figure 5-10), a full skimming regime is

not occurring; however, these steep, higher-flow measurements may have been collected in a transition zone. Comiti *et al.* (2009) found a sharp reduction in flow resistance in their mobile-bed laboratory study with a critical flow depth / average step height (h_c/z) ratio of 1.2 to 1.7; bankfull flows in FC-5 and FC-6 have h_c/z ratios of about 1.1 and 1.0, respectively. With a hypothesis of a shifting flow regime in the steepest reaches, four resistance measurements with residuals less than -1 (Figure 5-9), with slopes >18 percent, were eliminated from the h_m/σ_z model to reveal an increase in explained variance in f from 80 to 83 percent. Even though these reaches are well within the subcritical range, there appears to be a different resistance mechanism occurring in these steeper streams, at higher flows, than in the lower-gradient cascade and step-pool stream reaches.



Figure 5-10: Bankfull flow in reach FC-6.

Excluding resistance measurements for other reaches where bedform appears to not be the primary driver of flow resistance, as indicated by the residuals, can provide a greater understanding of the limits of relative bedform submergence for prediction in this dataset. Specifically, eliminating the reaches with substantial instream wood (>1 percent: ESL-2, ESL-5, FC-2, and FC-3), in addition to the measurements that are approaching skimming flow, increases the explained variance in f from 80 to 84 percent, with a sample size of 39.

A substantial amount of the flow resistance variation has been explained using variables describing bedform. However, the residual analysis indicates other potential sources of flow resistance beyond step resistance that may explain additional flow resistance, including instream wood. Additionally, variables describing bank variability may explain a substantial amount of flow resistance.

5.2.3 Bank Variability

The impact of bank variability on flow resistance was investigated using three measures in regression models (Figures 5-11 and 5-12, Table C-2): (1) average bank sinuosity (K_b); (2) horizontally-corrected average bank sinuosity (K_{bh}); and (3) the 2-D standard deviation of the residuals of a bank profile regression (σ_y). The horizontal length correction was tested to examine the influence of slope on computations. Using the entire dataset, bank sinuosity with a horizontal correction explained the most variance in the data ($R^2 = 0.47$ for n , 0.38 for f), with a slope correction to the straight-line distance increasing the explained variance by 4 percent. The bank variability variable σ_y , which is analogous to σ_z , explained little variance in the data alone ($R^2 = 0.13$ for f), although it

did explain up to 40 percent of the variance when normalized with the hydraulic radius. These variables show potential for explaining additional variance in multiple regression models when combined with relative bedform submergence.

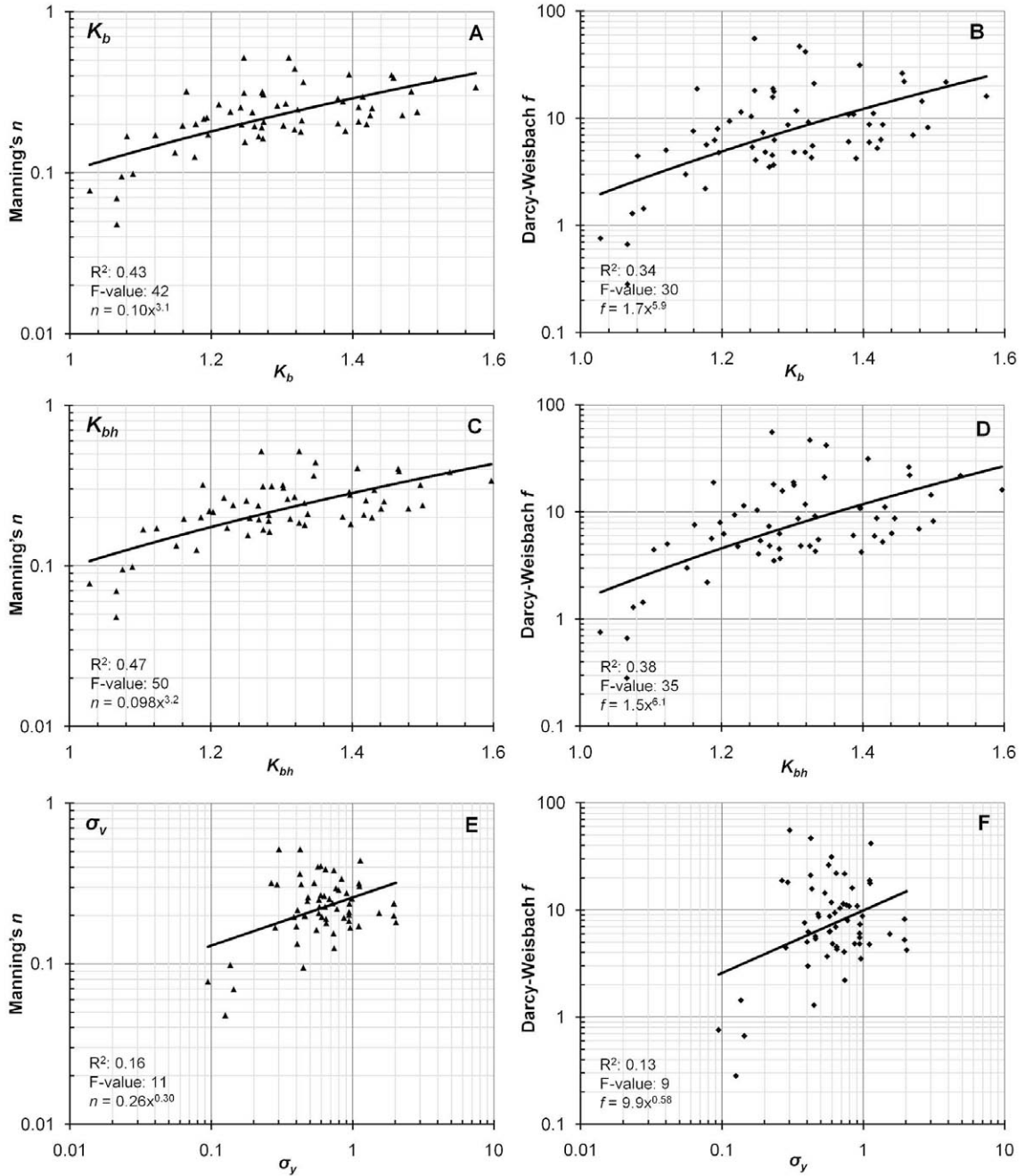


Figure 5-11: Resistance coefficients prediction with bank variability variables K_b , K_{bh} , and σ_y .

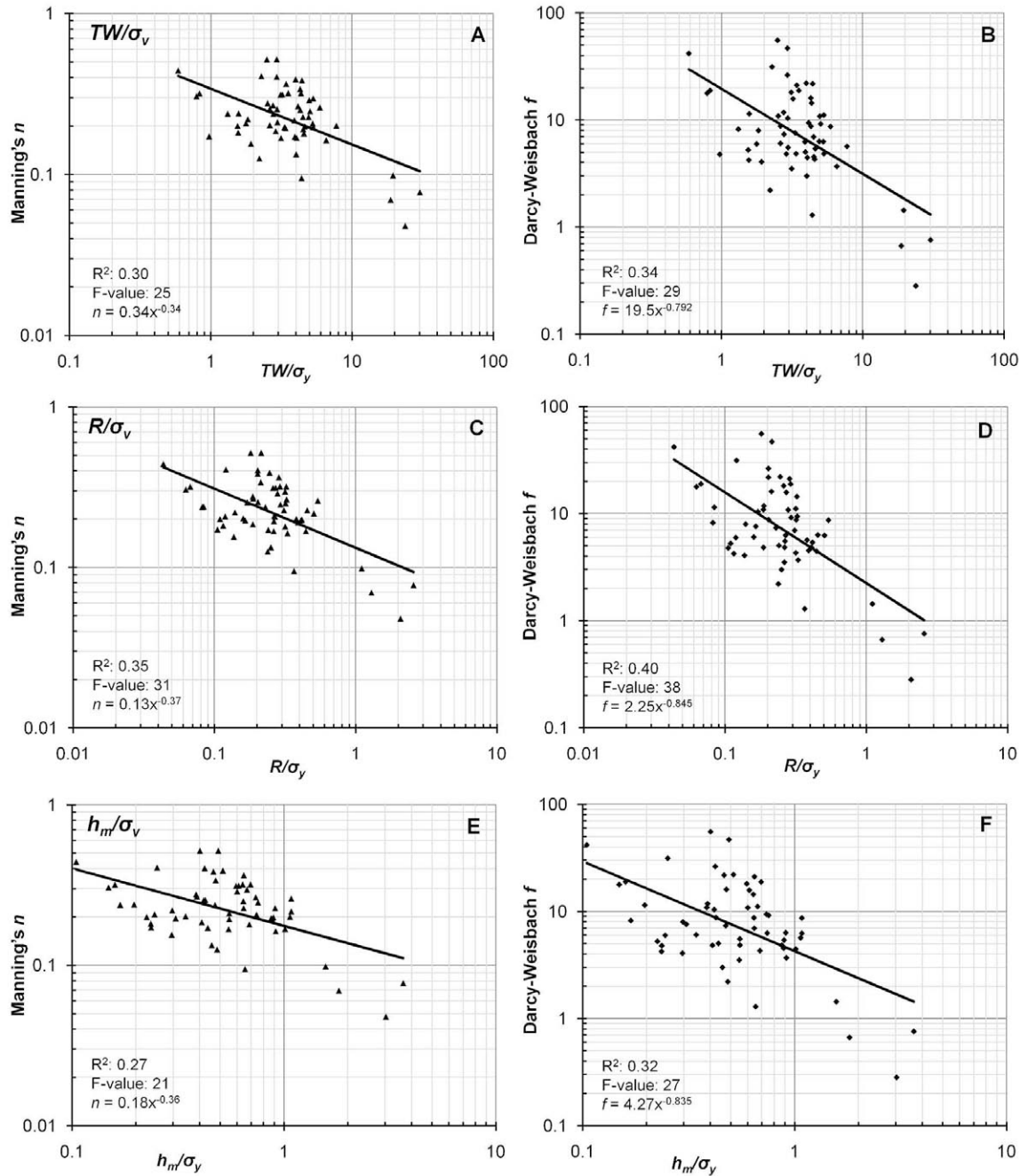


Figure 5-12: Resistance coefficients prediction with bank variability variables TW/σ_y , R/σ_y , and h_m/σ_y .

5.2.4 Instream Wood

The influence of non-step-forming instream wood on flow resistance was explored using univariate regression and a volumetric approach, with the variables computed as percentage ratios to the overall flow volume (V). Investigated variables included the instream wood volume (V_w); projected instream wood volume (V_{wp}), with an influence correction for angle of attack; branched instream wood volume (V_{wb}), with a correction for instream wood that still has branches attached; and thalweg-distance reduced instream wood volume (V_{wd}), to account for velocity variation and less effective resistance elements within the channel but distant from the highest velocities (Figures 5-13 through 5-15, Table C-3). Methods used to compute these variables are provided in the methods chapter. Additionally, combinations of the above variables were also investigated. Only non-step instream wood was included in this analysis, to avoid multicollinearity with relative bedform submergence. Low-flow measurements were excluded from the dataset, to minimize error induced by the LiDAR scans being collected during low flow. The extent of wood below the low flow water surface was estimated, with a greater proportion of the overall wood volume for low flow measurements resulting from these estimates and potentially reducing explained variance. The percent volume of the instream wood ranged from nearly 0 to 4.3 percent (FC-3). Reaches with instream wood percentages greater than 1 percent include ESL-2, ESL-5, FC-2, and FC-3.

In general, instream wood volume ratios explained little variance in the dataset, with the best correlation ($R^2 = 0.14$ for n) found with the branched, projected ratio (Figures 5-15A and 5-15B). Including a correction for branches increased the correlation;

strainers appear to be adding to overall flow resistance. Additionally, correcting for angle of attack with respect to the measured flow paths also increased correlation. A correction for distance from the thalweg did not enhance the correlation. Hence, inclusion of a variable quantifying branched, projected instream wood volume may have potential for explaining additional variance in multiple regression models, when combined with relative bedform submergence and bank sinuosity.

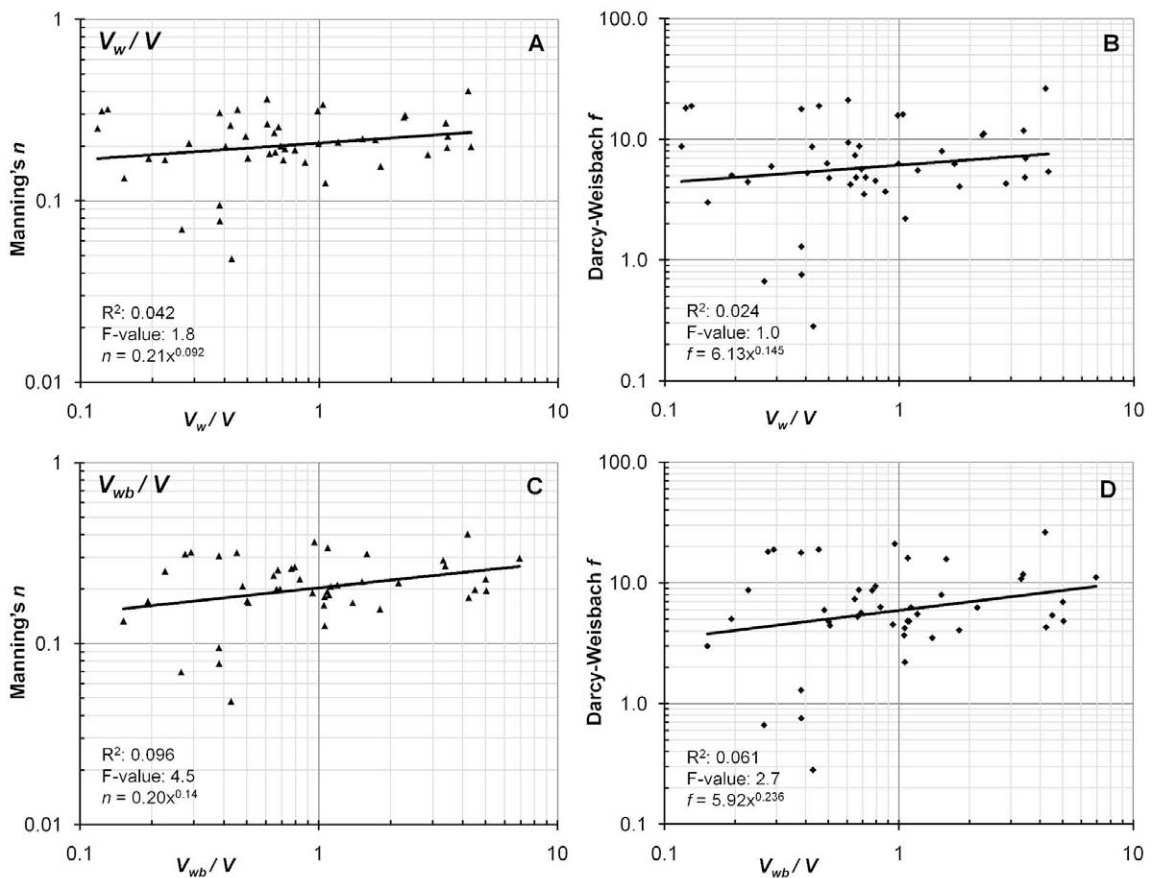


Figure 5-13: Resistance coefficients prediction with instream wood variables V_w/V and V_{wb}/V .

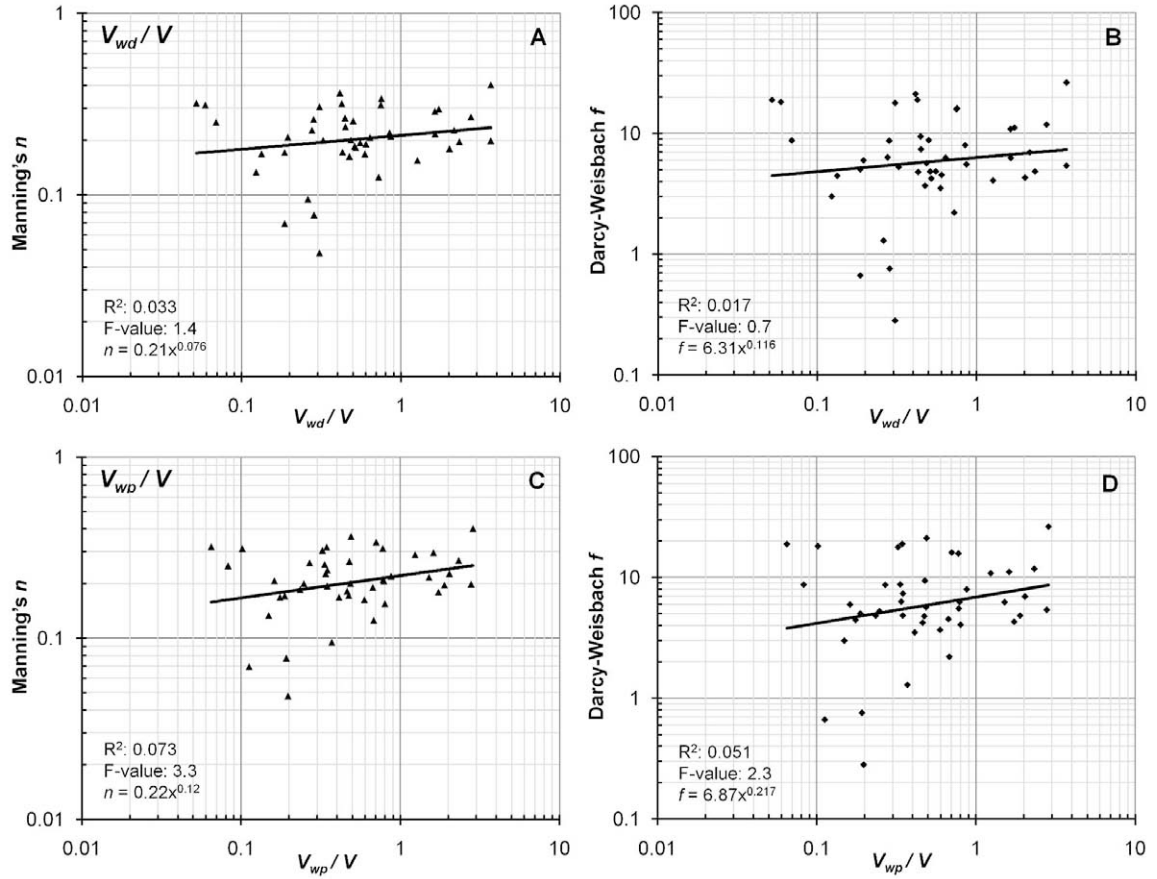


Figure 5-14: Resistance coefficients prediction with in-stream wood variables V_{wd}/V and V_{wp}/V .

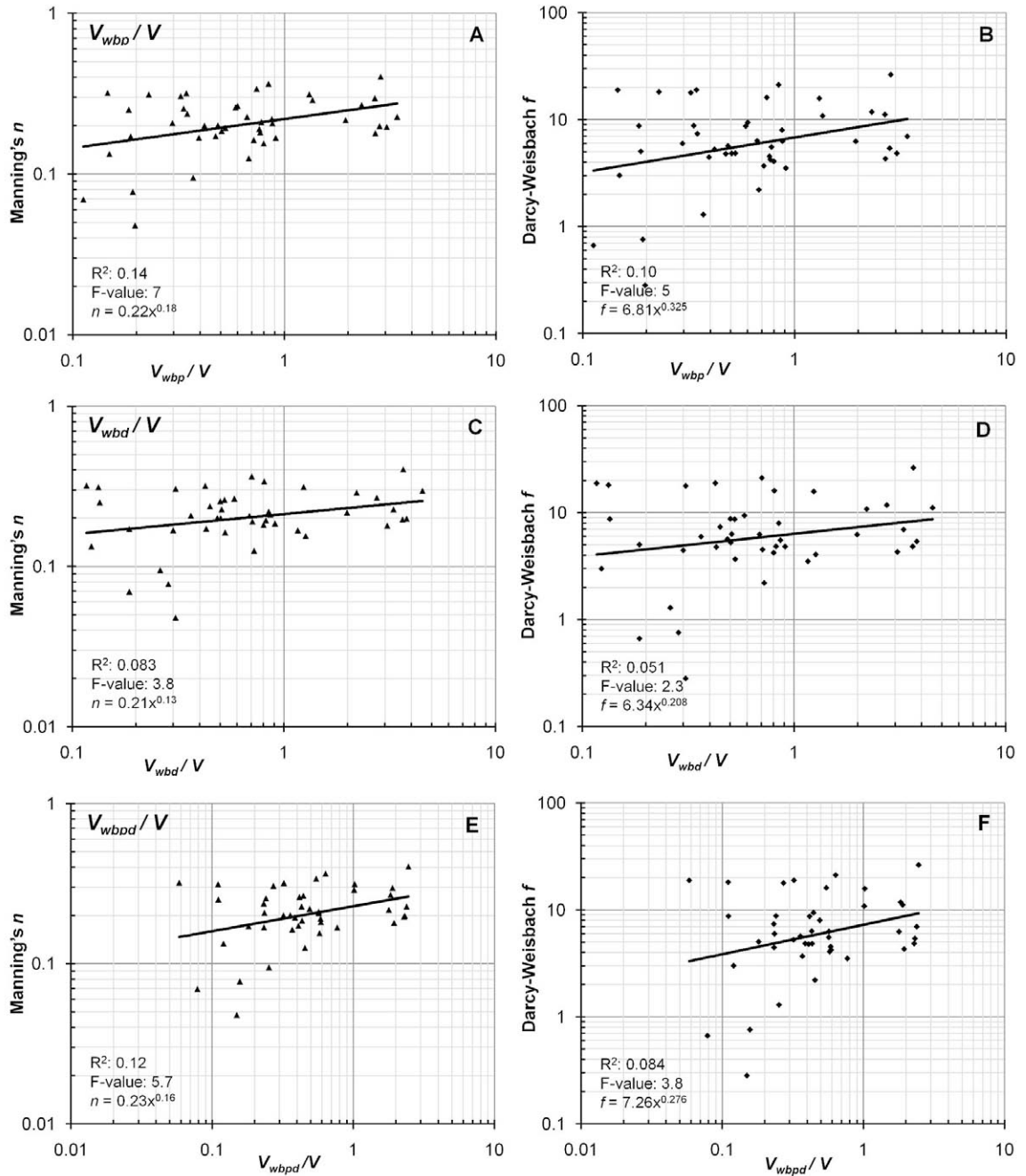


Figure 5-15: Resistance coefficients prediction with instream wood variables V_{wbp}/V , V_{wbd}/V , and V_{wbpd}/V .

5.3 Performance of Prior Prediction Methodologies

Existing methods for predicting flow resistance coefficients were tested to assess their relevance in these cascade, step-pool, and plane-bed stream reaches. Seven equations (Table 2-1) for predicting Manning's n and Darcy-Weisbach f in these stream types were tested with this dataset. Plots of measured versus predicted values are provided in Figure 5-16, for each tested relationship. The univariate regression models based upon relative bedform submergence are also provided (Figure 5-16-C and -D), for reference. They are referred to as the optimized models. An error analysis is provided for the dataset (Table 5-4), at several slope ranges, specifically less than 4 percent, 5 to 10 percent, 10 to 15 percent, and 15 to 20 percent. In general, existing flow resistance prediction equations tend to underpredict flow resistance in these stream reaches. Overall, the Jarrett (1984) equation provides a better fit than Soto and Madrid-Aris (1994) for Manning's n , while the equation developed by Aberle and Smart (2003) provides the best fit for the Darcy-Weisbach f . Relationships that rely solely upon the relative grain submergence, such as Bathurst (1985) and Lee and Ferguson (2002), performed the most poorly for these stream reaches. For measurements with slopes less than 10 percent, n was best predicted by Jarrett (1984), while Soto and Madrid-Aris (1994) provided better predictions at slopes from 10 to 20 percent. The relationship developed by Mussetter (1988) provided the best predictions of f at slopes less than 5 percent, while Aberle and Smart (2003) provided the best predictions for slopes from 5 to 20 percent.

Table 5-4: Error analysis of tested resistance relationships, by slope.

Friction slope (%), S_f	Number of points	Manning's n						Darcy-Weisbach f											
		Jarrett (1984)		Soto and Madrid-Aris (1994)		optimized.		Bathurst (1985)		Mussetter (1988)		Lee and Ferguson (2002)		Aberle and Smart (2003)		Comiti et al. (2007)		optimized	
		σ	e	σ	e	σ	e	σ	e	σ	e	σ	e	σ	e	σ	e	σ	e
All	59	0.078	16	0.083	-29	0.063	-6	11	94	10	31	11	96	7.6	35	8.2	72	7.5	-23
< 5	4	0.023	-31	0.015	-226	0.016	-18	0.45	70	0.36	-48	0.47	98	0.36	70	0.40	86	0.29	-37
5 – 10	28	0.067	17	0.073	-28	0.057	-8	7.1	94	7.2	19	7.1	96	5.4	35	6.9	74	5.1	-26
10 – 15	18	0.076	27	0.068	-2	0.053	8	10	97	10	55	10	97	7.9	42	7.7	71	7.5	3
15 – 20	9	0.11	14	0.090	2	0.081	-22	17	97	15	57	16	95	13	6	12	62	13	-55

Notes: σ = standard deviation of the prediction residuals and e = average percentage error of the prediction (measured – predicted).

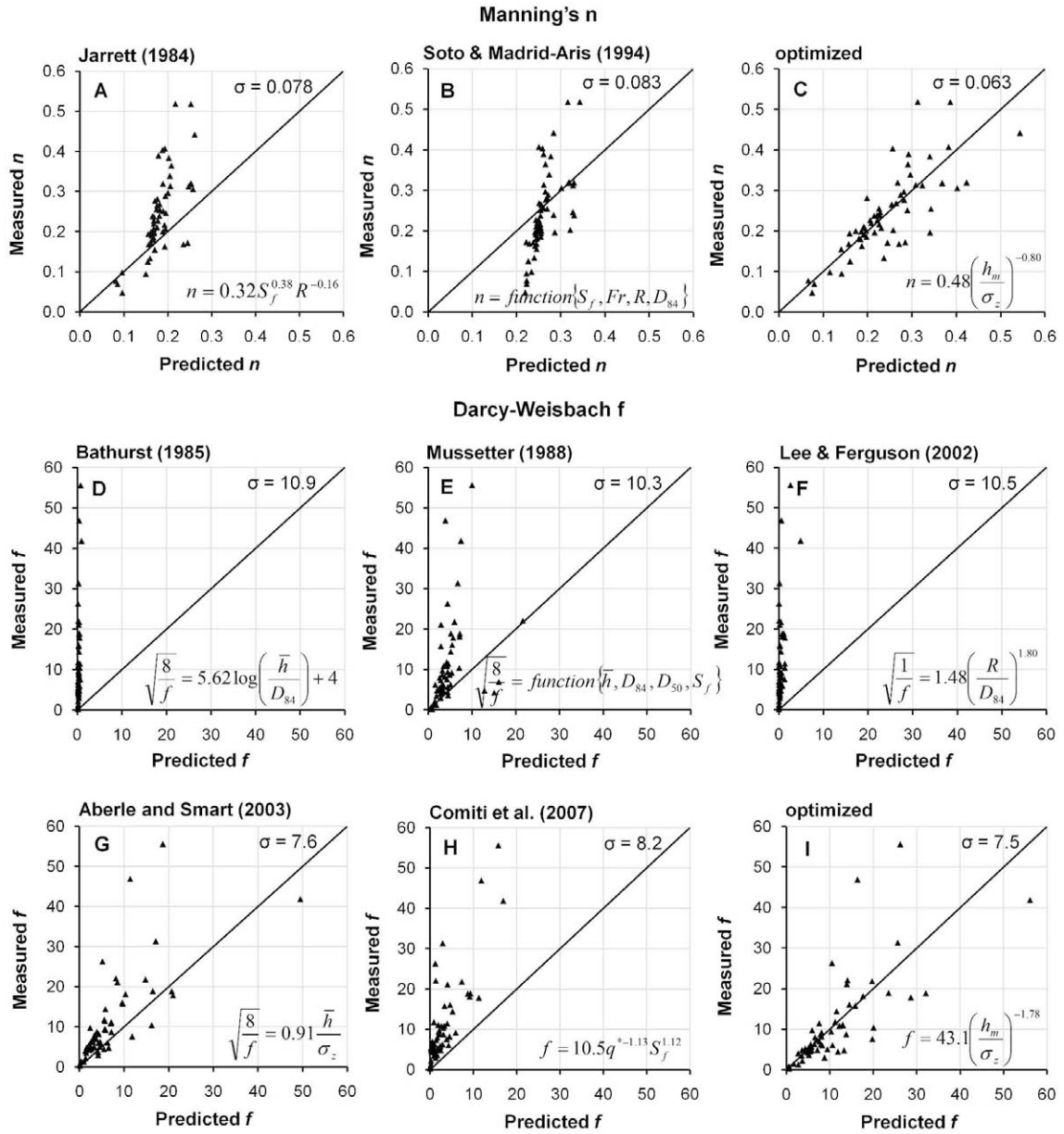


Figure 5-16: Flow resistance coefficients prediction testing, using Fraser database.

Existing flow resistance prediction equations were found to typically overpredict n at lower-resistance (lower-gradient) streams and underpredict n in higher-resistance streams. Of the two methods for predicting Manning's n , the Jarrett (1984) equation provides a better fit to the entire dataset. However, on steeper slopes (>10 percent) the equation developed by Soto and Madrid-Aris (1994) performed better (Table 5-4), which

is not unexpected considering the Jarrett equation was developed in streams with slopes less than 3.4 percent (Table 2-1). As shown in Figure 5-15-A, the Jarrett equation tends to predict fairly well for streams with lower flow resistance and predicts much more poorly in streams with Manning's n values greater than 0.17. This is understandable considering that the highest n measured in Jarrett's dataset was 0.16; this result indicates that extrapolation of the Jarrett equation into step-pool and cascade streams, where the Manning's n is typically greater than 0.16, is likely inappropriate and will substantially underestimate actual flow resistance. Though the heavily-parameterized Soto and Madrid-Aris equation provides a better prediction than Jarrett's equation in steeper reaches, this relationship fits the dataset poorly (Figure 5-16B) and is also likely inappropriate for application in step-pool and cascade channels.

Existing flow resistance prediction equations were also found to typically underpredict f . Equations that rely solely upon the relative grain submergence (Bathurst 1985; Lee and Ferguson 2002) performed least well in these stream reaches. The relatively poor performance of the Bathurst equation (Figure 5-16-D, Table 5-4) is not unexpected since it was developed in different stream types, at slopes less than 3.7 percent. It was shown to provide more accurate predictions in plane-bed reaches. However, the Lee and Ferguson equation was developed for step-pool and cascade streams in a similar slope range, using both field and laboratory data. Importantly, these steps (Lee and Ferguson 2002) were typically formed by clasts, not a combination of clasts and instream wood, as is the case for the Fraser data. This may explain the poor performance and illustrates that the usefulness of an explanatory variable that explains flow resistance in steps formed by both clasts and instream wood, and clasts alone. The

Mussetter (1988) equation, which relies upon \bar{h}/D_{84} as well as the ratio D_{84}/D_{50} and slope, performed better than methods that rely solely upon relative grain submergence, but substantially underpredicted flow resistance in the Fraser streams for slopes greater than 10 percent. The equation developed by Comiti *et al.* (2007) applied fairly well to the Fraser dataset but consistently underpredicted the flow resistance (Figure 5-16-H). This equation also relies upon the bed-material grain size, in combination with the unit discharge and slope.

Of the previously available methods, the equation developed by Aberle and Smart (2003) provided the best fit to the measured Darcy-Weisbach f values. This is surprising considering that the dataset was developed entirely in the laboratory, on self-formed alluvial steps as presented in Rosport (1997) and Koll (2002). This reinforces the finding that relative bedform submergence is a powerful tool for flow resistance prediction in these stream types. A key advantage of the standard deviation of the residuals of a bed profile regression in predicting resistance in these stream types is that it captures the influence of the largest clasts, the joint influence of clasts and instream wood, and bedrock in forming steps. Additionally, Aberle *et al.* (2010) found that the standard deviation of 3-D bed elevations in a sand-bedded river can be closely correlated with discharge. The use of standard deviations of bed elevations for prediction may be relevant for general use in open-channel flow where bedforms are present and contribute substantially to flow resistance.

5.4 Resistance Prediction Using 3-D Spatial Analysis

The LiDAR dataset provides a unique opportunity to explore the dataset using 3-D measures of geometric variability. Specifically, the variation in depth and detrended elevations were investigated to assess correlation with flow resistance. For each of the 44 non-low-flow resistance measurements, variation was assessed for both the entire channel width and for the centered 50 percent of the channel width, to eliminate bank effects. These variables are analogous to the 2-D variation terms quantified using the longitudinal profiles; the 3-D variables incorporate elevation and depth variability due to bedform, instream wood, and, in the case of the full channel width analysis, bankform. Variables of this form include variability across the y (width) dimension but have a lower resolution in the deeper portions of the channels, where the gridded laser theodolite data were used to fill gaps in the LiDAR dataset. Detrending was necessary, to exclude variation due to slope. With the 2-D data, it was found that not detrending the data reduced explained variance for f versus h_m/σ_z from 80 to 58 percent.

Example plots illustrating depth variability for the full width and 50-percent width are provided in Figure 5-17 for reach ESL-1 during bankflow conditions. Depth variability grids for each non-low-flow resistance measurement are provided in Appendix D. The pixel size of these data is 5 cm, which provides from 3,900 to 32,300 depth measurements per reach. These grids show depth variability due to bedform, large clasts, instream wood, and bank effects (Figure 5-17). Like the 2-D data, these 3-D spatial data (Table C-4) explain a substantial amount of the variance in both n and f (Figures 5-18 and 5-19). With variation that includes bank effects, up to 69 percent of the variance was explained using h_{a3}/σ_{z3} . Excluding bank effects increases the explained variance using

h_{a3}/σ_{z3} to 77 percent for n and 81 percent for f , with these 44 observations. In comparison, h_m/σ_z explains 74 percent of the variation in n and 80 percent of the variation in f with the same data. Hence, the best single variable for explaining flow resistance in this dataset is the 50%-width 3-D relative resistance element submergence term h_{a3}/σ_{z3} . The increase in explained variance by elimination of bank effects indicates that depth and elevation variability predict poorly in the near-bank zone of these streams in comparison to thalweg depth and elevation variability. The marginal increase in explained variance between the 2-D and 3-D measures indicates a non-linear contribution of individual flow resistance elements to overall flow resistance. A strong correlation ($r = 0.91$) exists between h_m/σ_z and h_{a3}/σ_{z3} (Figure 5-20) indicating redundancy between bed variability defined using longitudinal profiles and variability as defined through the 3-D spatial analysis.

Regression plots of the 3-D variables suggested potential clusters of sites within the dataset (Figures 5-18 and 5-19). As with relative bedform submergence, the inspection of residuals can be helpful in understanding underlying processes contributing to flow resistance as well as identify potential grouping within the non-low-flow dataset. An examination of Student residuals of the regression of n versus h_{a3}/σ_{z3} , with reach descriptions (Figure 5-21) indicated that h_{a3}/σ_{z3} underpredicted n in reaches with substantial non-step-forming instream wood and overpredicted n in steep-cascade and plane-bed reaches. The plane-bed reaches were more substantially and consistently overpredicted using the 3-D variables.

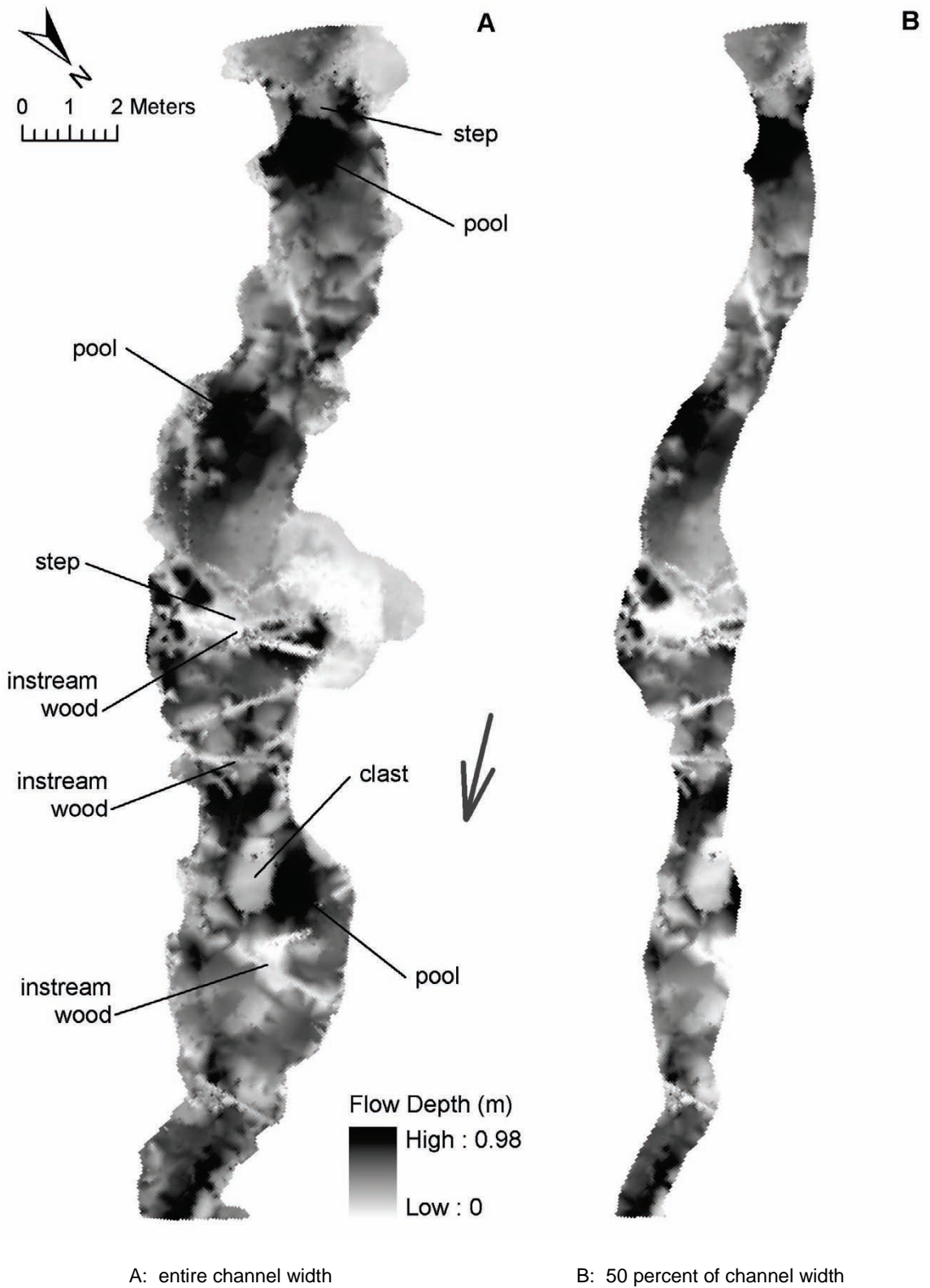


Figure 5-17: Depth variability for bankfull flow, reach ESL-1. Pixel size is 5 cm, for a total of 32,300 geo-referenced points.

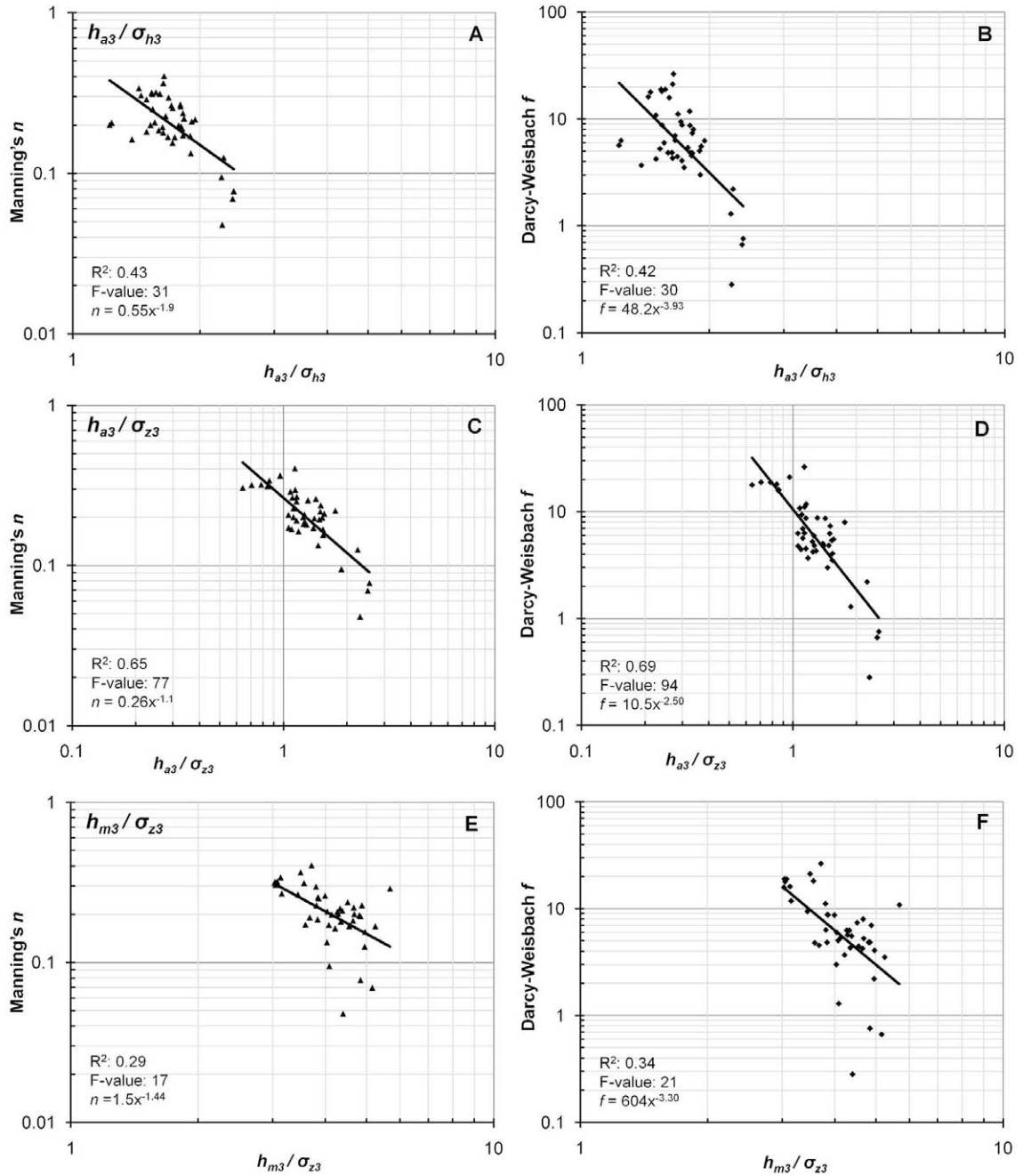


Figure 5-18: Resistance coefficients prediction with 3-D variables h_{a3}/σ_{h3} , h_{a3}/σ_{z3} , and h_{m3}/σ_{z3} , for the entire channel width.

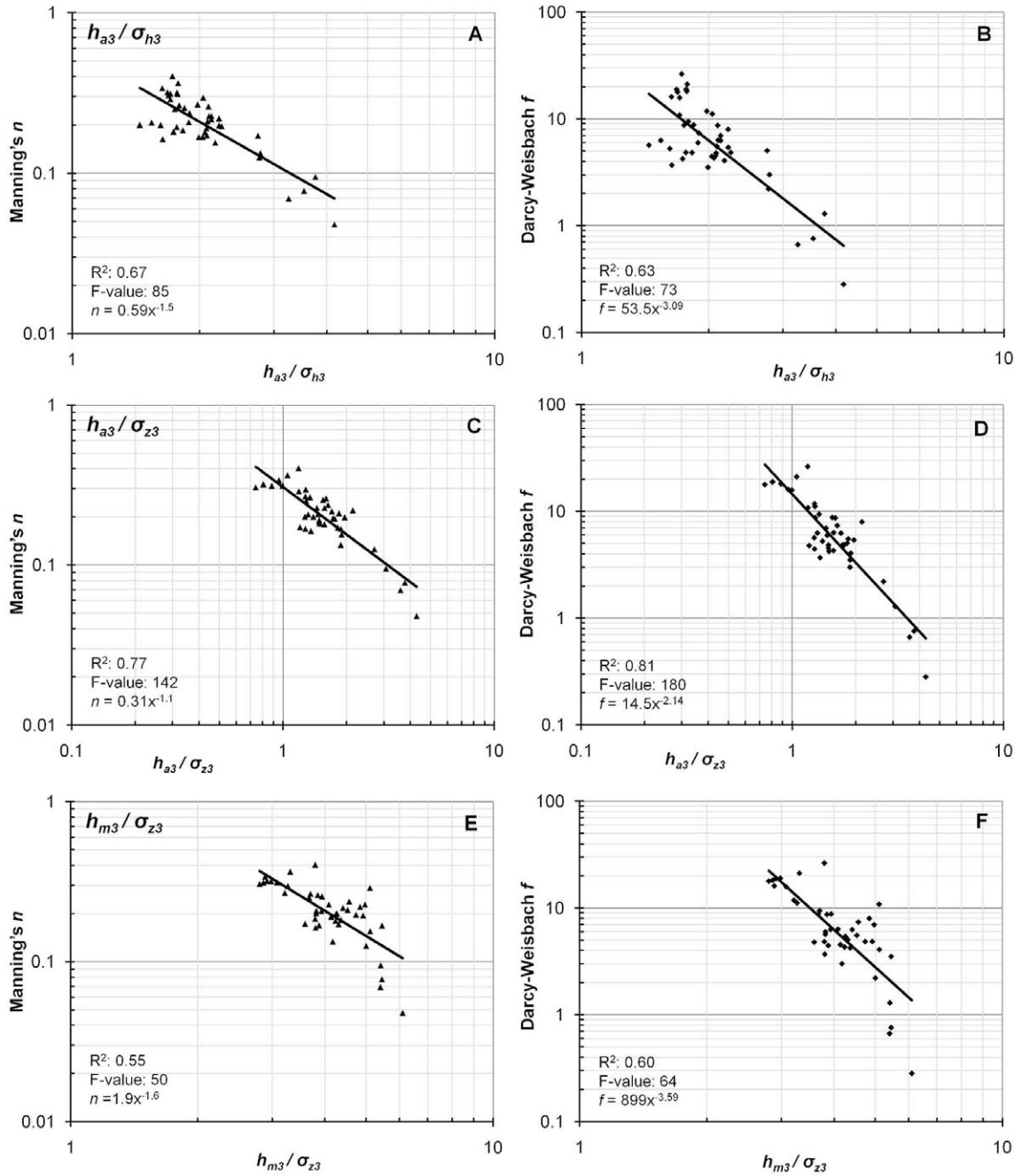


Figure 5-19: Resistance coefficients prediction with 3-D variables h_{a3}/σ_{h3} , h_{a3}/σ_{z3} , and h_{m3}/σ_{z3} , for the center 50 percent of the channel width.

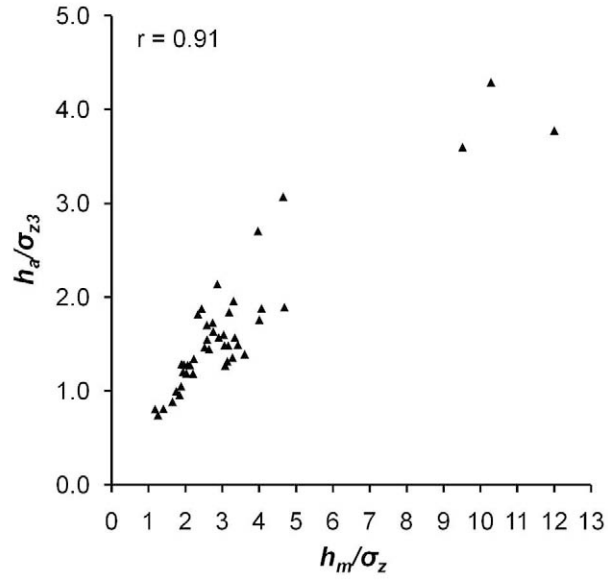


Figure 5-20: Correlation of relative bedform submergence with 3-D depth variability.

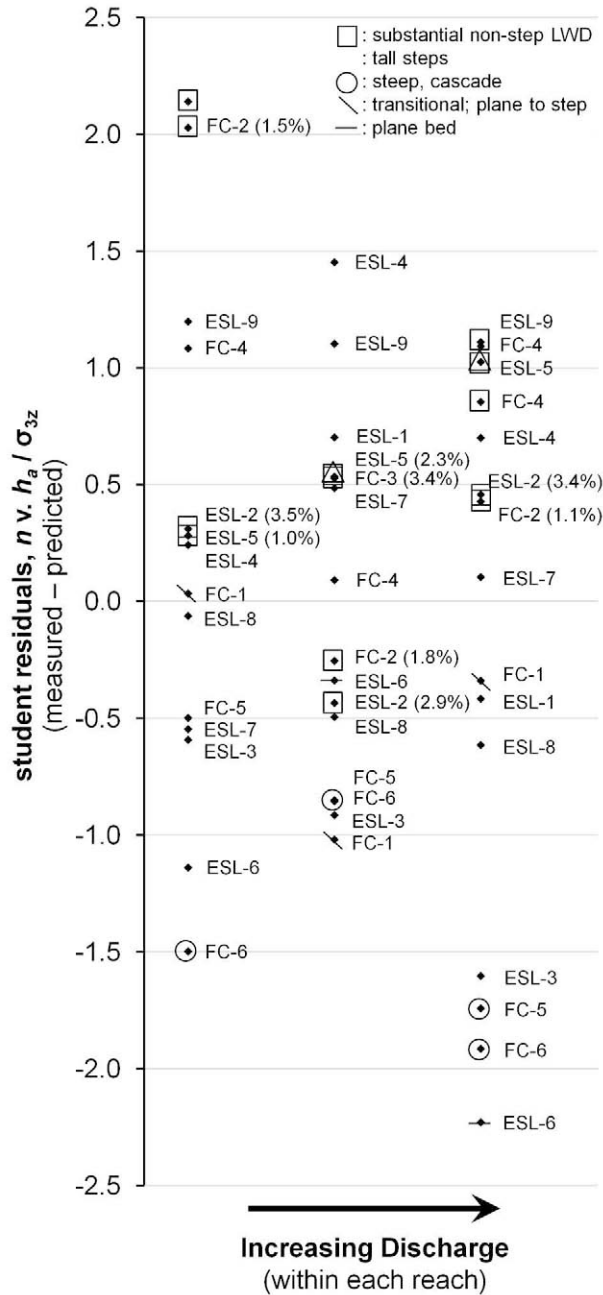


Figure 5-21: Student residuals of n versus h_m/σ_{z3} , in natural logarithm space with reach ID labels and outlying reach descriptions.

Flow resistance coefficients in FC-5 and FC-6, the steepest reaches, were consistently overpredicted. Exclusion of the measurements with the steepest slopes (>18 percent) increased the explained variance in f from 81 to 83 percent (40 points in the

dataset). Excluding the reaches with instream wood percentages greater than 1 percent, in addition to the reaches with the steepest slopes, increased the explained variance to 88 percent (28 points in the dataset). Excluding the plane-bed reach in addition decreased the explained variance to 74 percent (twenty-five points in the dataset). Hence, 3-D measurements of variability also show that flow characteristics may be shifting towards a skimming regime in the steepest reaches, and that flow resistance due to instream wood is ineffectively accounted for by variability in depth and elevation.

5.5 Multivariate Regression with Bedform, Bankform, and Instream Wood

The simple linear regression models have shown that bedform variables best explain the variance in flow resistance but provide poorer predictions in streams with substantial instream wood and bank effects. Using the variables describing bedform, bankform, and instream wood that were shown through simple linear regression to provide the greatest explanation of variance, multivariate regression models were developed to assess how much overall variance in the dataset can be explained with a suite of these descriptors.

A summary of the best-subset analyses for regression models describing bedform and bankform is provided in Table 5-5. For multivariate regressions with variables describing bedform and bankform, the following regression for Manning's n was developed, with 83 percent of the variance explained using all 59 resistance measurements:

$$n = 0.270 \left(\frac{h_m}{\sigma_z} \right)^{-0.645} (K_{bh})^{1.57} \quad (5-2)$$

Table 5-5: Multivariate regression results with entire database (n = 59), using variables describing bedform and bankform. Predictors significant with $\alpha = 0.01$.

Manning's n							Darcy-Weisbach f								
R^2	Cp	Adj. R^2	F-value	h_m/σ_z	R/σ_z	K_b	K_{bh}	R^2	Cp	Adj. R^2	F-value	h_m/σ_z	R/σ_z	K_b	K_{bh}
0.75			155	X				0.80			222	X			
0.76			178		X			0.80			221		X		
0.43			42			X		0.34			30			X	
0.47			50				X	0.38			35				X
0.84	2.3	0.83	142		X		X	0.84	-0.7	0.83	144	X			X
0.83	2.6	0.83	141		X	X		0.84	-0.5	0.83	144	X		X	
0.83	2.7	0.83	141	X			X	0.83	1.1	0.83	139		X		X
0.83	3.2	0.83	140	X		X		0.83	1.3	0.83	138		X	X	

Abbreviations: Adj. = Adjusted and Cp = Mallows' Cp.

Both variables are significant with $p < 0.0001$. With a correlation coefficient of -0.53 between relative bedform submergence and bank sinuosity (Figure 5-22), these two variables have a fairly weak linear relationship. For the Darcy-Weisbach f , the following regression explains 83 percent of the variance:

$$f = 17.1 \left(\frac{h_m}{\sigma_z} \right)^{-1.55} (K_{bh})^{2.34} \quad (5-3)$$

Both variables are significant, with a $p < 0.0001$ for relative bedform submergence and 0.0004 for bank sinuosity. Plots of measured versus predicted resistance coefficients are provided in Figure 5-23.

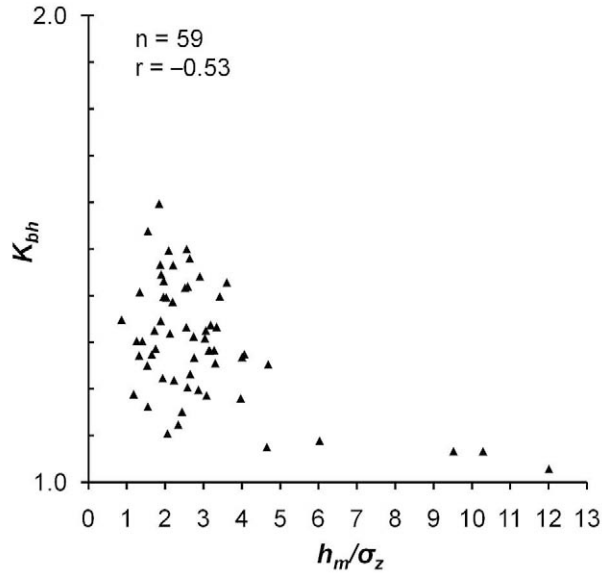


Figure 5-22: Correlation of relative bedform submergence with bank sinuosity.

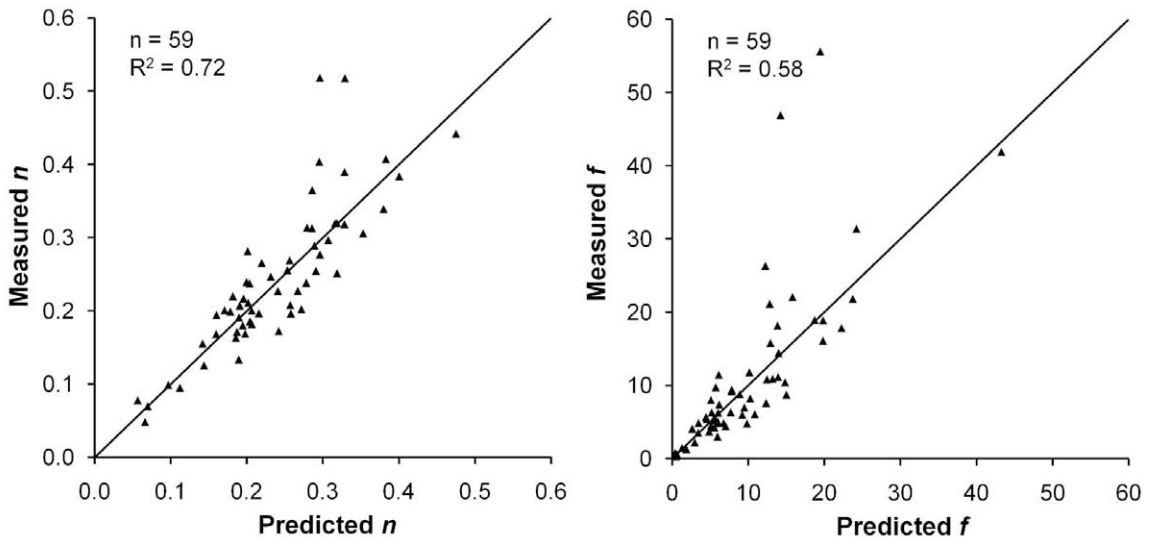


Figure 5-23: Measured versus predicted resistance coefficients, with predictors describing bedform and bankform.

A summary of the best-subset analyses for regression models describing bedform, bankform, and instream wood is provided in Tables 5-6 and 5-7. The following regression for Manning’s n was developed, with 87 percent of the variance explained with a dataset of forty-four resistance measurements (excluding low flow):

$$n = 0.288 \left(\frac{h_m}{\sigma_z} \right)^{-0.646} (K_{bh})^{1.28} \left(\frac{V_{wb}}{V} \right)^{0.063} \quad (5-4)$$

The variables are significant with $p < 0.0001$ for h_m/σ_z , 0.0004 for K_{bh} and 0.04 for V_{wb}/V . Using the 3-D spatial analysis results, the following regression equation was developed for n :

$$n = 0.242 \left(\frac{h_{a3}}{\sigma_{z3}} \right)^{-0.845} (K_b)^{0.976} \left(\frac{V_{wp}}{V} \right)^{0.068} \quad (5-5)$$

which explained 85 percent of the variance in the data. The variables are significant with $p < 0.0001$ for h_{a3}/σ_{z3} , 0.0086 for K_b , and 0.03 for V_{wp}/V . Correlations of h_m/σ_z versus V_{wb}/V and K_{bh} versus V_{wb}/V are shown in Figure 5-24. Correlations of h_{a3}/σ_{z3} versus K_b and V_{wb}/V are also provided. Relative bedform submergence and the 3-D analogy, h_{a3}/σ_{z3} , have low correlations with instream wood volume ratios. Bank variables and instream wood volume ratios also show low correlations. The most substantial correlation, with a still relatively weak $r = -0.58$, was found between h_{a3}/σ_{z3} and bank sinuosity. For the Darcy-Weisbach f , the following regression equation explains 87 percent of the variance:

$$f = 17.9 \left(\frac{h_m}{\sigma_z} \right)^{-1.52} (K_{bh})^{2.00} \left(\frac{V_w}{V} \right)^{0.109} \quad (5-6)$$

All variables are significant at $\alpha = 0.10$, with a $p < 0.0001$ for relative bedform submergence, 0.0051 for K_{bh} , and 0.074 for V_w/V . When performing a regression using the 3-D term, bank sinuosity lost significance. Using variables describing 3-D bed variability and instream wood, the following model provided the most explained variance with two independent variables ($R^2 = 0.84$):

$$f = 15.4 \left(\frac{h_{a3}}{\sigma_{z3}} \right)^{-2.15} \left(\frac{V_w}{V} \right)^{0.17} \quad (5-7)$$

The two variables are significant at $\alpha = 0.05$, with a $p < 0.0001$ for h_{a3}/σ_{z3} and 0.0059 for V_w/V . Significant models of this form are shown in Table 5-8. Plots of measured versus predicted resistance coefficients, for Equations 5-4 through 5-7, are provided in Figure 5-25.

Table 5-6: Multivariate regression results for Manning's n with exclusion of low-flow data ($n = 44$), using variables describing bedform, bankform, and instream wood. Predictors significant with $\alpha = 0.05$.

R ²	Cp	Adj. R ²	F-value	Bedform		Bankform		Instream Wood				
				h_m/σ_z	h_{a3}/σ_{z3}	K_b	K_{bh}	V_w/V	V_{wb}/V	V_{wp}/V	V_{wbd}/V	
0.77			77		X							
0.04			1.8					X				
0.10			4.5						X			
0.07			3.3							X		
0.08			3.8									X
0.87	-2.8	0.86	91	X			X		X			
0.87	-2.7	0.86	91	X		X			X			
0.87	-2.6	0.86	91	X			X	X				
0.87	-2.5	0.86	91	X		X		X				
0.87	-2.4	0.86	90	X			X					X
0.85	3.7	0.84	76		X	X				X		
0.85	3.7	0.84	76		X		X			X		

Table 5-7: Multivariate regression results for Darcy-Weisbach f with exclusion of low-flow data ($n = 44$), using variables describing bedform, bankform, and instream wood. Predictors significant with $\alpha = 0.10$.

R ²	Cp	Adj. R ²	F-value	Bedform	Bankform		instream wood	
				h_m/σ_z	K_b	K_{bh}	V_w/V	V_{wd}/V
0.02			1				X	
0.017			0.7					X
0.87	-2.2	0.86	91	X		X	X	
0.87	-2.2	0.86	91	X	X		X	
0.87	-1.9	0.86	90	X		X		X
0.87	-1.8	0.86	90	X	X			X

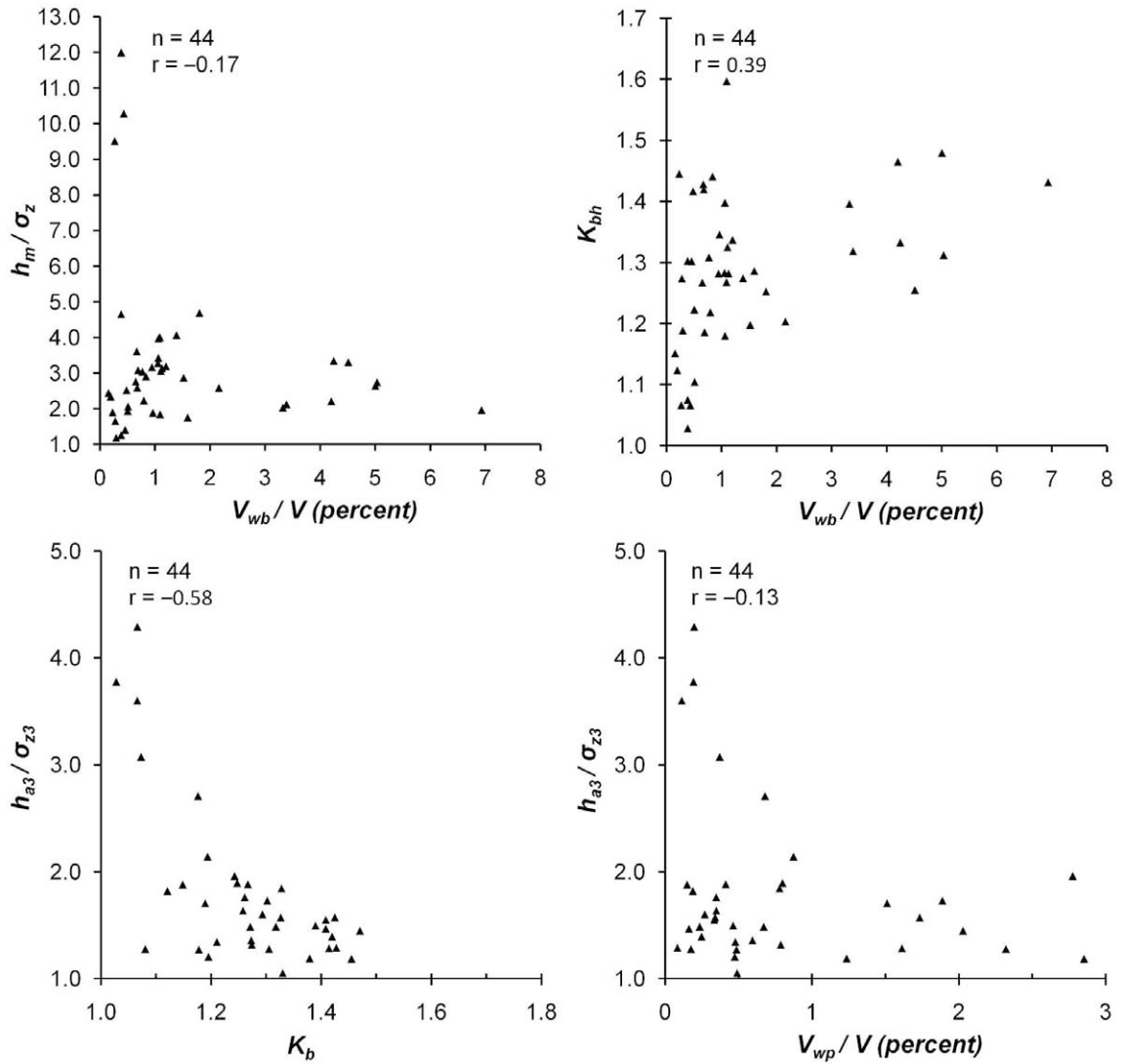


Figure 5-24: Correlation of predictors describing bedform, bankform, and instream wood ratios.

Table 5-8: Multivariate regression results for Darcy-Weisbach f with exclusion of low-flow data ($n = 44$), using variables describing 3-D bedform and instream wood. Predictors significant with $\alpha = 0.05$.

R^2	C_p	Adj. R^2	F-value	Bedform	instream wood			
				h_{a3}/σ_{z3}	V_w/V	V_{wd}/V	V_{wp}/V	V_{wbp}/V
0.81			180	X			X	
0.051			2.3					X
0.05			3.8					X
0.84	3.8	0.84	110	X	X			
0.84	4.0	0.83	109	X			X	
0.84	4.2	0.83	109	X				X
0.84	4.4	0.83	108	X		X		

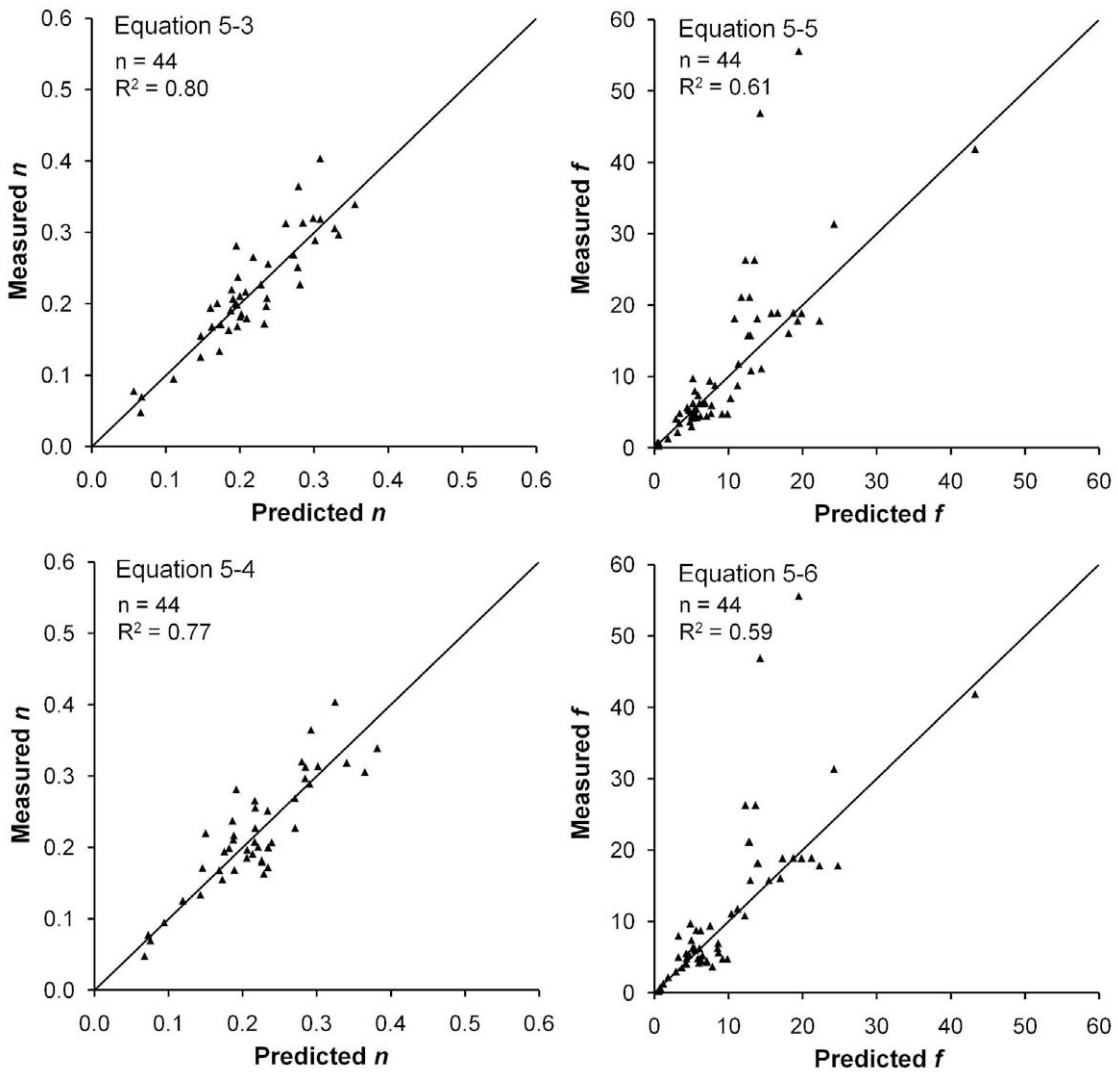


Figure 5-25: Measured versus predicted resistance coefficients, with predictors describing bedform, bankform, and instream wood.

In contrast to the simple linear regressions, where f was predicted with greater R^2 , both n and f were predicted with the same explained variance for both the 2- and 3-term predictor models. With up to 87 percent of the variance explained using variables that directly relate to sources of flow resistance, models generated from this dataset predict flow resistance coefficients with a greater explained variance than those generated in the research of Comiti *et al.* (2007), with up to 78 percent of the variance explained through reliance upon the dimensionless flow rate (unit discharge normalized by D_{84} grain size) and slope, and David *et al.* (2010), with up to 77 percent of the variance explained through slope and wood load. The inclusion of the plane-bed data substantially increases the explained variance of the dataset, from 78 to 87 percent for both n and f . These plane-bed data should not be considered outliers since they fall into a single log-space trend for the individual predictors and, hence, appear to be all part of the same population. There is observed bed variability in the plane-bed stream; this variability is an order of magnitude less than the bedforms quantified in the steeper streams, with a parallel decrease in flow resistance.

The significance levels of the explanatory variables in both the simple and multivariate regressions indicate that bedform flow characteristics, from form and spill resistance, are by far the greatest contributor to overall flow resistance, followed by form resistance generated by bankform, and lastly, by form resistance induced by non-step instream wood. The measured versus predicted plots indicate more accurate prediction of Manning's n for this dataset; this is in contrast to the typical preference of researchers for working with the Darcy-Weisbach f (Hey 1979; Comiti *et al.* 2007; David *et al.* 2010).

In general, there is relatively low correlation between explanatory variables, with the most substantial relationships found between bankform and both the 2-D and 3-D versions of bedform variables. The use of relative bedform submergence (h_m/σ_z) provides the best models for predicting n and f , outperforming both R/σ_z and the 3-D term h_{a3}/σ_{z3} . The use of horizontally-corrected bank sinuosity over non-corrected sinuosity in these steep streams consistently created slightly better models (as defined using Mallows' Cp), but did not substantially increase the explained variance of the multivariate regressions. In general, instream wood terms were less significant for prediction of f , than n . The best predictions of f obtained with instream wood terms used a simple percent volume term, without corrections for branches, angle of attack, and distance from thalweg. The simple instream wood percent volume term also performed well for n , however, the branch-corrected volume term performed slightly better. The use of a correction for the angle of attack was found to perform well when used with h_{a3}/σ_{z3} , but otherwise performed less well than other instream wood ratios.

Through these simple and multivariate regressions, the prediction of resistance coefficients has been explored. However, the primary use of resistance coefficients is for the estimation of velocity; the direct estimation of average reach velocity from the Fraser dataset is addressed in the following section.

5.6 Velocity Prediction

A multivariate regression model for predicting average reach velocity was developed using the explanatory variables found in the Manning's and Darcy-Weisbach equations: R and S . Relative bedform submergence, h_m/σ_z , was used as the roughness

term, since it has been shown to provide good prediction characteristics for this dataset though both simple linear and multivariate regressions. The relationship:

$$v = 1.37 \left(\frac{h_m}{\sigma_z} \right)^{0.78} R^{0.55} S^{0.40} \quad (5-8)$$

where v is the harmonic average reach velocity, provides the best fit ($n = 59$, $R^2 = 0.81$) to the dataset. Applying the best-performing 3-D spatial variable to all but the low-flow data provides the following equation ($n = 44$, $R^2 = 0.76$):

$$v = 2.10 \left(\frac{h_{a3}}{\sigma_{z3}} \right)^{0.95} R^{0.52} S^{0.42} \quad (5-9)$$

Analysis incorporating all data points indicates that, for the best fit to the measured average reach velocities using the hydraulic radius, slope, and the relative bedform submergence, the optimized exponent of R is 0.55, close to the exponent used in the Darcy-Weisbach equation (0.50) and more divergent from the exponent of the Manning's equation (0.67). The optimized exponent of S is 0.40, less than exponents used for both the Manning's and Darcy-Weisbach equations (0.50). These results using the entire dataset are plotted in Figure 5-26 alongside results presented by other researchers. Similar results were found using the 3-D term h_{a3}/σ_{z3} , using all but the low-flow data. With respect to the hydraulic radius, the best-fit exponent of 0.55 is substantially smaller than the 0.83 suggested by Jarrett (1984); and larger than the 0.40 computed by Dingman and Sharma (1997) in streams with slopes less than 4.2 percent and Lopez *et al.* (2007), who found that the most appropriate R exponent ranged from 0.77 to 0.82 in gravel-bed and mountain streams with slopes from 0.001 to 16 percent. In regard to slope, the best-fit exponent of 0.40 is substantially greater than the value of 0.17

suggested by Golubtsov (1969) for slopes over 0.4 percent, though less than the standard exponent of 0.5, as he suggested. Slope exponents less than 0.5 have also been suggested by Williams (1978), who found that an exponent of 0.28 provided the best fit for predicting bankfull discharge in streams with slopes less than 5 percent; Bray (1979), who found that an exponent of 0.29 provided the best fit in streams with slopes less than 1.5 percent; Jarrett (1984), who determined that the most appropriate exponent is 0.12; Dingman and Sharma (1997), who found the best exponent to be 0.34; and Lopez *et al.* (2007), who argued that this exponent may be close to 0.25. Additionally, Bjerklie *et al.* (2005) found that the use of a slope exponent of 0.33 reduced the variance of flow resistance estimates. Hence, the literature and this research indicate that, in higher gradient streams, the most appropriate exponent for the hydraulic radius can vary substantially, from 0.55 to 0.82, and that the slope should have an exponent less than 0.5, with a potential range of 0.12 to 0.40.

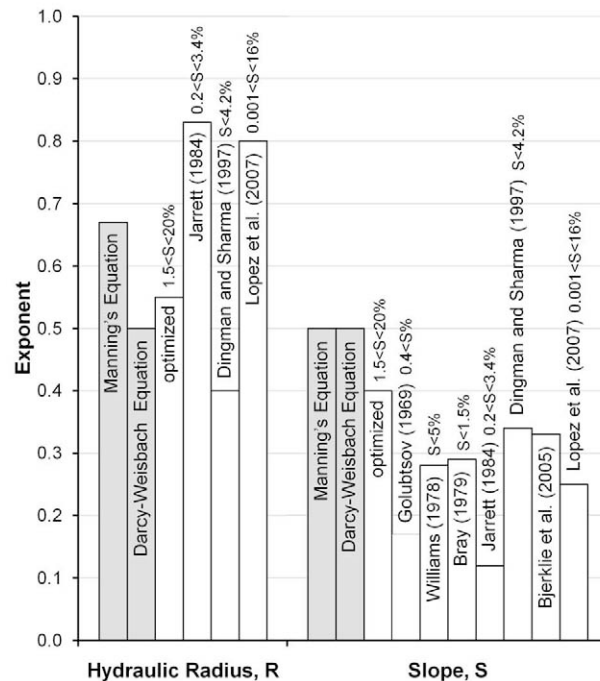


Figure 5-26: Most effective exponents of *R* and *S*.

5.7 Flow Path Influence on Resistance Estimates and Prediction

It was observed in the field that, due to rectangular section geometry, the deepest portion of the stream reaches was often not readily identifiable. Point velocities varied substantially across each section, with the locations of highest velocity in each section often varying by stage. The measured flow path lengths, as opposed to simply being defined by the deepest portion of the channel, instead followed the path of the estimated center of mass of the flow (Figure 3-6). These flow path lengths follow the deepest portion of the channel when it can be readily identified but vary in rectangular sections where a single maximum depth is not observed. In these areas, large clasts and instream wood divert the flow in a complex manner that varies by discharge. Surveying the longitudinal profiles along the observed flow paths, which is repeatable during any particular resistance measurement, has the advantage of providing the most hydraulically-representative reach lengths for a specific flow while defining what specific resistance elements are in high- and low-velocity zones within the stream channel. It has the disadvantage of not being known *a priori*, for prediction.

The impact of flow path variation can be substantial – the thalweg length varied by up to 21 percent for lesser flows. This can lead to overestimation of slope and underestimation of velocity, with the differences compounding the impact upon resistance coefficients. In the most extreme case, if the bankfull thalweg length of 12.5 m for ESL-5 was used for the resistance coefficient computation, instead of the measured length of 15.1 m, the Manning's n would be 0.51 instead of the 0.38. Discrepancies of

this magnitude can obscure potential statistical relationships, especially if the field methods are inconsistent.

The field techniques of researchers who have collected data in high-gradient streams have not addressed variation in flow paths by discharge, with lower flows corresponding to longer flow paths. The result is higher flow resistance coefficients computed for low flow. To explore the impact of this phenomenon upon the Fraser dataset, flow paths, velocities, resistance coefficients, and selected statistical relationships were computed using the shortest potential flow paths and the results compared to those computed using measured flow paths. The shortest potential flow path refers to a smooth curve near the stream centerline that represents the shortest potential flow length (Figure 4-1). The results with computations performed using the shortest potential flow paths are provided in Table 4-4.

In general, the use of shortest potential flow paths increases flow resistance coefficients (Figure 5-27), with increasing median and average values. Overall, the average n and f based upon measured flow paths are 0.24 and 11.1, respectively, while the averages based upon the shortest potential flow path are 0.29 and 16.6. The lowest flows have the longest measured flow paths. Hence, bankfull flows have the least differences while low-flow values have the greatest.

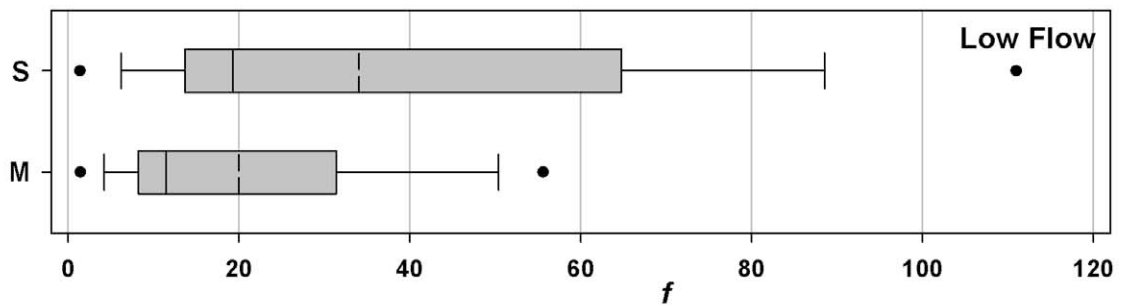
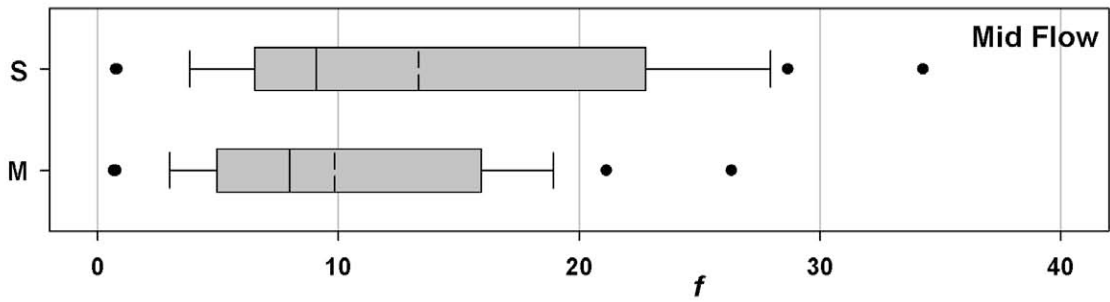
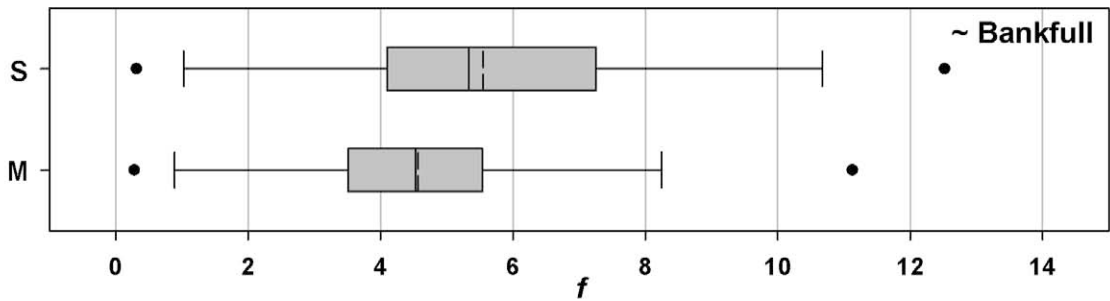
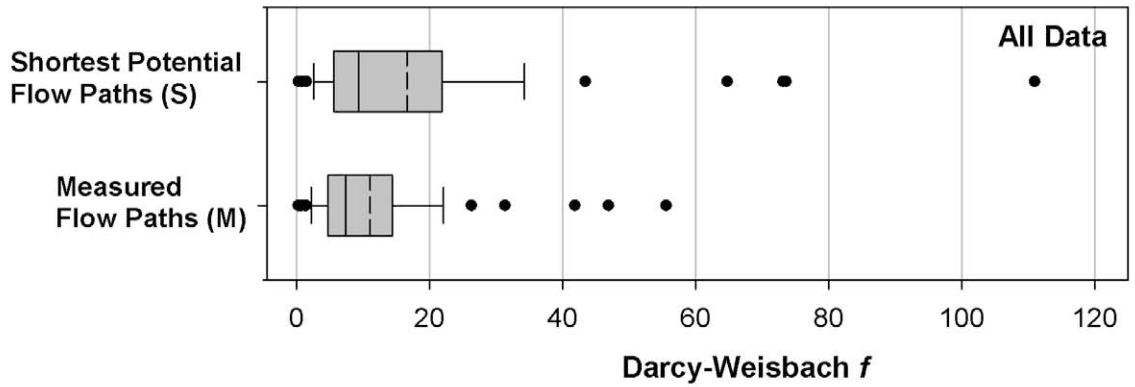


Figure 5-27: Comparison of Darcy-Weisbach f , shortest potential (S) versus measured (M) flow paths.

The effect of the implemented flow path methodology upon the predictive power of relative bedform submergence is minimal. This characteristic provides good predictions for both datasets, as long as consistent methodologies are used. Figure 5-28 provides prediction of n and f using shortest potential flow paths and relative bedform submergence. Explained variance drops from 0.75 to 0.74 and 0.80 to 0.78, respectively, for n and f with the use of shortest potential flow paths. For research, the use of the actual measured flow paths is more applicable because it best reflects flow interactions with resistance elements, as indicated by the slight increase in explained variance when using this methodology. However, for *a priori* resistance prediction the use of shortest potential flow paths is likely the most appropriate, since these thalweg paths are those most typically and easily measured in the field. In any case, a consistent methodology is required.

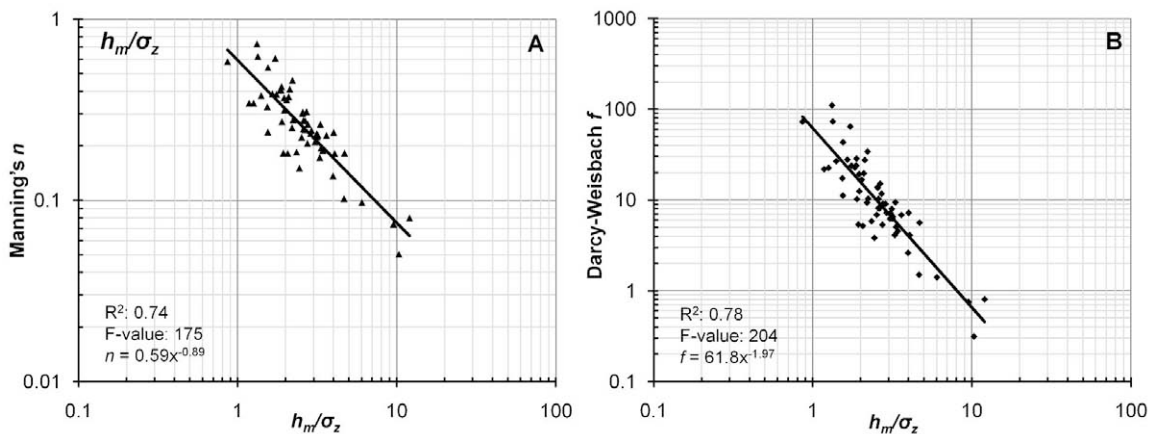


Figure 5-28: Prediction of n and f using relative bedform submergence, with shortest potential flow paths.

5.8 Future Research

Relative bedform submergence derived from longitudinal surveys, in both the form of h_m/σ_z and R/σ_z , has been shown to provide substantial variance explanation for the Fraser dataset, in cascade, step-pool, and plane-bed stream reaches. This variable is quantifying the bed variability that leads to the development of both form and spill resistance due to clasts and step-forming instream wood. The standard deviation of bed residuals has also been shown to be well correlated with discharge in sand-bed streams (Aberle *et al.* 2010). Quantitative methodologies for predicting flow resistance are a critical need for research and applied hydrology; the potential of relative bedform submergence for providing such a methodology is substantial. Research that focuses on the collection of additional measurements of flow resistance in other streams where bedform may be the primary source of flow resistance is needed. In such research, it is critical that field data-collection methodologies are rigorous and appropriate for the purpose.

The collected LiDAR data provide a unique dataset for analysis of resistance characteristics. Beyond the characterization of elevation and depth variability, other opportunities for analysis exist, including 2-D spectral analysis of the bedforms (Aberle *et al.* 2010). The key weakness of this dataset is that points below the low-flow water surface were collected by a laser theodolite at a necessarily much lower resolution than the LiDAR data. Research that takes advantage of a stream that is dry for portions of the year but still provides bed characteristics of interest would be an interesting succession from this work. Additionally, field methodologies that can link LiDAR data with sonar

soundings of below-water features could be a valid technique for developing a more comprehensive dataset.

Considering wake interference and its impact upon the influence of individual resistance elements, spatial statistics may be a helpful tool for exploring how resistance elements interact with each other. However, the practical application of available techniques is problematic. To use a function such as Ripley's K to perform a point cluster analysis, there is a practical problem of determining what type of and specific individual elements to include. For example, clusters of larger clasts are likely to interact with each other to vary each elements' contribution to overall flow resistance. But what clast size should be used in this analysis? The answer is likely that numerous clast sizes should be analyzed to determine the minimum element scale that significantly contributes to flow resistance. Such an analysis would require a comprehensive dataset of uniform resolution, as discussed above.

The scale issue is also relevant for instream wood, with additional issues of these features being linear instead of points and that branches on instream wood cause complex flow patterns that contribute to resistance that need to be represented. Furthermore, since bedform is the most substantial contributor to flow resistance in these stream types, it is essential that steps and pools are incorporated into the spatial analysis. What is needed is a methodology that implements the use of comprehensive raster data of bed and depth variability (Figure 5-17) in the spatial statistical analysis, to remove subjective decisions and evaluate the spatial variability and interaction of all the geometric characteristics. Because the manner in which resistance varies *within* each reach is unknown, with reach average characteristics being known instead, such a method needs to relate some

quantified characteristics of the gridded bed and depth variability to average reach travel time, velocity, or flow resistance coefficient. A method for performing such an analysis was not found in the literature but the development of such a statistical tool may be a worthy contribution. However, the issue of non-linear contributions of flow resistance element types to overall flow resistance may also be problematic.

Finally, one of the most pressing needs of the applied hydrologic community is a comprehensive tool for estimating flow resistance in all stream channel types. Such a method should include both photographic guides, for general selection, as well as quantitative techniques for resistance coefficient selection. Guidance for both Manning's n and Darcy-Weisbach f should be provided, to satisfy the needs of all users. From the reviews I have performed over the years, as well as through discussions I have had with professionals, it is clear to me that the lack of such comprehensive guidance is a fundamental weakness in the hydrologic community, one that can have substantial negative impacts upon the accuracy of hydraulic modeling, stream restoration design, geomorphic analyses, and ecological studies.

CHAPTER 6

SUMMARY AND CONCLUSIONS

Flow resistance measurements were collected in the Fraser Experimental Forest, Colorado, on fifteen reaches of East Saint Louis and Fool Creeks for bankfull through low flow. Data were collected on five cascade, eight step-pool, a transitional and one plane-bed stream reaches, with substantial instream wood present. Data collection was composed of longitudinal water surface profiles; bed, bank, and floodplain surveying using a LiDAR scanner and laser theodolite; bed-material characterization using a 300-point pebble count; and average reach velocity measurements using Rhodamine WT tracer and spatial harmonic travel times. A total of 59 resistance measurements were collected, with Manning's n varying from 0.05 to 0.52 and the Darcy-Weisbach f varying from 0.28 to 55.6.

Resistance coefficients were higher than many commonly-cited references indicate for mountain streams, though the work of other researchers (Reid and Hickin 2008; Comiti *et al.* 2007; Lee and Ferguson 2002) confirm higher values. All measurements indicated fully-subcritical reach-average conditions, with Froude numbers varying from 0.15 to 0.78 in channels with up to 20 percent slope. Counter intuitively, the highest Froude numbers were measured in the channel with the lowest-gradient slope. This is opposed to a common perception that high-gradient streams have high Froude

numbers and are typically dominated by supercritical flow. The underestimation of resistance coefficients and resultant miscategorization of flow regime can lead to substantially-overestimated flow velocities, underestimated travel times and computational instability, negatively impacting the accuracy of hydraulic models, stream restoration designs and ecological studies.

Relative bedform submergence provided the highest levels of explained variance, explaining 75 and 80 percent of the variance of n and f , respectively. A key advantage of the standard deviation of the residuals of a bed profile regression in predicting resistance for these stream types is that it captures the influence of the largest clasts, the combined influence of clasts and instream wood, and bedrock in forming steps. The standard deviation of a bed profile regression is a detrended bed variability term. Detrending is important; not detrending reduced the explained variance for f from 80 to 58 percent. Relative grain submergence was a poor predictor of flow resistance, explaining only 25 and 30 percent of the variance of n and f . Of available prior prediction methodologies, the relationship developed by Aberle and Smart (2003) provided the best fit of f through the use of relative bedform submergence. This was especially surprising since the relationship was developed solely using laboratory data. The use of the standard deviation of bed elevations and relative bedform submergence for prediction may be relevant for general use in open-channel flow where bedforms are present and contribute substantially to flow resistance. In the steepest reaches, with slopes over about 18 percent, relative bedform submergence overpredicted resistance; the data indicate a possible shift towards a skimming regime, with a partial submergence of bedforms and a stepped reduction in flow resistance. Using variables describing bedform, bankform, and

instream wood, multivariate regression models were developed which explained 87 percent of the variance in n and f . Bedform flow characteristics, from form and spill resistance, are by far the greatest contributor to overall flow resistance, followed by form resistance generated by bankform, and lastly, by form resistance induced by non-step instream wood. With a density of up to 4.3 percent, non-step instream wood was found to contribute relatively little resistance in these stream reaches.

Through the use of a sensitivity analysis to explore the impact of the longitudinal profile point density on the power of relative bedform submergence for prediction, it was found that reducing the point density by 25 and 50 percent had a small but detectable impact on the predictions while point density reductions of 75 percent had a more substantial negative influence upon the predictions. The resilience of predictions despite point densities variations indicate resiliency in the predictor. Longitudinal profiles should be measured with uniform spacing at sufficient scale for quantifying bed variability in the streams being assessed. In this study streams surveyed with average width-spacing ratios >6 provided sufficient resolution to define the bed variability and effectively predicted flow resistance.

The use of 3-D measures of geometric variability indicated, at best, a marginal increase in predictive power, with h_{a3}/σ_{z3} explaining 77 percent of the variance in n and 81 percent in f . Variability included in these grids was due to bedform, large clasts, and instream wood. The exclusion of bank effects was necessary – depth and elevation variability predict poorly in the near-bank zone of these streams. A strong correlation ($r = 0.91$) exists between h_m/σ_z and h_{a3}/σ_{z3} , indicating redundancy between bed variability defined using longitudinal profiles and variability as defined through the 3-D spatial

analysis. The marginal increase in explained variance between the 2-D and 3-D measures indicates a non-linear contribution of individual flow resistance elements to overall flow resistance, with the gain in explained variance of questionable value considering the extensive additional analysis required.

The ability to predict flow resistance is essential for numerous practical applications including hydraulic modeling, stream restoration planning and design, geomorphic analysis, and quantification of ecological habitat characteristics for endangered and other species of interest. With an understanding that bedform is the largest contributor to flow resistance in these stream types and that relative bedform submergence is effective for flow resistance prediction, especially when combined with other variables that describe flow resistance contributions due to bank and instream wood, it is reasonable to have optimism that flow resistance can be effectively predicted in these stream types on a general basis given additional compatible and spatially-diverse data for analysis. Other uses of the standard deviations of bed residuals for flow resistance predictions may be possible, such as in the design of concrete and rock structures for stabilizing steep channels and dam outlet works.

REFERENCES

- Aberle, J., A. Dittrich, and F. Nestmann (1999), Description of steep stream roughness with the standard deviation S , In: Proceedings of the 28th Congress of the IAHR, Graz, Austria.
- Aberle, J., and G. M. Smart (2003), The influence of roughness structure on flow resistance on steep slopes, *Journal of Hydraulic Research*, 41(3), 259–269.
- Aberle, J., V. Nikora, M. Henning, B. Ettmer, and B. Hentschel (2010), Statistical characterization of bed roughness due to bed forms: a field study in the Elbe River at Aken, Germany, *Water Resources Research*, 46, W03521.
- Abrahams, A. D., G. Li, and J. F. Atkinson (1995), Step-pool streams: adjustment to maximum flow resistance, *Water Resources Research*, 31(10), 2593–2602.
- Abt, S. R., R. J. Wittier, J. K. Ruff, and M. S. Khattak (1988), Resistance to flow over riprap in steep channels, *Water Resources Bulletin*, 24(6), 1193–1200.
- Aldridge, B. N., and J. M. Garrett (1973), Roughness Coefficients for Stream Channels in Arizona, *U. S. Geological Survey Open-File Report*, Tucson, Arizona.
- Arcement, G. J., and V. R. Schneider (1989), Guide for Selecting Manning's Roughness Coefficients for Natural Channels and Flood Plains, *U. S. Geological Survey Water-Supply Paper 2339*.

- Ataman, E., V. K. Aatre, and K. M. Wong (1981), Some statistical properties of median filters, *IEEE Transactions on Acoustics, Speech, and Signal Processing*, 29(5), 1073–1075.
- Barnes, H. H. (1967), Roughness Characteristics of Natural Channels, *U. S. Geological Survey Water-Supply Paper 1849*.
- Bathurst, J. C. (1985), Flow resistance estimation in mountain rivers, *Journal of Hydraulic Engineering*, 111(4), 625–643.
- Beauchamp, J. T., and J. S. Olson (1973), Corrections for bias in regression estimates after logarithmic transformation, *Ecology*, 54(6), 1403–1407.
- Behrens, H, U. Beims, H. Dieter, G. Dietze, T. Eikmann, T. Grummt, H. Hanisch, H. Henseling, W. Käß, H. Kerndorff, C. Leibundgut, U. Müller-Wegener, I. Rönnefahrt, B. Scharenberg, R. Schleyer, W. Schloz, and F. Tilkes (2001), Toxicological and ecotoxicological assessment of water tracers, *Hydrogeology Journal*, 9, 321–325.
- Bjerklie, D. M., S. L. Dingman, and C. H. Bolster (2005), Comparison of constitutive flow resistance equations based on the Manning and Chezy equations applied to natural rivers, *Water Resources Research*, 41.
- Bray, D. I. (1979), Estimating average velocity in gravel-bed rivers, *Journal of the Hydraulics Division*, 105(9), 1103–1123.
- Brunner, G. W. (2008), HEC-RAS River Analysis System Hydraulic Reference Manual, *Report CPD-69*, U. S. Army Corps of Engineers, Hydrologic Engineering Center.

- Buffington, J. M., and D. R. Montgomery (1999), Effects of hydraulic roughness on surface textures of gravel-bed rivers, *Water Resources Research*, 35(11), 3507–3521.
- Chin, A., and J. D. Phillips (2007), The self-organization of step-pools in mountain streams, *Geomorphology*, 83, 346–358.
- Chow, V. T. (1959), Open Channel Hydraulics, McGraw-Hill Book Company, New York.
- Comiti, F., A. Andreoli, L. Mao, and M. A. Lenzi (2008), Wood storage in three mountain streams of the Southern Andes and its hydro-morphological effects, *Earth Surface Processes and Landforms*, 33, 244–262.
- Comiti F., D. Cadol, and E. Wohl (2009), Flow regimes, bed morphology, and flow resistance in self-formed step-pool channels, *Water Resources Research*, 45, W04424.
- Comiti, F., L. Mao, A. Wilcox, E. E. Wohl, and M. A. Lenzi (2007), Field-derived relationships for flow velocity and resistance in high-gradient streams, *Journal of Hydrology*, 340, 48–62.
- Cowan, W. L. (1956), Estimating hydraulic roughness coefficients, *Agricultural Engineering*, 37, 473–475.
- Curran, J. H. and E. E. Wohl (2003), Large woody debris and flow resistance in step-pool channels, Cascade Range, Washington, *Geomorphology*, 51(1-3), 141–157.
- Daly, C., R. P. Neilson, and D. L. Phillips (1994), A statistical-topographic model for mapping climatological precipitation over mountainous terrain, *Journal of Applied Meteorology*, 33(2), 140–158.

- Daugherty, R. L., J. B. Franzini, and J. E. Finnemore (1985), Fluid Mechanics with Engineering Applications, Eighth Edition, McGraw-Hill Book Company, New York.
- David, G. E. (2010), Characterizing Flow Resistance in Steep Mountain Streams, Fraser Experimental Forest, CO, *PhD Dissertation*, Colorado State University, Fort Collins, Colorado.
- David, G. C. L., Wohl, E., Yochum, S. E. and Bledsoe, B. P. (2010). Controls on spatial variations in flow resistance along steep mountain streams, *Water Resources Research* 46, W03513.
- Dingman, S. L., and K. P. Sharma (1997), Statistical development and validation of discharge equations for natural channels, *Journal of Hydrology*, 199, 13–35.
- Field, M. S., R. G. Wilhelm, J. F. Quinlan, and T. J. Aley (1995), An assessment of the potential adverse properties of fluorescent tracer dyes used for groundwater tracing, *Environmental Monitoring and Assessment*, 38, 75–96.
- Ferguson, R. I. (1987), Accuracy and precision of methods for estimating river loads, *Earth Surfaces Processes and Landforms*, 12(1), 95–104.
- Ferguson, R. (2007), Flow resistance equations for gravel- and boulder-bed streams, *Water Resources Research*, 43.
- Gallagher, N. C., and G. L. Wise (1981), A theoretical analysis of the properties of median filters, *IEEE Transactions on Acoustics, Speech, and Signal Processing*, 29(6), 1136–1141.
- Ganguillet, E., and Kutter, W. R. (1869). Versuch zur Augstellung einer neuen allgeneinen Formel für die gleichformige Bewegung des Wassers in Canalen und

- Flussen, Zeitschrift des Osterreichischen Ingenieur – und Architekten-Vereines, 21, (1) 6–25, and (2) 46–59. [Translated into English by: R. Hering and J. C. Trautwine (1888 and 1891). A General Formula for the Uniform Flow of Water in Rivers and Other Channels. John Wiley & Sons, New York, New York.]
- Gauckler, P. (1868), Du mouvement de l'eau dans les conduites, *Annales des Ponts et Chaussées*, 15, 229–281.
- Ghisalberti, M., and H. M. Nepf (2002), Mixing layers and coherent structures in vegetated aquatic flows, *Journal of Geophysical Research*, 107(C2).
- Grant, G. E. (1997), Critical flow constraints flow hydraulics in mobile-bed stream: a new hypothesis, *Water Resources Research*, 33(2), 349–358.
- Golubtsov, W. (1969), Hydraulic resistance and formula for computing the average flow velocity of mountain rivers, *Soviet Hydrology*, 5, 500–511.
- Hagen, G. W. (1881), Neuere Beobachtung über die gleichförmige Bewegung des Wassers, *Zeitschrift für Bauwesen*, 31, 221–223.
- Henderson, F. M. (1966), Open Channel Flow, MacMillan Publishing Company, New York.
- Hey, R. D. (1979), Flow resistance in gravel-bed rivers, *Journal of the Hydraulics Division*, 105(4), 365–379.
- Jarrett, R. D. (1984), Hydraulics of high-gradient streams, *Journal of Hydraulic Engineering*, 110(11), 1519–1539.
- Jarrett, R. D. (1991), Wading measurements of vertical velocity profiles, *Geomorphology*, 4, 243–247.

- Katul, G., P. Wiberg, J. Albertson, and G. Hornberger (2002), A mixing layer theory for flow resistance in shallow streams, *Water Resources Research*, 38(11).
- Kean, J. W., and J. D. Smith (2005), Generation and verification of theoretical rating curves in the Whitewater River basin, Kansas, *Journal of Geophysical Research*, 110.
- Kean, J. W., and J. D. Smith (2006a), Form drag in rivers due to small-scale natural topographic features: 1. regular sequences, *Journal of Geophysical Research*, 111.
- Kean, J. W., and J. D. Smith (2006b), Form drag in rivers due to small-scale natural topographic features: 2. irregular sequences, *Journal of Geophysical Research*, 111.
- Kilpatrick F. A. (1970), Dosage requirements for slug injection of rhodamine BA and WT dyes, *U.S Geological Survey Professional Paper 700-B*.
- Koll, K. (2002). Feststofftransport und Geschwindigkeitsverteilung in Raugerinnen *Diss., Univ. Karlsruhe, Fak. f. Bauingenieur- und Vermessungswesen*.
- Kratzer, C. R., and R. N. Biagtan (1997), Determination of travel times in the Lower San Joaquin River Basin, California, from dye-tracer studies during 1994-1995, *U.S. Geological Survey Water Resources Investigation Report 97-4018*.
- Lee, A. J., and R. I. Ferguson (2002), Velocity and flow resistance in step-pool streams, *Geomorphology*, 46, 59–71.
- Lee, K. K. (1995), Stream velocity and dispersion characteristics determined by dye-tracer studies on selected stream reaches in the Willamette River Basin, Oregon, *U.S. Geological Survey Water Resources Investigation Report 95-4078*.

- Leopold, L. B., R. A. Bagnold, M. G. Wolman, and L. M. Brush (1960), Flow Resistance in Sinuous or Irregular Channels, *Geological Survey Professional Paper 282-D*.
- Limerinos, J. T. (1970), Determination of the Manning Coefficient from Measured Bed Roughness in Natural Channels, *U.S. Geological Survey Water-Supply Paper 1898-B*.
- Lopez, R., J. Barragan, and M. A. Colomer (2007), Flow resistance equations without explicit estimation of the resistance coefficient for coarse-grained rivers, *Journal of Hydrology*, 338, 113–121.
- MacFarlane, W. A., and E. Wohl (2003), Influence of step composition on step geometry and flow resistance in step-pool streams of the Washington Cascades, *Water Resources Research*, 39(2).
- Manga, M., and J. W. Kirchner (2000), Stress partitioning in streams by large woody debris, *Water Resources Research*, 36(8), 2373–2379.
- Marchand, J. P., R. D. Jarrett, and L. L. Jones (1984), Velocity profile, water-surface slope and bed-material size for selected streams in Colorado, *U. S. Geological Survey Open-File Report 84-733*.
- Marcus, W. A., K. Roberts, L. Harvey, and G. Tackman (1992), An evaluation of methods for estimating Manning's n in small mountain stream, *Mountain Research and Development*, 12(3), 227–239.
- Mason, P. D. and Hicks, D.M. (1999), Roughness characteristics of New Zealand rivers: a handbook for assigning hydraulic roughness coefficients to river reaches by the "visual comparison" approach. Wellington, N.Z.: Water Resources Survey, DSIR Marine and Freshwater.

- Masterman, R., and C. R. Thorne (1994), Analytical approach to flow resistance in gravel-bed channels vegetated banks, In: M. J. Kirkby (Ed.), Process Models and Theoretical Geomorphology, John Wiley and Sons Ltd.
- McCuen, R. H., R. B. Leahy, and P. A. Johnson (1990), Problems with logarithmic transformations in regression, *Journal of Hydraulic Engineering*, 116(3), 414–428.
- Montgomery, D. R., and J. M. Buffington (1997), Channel reach morphology in mountain drainage basins, *Geological Society of America Bulletin*, 109(5), 596–611.
- Mussetter, R. A. (1988), Dynamics of Mountain Streams, *PhD Dissertation*, Colorado State University, Fort Collins, Colorado.
- Nepf, H. M. (1999), Drag, turbulence, and diffusion in flow through emergent vegetation, *Water Resources Research*, 35(2), 479–489.
- Newman, M. C. (1993), Regression analysis of log-transformed data: statistical bias and its correction, *Environmental Toxicology and Chemistry*, 12, 1129–1133.
- Orlandini, S., C. Boaretti, V. Guidi, and G. Sfondrini (2006), Field determination of the spatial variation of resistance to flow along a steep Alpine stream, *Hydrological Processes*, 20, 3897–3913.
- Pagliara, S., and P. Chiavaccini (2006), Flow resistance of rock chutes with protruding boulders, *Journal of Hydraulic Engineering*, 132(6), 545–552.
- Recking, A., P. Frey, A. Paquier, P. Belleudy, and J. Y. Champagne (2008), Feedback between bed load transport and flow resistance in gravel and cobble bed rivers, *Water Resources Research*, 44.

- Reid, D. E., and E. J. Hickin (2008), Flow resistance in steep mountain streams, *Earth Surface Processes Landforms*, 33, 2211–2240.
- Retzer, J. L. (1962). Soil survey of Fraser alpine area, Colorado, *Soil Survey Series 1956*, 20, March, U. S. Department of Agriculture, Forest Service and Soil Conservation Service, 47 p.
- Rice, C. E., K. C. Kadavy, and K. M. Robinson (1998), Roughness of loose rock riprap on steep slopes, *Journal of Hydraulic Engineering*, 124(2), 179–185.
- Rospport, M. (1997). Fließwiderstand und Sohlstabilität steiler Fließgewässer unter Berücksichtigung gebirgsbachtypischer Sohlstrukturen, *Mitt. des Instituts für Wasserwirtschaft und Kulturtechnik, Univ. Karlsruhe*, Heft 196.
- Rouse, H. (1965), Critical analysis of open-channel resistance, *ASCE Journal of the Hydraulics Division*, 91, 1–25.
- Soto, A. U., and M. Madrid-Aris (1994), Roughness coefficients in mountain rivers, *Hydraulic Engineering 1994 – Volume I*, American Society of Civil Engineers, New York.
- Tukey, J. W. (1974), Nonlinear (nonsuperposable) methods for smoothing data, *IEEE Electronics and Aerospace Systems Convention*, 673.
- Walden, M. G. (2004), Estimation of average stream velocity, *ASCE, Journal of Hydraulic Engineering*, 130(11), 1119–1122.
- Wilcox, A. C., and E. E. Wohl (2006), Flow resistance dynamics in step-pool stream channels: 1. large woody debris and controls on total resistance, *Water Resources Research*, 42.

- Wilcox, A. C., J. M. Nelson, and E. E. Wohl (2006), Flow resistance dynamics in step-pool stream channels: 2. partitioning between grain, spill and woody debris resistance, *Water Resources Research*, 42.
- Williams, G. P. (1978), Bank-full discharge in rivers, *Water Resources Research*, 14(6), 1141–1154.
- Wohl, E., J. N. Kuzma, and N.E. Brown (2004), Reach-scale channel geometry of a mountain river, *Earth Surface Processes and Landforms*, 29, 969–981.
- Wohl, E., S. Madsen, and L. MacDonald (1997), Characteristics of log and clast bed-steps in step-pool streams of northwestern Montana, USA, *Geomorphology*, 20, 1–10.
- Wohl, E., and D. Merritt (2005), Prediction of mountain stream morphology, *Water Resources Research*, 41, 1–10.
- Wohl, E., and D. M. Merritt (2008), Reach-scale channel geometry of mountain streams, *Geomorphology*, 93, 168–185.
- Wohl, E. E., and A. Wilcox (2005), Channel geometry of mountain streams in New Zealand, *Journal of Hydrology*, 300(1-4), 252–266.
- Yochum, S., and Bledsoe, B. (2010), Flow resistance estimation in high-gradient streams, In: 4th Federal Interagency Hydrologic Modeling Conference, June 27 - July 1, Las Vegas, Nevada.
- Zimmermann, A., and M. Church (2001), Channel morphology, gradient profiles and bed stresses during flood in a step-pool channel, *Geomorphology*, 40, 311–327.

Zimmermann, A. (2009), Experimental Investigations of Step-pool Channel Formation and Stability, *PhD Dissertation*, The University of British Columbia, Vancouver, BC, Canada.

APPENDIX A

2007 AND 2008 DAILY DISCHARGE DATA

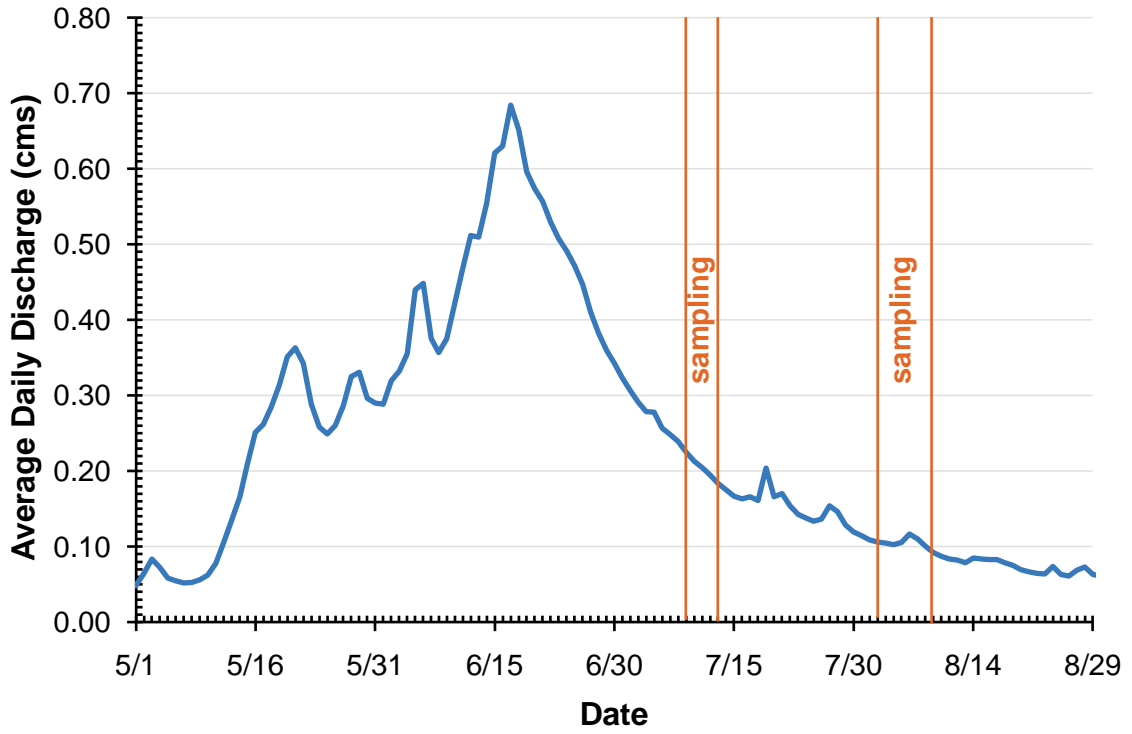


Figure A-1: East Saint Louis Creek average daily streamflow, 2007.

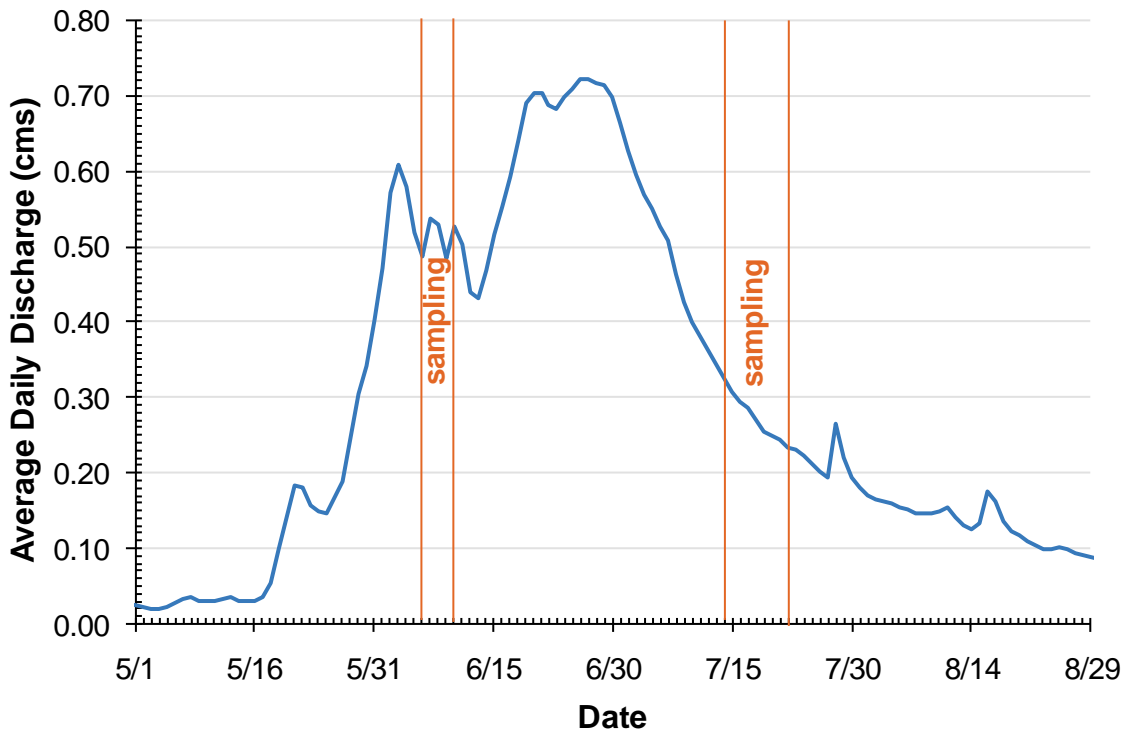


Figure A-2: East Saint Louis Creek average daily streamflow, 2008.

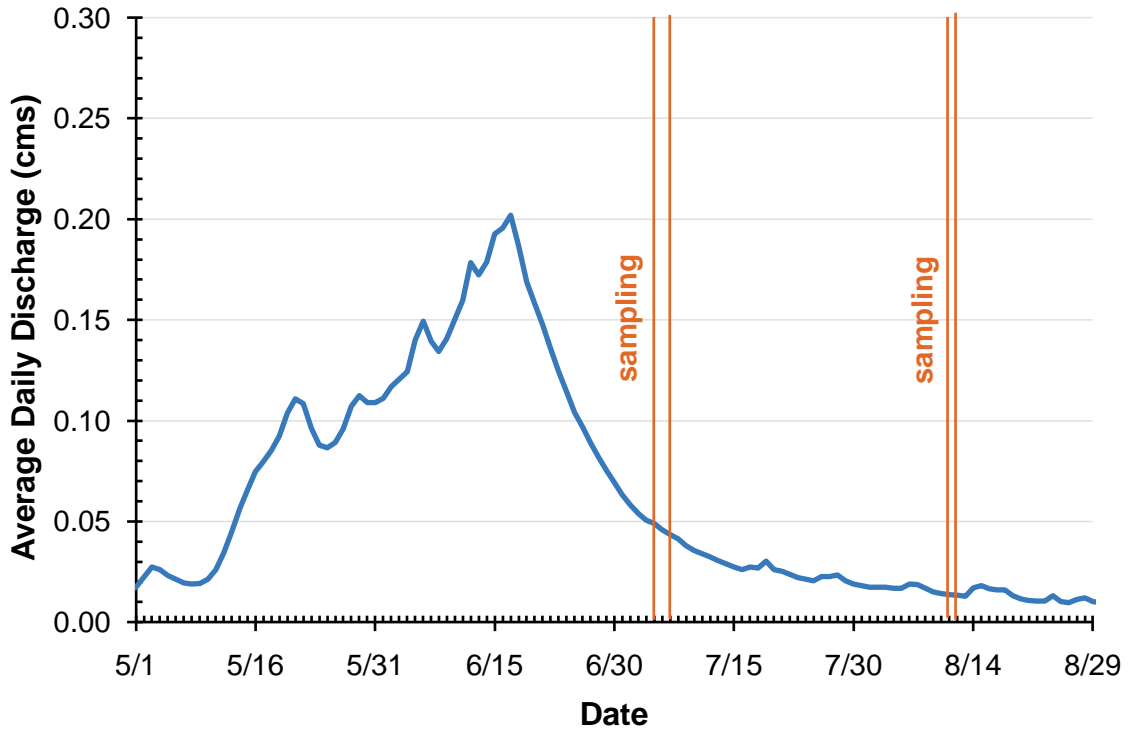


Figure A-3: Lower Fool Creek average daily streamflow, 2007

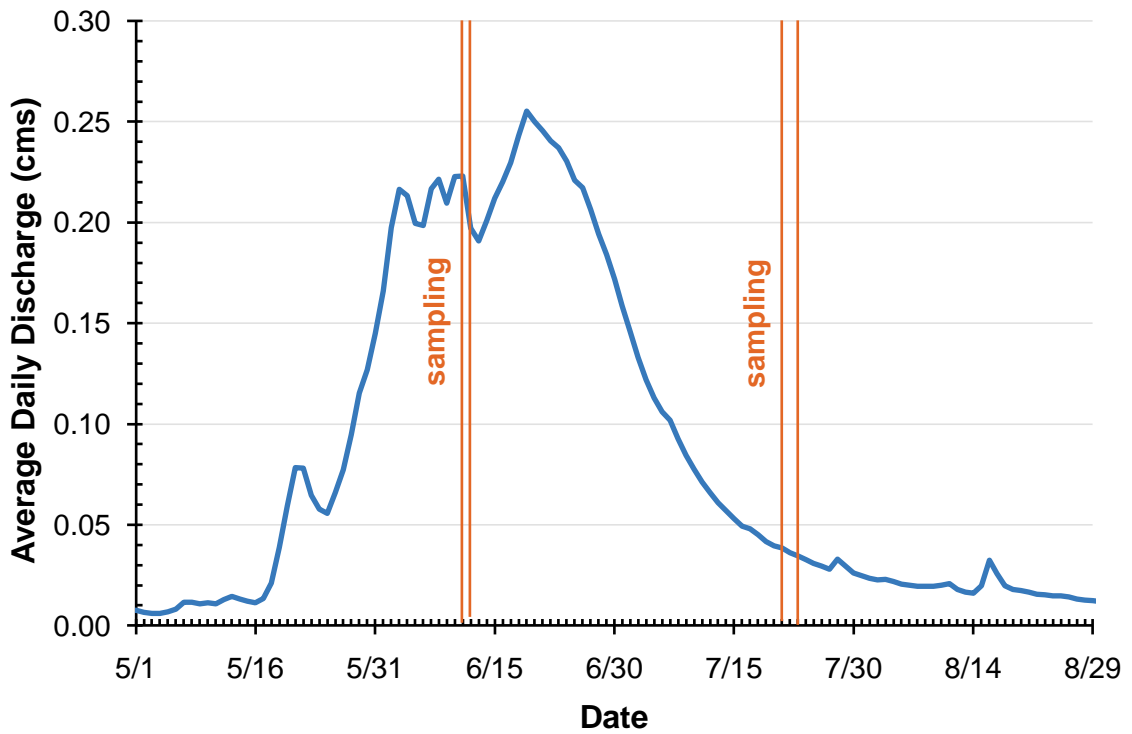


Figure A-4: Lower Fool Creek average daily streamflow, 2008

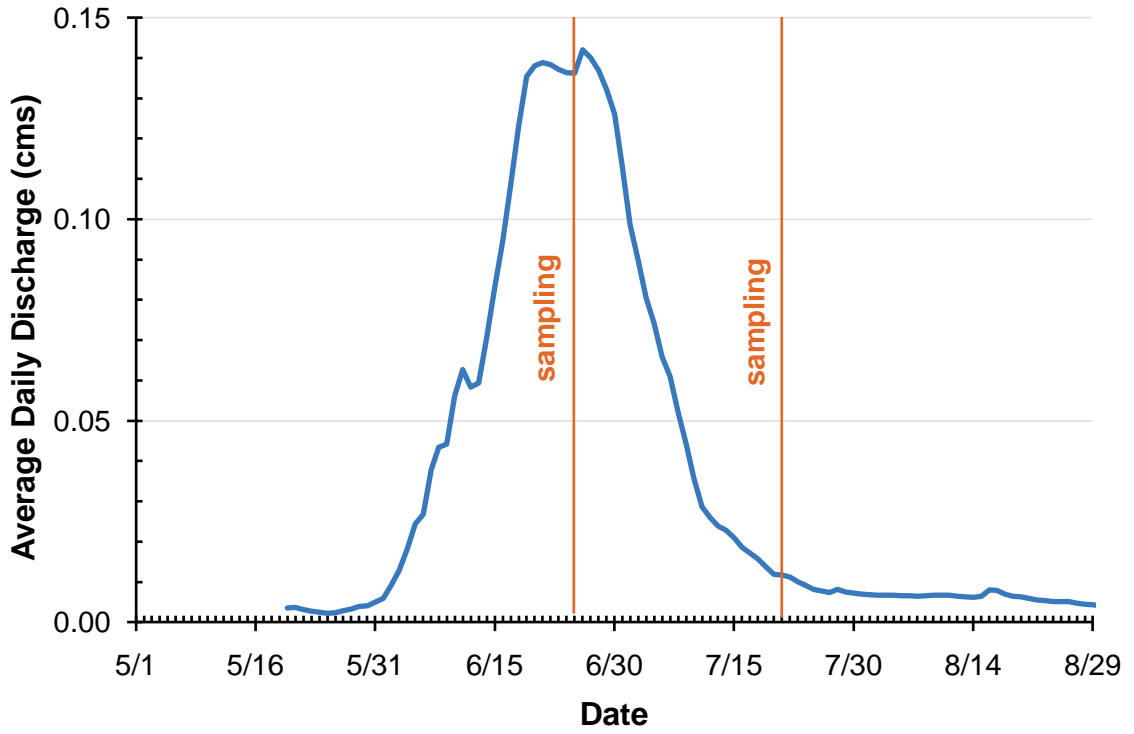


Figure A-5: Upper Fool Creek average daily streamflow, 2008

APPENDIX B

LOG-PEARSON FREQUENCY ANALYSIS SPREADSHEETS

Project: Fraser Flow Resistance
 Streamgage: East Saint Louis
 Date: 5/6/2010 Performed By: Yochum

Without Generalized Skew

Average: -0.1338
 Standard Deviation: 0.44333079
 Skew Coefficient⁽¹⁾: -0.7399298
 Length of systematic record: 64
 Number of historic peaks: 0
 Length of Data Record: 64
 Length of Historic Record:⁽⁵⁾ ----

Recurrence Interval ⁽²⁾ (years)	Percent Chance	K-Value	Ln(Q)	Peak ⁽⁴⁾ Discharge (cfs)	95% Confidence Limits	
					Upper (cfs)	Lower (cfs)
200	0.5	1.890	0.7043	2.02	2.41	1.76
100	1	1.777	0.6539	1.92	2.27	1.68
50	2	1.640	0.5934	1.81	2.12	1.59
25	4	1.472	0.5188	1.68	1.95	1.49
10	10	1.176	0.3877	1.47	1.68	1.32
5	20	0.857	0.2460	1.28	1.44	1.16
2	50	0.122	-0.0795	0.92	1.01	0.84
1.25	80	-0.786	-0.4823	0.62	0.68	0.55
1.05	95	-1.827	-0.9438	0.39	0.45	0.33
200	0.5	2.576	1.0082	----	----	----
100	1	2.326	0.8974	----	----	----
50	2	2.054	0.7768	----	----	----
25	4	1.751	0.6425	----	----	----
10	10	1.282	0.4346	----	----	----
5	20	0.842	0.2395	----	----	----
2	50	0.000	-0.1338	----	----	----
1.25	80	-0.842	-0.5071	----	----	----
1.05	95	-1.645	-0.8631	----	----	----

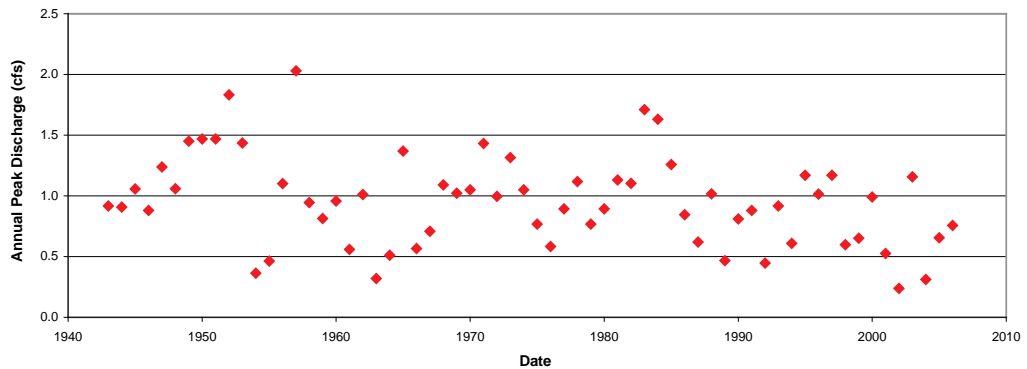
With Weighted Generalized Skew

Generalized Skew Coefficient⁽³⁾:
 Variance of Generalized Skew⁽³⁾:
 A: -0.270806
 B: 0.747618
 station skew: -0.739930
 MSE Station Skew: 0.13380721
 Weighted skew coefficient⁽¹⁾: 0

- (1) Station and generalized skews must be between -2.00 and +3.00 in this spreadsheet.
- (2) Considering the relatively short length of most gage records, less frequent peak estimates need to be used with considerable care.
- (3) Computed one of four ways (see "generalized skew coefficient" worksheet): Mean and variance (standard deviation²) of station skews coefficients in region; skew isolines drawn on a map or regions; skew prediction equations; read from Plate 1 of Bulletin 17B (reproduced in this spreadsheet), with Variance of Generalized Skew = 0.302.
- (4) Results are automatically rounded to three significant figures, the dominant number of significant figures in the K-Value table.
- (5) Historic frequency analysis assumes that intervening years reflect systematic record.

Comments:

Data Plot:



Peak Timing:

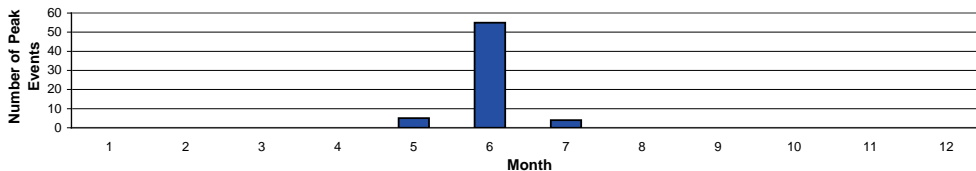


Figure B-1: East Saint Louis Log-Pearson Frequency Analysis Spreadsheet.

Log-Pearson Frequency Analysis Spreadsheet, Version 2.3, 1/2005.

Project: Fraser Flow Resistance
 Streamgage: East Saint Louis
 Date: 5/6/2010

Performed By: Yochum

Input Data

Station ID: 0
 Drainage Area (mi²): 0
 Number of low outliers eliminated: 0

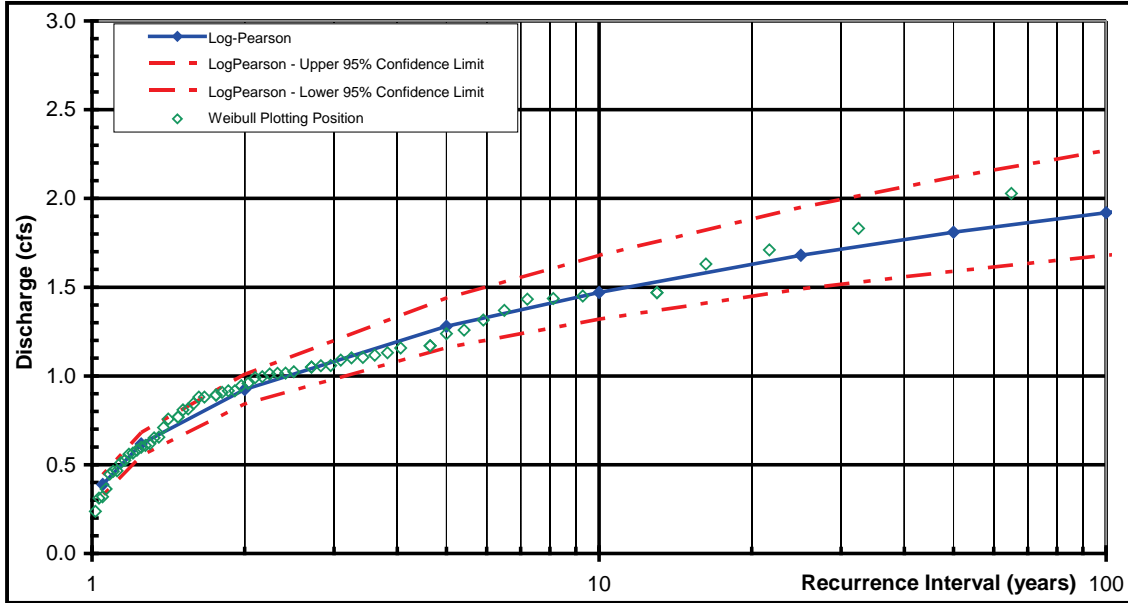
Latitude, Longitude: -- --
 County: Grand County
 State: Colorado

	Date	Discharge (cfs)	Historic?	Outlier?		Date	Discharge (cfs)	Historic?	Outlier?		Date	Discharge (cfs)	Historic?	Outlier?
1	06/22/1943	0.92	n	n	51	06/17/1993	0.92	n	n	101	----	----	n	n
2	06/21/1944	0.91	n	n	52	06/01/1994	0.61	n	n	102	----	----	n	n
3	06/24/1945	1.06	n	n	53	06/17/1995	1.17	n	n	103	----	----	n	n
4	06/10/1946	0.88	n	n	54	06/15/1996	1.02	n	n	104	----	----	n	n
5	06/20/1947	1.24	n	n	55	06/19/1997	1.17	n	n	105	----	----	n	n
6	06/03/1948	1.06	n	n	56	06/03/1998	0.60	n	n	106	----	----	n	n
7	06/17/1949	1.45	n	n	57	06/22/1999	0.65	n	n	107	----	----	n	n
8	06/16/1950	1.47	n	n	58	05/29/2000	0.99	n	n	108	----	----	n	n
9	06/21/1951	1.47	n	n	59	06/01/2001	0.53	n	n	109	----	----	n	n
10	06/10/1952	1.83	n	n	60	05/30/2002	0.24	n	y	110	----	----	n	n
11	06/13/1953	1.44	n	n	61	06/01/2003	1.16	n	n	111	----	----	n	n
12	05/20/1954	0.36	n	n	62	06/08/2004	0.31	n	n	112	----	----	n	n
13	06/13/1955	0.46	n	n	63	07/24/2005	0.66	n	n	113	----	----	n	n
14	06/02/1956	1.10	n	n	64	06/06/2006	0.76	n	n	114	----	----	n	n
15	07/03/1957	2.03	n	n	65	----	----	n	n	115	----	----	n	n
16	06/06/1958	0.94	n	n	66	----	----	n	n	116	----	----	n	n
17	06/20/1959	0.81	n	n	67	----	----	n	n	117	----	----	n	n
18	06/17/1960	0.96	n	n	68	----	----	n	n	118	----	----	n	n
19	06/12/1961	0.56	n	n	69	----	----	n	n	119	----	----	n	n
20	06/30/1962	1.01	n	n	70	----	----	n	n	120	----	----	n	n
21	06/16/1963	0.32	n	n	71	----	----	n	n	121	----	----	n	n
22	06/10/1964	0.51	n	n	72	----	----	n	n	122	----	----	n	n
23	06/17/1965	1.37	n	n	73	----	----	n	n	123	----	----	n	n
24	07/22/1966	0.57	n	n	74	----	----	n	n	124	----	----	n	n
25	06/18/1967	0.71	n	n	75	----	----	n	n	125	----	----	n	n
26	06/20/1968	1.09	n	n	76	----	----	n	n	126	----	----	n	n
27	05/30/1969	1.02	n	n	77	----	----	n	n	127	----	----	n	n
28	06/22/1970	1.05	n	n	78	----	----	n	n	128	----	----	n	n
29	06/24/1971	1.43	n	n	79	----	----	n	n	129	----	----	n	n
30	06/07/1972	1.00	n	n	80	----	----	n	n	130	----	----	n	n
31	06/26/1973	1.31	n	n	81	----	----	n	n	131	----	----	n	n
32	06/18/1974	1.05	n	n	82	----	----	n	n	132	----	----	n	n
33	07/02/1975	0.77	n	n	83	----	----	n	n	133	----	----	n	n
34	06/08/1976	0.58	n	n	84	----	----	n	n	134	----	----	n	n
35	06/09/1977	0.89	n	n	85	----	----	n	n	135	----	----	n	n
36	06/15/1978	1.12	n	n	86	----	----	n	n	136	----	----	n	n
37	06/16/1979	0.77	n	n	87	----	----	n	n	137	----	----	n	n
38	06/12/1980	0.89	n	n	88	----	----	n	n	138	----	----	n	n
39	06/09/1981	1.13	n	n	89	----	----	n	n	139	----	----	n	n
40	06/30/1982	1.10	n	n	90	----	----	n	n	140	----	----	n	n
41	06/27/1983	1.71	n	n	91	----	----	n	n	141	----	----	n	n
42	06/30/1984	1.63	n	n	92	----	----	n	n	142	----	----	n	n
43	06/08/1985	1.26	n	n	93	----	----	n	n	143	----	----	n	n
44	06/07/1986	0.84	n	n	94	----	----	n	n	144	----	----	n	n
45	06/09/1987	0.62	n	n	95	----	----	n	n	145	----	----	n	n
46	06/21/1988	1.02	n	n	96	----	----	n	n	146	----	----	n	n
47	05/30/1989	0.47	n	n	97	----	----	n	n	147	----	----	n	n
48	06/10/1990	0.81	n	n	98	----	----	n	n	148	----	----	n	n
49	06/11/1991	0.88	n	n	99	----	----	n	n	149	----	----	n	n
50	06/12/1992	0.45	n	n	100	----	----	n	n	150	----	----	n	n

Figure B-1 (continued): East Saint Louis Log-Pearson Frequency Analysis Spreadsheet.

Project: Fraser Flow Resistance
 Streamgage: East Saint Louis
 Date: 5/6/2010 Performed By: Yochum

Discharge-Frequency, with Gage Skew
 East Saint Louis



Discharge-Frequency, with Weighted Generalized Skew
 East Saint Louis

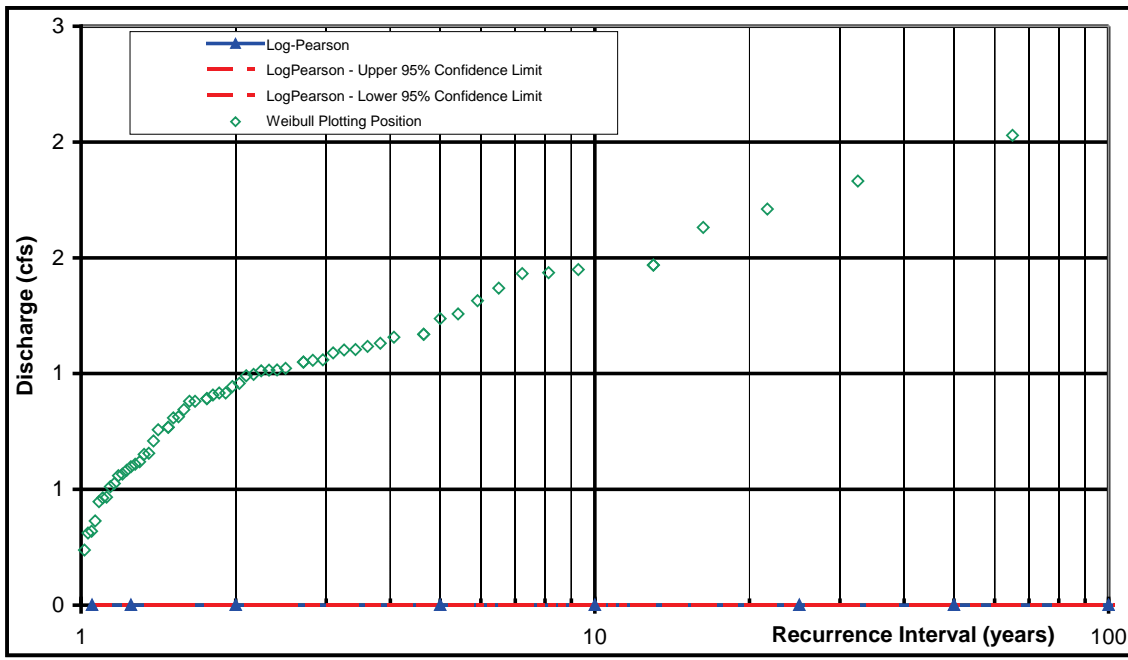


Figure B-1 (continued): East Saint Louis Log-Pearson Frequency Analysis Spreadsheet.

Project: Fraser Flow Resistance
 Streamgauge: Lower Fool Creek
 Date: 5/6/2010 Performed By: Yochum

Without Generalized Skew

Average: -1.3357
 Standard Deviation: 0.55455045
 Skew Coefficient⁽¹⁾: -1.1577507
 Length of systematic record: 67
 Number of historic peaks: 0
 Length of Data Record: 67
 Length of Historic Record:⁽⁶⁾ ----

Recurrence Interval ⁽²⁾ (years)	Percent Chance	K-Value	Ln(Q)	Peak ⁽⁴⁾ Discharge (cfs)	95% Confidence Limits	
					Upper (cfs)	Lower (cfs)
200	0.5	1.535	-0.4846	0.62	0.74	0.53
100	1	1.478	-0.5160	0.60	0.72	0.52
50	2	1.403	-0.5579	0.57	0.68	0.50
25	4	1.300	-0.6149	0.54	0.64	0.47
10	10	1.095	-0.7285	0.48	0.56	0.42
5	20	0.846	-0.8667	0.42	0.48	0.37
2	50	0.189	-1.2311	0.29	0.33	0.26
1.25	80	-0.737	-1.7447	0.18	0.20	0.15
1.05	95	-1.903	-2.3911	0.09	0.11	0.07
200	0.5	2.576	0.0928	----	----	----
100	1	2.326	-0.0458	----	----	----
50	2	2.054	-0.1966	----	----	----
25	4	1.751	-0.3647	----	----	----
10	10	1.282	-0.6248	----	----	----
5	20	0.842	-0.8688	----	----	----
2	50	0.000	-1.3357	----	----	----
1.25	80	-0.842	-1.8026	----	----	----
1.05	95	-1.645	-2.2479	----	----	----

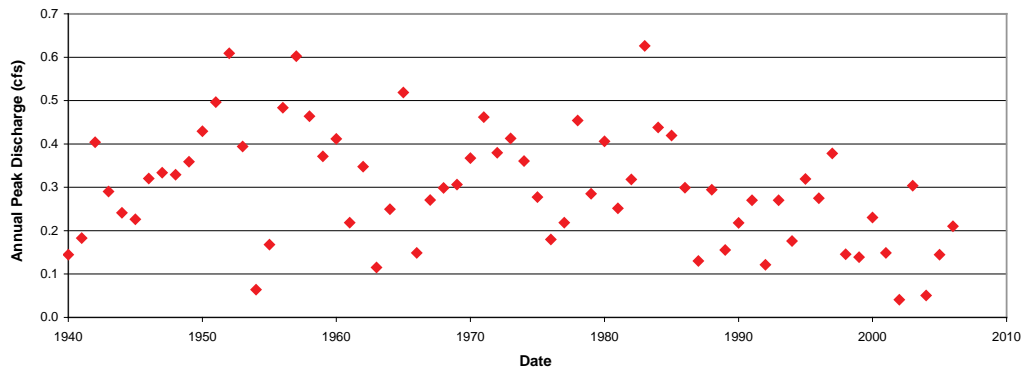
With Weighted Generalized Skew

Generalized Skew Coefficient⁽³⁾:
 Variance of Generalized Skew⁽³⁾:
 A: -0.172675
 B: 0.638985
 station skew: -1.157751
 MSE Station Skew: 0.19928562
 Weighted skew coefficient⁽¹⁾: 0

- (1) Station and generalized skews must be between -2.00 and +3.00 in this spreadsheet.
- (2) Considering the relatively short length of most gage records, less frequent peak estimates need to be used with considerable care.
- (3) Computed one of four ways (see "generalized skew coefficient" worksheet): Mean and variance (standard deviation²) of station skews coefficients in region; skew isolines drawn on a map or regions; skew prediction equations; read from Plate 1 of Bulletin 17B (reproduced in this spreadsheet), with Variance of Generalized Skew = 0.302.
- (4) Results are automatically rounded to three significant figures, the dominant number of significant figures in the K-Value table.
- (5) Historic frequency analysis assumes that intervening years reflect systematic record.

Comments:

Data Plot:



Peak Timing:

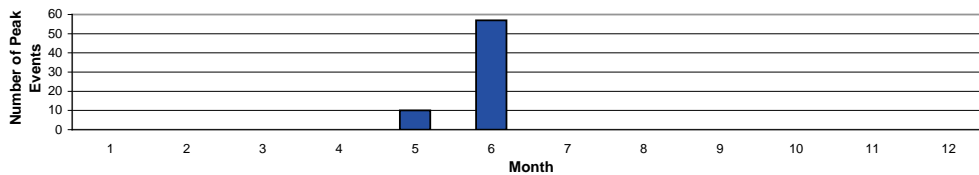


Figure B-2: Lower Fool Creek Log-Pearson Frequency Analysis Spreadsheet.

Project: Fraser Flow Resistance
 Streamgauge: Lower Fool Creek
 Date: 5/6/2010

Performed By: Yochum

Input Data

Station ID: 0
 Drainage Area (mi²): 0
 Number of low outliers eliminated: 0

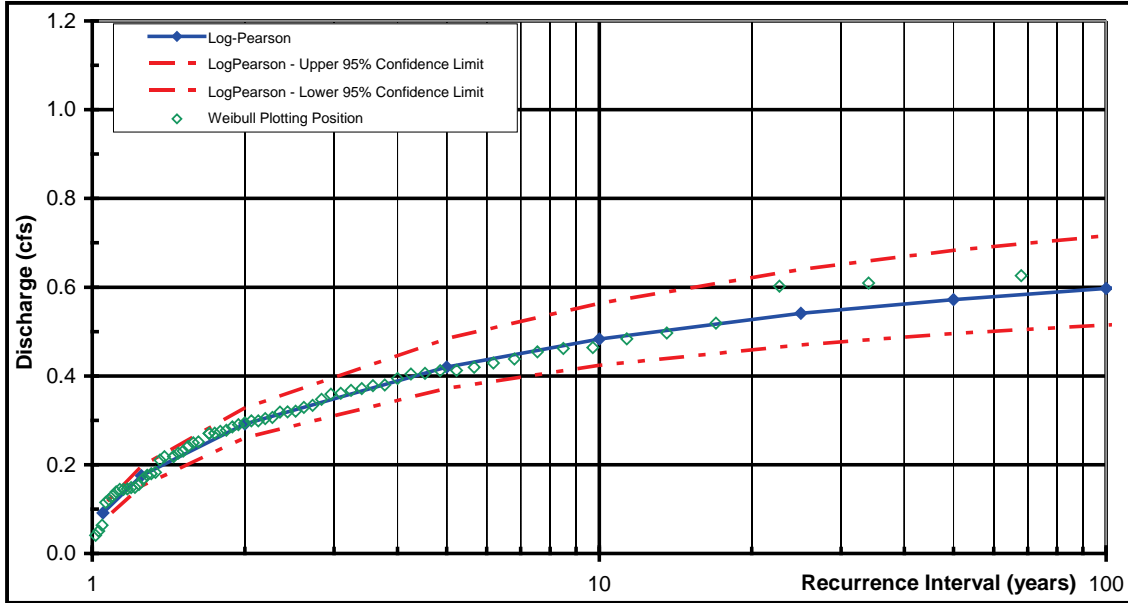
Latitude, Longitude: -- --
 County: Grand County
 State: Colorado

	Date	Discharge (cfs)	Historic?	Outlier?		Date	Discharge (cfs)	Historic?	Outlier?		Date	Discharge (cfs)	Historic?	Outlier?
1	06/05/1940	0.14	n	n	51	06/12/1990	0.22	n	n	101	----	----	n	n
2	06/08/1941	0.18	n	n	52	06/07/1991	0.27	n	n	102	----	----	n	n
3	06/17/1942	0.40	n	n	53	05/27/1992	0.12	n	n	103	----	----	n	n
4	06/20/1943	0.29	n	n	54	06/18/1993	0.27	n	n	104	----	----	n	n
5	06/15/1944	0.24	n	n	55	06/02/1994	0.18	n	n	105	----	----	n	n
6	06/24/1945	0.23	n	n	56	06/18/1995	0.32	n	n	106	----	----	n	n
7	06/10/1946	0.32	n	n	57	06/09/1996	0.27	n	n	107	----	----	n	n
8	06/20/1947	0.33	n	n	58	06/06/1997	0.38	n	n	108	----	----	n	n
9	06/03/1948	0.33	n	n	59	06/04/1998	0.15	n	n	109	----	----	n	n
10	06/17/1949	0.36	n	n	60	06/16/1999	0.14	n	n	110	----	----	n	n
11	06/16/1950	0.43	n	n	61	05/30/2000	0.23	n	n	111	----	----	n	n
12	06/20/1951	0.50	n	n	62	06/03/2001	0.15	n	n	112	----	----	n	n
13	06/10/1952	0.61	n	n	63	06/04/2002	0.04	n	y	113	----	----	n	n
14	06/13/1953	0.39	n	n	64	06/01/2003	0.30	n	n	114	----	----	n	n
15	06/05/1954	0.06	n	n	65	06/09/2004	0.05	n	y	115	----	----	n	n
16	06/08/1955	0.17	n	n	66	06/03/2005	0.14	n	n	116	----	----	n	n
17	06/02/1956	0.48	n	n	67	06/06/2006	0.21	n	n	117	----	----	n	n
18	06/28/1957	0.60	n	n	68	----	----	n	n	118	----	----	n	n
19	05/29/1958	0.46	n	n	69	----	----	n	n	119	----	----	n	n
20	06/09/1959	0.37	n	n	70	----	----	n	n	120	----	----	n	n
21	06/05/1960	0.41	n	n	71	----	----	n	n	121	----	----	n	n
22	06/08/1961	0.22	n	n	72	----	----	n	n	122	----	----	n	n
23	06/13/1962	0.35	n	n	73	----	----	n	n	123	----	----	n	n
24	05/09/1963	0.12	n	n	74	----	----	n	n	124	----	----	n	n
25	05/26/1964	0.25	n	n	75	----	----	n	n	125	----	----	n	n
26	06/16/1965	0.52	n	n	76	----	----	n	n	126	----	----	n	n
27	05/31/1966	0.15	n	n	77	----	----	n	n	127	----	----	n	n
28	06/06/1967	0.27	n	n	78	----	----	n	n	128	----	----	n	n
29	06/18/1968	0.30	n	n	79	----	----	n	n	129	----	----	n	n
30	05/30/1969	0.31	n	n	80	----	----	n	n	130	----	----	n	n
31	05/30/1970	0.37	n	n	81	----	----	n	n	131	----	----	n	n
32	06/18/1971	0.46	n	n	82	----	----	n	n	132	----	----	n	n
33	06/05/1972	0.38	n	n	83	----	----	n	n	133	----	----	n	n
34	06/13/1973	0.41	n	n	84	----	----	n	n	134	----	----	n	n
35	05/29/1974	0.36	n	n	85	----	----	n	n	135	----	----	n	n
36	06/16/1975	0.28	n	n	86	----	----	n	n	136	----	----	n	n
37	06/10/1976	0.18	n	n	87	----	----	n	n	137	----	----	n	n
38	06/09/1977	0.22	n	n	88	----	----	n	n	138	----	----	n	n
39	06/15/1978	0.45	n	n	89	----	----	n	n	139	----	----	n	n
40	06/16/1979	0.29	n	n	90	----	----	n	n	140	----	----	n	n
41	06/12/1980	0.41	n	n	91	----	----	n	n	141	----	----	n	n
42	06/09/1981	0.25	n	n	92	----	----	n	n	142	----	----	n	n
43	06/18/1982	0.32	n	n	93	----	----	n	n	143	----	----	n	n
44	06/27/1983	0.63	n	n	94	----	----	n	n	144	----	----	n	n
45	06/01/1984	0.44	n	n	95	----	----	n	n	145	----	----	n	n
46	06/08/1985	0.42	n	n	96	----	----	n	n	146	----	----	n	n
47	06/09/1986	0.30	n	n	97	----	----	n	n	147	----	----	n	n
48	06/10/1987	0.13	n	n	98	----	----	n	n	148	----	----	n	n
49	06/11/1988	0.29	n	n	99	----	----	n	n	149	----	----	n	n
50	05/31/1989	0.16	n	n	100	----	----	n	n	150	----	----	n	n

Figure B-2 (continued): Lower Fool Creek Log-Pearson Frequency Analysis Spreadsheet.

Project: Fraser Flow Resistance
 Streamgage: Lower Fool Creek
 Date: 5/6/2010 Performed By: Yochum

Discharge-Frequency, with Gage Skew
 Lower Fool Creek



Discharge-Frequency, with Weighted Generalized Skew
 Lower Fool Creek

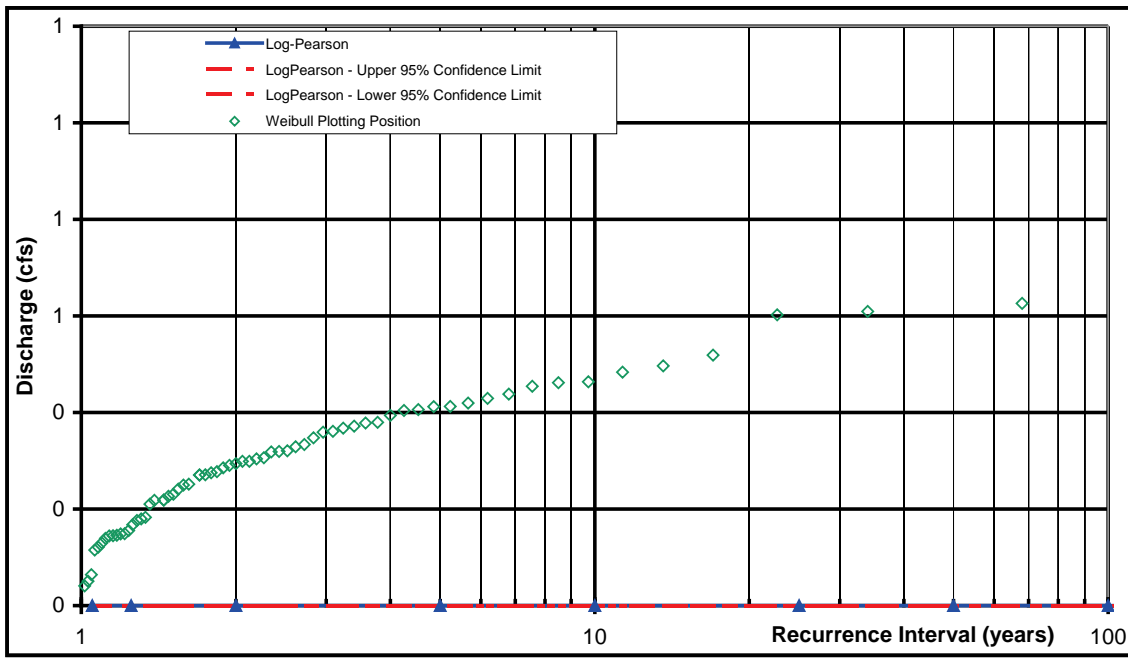


Figure B-2 (continued): Lower Fool Creek Log-Pearson Frequency Analysis Spreadsheet.

Project: Fraser Flow Resistance
 Streamgage: Upper Fool Creek
 Date: 5/6/2010 Performed By: Yochum

Without Generalized Skew

Average: -2.0516
 Standard Deviation: 0.55549316
 Skew Coefficient⁽¹⁾: -1.3391014
 Length of systematic record: 21
 Number of historic peaks: 0
 Length of Data Record: 21
 Length of Historic Record⁽⁵⁾: ----

Recurrence Interval ⁽²⁾ (years)	Percent Chance	K-Value	Ln(Q)	Peak ⁽⁴⁾ Discharge (cfs)	95% Confidence Limits	
					Upper (cfs)	Lower (cfs)
200	0.5	1.395	-1.2765	0.28	0.40	0.22
100	1	1.358	-1.2975	0.27	0.39	0.22
50	2	1.303	-1.3279	0.27	0.37	0.21
25	4	1.224	-1.3719	0.25	0.35	0.20
10	10	1.055	-1.4656	0.23	0.31	0.19
5	20	0.836	-1.5874	0.20	0.27	0.17
2	50	0.216	-1.9317	0.15	0.18	0.12
1.25	80	-0.714	-2.4480	0.09	0.11	0.07
1.05	95	-1.930	-3.1238	0.04	0.06	0.03
200	0.5	2.576	-0.6207	----	----	----
100	1	2.326	-0.7595	----	----	----
50	2	2.054	-0.9106	----	----	----
25	4	1.751	-1.0790	----	----	----
10	10	1.282	-1.3395	----	----	----
5	20	0.842	-1.5839	----	----	----
2	50	0.000	-2.0516	----	----	----
1.25	80	-0.842	-2.5193	----	----	----
1.05	95	-1.645	-2.9654	----	----	----

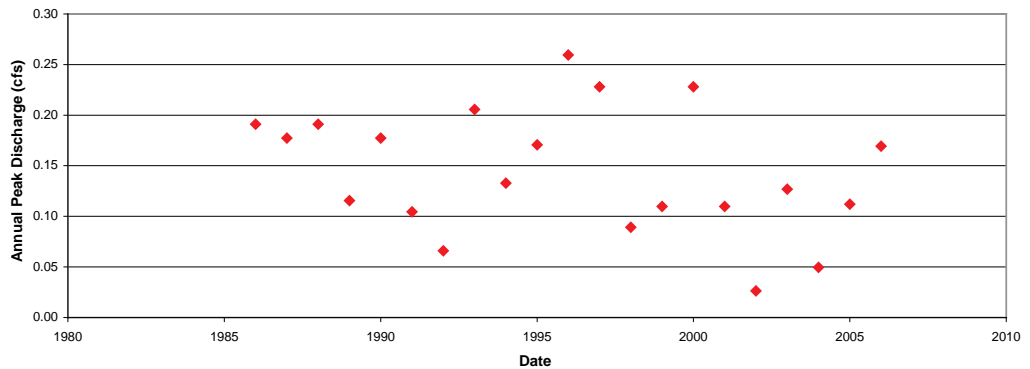
With Weighted Generalized Skew

Generalized Skew Coefficient⁽³⁾:
 Variance of Generalized Skew⁽³⁾:
 A: -0.118270
 B: 0.591834
 station skew: -1.339101
 MSE Station Skew: 0.490942
 Weighted skew coefficient⁽¹⁾: 0

- (1) Station and generalized skews must be between -2.00 and +3.00 in this spreadsheet.
- (2) Considering the relatively short length of most gage records, less frequent peak estimates need to be used with considerable care.
- (3) Computed one of four ways (see "generalized skew coefficient" worksheet): Mean and variance (standard deviation²) of station skews coefficients in region; skew isolines drawn on a map or regions; skew prediction equations; read from Plate 1 of Bulletin 17B (reproduced in this spreadsheet), with Variance of Generalized Skew = 0.302.
- (4) Results are automatically rounded to three significant figures, the dominant number of significant figures in the K-Value table.
- (5) Historic frequency analysis assumes that intervening years reflect systematic record.

Comments:

Data Plot:



Peak Timing:

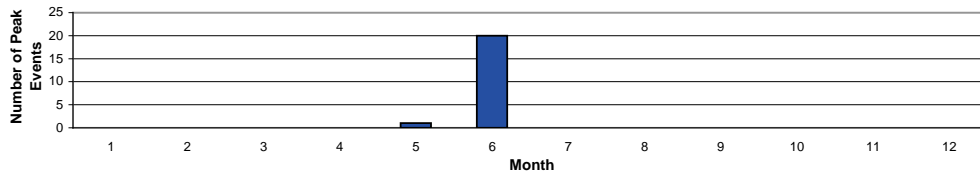


Figure B-3: Upper Fool Creek Log-Pearson Frequency Analysis Spreadsheet.

Project: *Fraser Flow Resistance*
 Streamgage: *Upper Fool Creek*
 Date: *5/6/2010*

Performed By: *Yochum*

Input Data

Station ID: *0*
 Drainage Area (mi²): *0*
 Number of low outliers eliminated: *0*

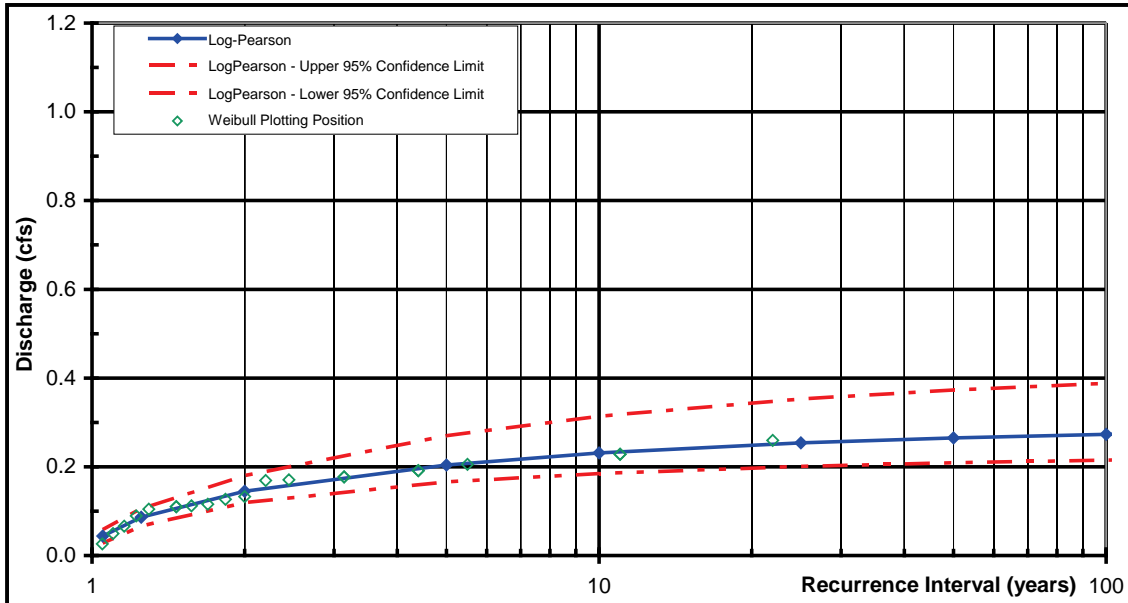
Latitude, Longitude: *-- --*
 County: *Grand County*
 State: *Colorado*

	Date	Discharge (cfs)	Historic?	Outlier?		Date	Discharge (cfs)	Historic?	Outlier?		Date	Discharge (cfs)	Historic?	Outlier?
1	06/08/1986	0.19	n	n	51	----	----	n	n	101	----	----	n	n
2	06/09/1987	0.18	n	n	52	----	----	n	n	102	----	----	n	n
3	06/10/1988	0.19	n	n	53	----	----	n	n	103	----	----	n	n
4	06/16/1989	0.12	n	n	54	----	----	n	n	104	----	----	n	n
5	06/11/1990	0.18	n	n	55	----	----	n	n	105	----	----	n	n
6	06/18/1991	0.10	n	n	56	----	----	n	n	106	----	----	n	n
7	06/12/1992	0.07	n	n	57	----	----	n	n	107	----	----	n	n
8	06/22/1993	0.21	n	n	58	----	----	n	n	108	----	----	n	n
9	06/04/1994	0.13	n	n	59	----	----	n	n	109	----	----	n	n
10	06/21/1995	0.17	n	n	60	----	----	n	n	110	----	----	n	n
11	06/15/1996	0.26	n	n	61	----	----	n	n	111	----	----	n	n
12	06/19/1997	0.23	n	n	62	----	----	n	n	112	----	----	n	n
13	06/21/1998	0.09	n	n	63	----	----	n	n	113	----	----	n	n
14	06/18/1999	0.11	n	n	64	----	----	n	n	114	----	----	n	n
15	05/30/2000	0.23	n	n	65	----	----	n	n	115	----	----	n	n
16	06/03/2001	0.11	n	n	66	----	----	n	n	116	----	----	n	n
17	06/06/2002	0.03	n	y	67	----	----	n	n	117	----	----	n	n
18	06/14/2003	0.13	n	n	68	----	----	n	n	118	----	----	n	n
19	06/08/2004	0.05	n	n	69	----	----	n	n	119	----	----	n	n
20	06/19/2005	0.11	n	n	70	----	----	n	n	120	----	----	n	n
21	06/06/2006	0.17	n	n	71	----	----	n	n	121	----	----	n	n
22	----	----	n	n	72	----	----	n	n	122	----	----	n	n
23	----	----	n	n	73	----	----	n	n	123	----	----	n	n
24	----	----	n	n	74	----	----	n	n	124	----	----	n	n
25	----	----	n	n	75	----	----	n	n	125	----	----	n	n
26	----	----	n	n	76	----	----	n	n	126	----	----	n	n
27	----	----	n	n	77	----	----	n	n	127	----	----	n	n
28	----	----	n	n	78	----	----	n	n	128	----	----	n	n
29	----	----	n	n	79	----	----	n	n	129	----	----	n	n
30	----	----	n	n	80	----	----	n	n	130	----	----	n	n
31	----	----	n	n	81	----	----	n	n	131	----	----	n	n
32	----	----	n	n	82	----	----	n	n	132	----	----	n	n
33	----	----	n	n	83	----	----	n	n	133	----	----	n	n
34	----	----	n	n	84	----	----	n	n	134	----	----	n	n
35	----	----	n	n	85	----	----	n	n	135	----	----	n	n
36	----	----	n	n	86	----	----	n	n	136	----	----	n	n
37	----	----	n	n	87	----	----	n	n	137	----	----	n	n
38	----	----	n	n	88	----	----	n	n	138	----	----	n	n
39	----	----	n	n	89	----	----	n	n	139	----	----	n	n
40	----	----	n	n	90	----	----	n	n	140	----	----	n	n
41	----	----	n	n	91	----	----	n	n	141	----	----	n	n
42	----	----	n	n	92	----	----	n	n	142	----	----	n	n
43	----	----	n	n	93	----	----	n	n	143	----	----	n	n
44	----	----	n	n	94	----	----	n	n	144	----	----	n	n
45	----	----	n	n	95	----	----	n	n	145	----	----	n	n
46	----	----	n	n	96	----	----	n	n	146	----	----	n	n
47	----	----	n	n	97	----	----	n	n	147	----	----	n	n
48	----	----	n	n	98	----	----	n	n	148	----	----	n	n
49	----	----	n	n	99	----	----	n	n	149	----	----	n	n
50	----	----	n	n	100	----	----	n	n	150	----	----	n	n

Figure B-3 (continued): Upper Fool Creek Log-Pearson Frequency Analysis Spreadsheet.

Project: Fraser Flow Resistance
 Streamgage: Upper Fool Creek
 Date: 5/6/2010 Performed By: Yochum

Discharge-Frequency, with Gage Skew
 Upper Fool Creek



Discharge-Frequency, with Weighted Generalized Skew
 Upper Fool Creek

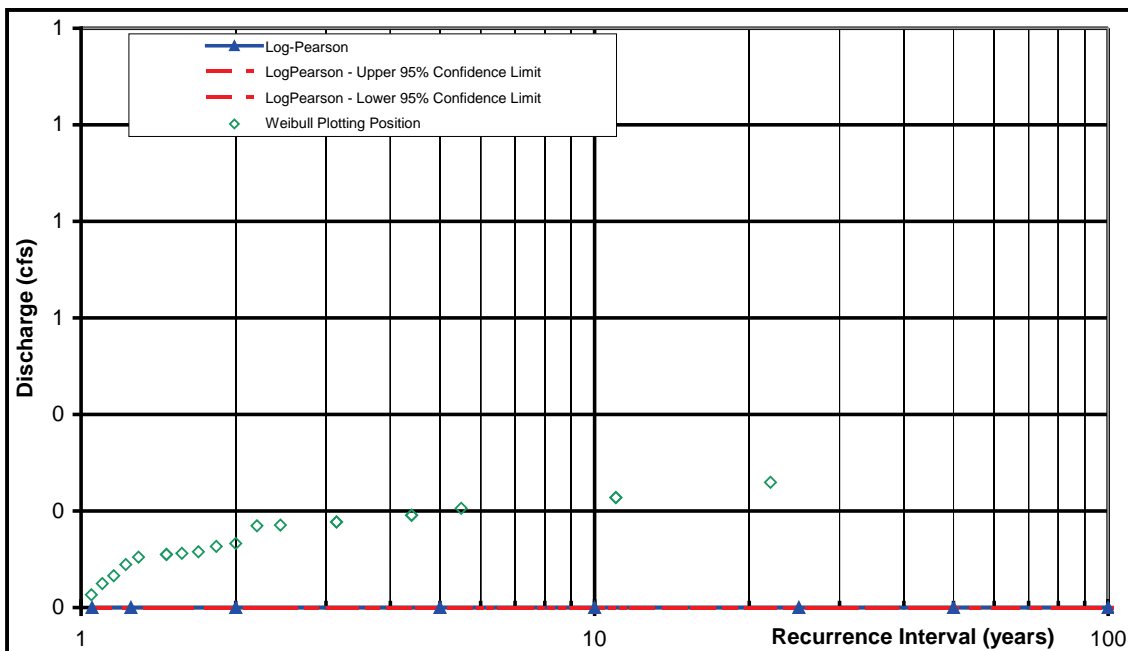


Figure B-3 (continued): Upper Fool Creek Log-Pearson Frequency Analysis Spreadsheet.

APPENDIX C
BED AND BANK DATA

Table C-1: Bed data.

Reach ID	Date	n	f	R/D_{84}	A/SDA	R/SDR	h_m/SDh_m	R/δ_m	h_m/δ_m	R/σ_z	h_m/σ_z
ESL-1	2-Aug-07	0.25	10.4	0.75	1.52	2.13	2.32	0.19	0.47	0.63	1.54
	10-Jun-08	0.19	4.5	1.62	3.11	3.30	3.44	0.42	0.95	1.39	3.16
	22-Jul-08	0.27	9.4	1.30	2.45	2.76	3.35	0.33	0.74	0.98	2.23
ESL-2	9-Jul-07	0.23	7.0	2.81	2.33	4.34	4.43	0.59	1.24	1.27	2.64
	9-Aug-07	0.39	22.1	2.24	1.98	3.93	4.08	0.35	0.74	0.89	1.87
	6-Jun-08	0.20	4.8	3.51	2.89	5.10	4.80	0.52	1.12	1.29	2.74
	15-Jul-08	0.18	4.3	2.92	2.31	3.88	3.63	0.51	1.10	1.54	3.34
ESL-3	10-Jul-07	0.21	6.3	1.02	1.95	3.84	5.32	0.58	1.60	1.13	3.14
	9-Aug-07	0.25	9.2	0.92	1.79	2.75	4.32	0.45	1.15	0.99	2.55
	7-Jun-08	0.16	3.7	1.20	2.50	3.91	6.45	0.55	1.52	1.18	3.28
	15-Jul-08	0.20	5.7	1.15	2.62	4.27	6.19	0.64	1.80	1.09	3.08
ESL-4	10-Jul-07	0.25	8.7	1.06	2.14	2.65	3.04	0.36	0.73	0.94	1.90
	6-Aug-07	0.32	14.4	0.99	2.02	2.48	3.00	0.38	0.76	1.05	2.09
	7-Jun-08	0.23	6.3	1.52	2.63	3.05	3.47	0.53	1.07	1.45	2.90
	14-Jul-08	0.26	8.7	1.34	2.21	2.82	3.14	0.56	1.12	1.35	2.71
ESL-5	12-Jul-07	0.34	16.1	1.23	2.69	4.20	3.25	0.34	0.77	0.82	1.84
	8-Aug-07	0.38	21.8	1.04	2.43	3.72	2.92	0.28	0.64	0.67	1.55
	9-Jun-08	0.30	11.1	1.67	3.26	6.48	3.80	0.44	0.92	0.93	1.96
	14-Jul-08	0.29	10.8	1.55	2.52	4.85	3.20	0.38	0.82	0.94	2.03
ESL-6	13-Jul-07	0.07	0.7	2.41	6.47	6.32	5.80	2.69	3.78	6.77	9.52
	8-Aug-07	0.10	1.4	1.95	4.64	4.80	4.85	1.85	2.64	4.22	6.03
	9-Jun-08	0.05	0.3	3.37	8.35	11.51	8.92	3.86	5.64	7.04	10.29
	14-Jul-08	0.08	0.8	3.14	8.04	9.22	7.92	3.69	5.26	8.42	12.01
ESL-7	12-Jul-07	0.19	4.8	1.01	4.06	5.47	4.54	0.50	1.09	1.40	3.06
	4-Aug-07	0.20	6.0	0.86	3.42	4.47	4.93	0.42	0.90	1.02	2.19
	8-Jun-08	0.17	3.5	1.45	3.00	4.32	4.18	0.81	1.68	1.95	4.07
	15-Jul-08	0.19	4.8	1.31	2.01	3.45	4.22	0.61	1.27	1.91	4.01
ESL-8	11-Jul-07	0.21	6.0	1.06	3.48	4.26	5.30	0.39	0.80	1.22	2.52
	5-Aug-07	0.24	8.2	0.93	2.91	4.36	5.22	0.34	0.70	1.24	2.56
	9-Jun-08	0.18	4.2	1.35	2.98	5.81	6.97	0.56	1.14	1.68	3.42
	16-Jul-08	0.20	5.3	1.24	3.19	4.91	5.67	0.55	1.13	1.75	3.61
ESL-9	11-Jul-07	0.26	8.8	1.31	2.93	3.66	5.39	0.43	0.89	1.24	2.59
	6-Aug-07	0.28	10.9	1.11	2.84	3.57	3.98	0.38	0.78	0.95	1.96
	8-Jun-08	0.21	5.5	1.64	3.35	4.47	4.58	0.78	1.63	1.53	3.19
	16-Jul-08	0.24	7.4	1.42	3.28	3.77	4.58	0.47	0.97	1.33	2.76
FC-1	5-Jul-07	0.13	3.0	1.21	4.49	5.13	6.86	0.49	0.89	1.34	2.44
	12-Aug-07	0.20	7.6	0.75	2.50	3.88	4.68	0.31	0.57	0.83	1.55
	11-Jun-08	0.09	1.3	1.95	4.84	7.36	10.09	1.10	1.98	2.60	4.65
	23-Jul-08	0.17	5.0	1.15	2.91	4.64	5.89	0.60	1.09	1.29	2.34
FC-2	7-Jul-07	0.16	4.1	1.23	3.98	4.88	5.53	0.68	1.46	2.17	4.69
	12-Aug-07	0.24	11.4	0.74	3.04	3.21	3.90	0.35	0.82	1.13	2.65
	11-Jun-08	0.13	2.2	2.16	4.23	6.83	6.16	0.71	1.44	1.95	3.97
	23-Jul-08	0.22	8.0	1.33	2.23	3.46	3.74	0.58	1.23	1.35	2.87

Table C-1 (continued): Bed data.

Reach ID	Date	<i>n</i>	<i>f</i>	<i>R/D</i>₈₄	<i>A/SDA</i>	<i>R/SDR</i>	<i>h_m/SDh_m</i>	<i>R/δ_m</i>	<i>h_m/δ_m</i>	<i>R/σ_z</i>	<i>h_m/σ_z</i>
FC-3	6-Jul-07	0.27	11.8	2.24	2.23	3.34	3.35	0.41	0.85	1.03	2.12
	11-Aug-07	0.41	31.4	1.44	1.47	2.84	2.51	0.23	0.48	0.64	1.34
	12-Jun-08	0.20	5.4	3.83	3.27	5.26	4.28	0.67	1.44	1.54	3.31
	22-Jul-08	0.40	26.3	2.31	2.07	2.74	3.12	0.49	1.02	1.06	2.21
FC-4	7-Jul-07	0.36	21.1	1.27	2.02	2.86	3.29	0.26	0.60	0.83	1.88
	11-Aug-07	0.52	46.9	0.95	1.73	2.76	2.43	0.24	0.54	0.75	1.72
	12-Jun-08	0.22	6.3	2.15	3.06	4.34	4.84	0.45	0.96	1.20	2.58
	21-Jul-08	0.31	15.8	1.23	2.83	3.59	3.03	0.24	0.55	0.78	1.75
FC-5	8-Jul-07	0.31	18.2	0.86	2.45	4.02	3.46	0.21	0.48	0.72	1.65
	10-Aug-07	0.52	55.6	0.62	1.28	2.77	2.71	0.18	0.40	0.59	1.32
	25-Jun-08	0.17	4.5	1.43	2.52	7.27	4.35	0.36	0.83	0.90	2.06
	17-Jul-08	0.32	18.9	0.88	1.85	3.26	2.57	0.20	0.48	0.49	1.18
FC-6	8-Jul-07	0.31	17.8	0.74	1.54	2.40	2.23	0.23	0.55	0.53	1.26
	10-Aug-07	0.44	41.9	0.52	1.19	1.85	1.72	0.17	0.41	0.36	0.86
	25-Jun-08	0.17	4.8	1.22	2.72	3.92	2.93	0.32	0.72	0.86	1.94
	17-Jul-08	0.32	18.9	0.79	1.86	2.81	2.49	0.20	0.48	0.59	1.40

Table C-2: Bank data.

Reach ID	Date	n	f	K_b	K_{bh}	σ_y (m)	TW/σ_y	R/σ_y	h_m/σ_y
ESL-1	2-Aug-07	0.25	10.4	1.24	1.25	0.68	2.95	0.17	0.42
	10-Jun-08	0.19	4.5	1.27	1.28	0.65	4.52	0.39	0.89
	22-Jul-08	0.27	9.4	1.21	1.22	0.63	4.15	0.32	0.74
ESL-2	9-Jul-07	0.23	7.0	1.47	1.48	0.64	4.49	0.31	0.65
	9-Aug-07	0.39	22.1	1.46	1.47	0.64	3.99	0.25	0.52
	6-Jun-08	0.20	4.8	1.30	1.31	0.60	5.32	0.41	0.87
	15-Jul-08	0.18	4.3	1.33	1.33	0.65	4.57	0.32	0.69
ESL-3	10-Jul-07	0.21	6.3	1.27	1.28	0.57	5.27	0.27	0.74
	9-Aug-07	0.25	9.2	1.32	1.33	0.48	5.05	0.29	0.76
	7-Jun-08	0.16	3.7	1.27	1.28	0.55	6.57	0.33	0.92
	15-Jul-08	0.20	5.7	1.18	1.19	0.46	7.74	0.38	1.07
ESL-4	10-Jul-07	0.25	8.7	1.43	1.45	0.58	4.30	0.32	0.64
	6-Aug-07	0.32	14.4	1.48	1.50	0.53	4.35	0.32	0.64
	7-Jun-08	0.23	6.3	1.42	1.44	0.58	4.93	0.45	0.91
	14-Jul-08	0.26	8.7	1.29	1.31	0.48	5.92	0.54	1.08
ESL-5	12-Jul-07	0.34	16.1	1.57	1.60	0.83	4.30	0.21	0.48
	8-Aug-07	0.38	21.8	1.52	1.54	0.74	4.42	0.20	0.46
	9-Jun-08	0.30	11.1	1.41	1.43	0.76	5.31	0.32	0.67
	14-Jul-08	0.29	10.8	1.38	1.40	0.79	4.97	0.28	0.60
ESL-6	13-Jul-07	0.07	0.7	1.07	1.07	0.14	18.76	1.29	1.82
	8-Aug-07	0.10	1.4	1.09	1.09	0.14	19.51	1.10	1.57
	9-Jun-08	0.05	0.3	1.07	1.07	0.13	23.78	2.07	3.03
	14-Jul-08	0.08	0.8	1.03	1.03	0.09	30.21	2.57	3.66
ESL-7	12-Jul-07	0.19	4.8	1.32	1.33	0.94	2.88	0.19	0.41
	4-Aug-07	0.20	6.0	1.38	1.39	0.94	2.62	0.16	0.34
	8-Jun-08	0.17	3.5	1.27	1.27	0.96	3.15	0.26	0.55
	15-Jul-08	0.19	4.8	1.26	1.27	0.87	3.38	0.26	0.55
ESL-8	11-Jul-07	0.21	6.0	1.41	1.42	1.54	1.78	0.12	0.25
	5-Aug-07	0.24	8.2	1.49	1.50	1.96	1.32	0.08	0.17
	9-Jun-08	0.18	4.2	1.39	1.40	2.02	1.56	0.12	0.24
	16-Jul-08	0.20	5.3	1.42	1.43	1.95	1.55	0.11	0.23
ESL-9	11-Jul-07	0.26	8.8	1.41	1.42	0.98	2.62	0.20	0.43
	6-Aug-07	0.28	10.9	1.39	1.40	0.90	2.53	0.19	0.39
	8-Jun-08	0.21	5.5	1.33	1.34	0.94	2.97	0.27	0.55
	16-Jul-08	0.24	7.4	1.26	1.27	0.95	2.78	0.23	0.47
FC-1	5-Jul-07	0.13	3.0	1.15	1.15	0.40	4.02	0.25	0.46
	12-Aug-07	0.20	7.6	1.16	1.16	0.38	3.33	0.16	0.31
	11-Jun-08	0.09	1.3	1.07	1.08	0.45	4.40	0.37	0.66
	23-Jul-08	0.17	5.0	1.12	1.12	0.40	3.93	0.24	0.44
FC-2	7-Jul-07	0.16	4.1	1.25	1.25	0.73	1.93	0.14	0.30
	12-Aug-07	0.24	11.4	1.23	1.23	0.72	1.57	0.08	0.20
	11-Jun-08	0.13	2.2	1.18	1.18	0.74	2.21	0.24	0.48
	23-Jul-08	0.22	8.0	1.19	1.20	0.77	1.83	0.14	0.30

Table C-2 (continued): Bank data.

Reach ID	Date	<i>n</i>	<i>f</i>	<i>K_b</i>	<i>K_{bh}</i>	σ_y (m)	<i>TW</i>/σ_y	<i>R</i>/σ_y	<i>h_m</i>/σ_y
FC-3	6-Jul-07	0.27	11.8	1.31	1.32	0.59	2.76	0.19	0.39
	11-Aug-07	0.41	31.4	1.40	1.41	0.59	2.28	0.12	0.25
	12-Jun-08	0.20	5.4	1.24	1.26	0.46	4.62	0.42	0.89
	22-Jul-08	0.40	26.3	1.46	1.47	0.57	2.93	0.20	0.42
FC-4	7-Jul-07	0.36	21.1	1.33	1.35	0.42	3.42	0.29	0.65
	11-Aug-07	0.52	46.9	1.31	1.33	0.42	2.93	0.21	0.49
	12-Jun-08	0.22	6.3	1.19	1.20	0.41	3.91	0.51	1.08
	21-Jul-08	0.31	15.8	1.27	1.29	0.43	3.21	0.27	0.61
FC-5	8-Jul-07	0.31	18.2	1.25	1.27	0.29	3.12	0.26	0.59
	10-Aug-07	0.52	55.6	1.25	1.27	0.30	2.50	0.18	0.40
	25-Jun-08	0.17	4.5	1.08	1.10	0.28	4.05	0.44	1.01
	17-Jul-08	0.32	18.9	1.16	1.19	0.27	3.53	0.29	0.70
FC-6	8-Jul-07	0.31	17.8	1.27	1.30	1.11	0.79	0.06	0.15
	10-Aug-07	0.44	41.9	1.32	1.35	1.13	0.59	0.04	0.10
	25-Jun-08	0.17	4.8	1.20	1.22	1.10	0.97	0.10	0.24
	17-Jul-08	0.32	18.9	1.27	1.30	1.11	0.83	0.07	0.16

Table C-3: Instream wood data.

Reach ID	Date	<i>n</i>	<i>f</i>	Volumes (m ³)									<i>V_w/V</i>
				<i>V</i>	<i>V_w</i>	<i>V_{wb}</i>	<i>V_{wd}</i>	<i>V_{wp}</i>	<i>V_{wbp}</i>	<i>V_{wbd}</i>	<i>V_{wbpd}</i>		
ESL-1	10-Jun-08	0.19	4.5	25.81	0.204	0.942	0.156	0.173	0.197	0.183	0.152	0.0079	
	22-Jul-08	0.27	9.4	18.20	0.110	0.794	0.081	0.087	0.109	0.106	0.081	0.0060	
ESL-2	9-Jul-07	0.23	7.0	8.89	0.307	5.000	0.192	0.180	0.303	0.293	0.212	0.0345	
	6-Jun-08	0.20	4.8	12.94	0.444	5.032	0.301	0.244	0.395	0.471	0.297	0.0343	
	15-Jul-08	0.18	4.3	9.55	0.272	4.243	0.192	0.165	0.257	0.294	0.186	0.0285	
ESL-3	10-Jul-07	0.21	6.3	5.51	0.055	1.125	0.035	0.043	0.048	0.038	0.031	0.0099	
	7-Jun-08	0.16	3.7	7.94	0.069	1.051	0.038	0.047	0.057	0.042	0.029	0.0087	
	15-Jul-08	0.20	5.7	7.31	0.050	0.689	0.035	0.035	0.035	0.035	0.026	0.0069	
ESL-4	10-Jul-07	0.25	8.7	7.77	0.009	0.227	0.005	0.006	0.014	0.010	0.009	0.0012	
	7-Jun-08	0.23	6.3	13.29	0.065	0.833	0.037	0.045	0.089	0.068	0.057	0.0049	
	14-Jul-08	0.26	8.7	11.01	0.047	0.769	0.031	0.030	0.065	0.058	0.046	0.0042	
ESL-5	12-Jul-07	0.34	16.1	8.59	0.089	1.090	0.065	0.060	0.064	0.069	0.047	0.0103	
	9-Jun-08	0.30	11.1	13.41	0.307	6.929	0.232	0.216	0.359	0.606	0.255	0.0229	
	14-Jul-08	0.29	10.8	12.07	0.272	3.320	0.197	0.149	0.164	0.266	0.123	0.0226	
ESL-6	13-Jul-07	0.07	0.7	3.26	0.009	0.266	0.006	0.004	0.004	0.006	0.003	0.0027	
	9-Jun-08	0.05	0.3	5.28	0.023	0.429	0.016	0.010	0.010	0.016	0.008	0.0043	
	14-Jul-08	0.08	0.8	4.68	0.018	0.383	0.013	0.009	0.009	0.013	0.007	0.0038	
ESL-7	12-Jul-07	0.19	4.8	11.30	0.074	1.105	0.058	0.027	0.057	0.103	0.049	0.0065	
	8-Jun-08	0.17	3.5	19.39	0.137	1.387	0.115	0.080	0.176	0.226	0.149	0.0071	
	15-Jul-08	0.19	4.8	17.06	0.122	1.087	0.095	0.059	0.090	0.140	0.066	0.0072	
ESL-8	11-Jul-07	0.21	6.0	16.60	0.047	0.480	0.032	0.027	0.049	0.060	0.039	0.0028	
	9-Jun-08	0.18	4.2	25.61	0.158	1.058	0.133	0.118	0.197	0.205	0.151	0.0062	
	16-Jul-08	0.20	5.3	22.17	0.090	0.666	0.072	0.055	0.093	0.111	0.071	0.0040	
ESL-9	11-Jul-07	0.26	8.8	9.73	0.066	0.674	0.049	0.033	0.033	0.049	0.023	0.0067	
	8-Jun-08	0.21	5.5	14.01	0.168	1.197	0.121	0.109	0.109	0.121	0.080	0.0120	
	16-Jul-08	0.24	7.4	10.93	0.071	0.647	0.049	0.038	0.038	0.049	0.025	0.0065	
FC-1	5-Jul-07	0.13	3.0	3.88	0.006	0.152	0.005	0.006	0.006	0.005	0.005	0.0015	
	11-Jun-08	0.09	1.3	7.96	0.030	0.382	0.021	0.030	0.030	0.021	0.020	0.0038	
	23-Jul-08	0.17	5.0	3.65	0.007	0.193	0.007	0.007	0.007	0.007	0.007	0.0019	
FC-2	7-Jul-07	0.16	4.1	1.70	0.031	1.805	0.022	0.014	0.014	0.022	0.010	0.0180	
	11-Jun-08	0.13	2.2	3.83	0.041	1.060	0.028	0.026	0.026	0.028	0.017	0.0106	
	23-Jul-08	0.22	8.0	1.94	0.029	1.517	0.016	0.017	0.017	0.016	0.010	0.0152	
FC-3	6-Jul-07	0.27	11.8	2.43	0.082	3.385	0.067	0.056	0.056	0.067	0.045	0.0339	
	12-Jun-08	0.20	5.4	5.86	0.253	4.508	0.215	0.163	0.165	0.223	0.136	0.0432	
	22-Jul-08	0.40	26.3	2.60	0.109	4.200	0.095	0.074	0.074	0.095	0.064	0.0420	
FC-4	7-Jul-07	0.36	21.1	3.72	0.022	0.959	0.015	0.018	0.031	0.026	0.024	0.0060	
	12-Jun-08	0.22	6.3	7.85	0.135	2.157	0.129	0.118	0.153	0.156	0.140	0.0172	
	21-Jul-08	0.31	15.8	3.34	0.033	1.591	0.025	0.026	0.044	0.041	0.034	0.0098	
FC-5	8-Jul-07	0.31	18.2	0.91	0.001	0.276	0.001	0.001	0.002	0.001	0.001	0.0012	
	25-Jun-08	0.17	4.5	2.10	0.005	0.508	0.003	0.004	0.008	0.006	0.005	0.0023	
	17-Jul-08	0.32	18.9	1.04	0.001	0.292	0.001	0.001	0.002	0.001	0.001	0.0013	
FC-6	8-Jul-07	0.31	17.8	1.44	0.006	0.382	0.004	0.005	0.005	0.004	0.004	0.0038	
	25-Jun-08	0.17	4.8	3.00	0.015	0.502	0.013	0.014	0.014	0.013	0.012	0.0050	
	17-Jul-08	0.32	18.9	1.57	0.007	0.454	0.007	0.005	0.005	0.007	0.005	0.0045	

Table C-4: Three-dimensional spatial variability data.

Reach ID	Date	n	f	100% Channel Width			50% Channel Width		
				h_{a3}/σ_{h3}	h_{a3}/σ_{z3}	h_{m3}/σ_{z3}	h_{a3}/σ_{h3}	h_{a3}/σ_{z3}	h_{m3}/σ_{z3}
ESL-1	10-Jun-08	0.19	4.5	1.82	1.15	3.67	2.08	1.48	4.14
	22-Jul-08	0.27	9.4	1.71	1.10	3.44	1.79	1.34	3.69
ESL-2	9-Jul-07	0.23	7.0	1.66	1.11	4.88	2.13	1.45	4.97
	6-Jun-08	0.20	4.8	1.81	1.40	4.81	2.26	1.73	4.73
	15-Jul-08	0.18	4.3	1.64	1.29	4.35	2.06	1.57	4.23
ESL-3	10-Jul-07	0.21	6.3	1.24	1.06	4.26	1.54	1.32	3.92
	7-Jun-08	0.16	3.7	1.38	1.18	4.21	1.64	1.36	3.80
	15-Jul-08	0.20	5.7	1.22	1.11	4.28	1.44	1.27	3.81
ESL-4	10-Jul-07	0.25	8.7	1.55	1.15	3.85	1.75	1.29	3.67
	7-Jun-08	0.23	6.3	1.66	1.13	3.81	2.11	1.57	4.08
	14-Jul-08	0.26	8.7	1.80	1.42	3.99	2.10	1.60	3.84
ESL-5	12-Jul-07	0.34	16.1	1.44	0.86	3.13	1.63	0.96	2.89
	9-Jun-08	0.30	11.1	1.69	1.14	3.80	2.04	1.28	3.27
	14-Jul-08	0.29	10.8	1.50	1.08	5.68	1.71	1.19	5.11
ESL-6	13-Jul-07	0.07	0.7	2.39	2.50	5.16	3.25	3.60	5.41
	9-Jun-08	0.05	0.3	2.26	2.30	4.40	4.17	4.29	6.11
	14-Jul-08	0.08	0.8	2.41	2.55	4.84	3.53	3.78	5.45
ESL-7	12-Jul-07	0.19	4.8	1.60	1.26	3.83	1.83	1.49	3.79
	8-Jun-08	0.17	3.5	1.74	1.54	5.24	1.99	1.88	5.46
	15-Jul-08	0.19	4.8	1.63	1.48	4.84	1.77	1.76	4.92
ESL-8	11-Jul-07	0.21	6.0	1.56	1.26	4.04	1.89	1.47	3.81
	9-Jun-08	0.18	4.2	1.50	1.24	4.65	1.74	1.49	4.36
	16-Jul-08	0.20	5.3	1.53	1.24	4.68	1.62	1.39	4.27
ESL-9	11-Jul-07	0.26	8.8	1.72	1.30	3.84	1.84	1.55	3.93
	8-Jun-08	0.21	5.5	1.91	1.56	4.38	2.09	1.84	4.52
	16-Jul-08	0.24	7.4	1.82	1.50	4.51	1.89	1.63	4.56
FC-1	5-Jul-07	0.13	3.0	1.90	1.46	4.03	2.79	1.88	4.17
	11-Jun-08	0.09	1.3	2.25	1.88	4.08	3.76	3.07	5.42
	23-Jul-08	0.17	5.0	1.90	1.38	4.07	2.75	1.82	4.31
FC-2	7-Jul-07	0.16	4.1	1.72	1.54	4.96	2.18	1.89	5.11
	11-Jun-08	0.13	2.2	2.28	2.24	4.95	2.77	2.71	5.00
	23-Jul-08	0.22	8.0	1.83	1.76	4.66	2.22	2.14	4.84
FC-3	6-Jul-07	0.27	11.8	1.80	1.16	3.15	1.98	1.28	3.21
	12-Jun-08	0.20	5.4	1.78	1.53	4.14	2.23	1.96	4.25
	22-Jul-08	0.40	26.3	1.65	1.13	3.71	1.73	1.19	3.79
FC-4	7-Jul-07	0.36	21.1	1.64	0.96	3.49	1.78	1.05	3.31
	12-Jun-08	0.22	6.3	1.95	1.49	4.33	2.13	1.70	4.41
	21-Jul-08	0.31	15.8	1.61	0.85	3.03	1.71	1.00	3.08
FC-5	8-Jul-07	0.31	18.2	1.54	0.84	3.56	1.78	0.89	2.86
	25-Jun-08	0.17	4.5	1.68	1.09	4.55	2.03	1.28	3.87
	17-Jul-08	0.32	18.9	1.57	0.78	3.07	1.68	0.81	2.91
FC-6	8-Jul-07	0.31	17.8	1.45	0.64	3.05	1.69	0.74	2.80
	25-Jun-08	0.17	4.8	1.82	1.06	3.58	2.08	1.20	3.59
	17-Jul-08	0.32	18.9	1.54	0.71	3.04	1.77	0.81	2.98

APPENDIX D

DEPTH VARIABILITY GRIDS

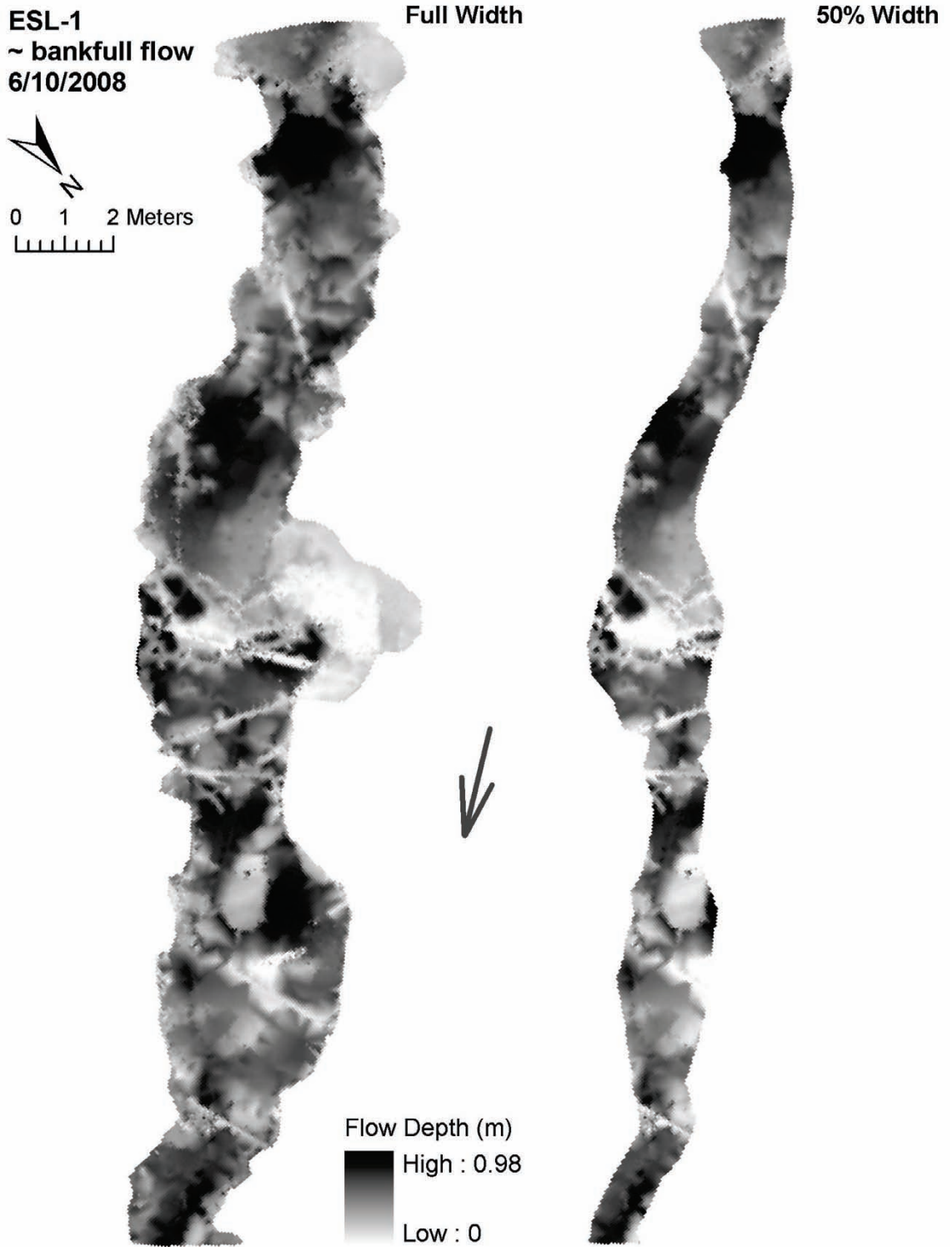


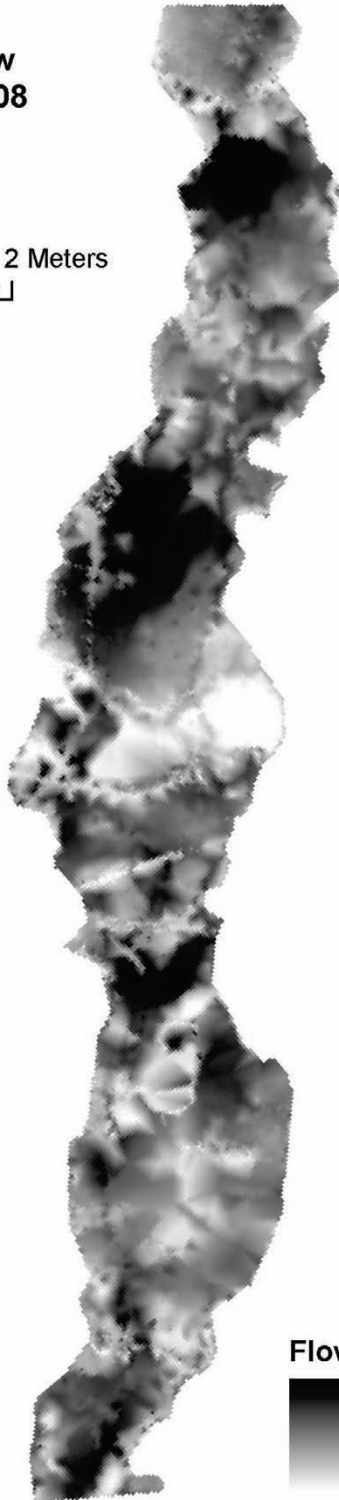
Figure D-1: Depth variability for ~bankfull flow, reach ESL-1 (6/10/2008).

ESL-1
mid flow
7/22/2008



0 1 2 Meters

Full Width



50% Width



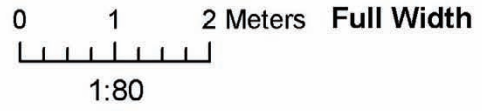
Flow Depth (m)

High : 0.76

Low : 0

Figure D-2: Depth variability for mid flow, reach ESL-1 (7/22/2008).

ESL-2
mid flow
7/9/2007



50% Width

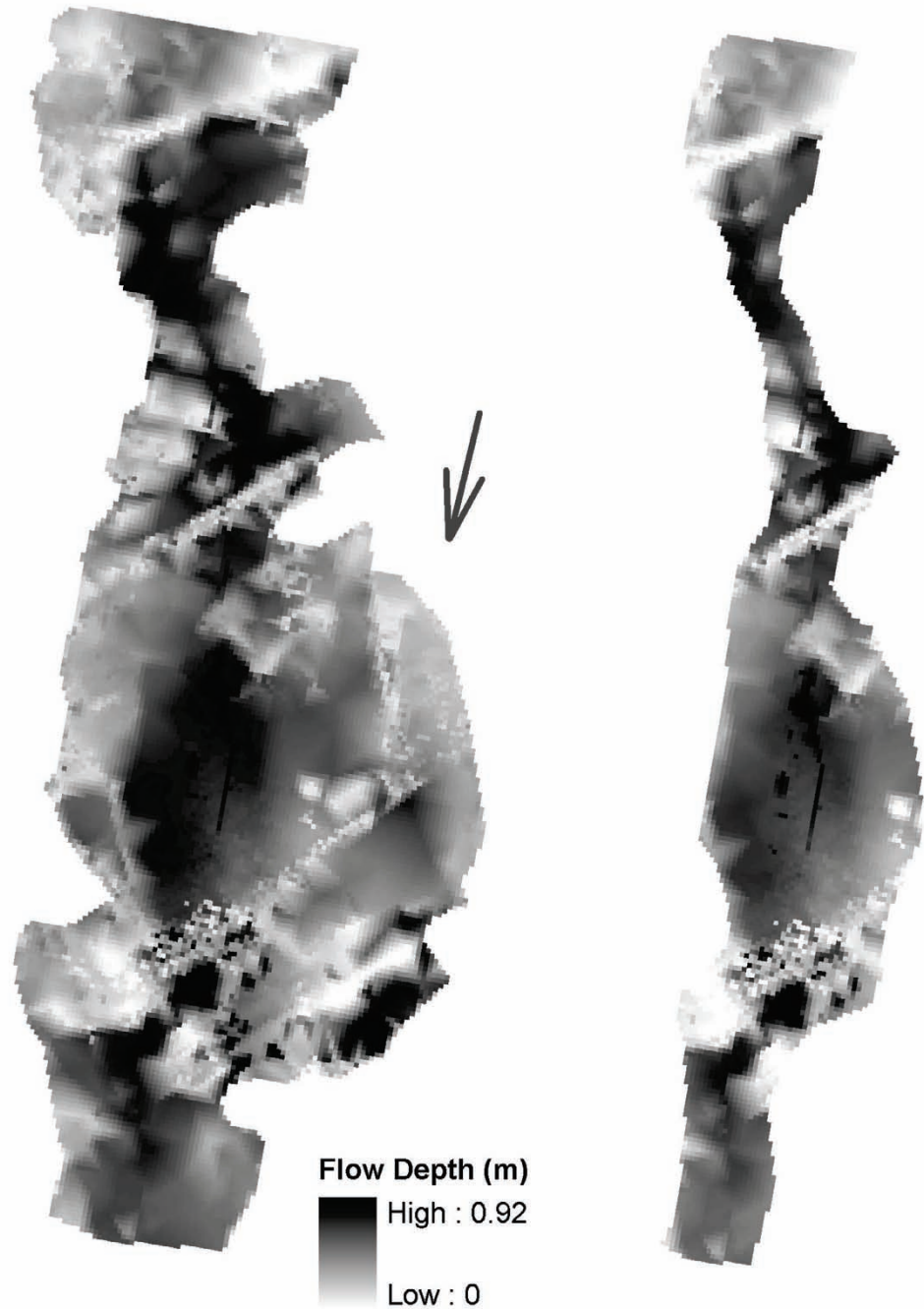


Figure D-3: Depth variability for mid flow, reach ESL-2 (7/9/2007).

ESL-2
~ bankfull flow
6/6/2008

Full Width
0 1 2 Meters
1:80

50% Width

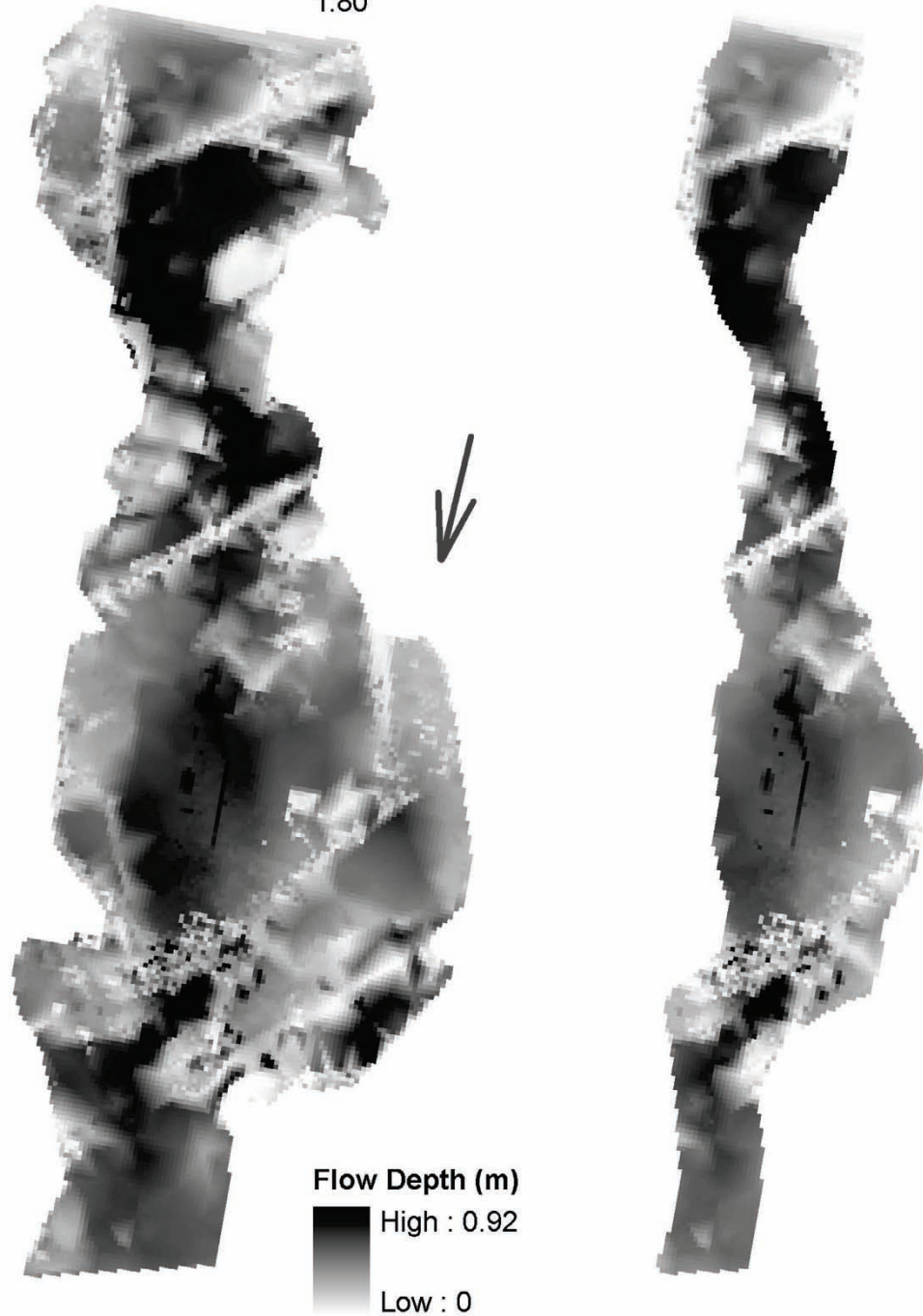


Figure D-4: Depth variability for ~bankfull flow, reach ESL-2 (6/6/2008).

ESL-2
mid flow
7/15/2008

Full Width
0 1 2 Meters
1:80

50% Width

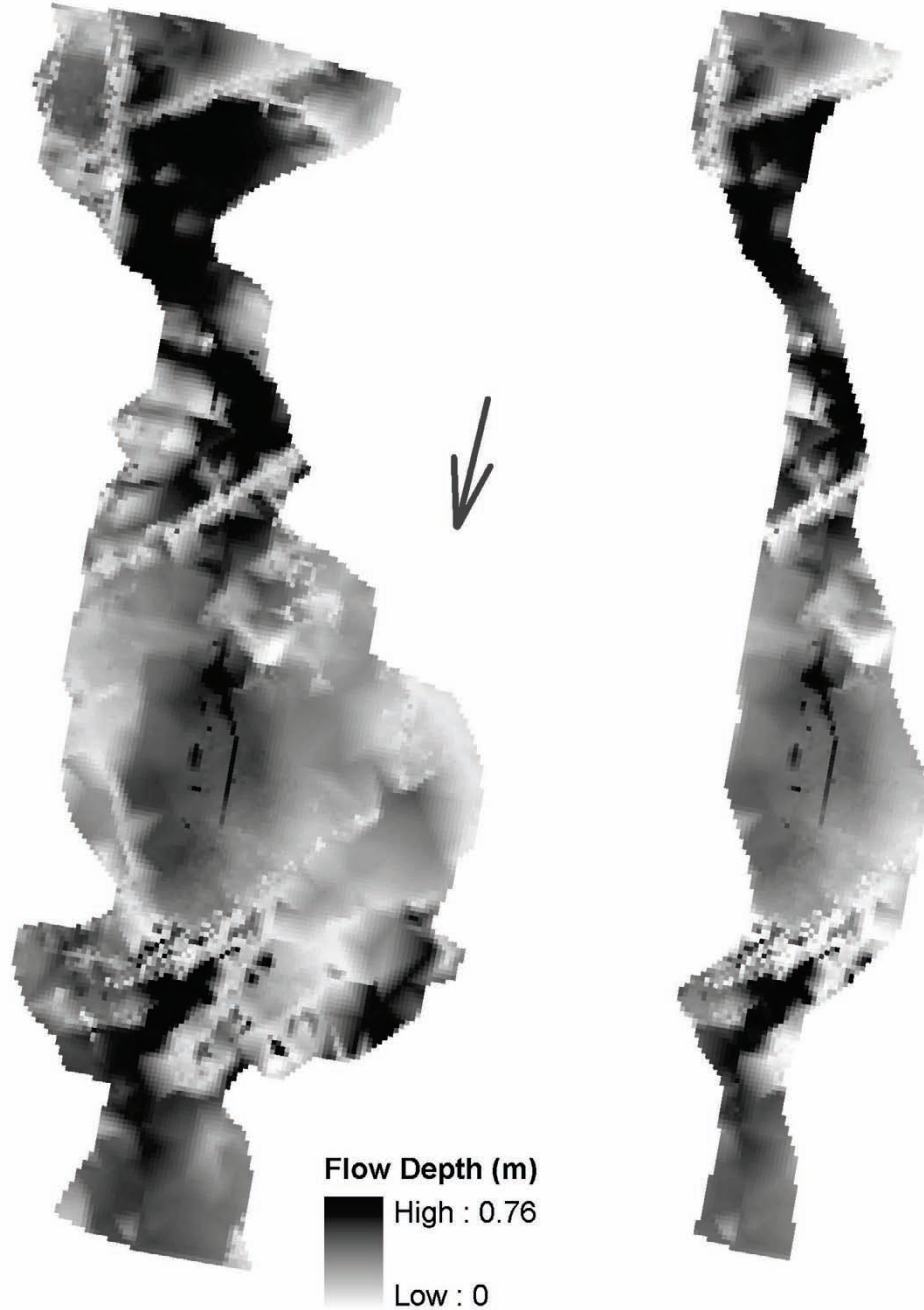
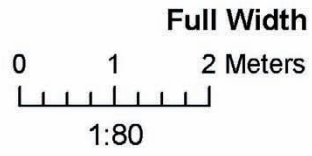


Figure D-5: Depth variability for mid flow, reach ESL-2 (7/15/2008).

ESL-3
mid flow
7/10/2007



50% Width

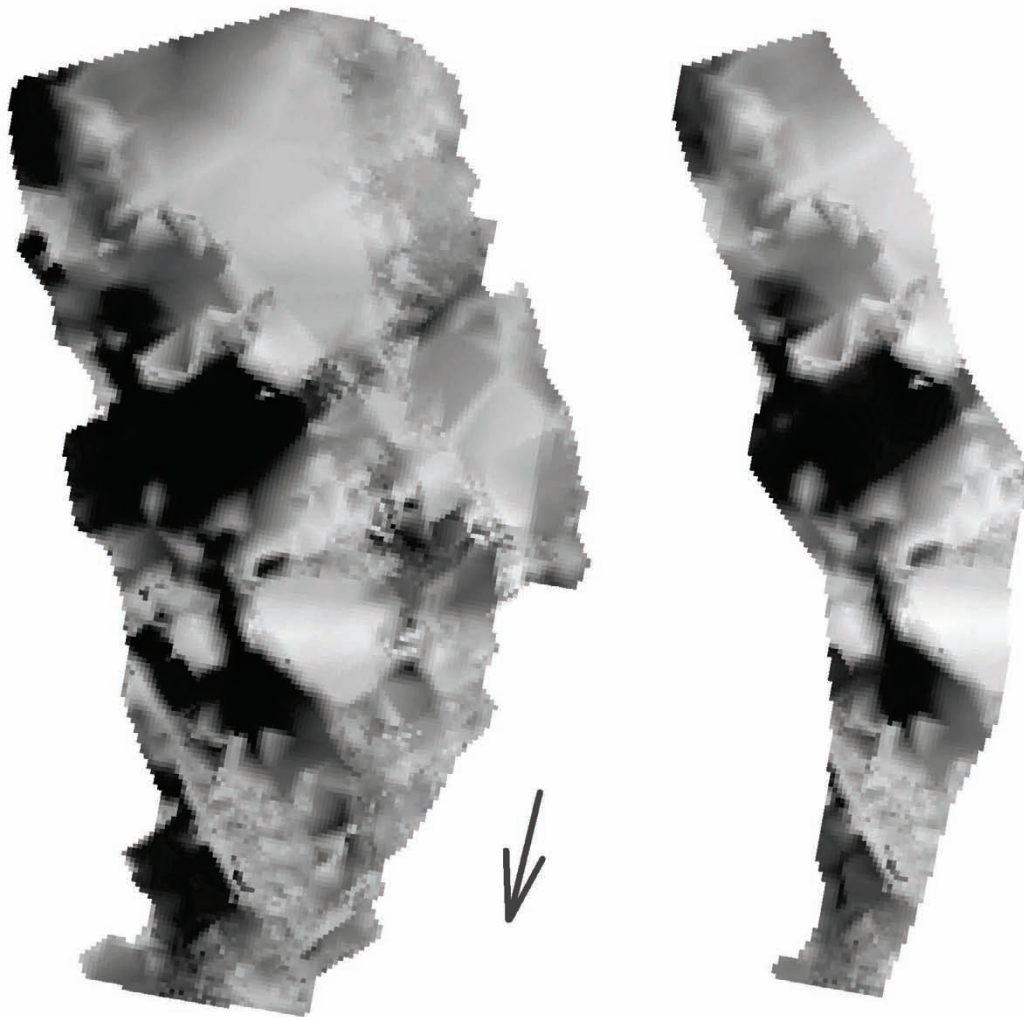


Figure D-6: Depth variability for mid flow, reach ESL-3 (7/10/2007).

ESL-3
~ bankfull flow
6/7/2008

Full Width
0 1 2 Meters
1:80

50% Width

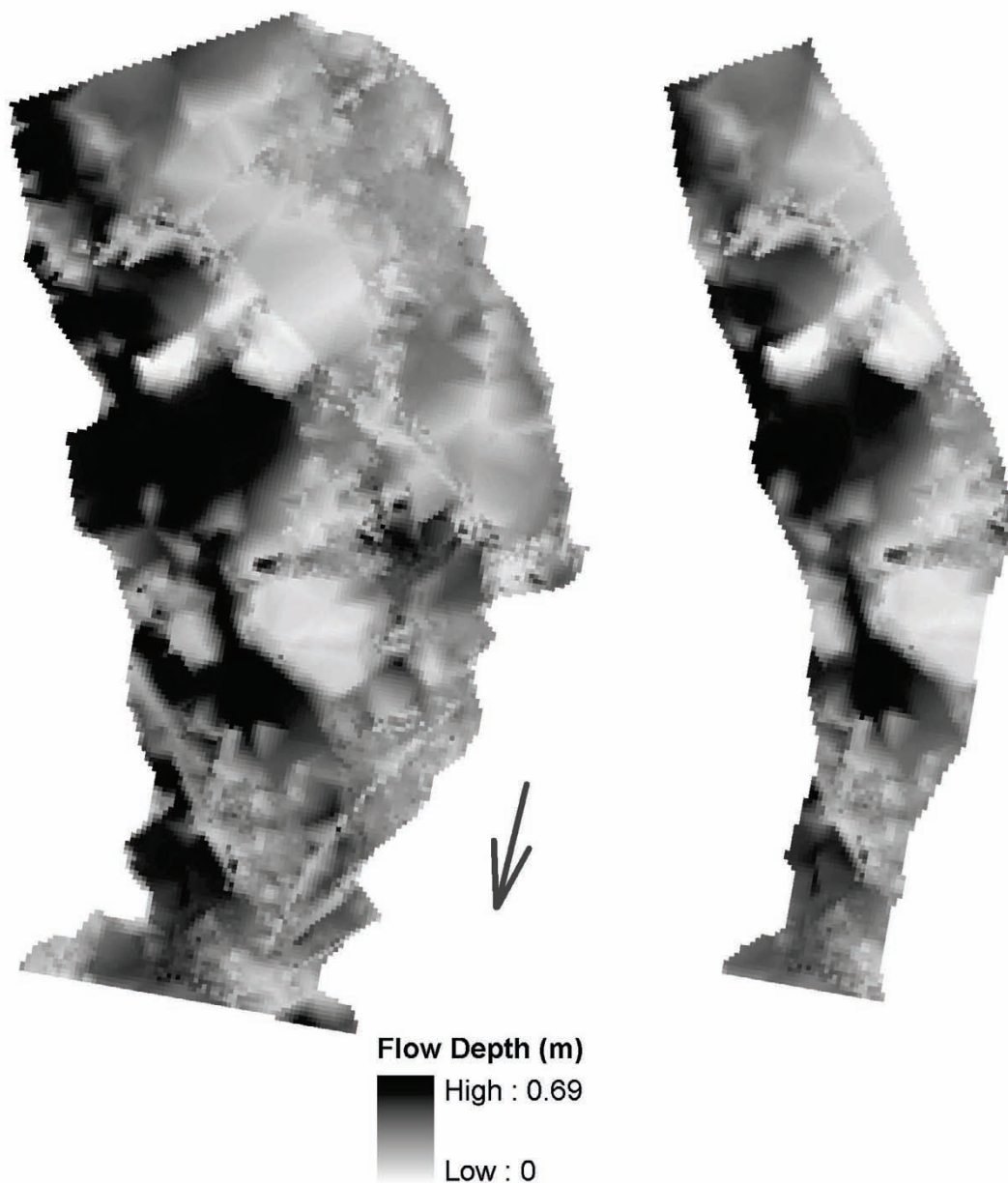
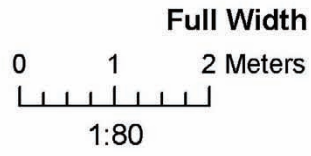
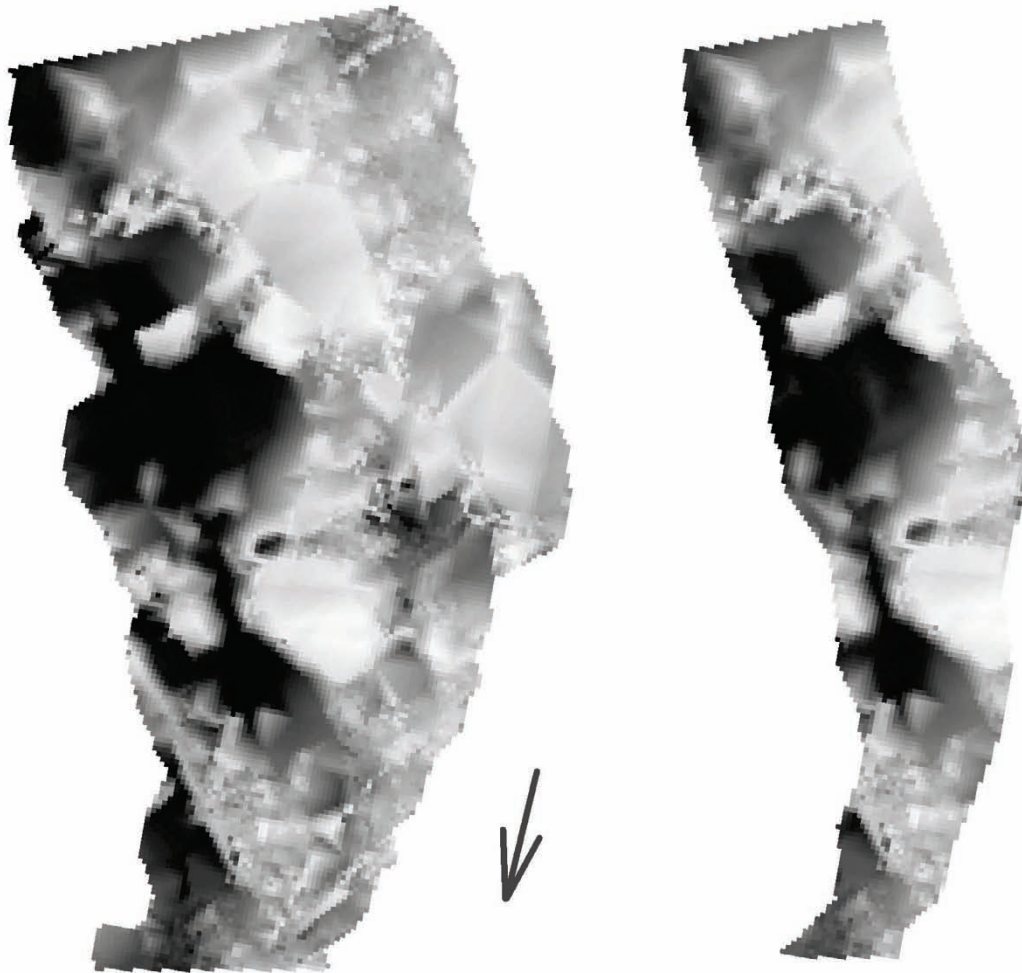


Figure D-7: Depth variability for ~bankfull flow, reach ESL-3 (6/7/2008).

ESL-3
mid flow
7/15/2008



50% Width



Flow Depth (m)



Figure D-8: Depth variability for mid flow, reach ESL-3 (7/15/2008).

ESL-4
mid flow
7/10/2007

Full Width
0 1 2 Meters
1:90

50% Width

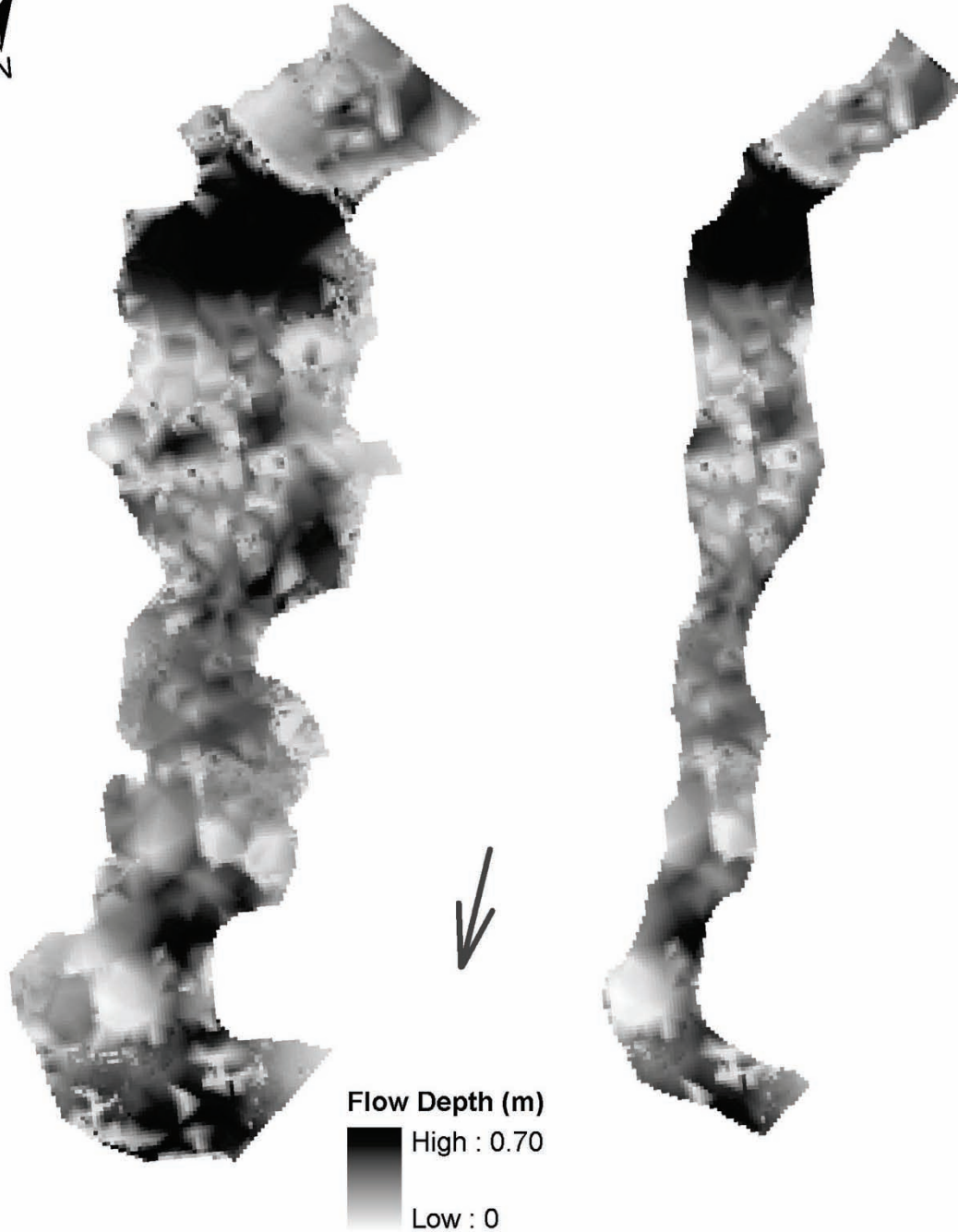


Figure D-9: Depth variability for mid flow, reach ESL-4 (7/10/2007).

ESL-4
~ bankfull flow
6/7/2008

Full Width
0 1 2 Meters
1:90

50% Width

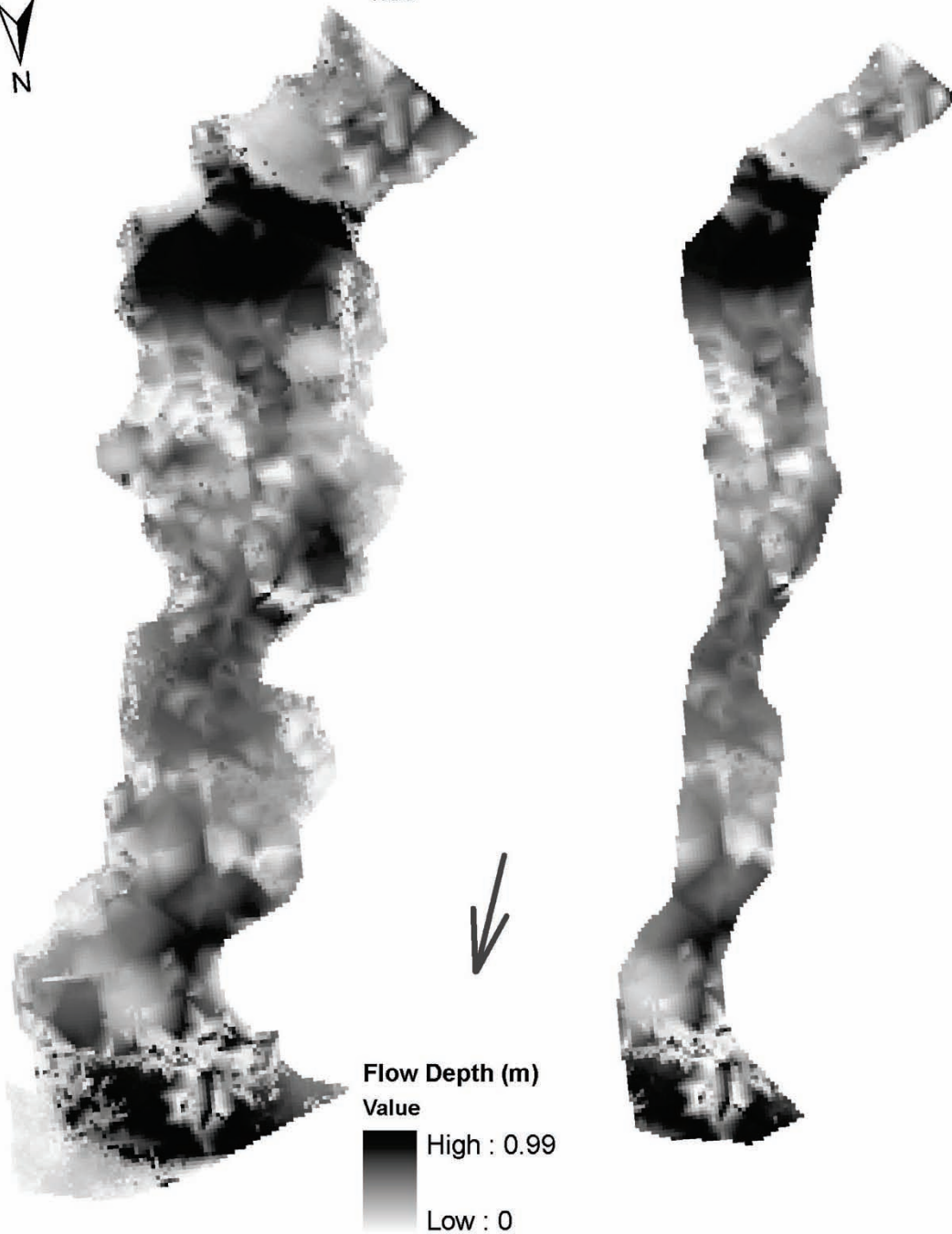


Figure D-10: Depth variability for ~bankfull flow, reach ESL-4 (6/7/2008).

ESL-4
mid flow
7/14/2008



Full Width
0 1 2 Meters
1:90

50% Width

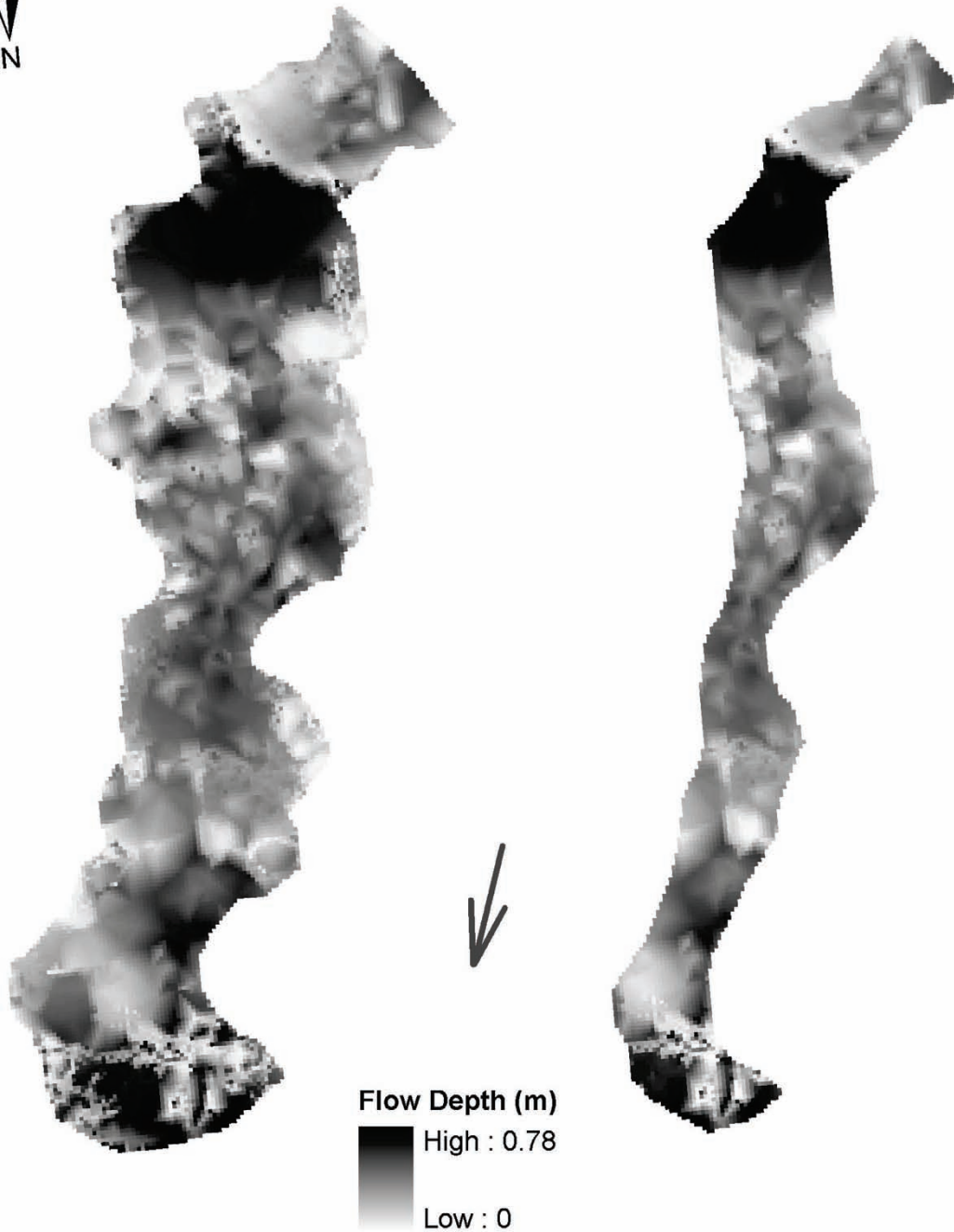


Figure D-11: Depth variability for mid flow, reach ESL-4 (7/14/2008).

ESL-5
mid flow
7/12/2007

Full Width
0 1 2 Meters
1:80

50% Width

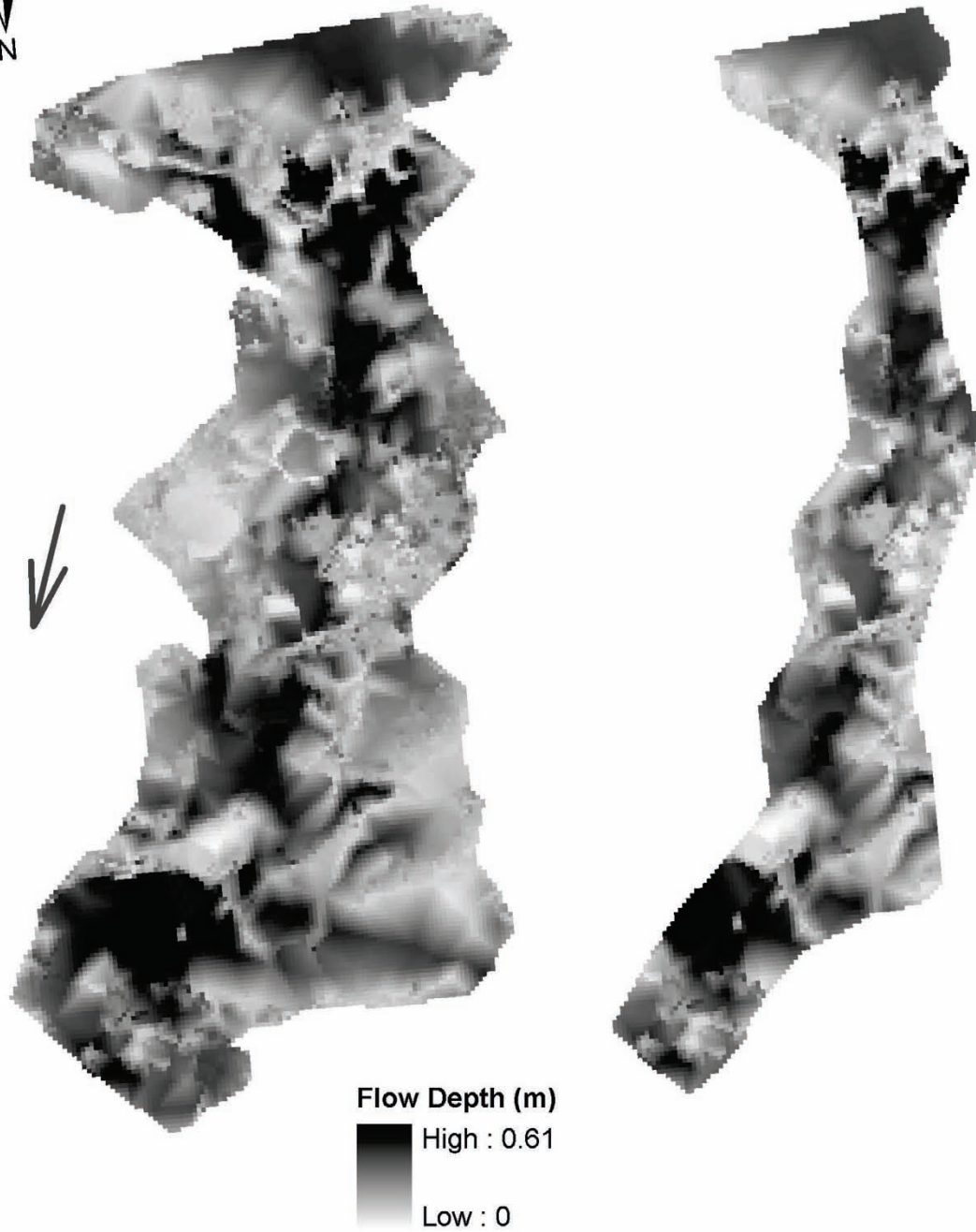


Figure D-12: Depth variability for mid flow, reach ESL-5 (7/12/2007).

ESL-5
~ bankfull flow
6/9/2008

Full Width
0 1 2 Meters
1:80

50% Width

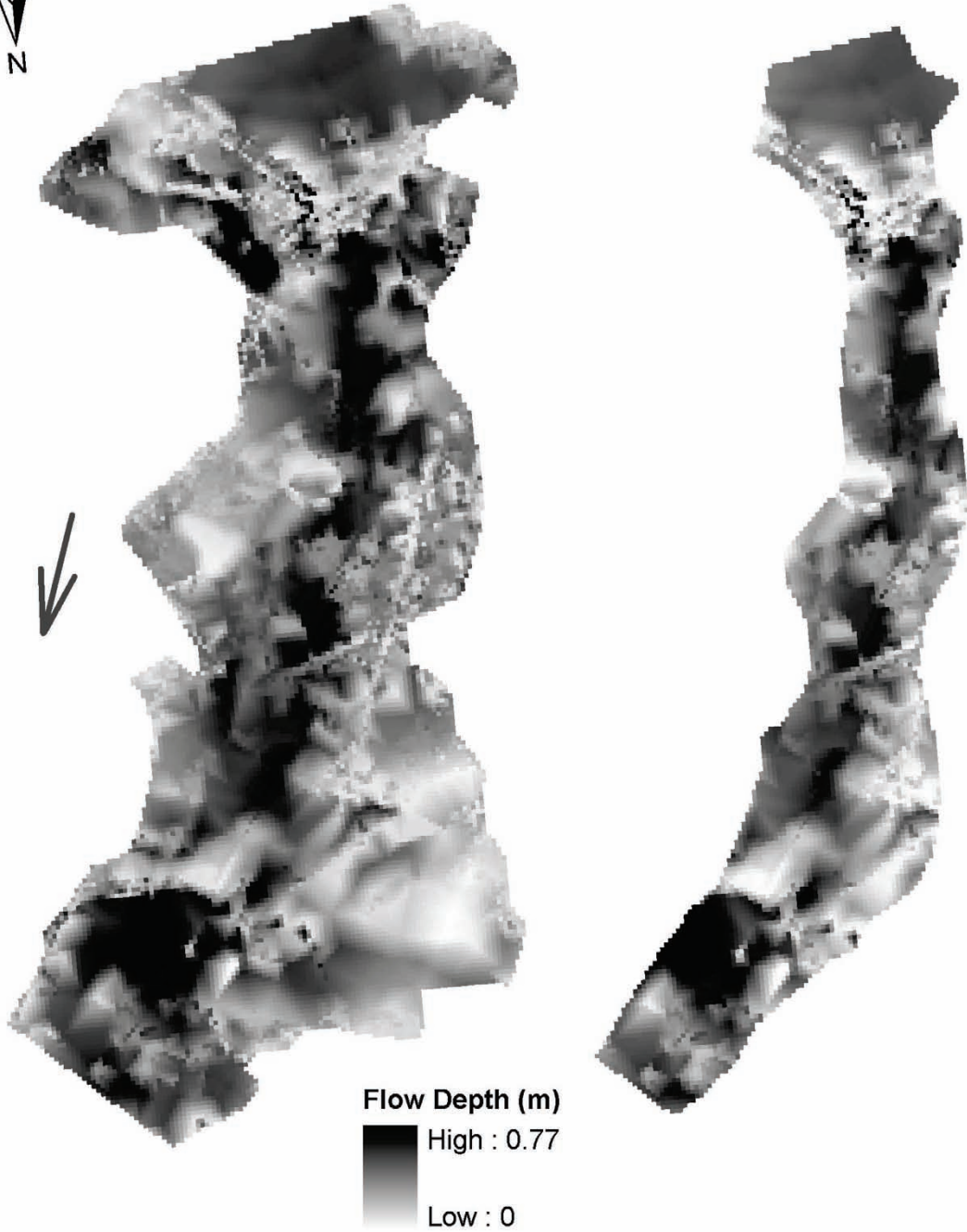


Figure D-13: Depth variability for ~bankfull flow, reach ESL-5 (6/9/2008).

ESL-5
mid flow
7/14/2008

Full Width
0 1 2 Meters
1:80

50% Width

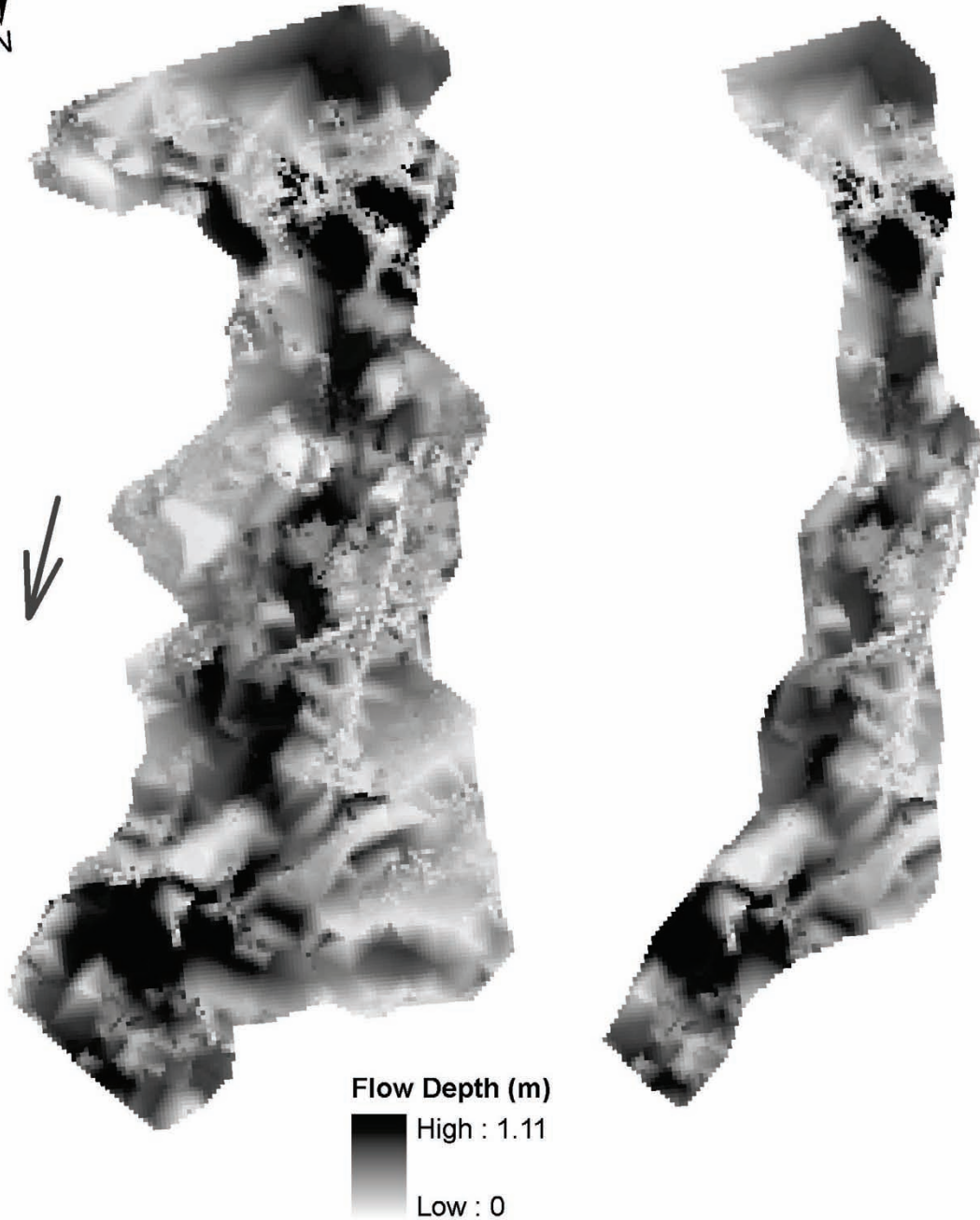
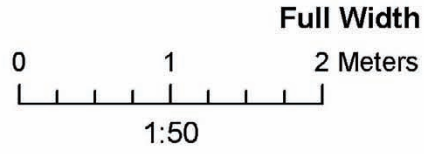


Figure D-14: Depth variability for mid flow, reach ESL-5 (7/14/2008).

ESL-6
mid flow
7/13/2007



50% Width

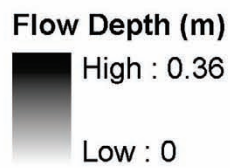


Figure D-15: Depth variability for mid flow, reach ESL-6 (7/13/2007).

ESL-6
~ bankfull flow
6/9/2008

Full Width

50% Width

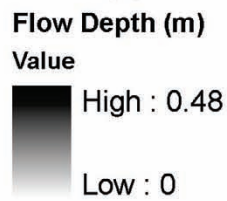
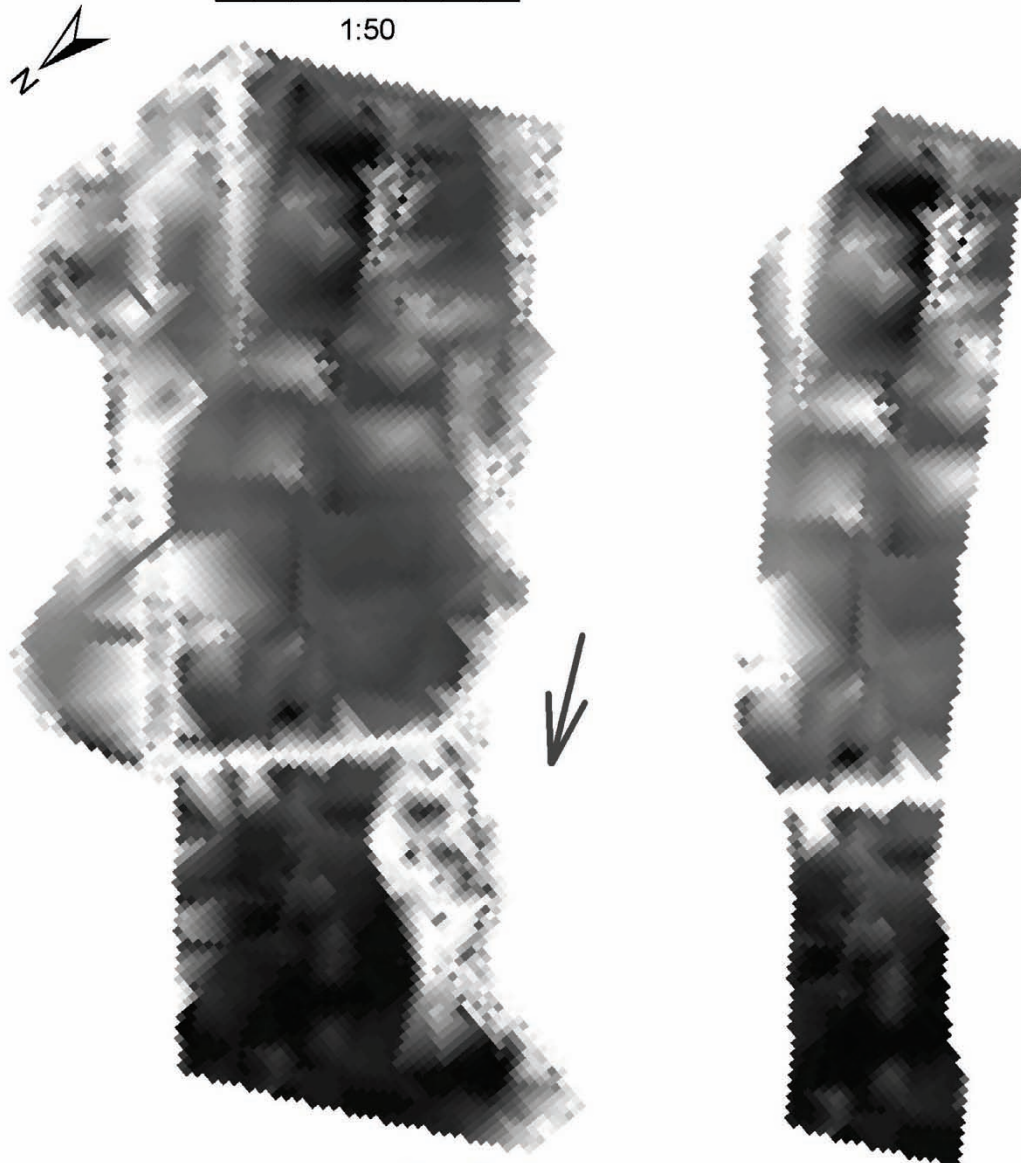
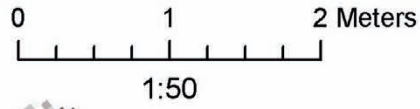
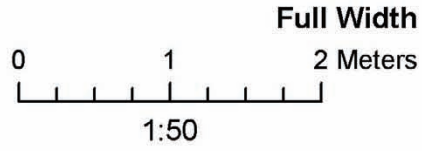


Figure D-16: Depth variability for ~bankfull flow, reach ESL-6 (6/9/2008).

ESL-6
mid flow
7/14/2008



50% Width

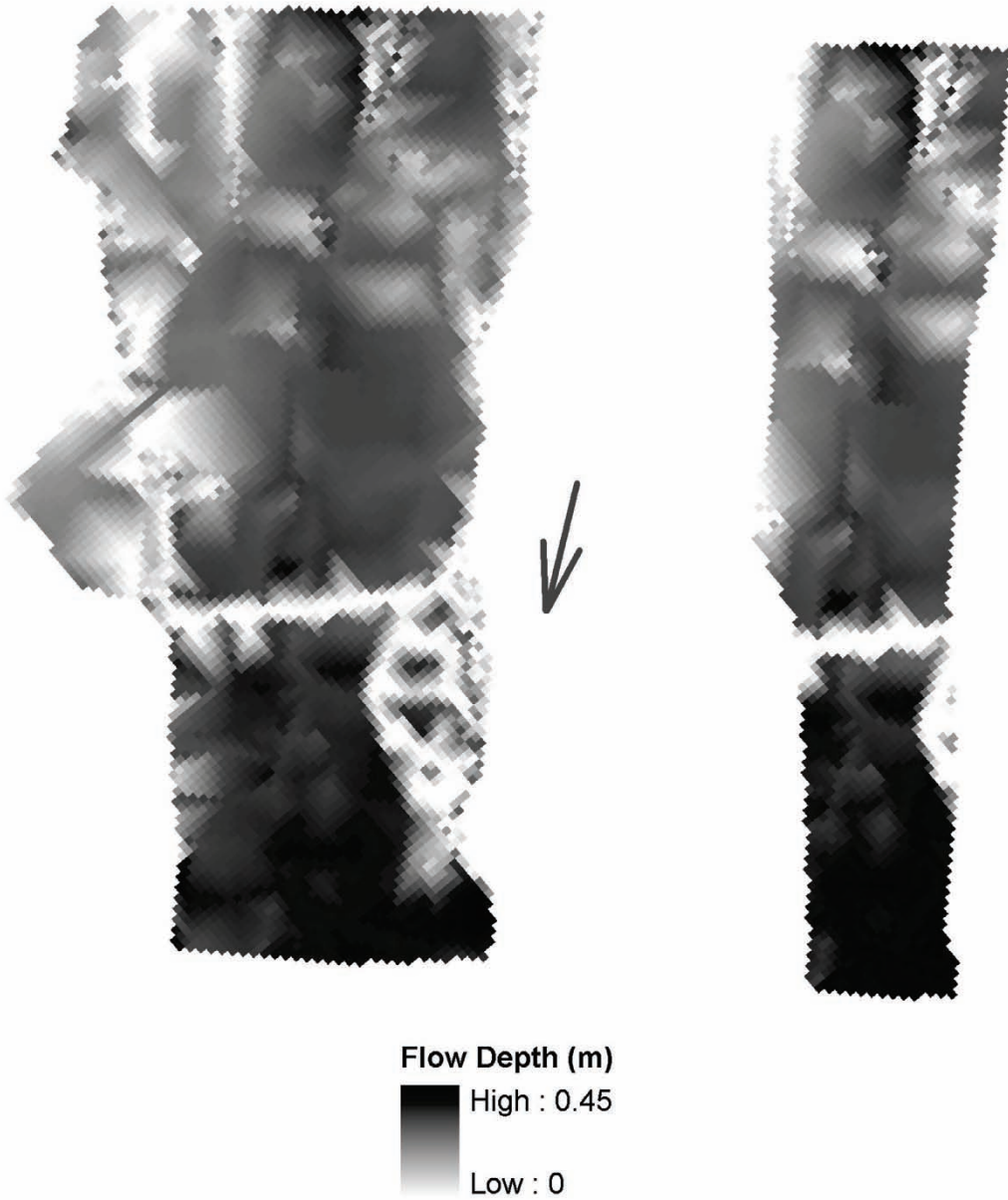


Figure D-17: Depth variability for mid flow, reach ESL-6 (7/14/2008).

ESL-7
mid flow
7/12/2007



Full Width
0 1 2 Meters
1:120

50% Width

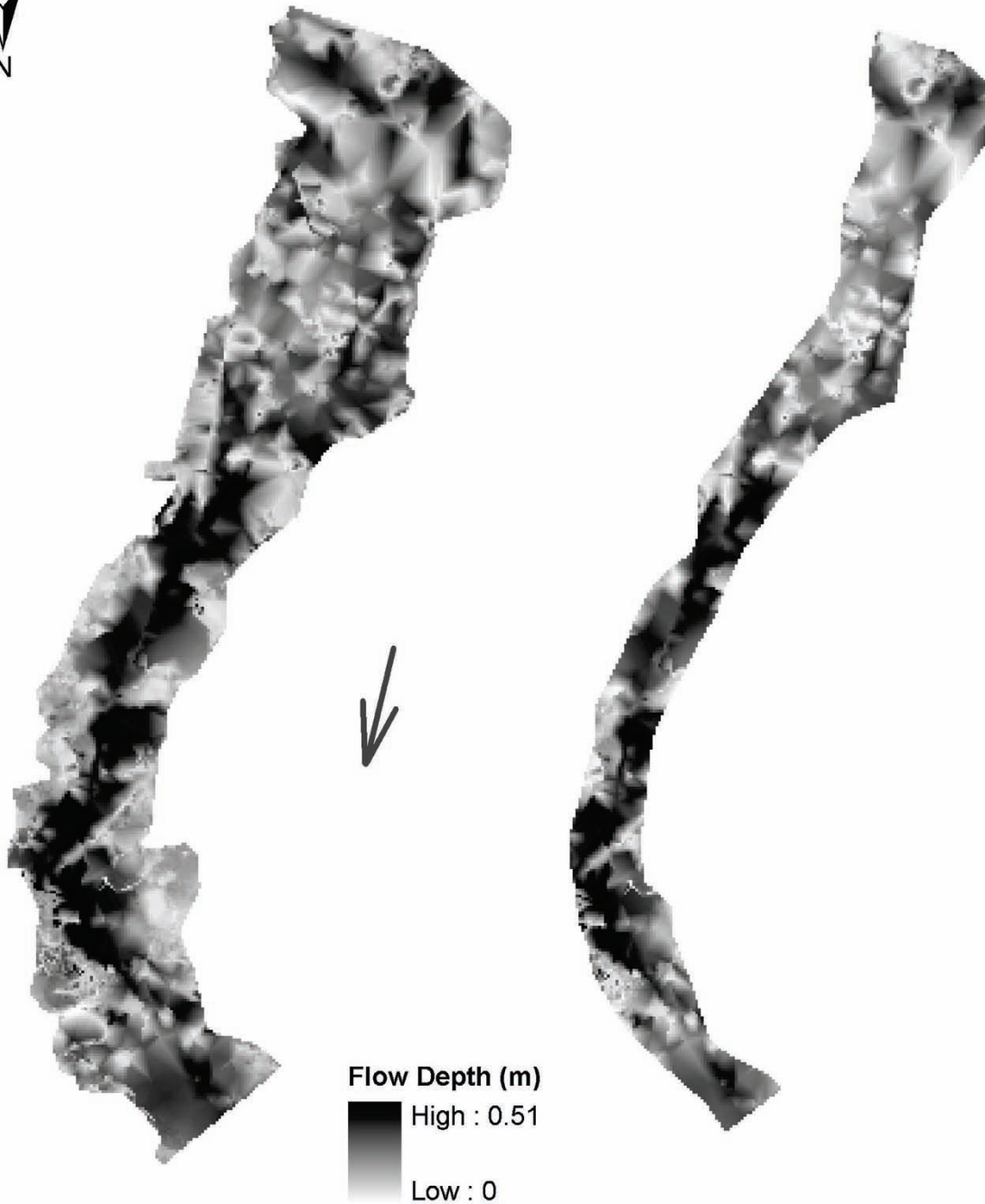


Figure D-18: Depth variability for mid flow, reach ESL-7 (7/12/2007).

ESL-7
~ bankfull flow
6/8/2008

Full Width
0 1 2 Meters
1:120

50% Width

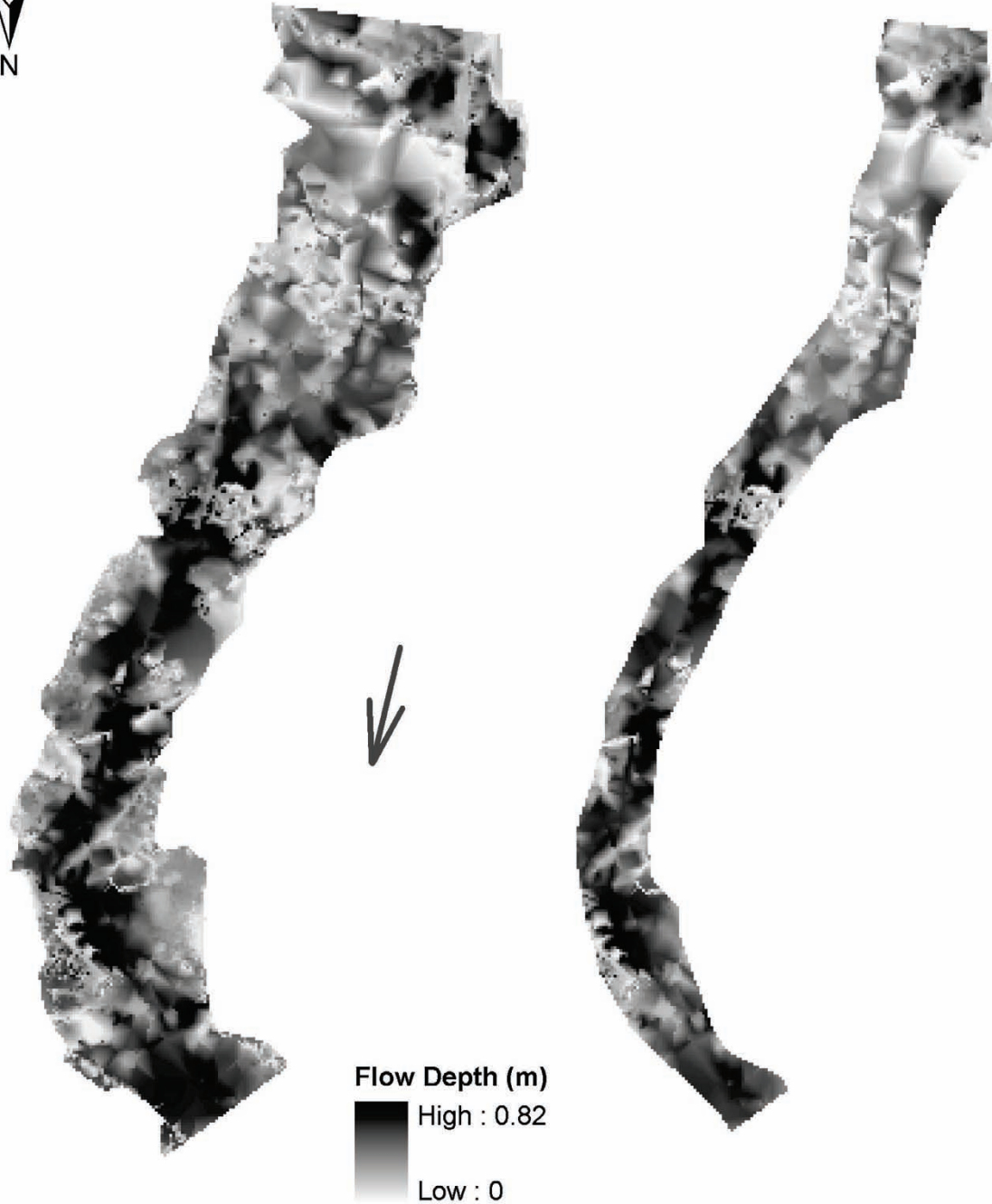
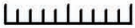


Figure D-19: Depth variability for ~bankfull flow, reach ESL-7 (6/8/2008).

ESL-7
mid flow
7/15/2008



Full Width
0 1 2 Meters

1:120

50% Width

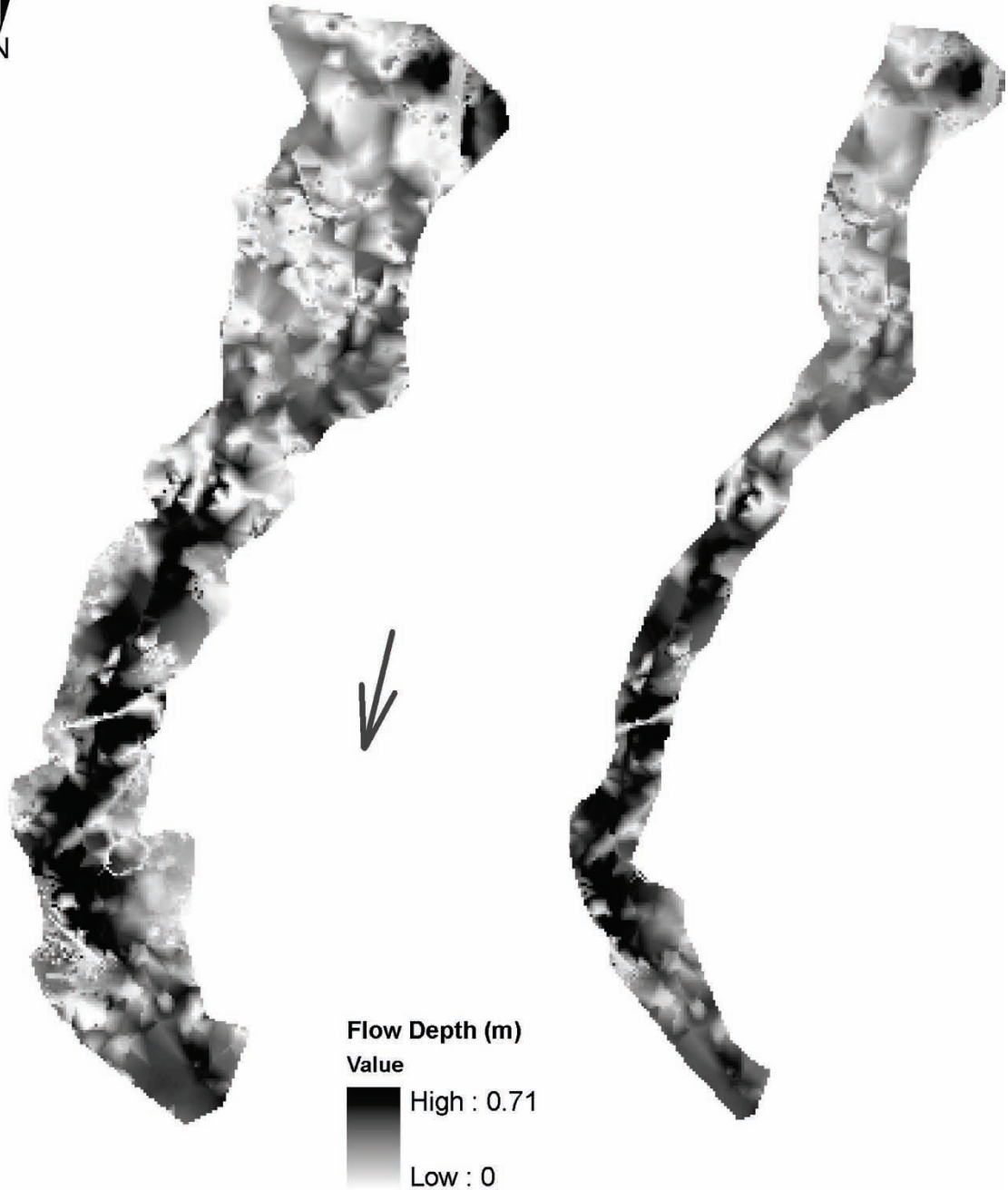


Figure D-20: Depth variability for mid flow, reach ESL-7 (7/15/2008).

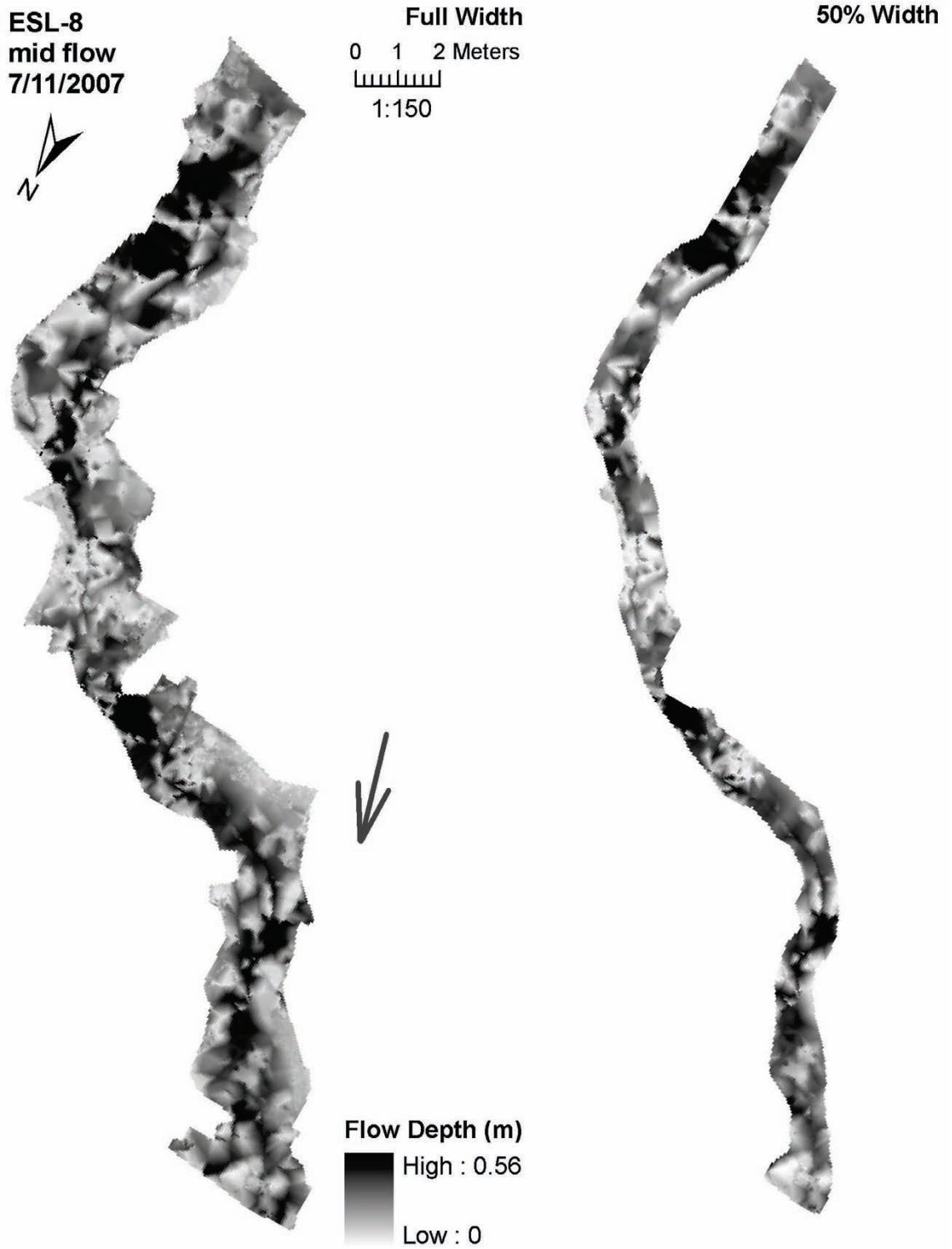


Figure D-21: Depth variability for mid flow, reach ESL-8 (7/11/2007).

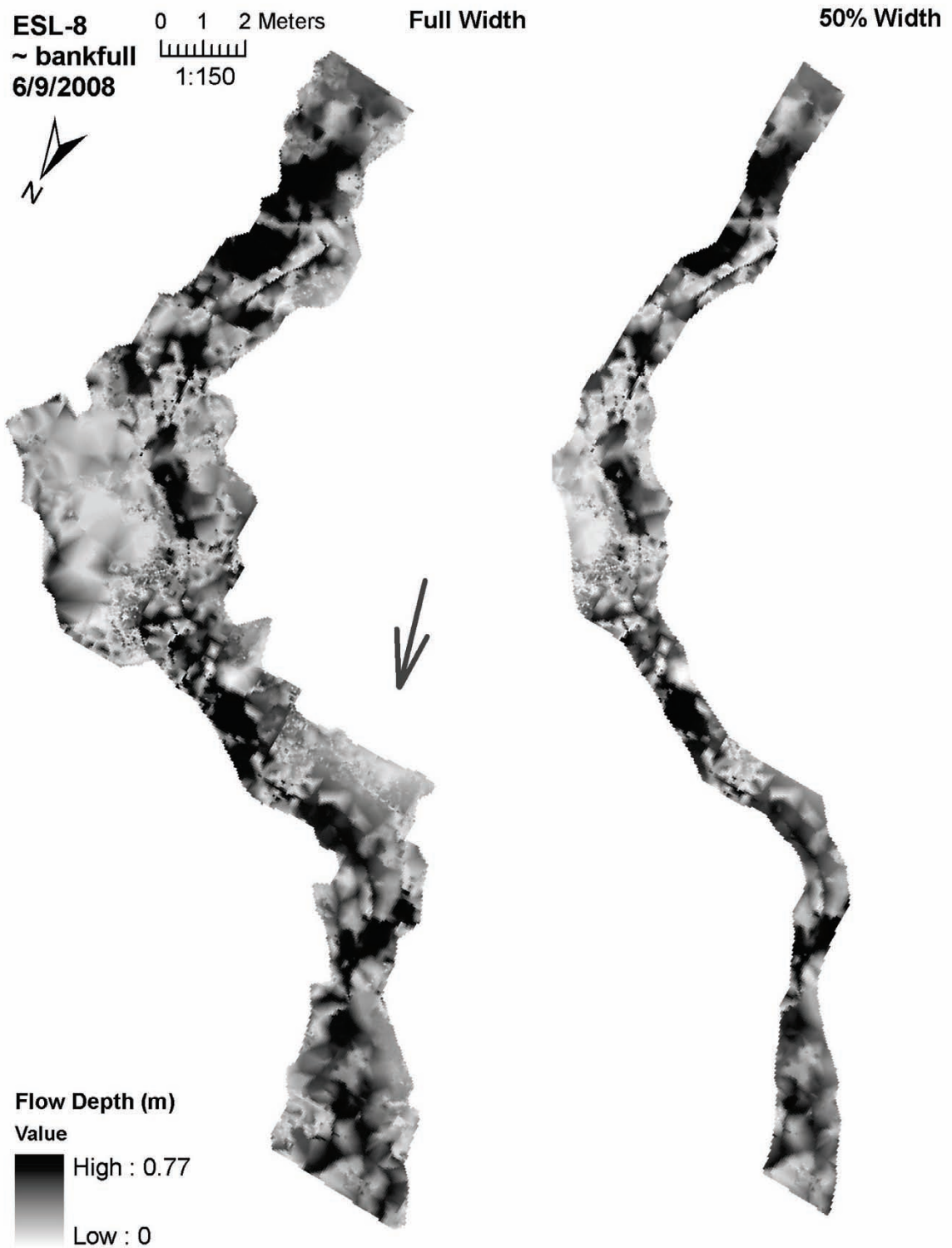


Figure D-22: Depth variability for ~bankfull flow, reach ESL-8 (6/9/2008).

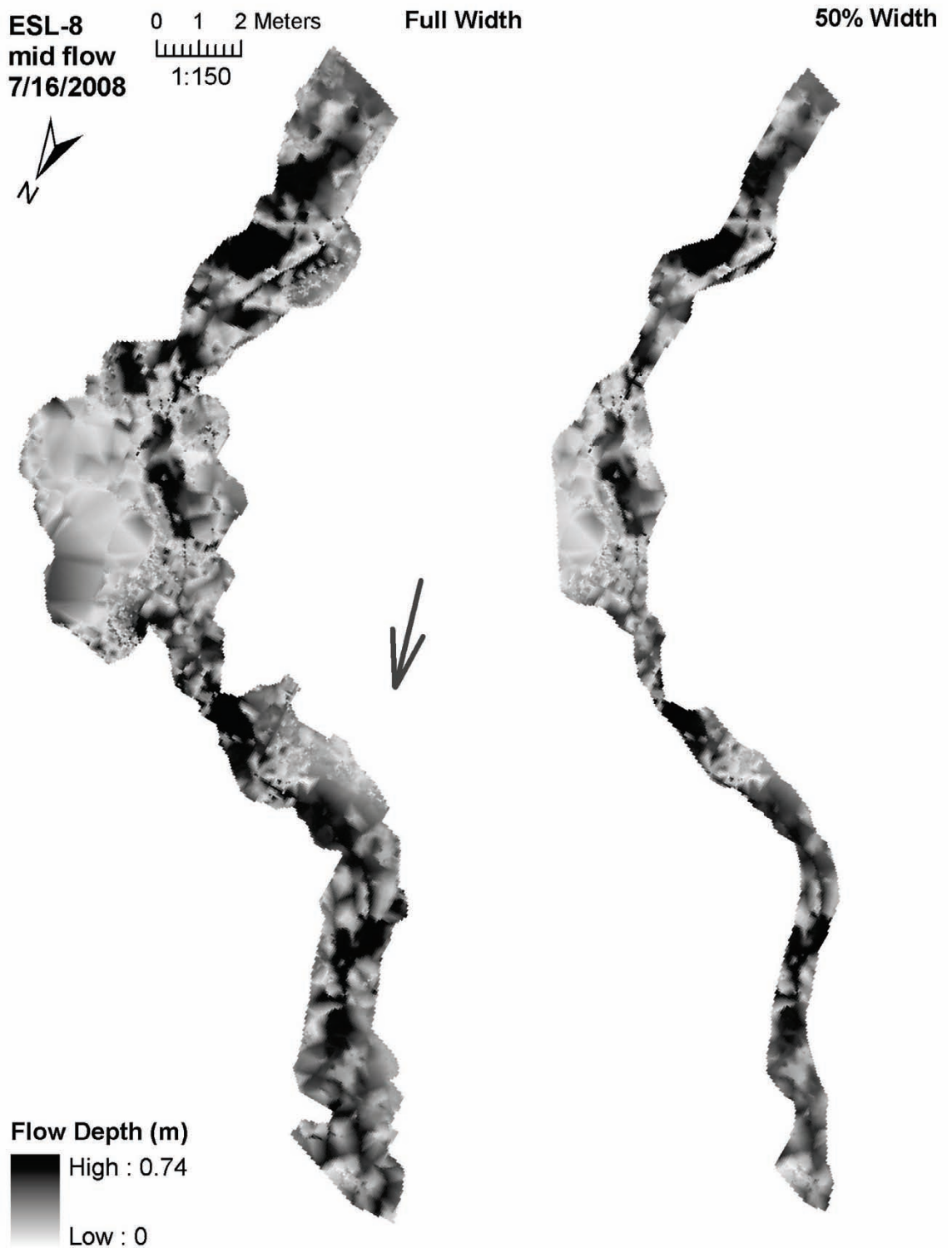
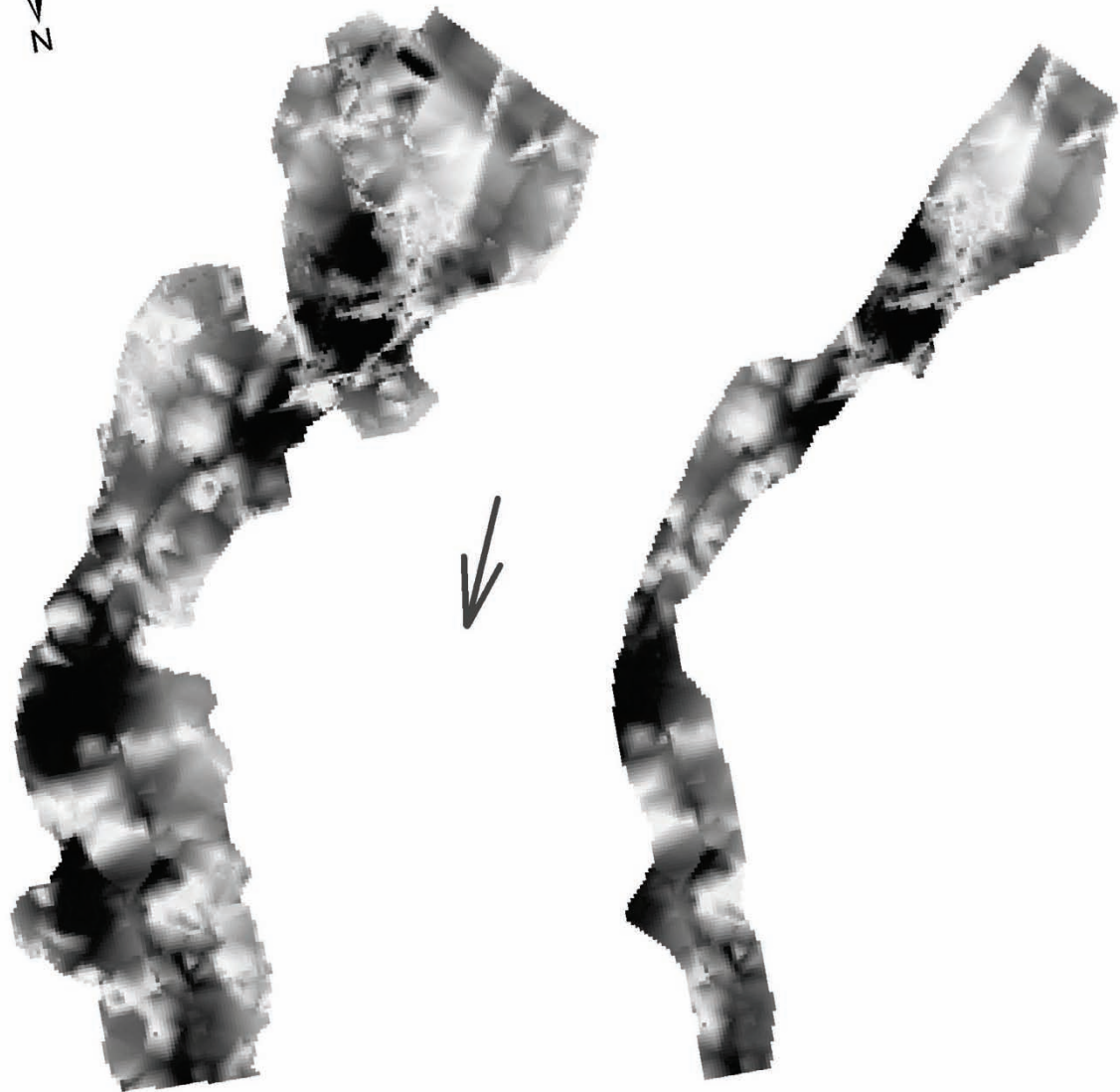


Figure D-23: Depth variability for mid flow, reach ESL-8 (7/16/2008).

ESL-9
mid flow
7/11/2007

Full Width
0 1 2 Meter
1:100

50% Width



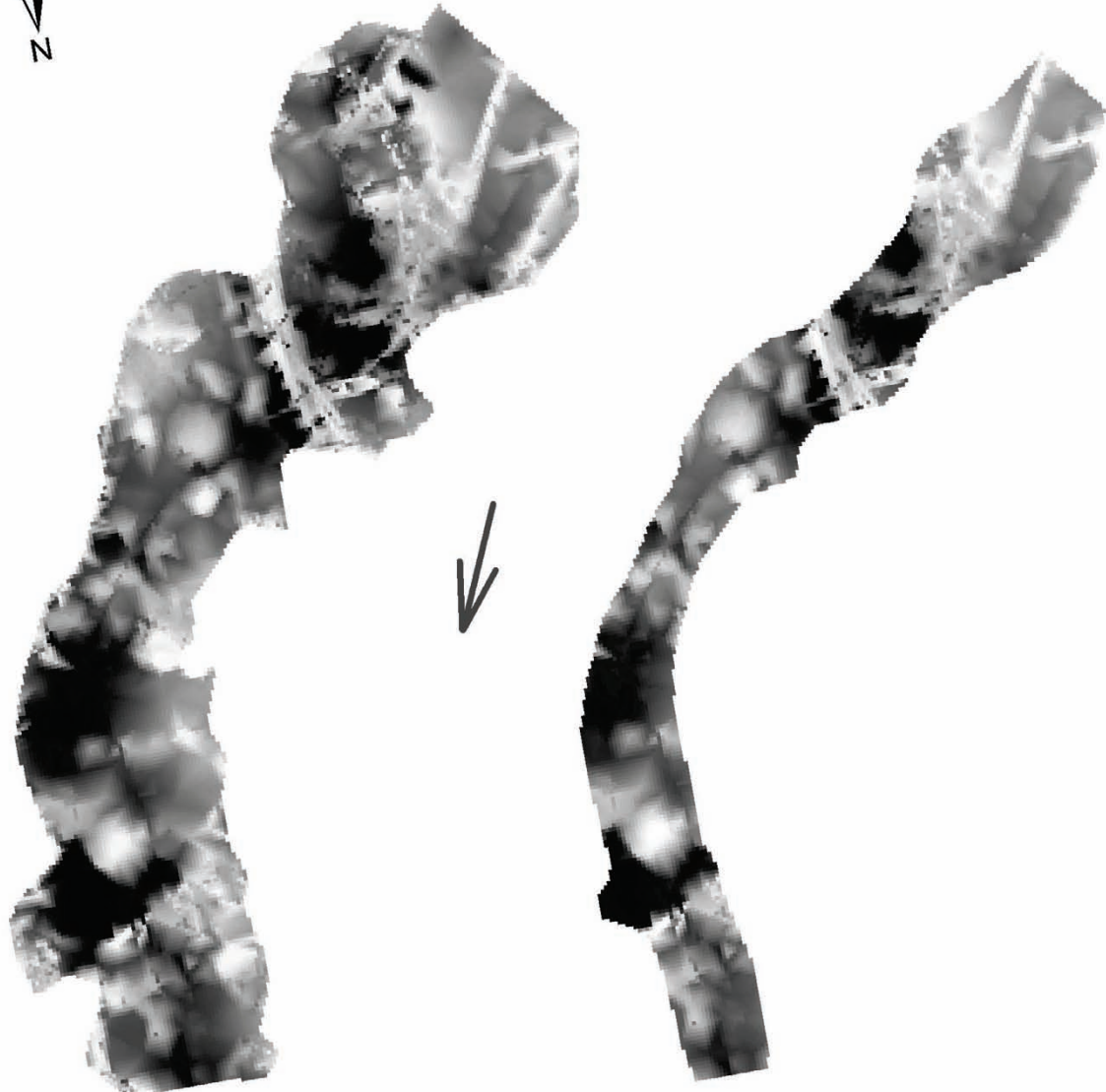
Flow Depth (m)
High : 0.63
Low : 0

Figure D-24: Depth variability for mid flow, reach ESL-9 (7/11/2007).

ESL-9
~ bankfull flow
6/8/2008

Full Width
0 1 2 Met
1:100

50% Width



Flow Depth (m)
Value
High : 0.8
Low : 0

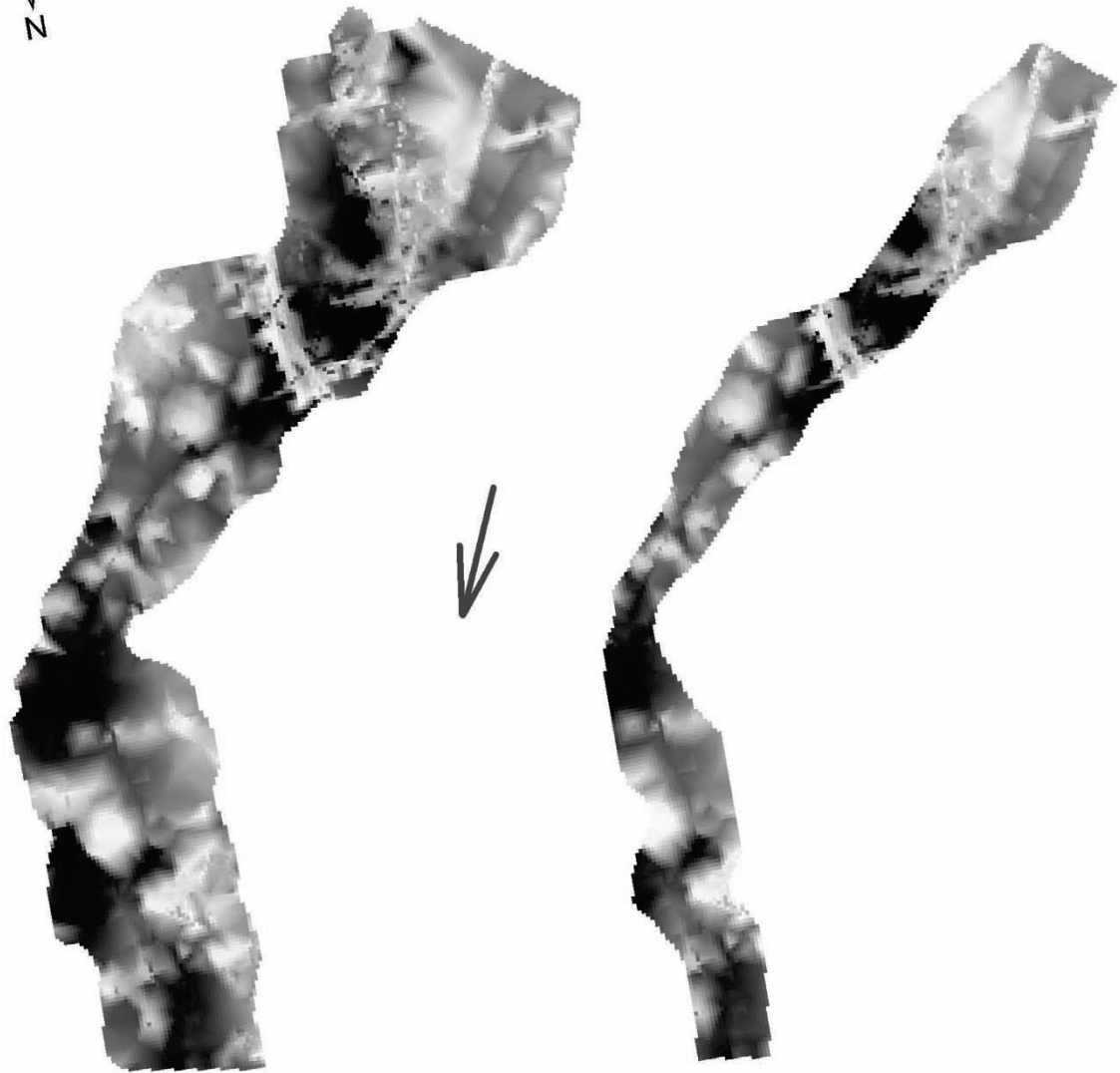
Figure D-25: Depth variability for ~bankfull flow, reach ESL-9 (6/8/2008).

ESL-9
mid flow
7/16/2008



Full Width
0 1 2 Met
1:100

50% Width



Flow Depth (m)
High : 0.7
Low : 0

Figure D-26: Depth variability for mid flow, reach ESL-9 (7/16/2008).

FC-1
mid flow
7/5/2007



Full Width
0 1 2 Meters
1:120

50% Width

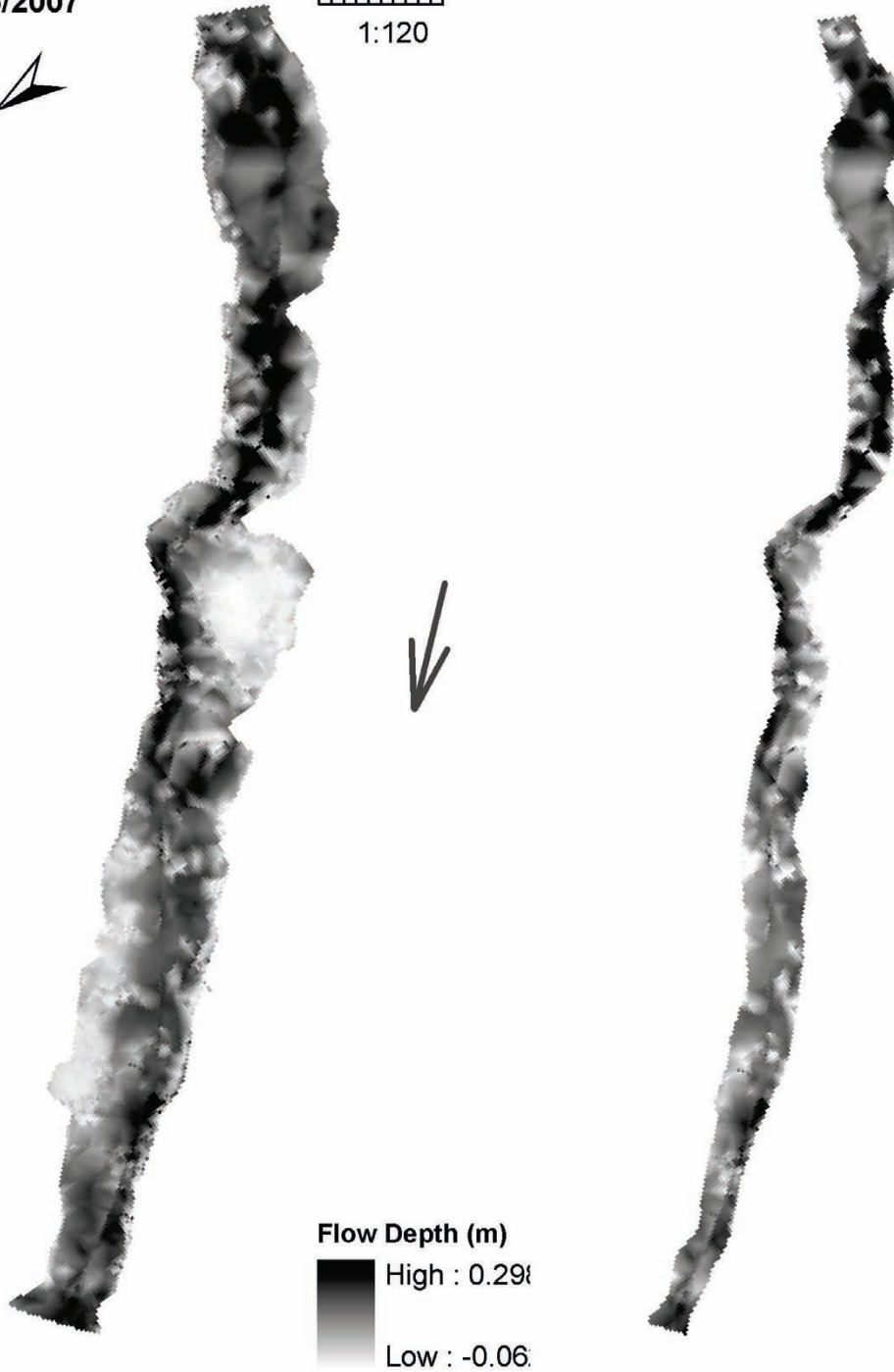


Figure D-27: Depth variability for mid flow, reach FC-1 (7/5/2007).

FC-1
~ bankfull
6/11/2008



Full Width
0 1 2 Meters
1:120

50% Width

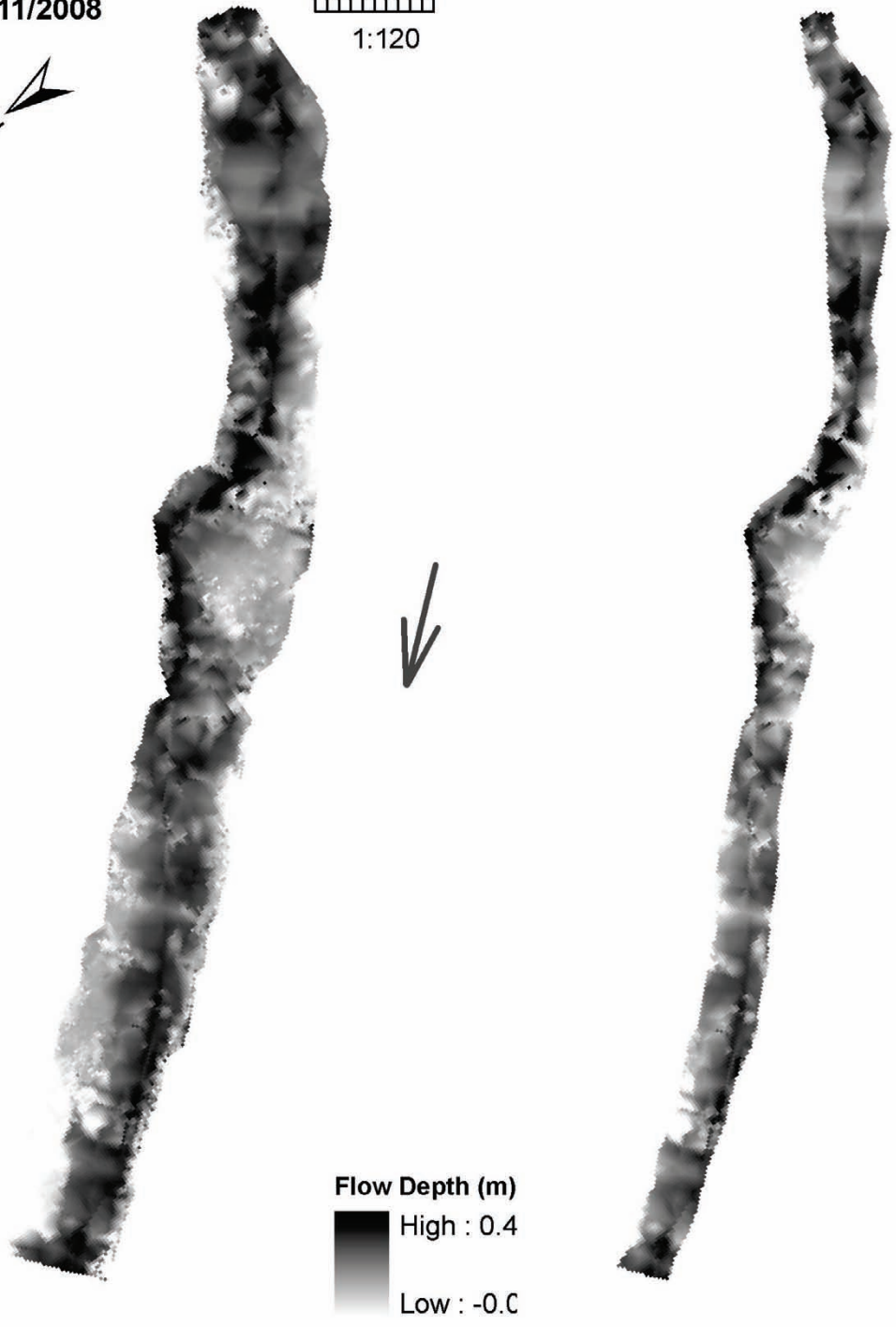


Figure D-28: Depth variability for ~bankfull flow, reach FC-1 (6/11/2008).

FC-1
mid flow
7/23/2008



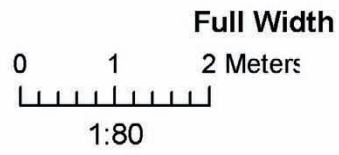
Full Width
0 1 2 Meters
1:120

50% Width



Figure D-29: Depth variability for mid flow, reach FC-1 (7/23/2008).

FC-2
mid flow
7/7/2007



50% Width

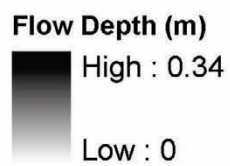
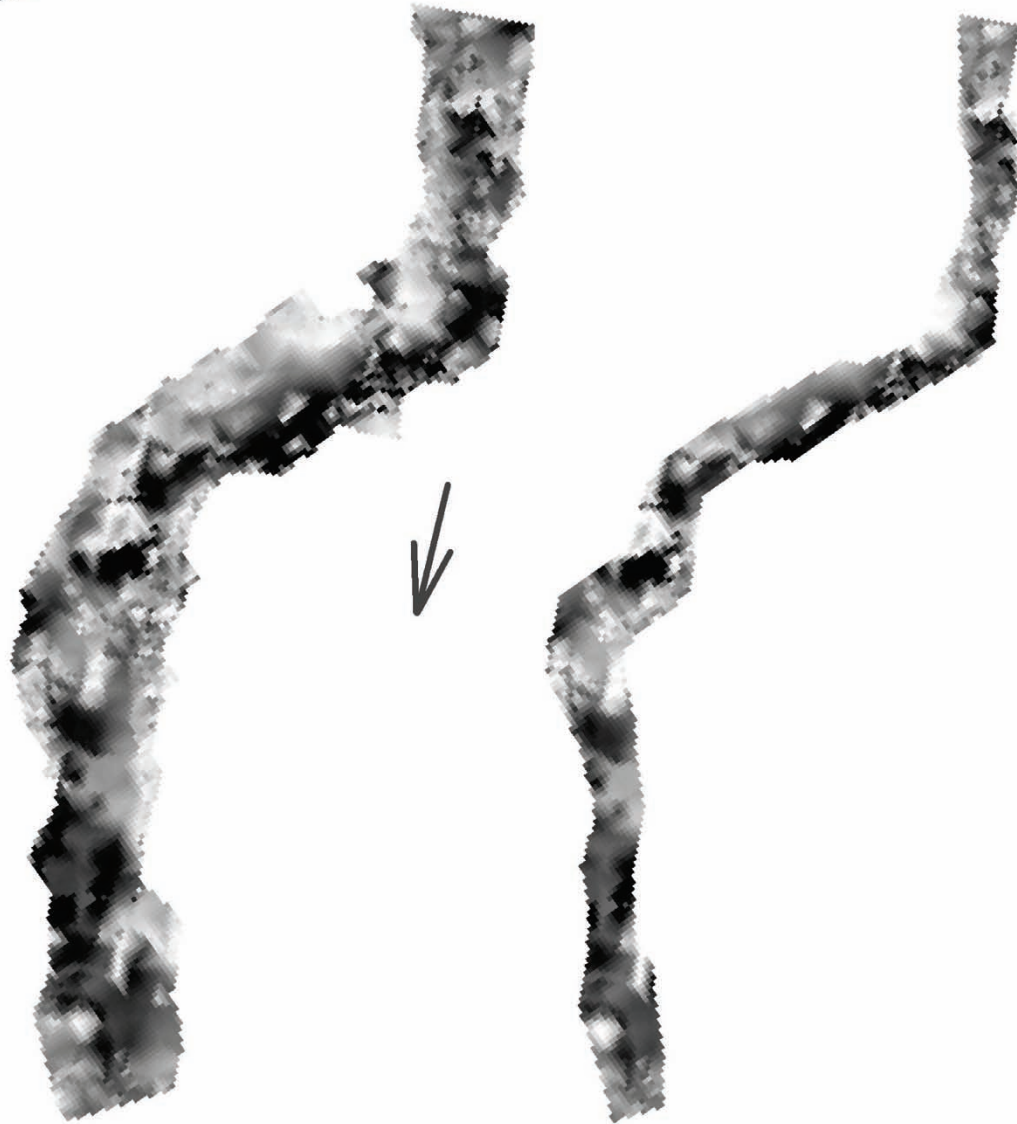
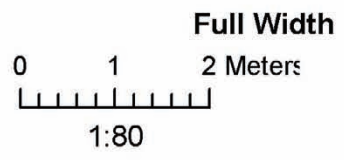


Figure D-30: Depth variability for mid flow, reach FC-2 (7/7/2007).

FC-2
~ bankfull
6/11/2008



50% Width

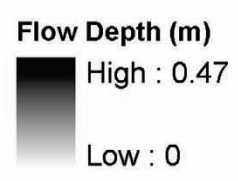
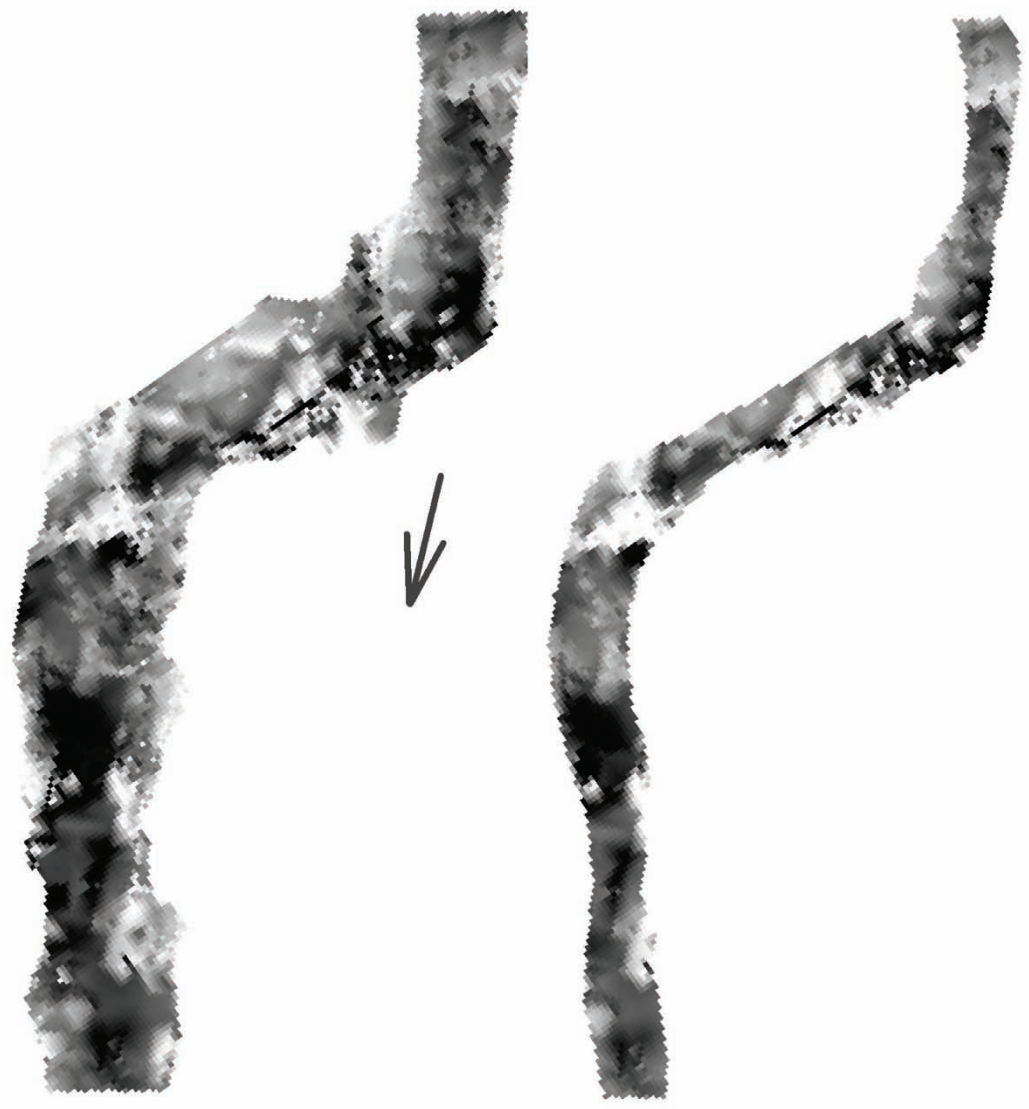
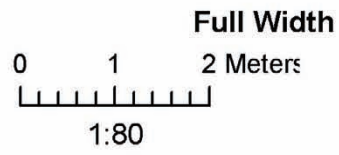


Figure D-31: Depth variability for ~bankfull flow, reach FC-2 (6/11/2008).

FC-2
mid flow
7/23/2008



50% Width

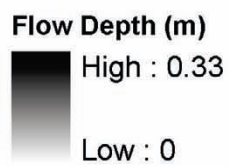


Figure D-32: Depth variability for mid flow, reach FC-2 (7/23/2008).

FC-3
mid flow
7/6/2007

Full Width
0 1 2 Met
1:70

50% Width

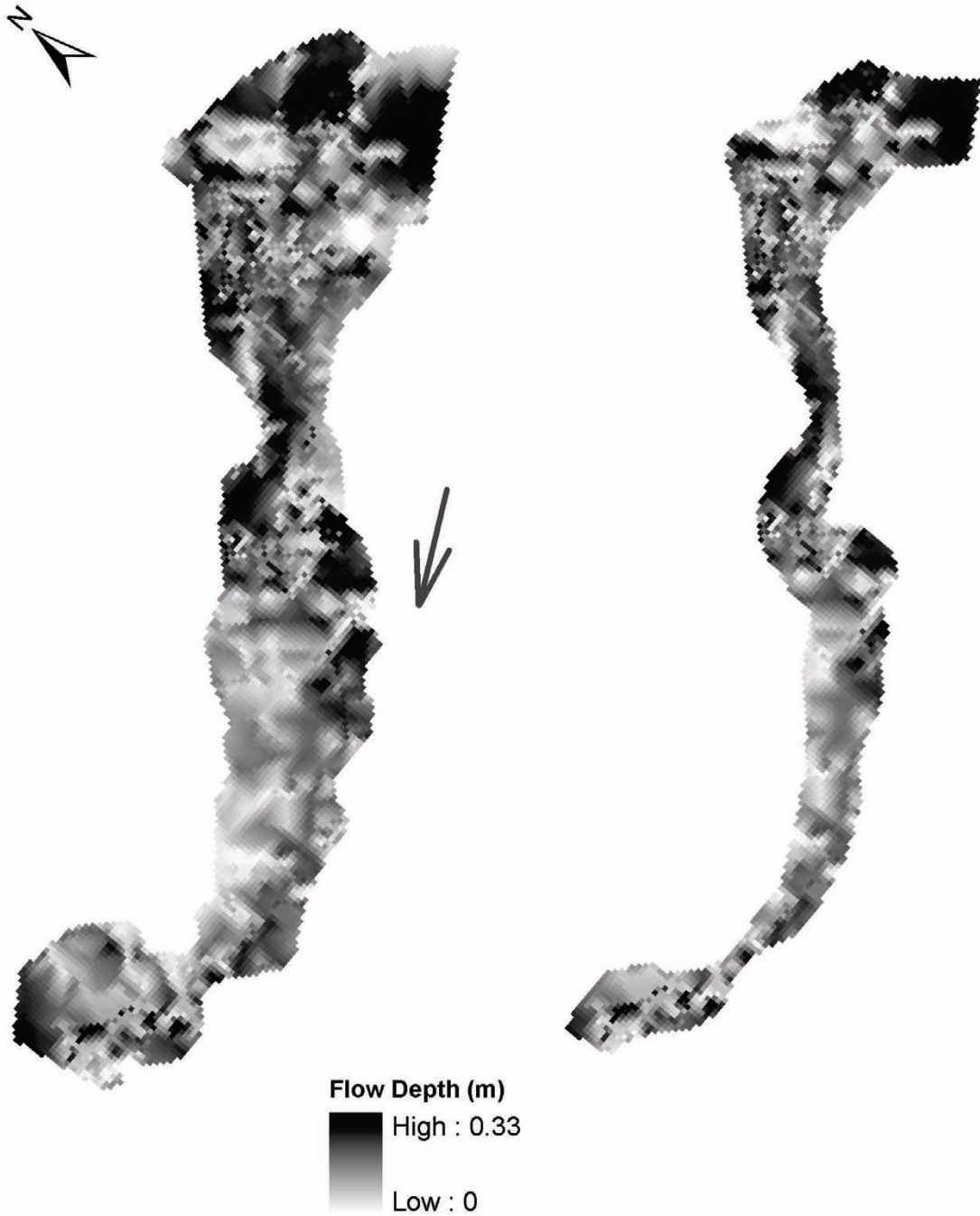


Figure D-33: Depth variability for mid flow, reach FC-3 (7/16/2007).

FC-3
~ bankfull
6/12/2008

Full Width
0 1 2 Met
1:70

50% Width

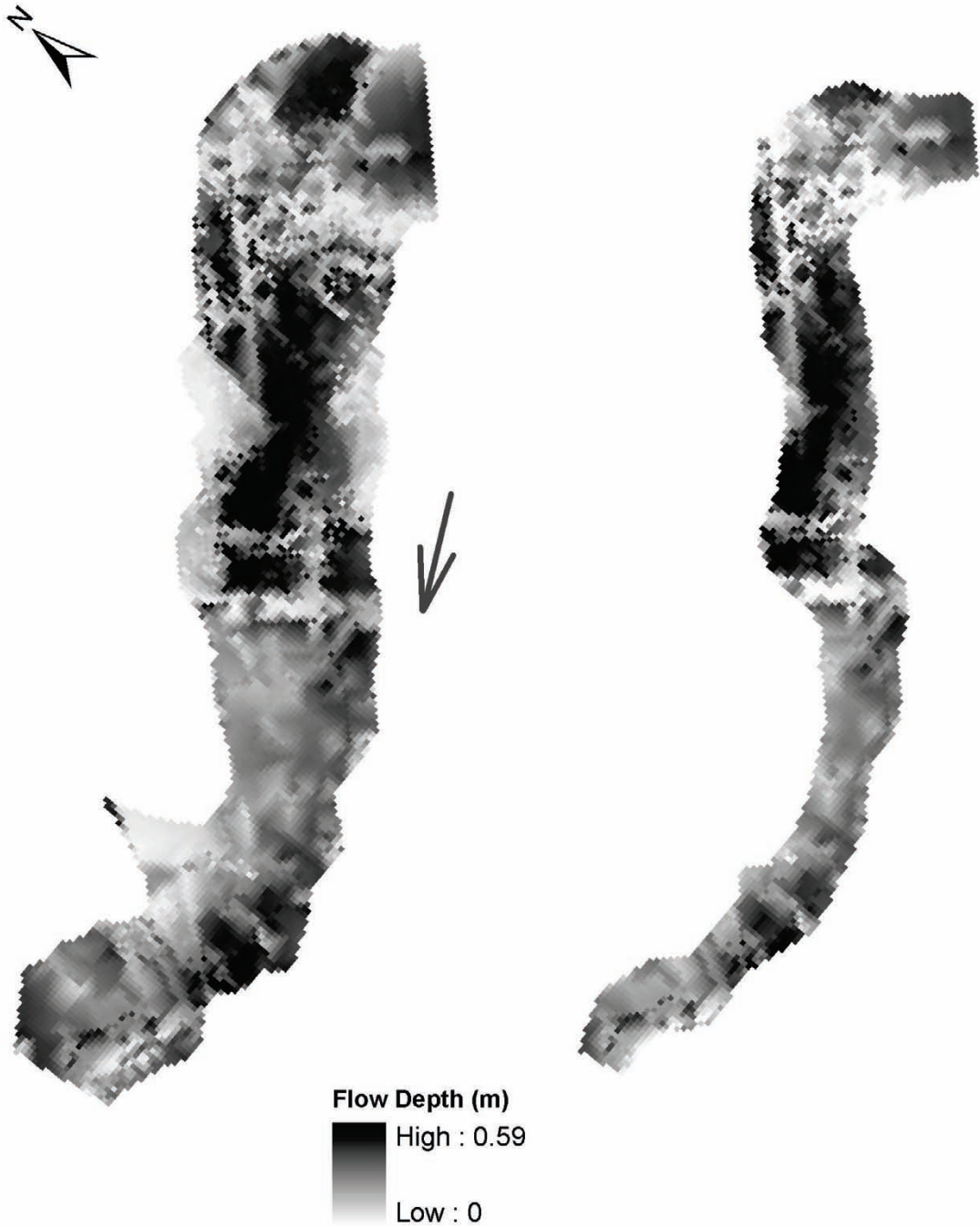


Figure D-34: Depth variability for ~bankfull flow, reach FC-3 (6/12/2008).

FC-3
mid flow
7/22/2008

Full Width
0 1 2 Met
1:70

50% Width

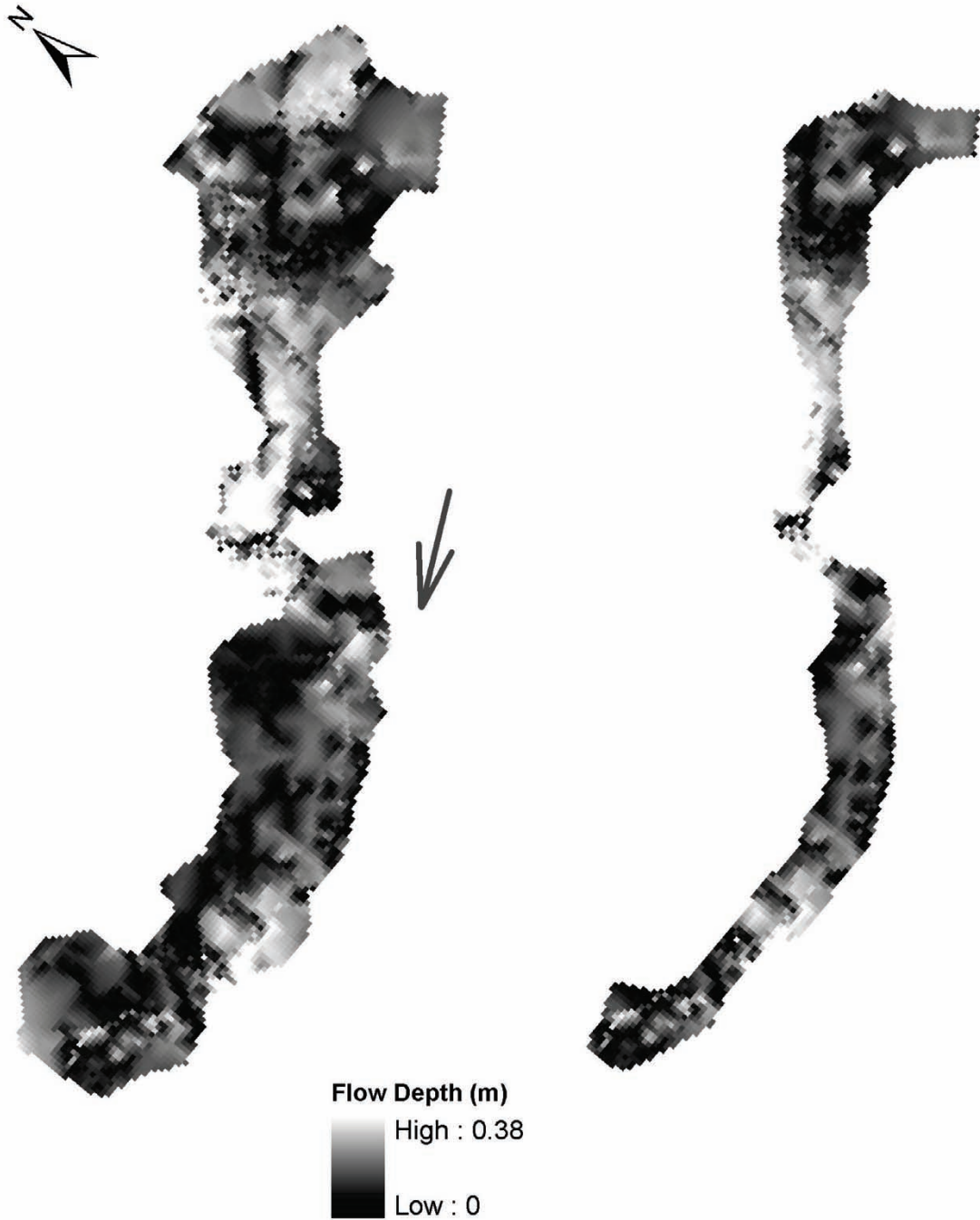


Figure D-35: Depth variability for mid flow, reach FC-3 (7/22/2008).

FC-4
mid flow
7/7/2007

Full Width
0 1 2 Meters
1:100

50% Width

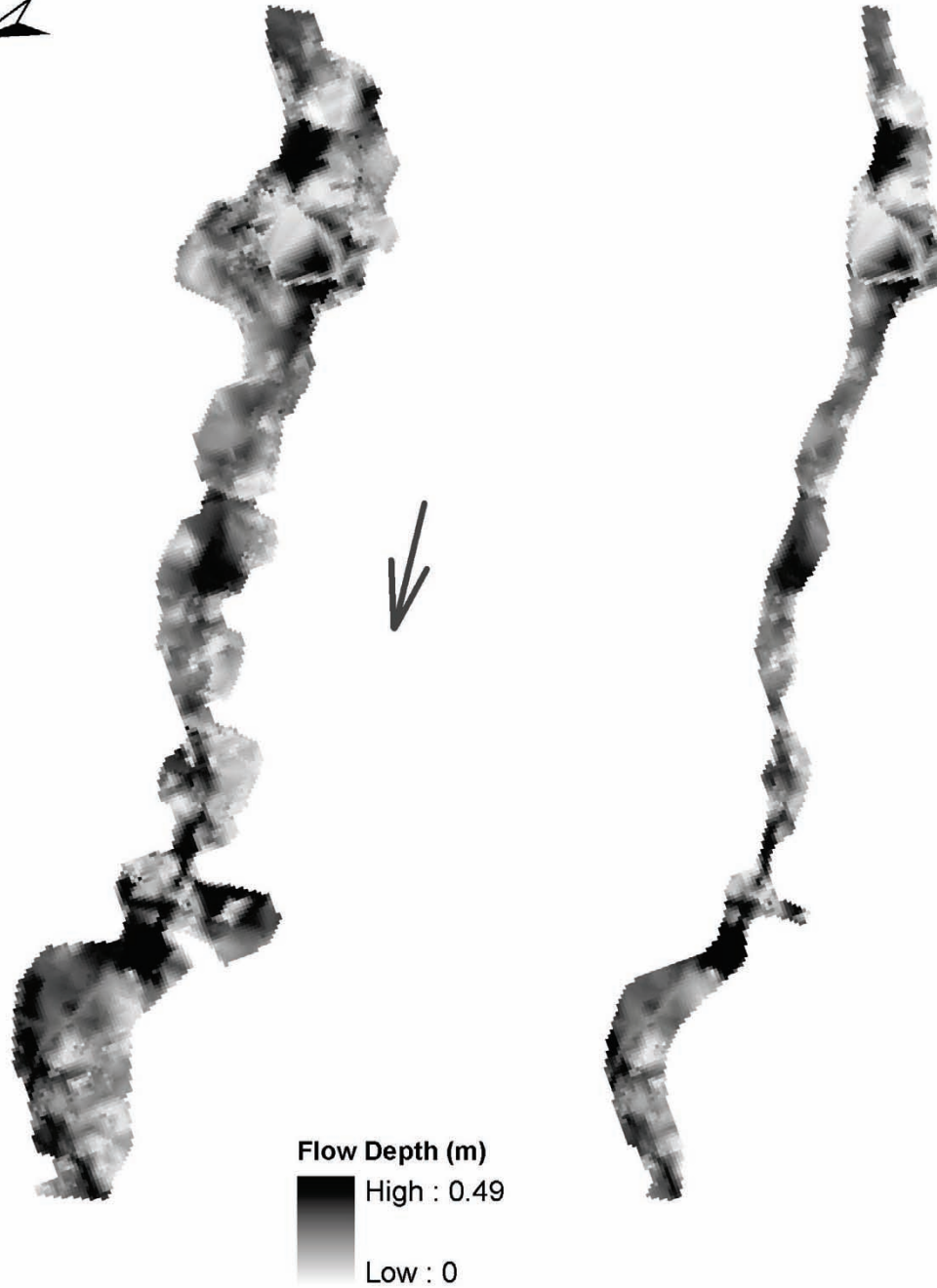


Figure D-36: Depth variability for mid flow, reach FC-4 (7/7/2007).

FC-4
~ bankfull
6/12/2008

Full Width
0 1 2 Meters
1:100

50% Width

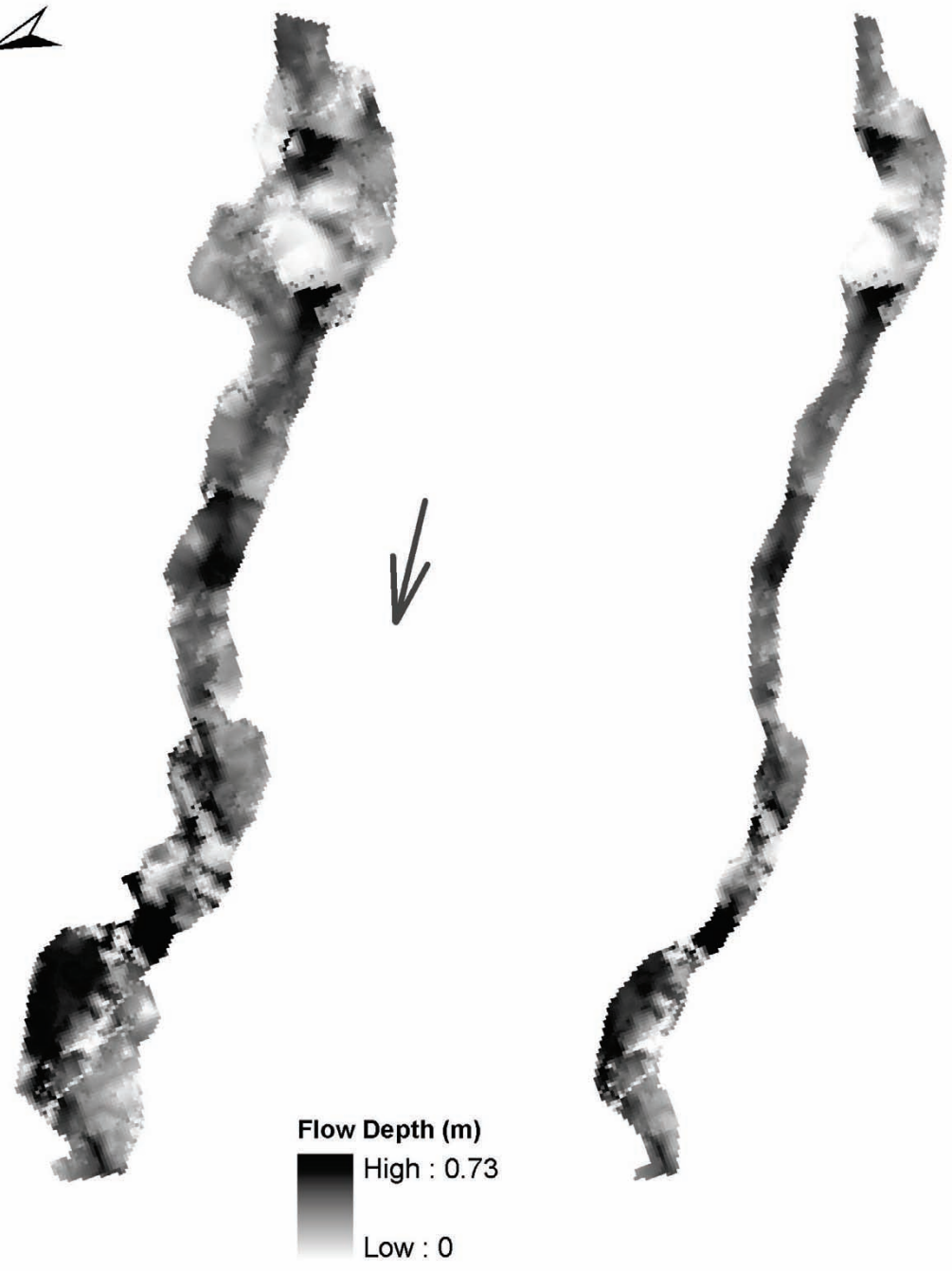


Figure D-37: Depth variability for ~bankfull flow, reach FC-4 (6/12/2008).

FC-4
mid flow
7/21/2008

Full Width
0 1 2 Meters
1:100

50% Width

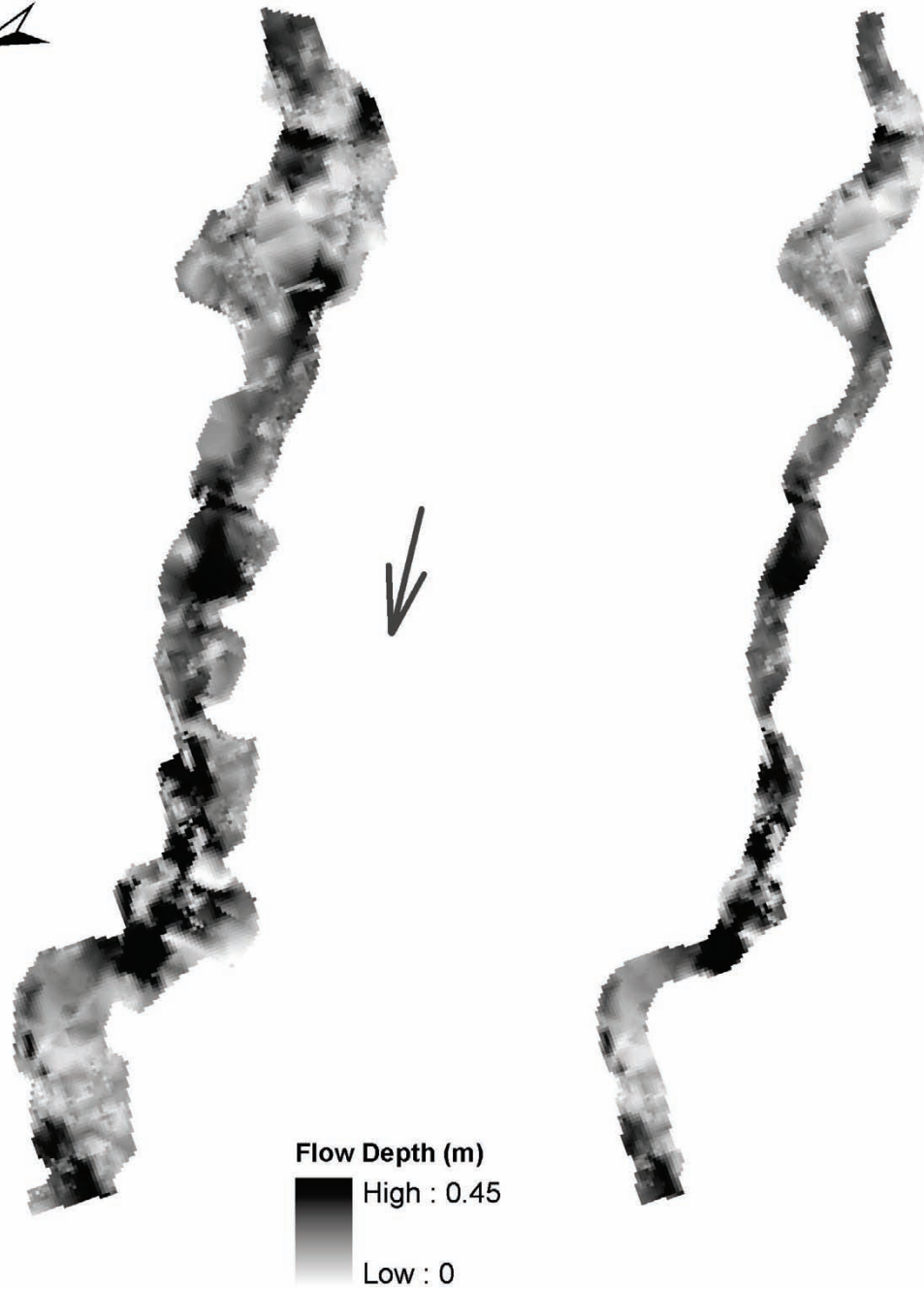


Figure D-38: Depth variability for mid flow, reach FC-4 (7/21/2008).

FC-5
mid flow
7/8/2007



Full Width
0 1 2 Meters
1:60

50% Width

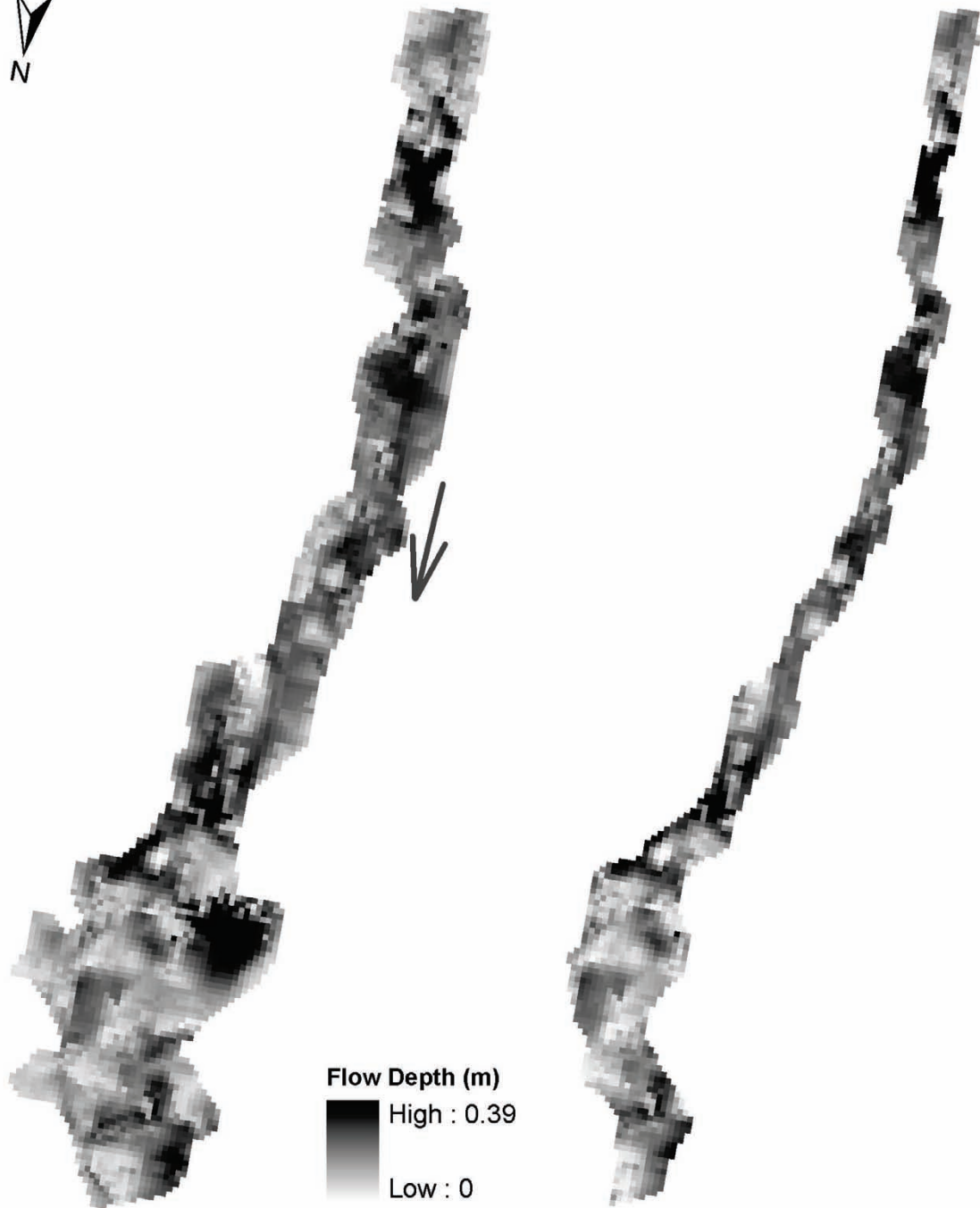


Figure D-39: Depth variability for mid flow, reach FC-5 (7/8/2007).

FC-5
~ bankflow
6/25/2008



Full Width

50% Width

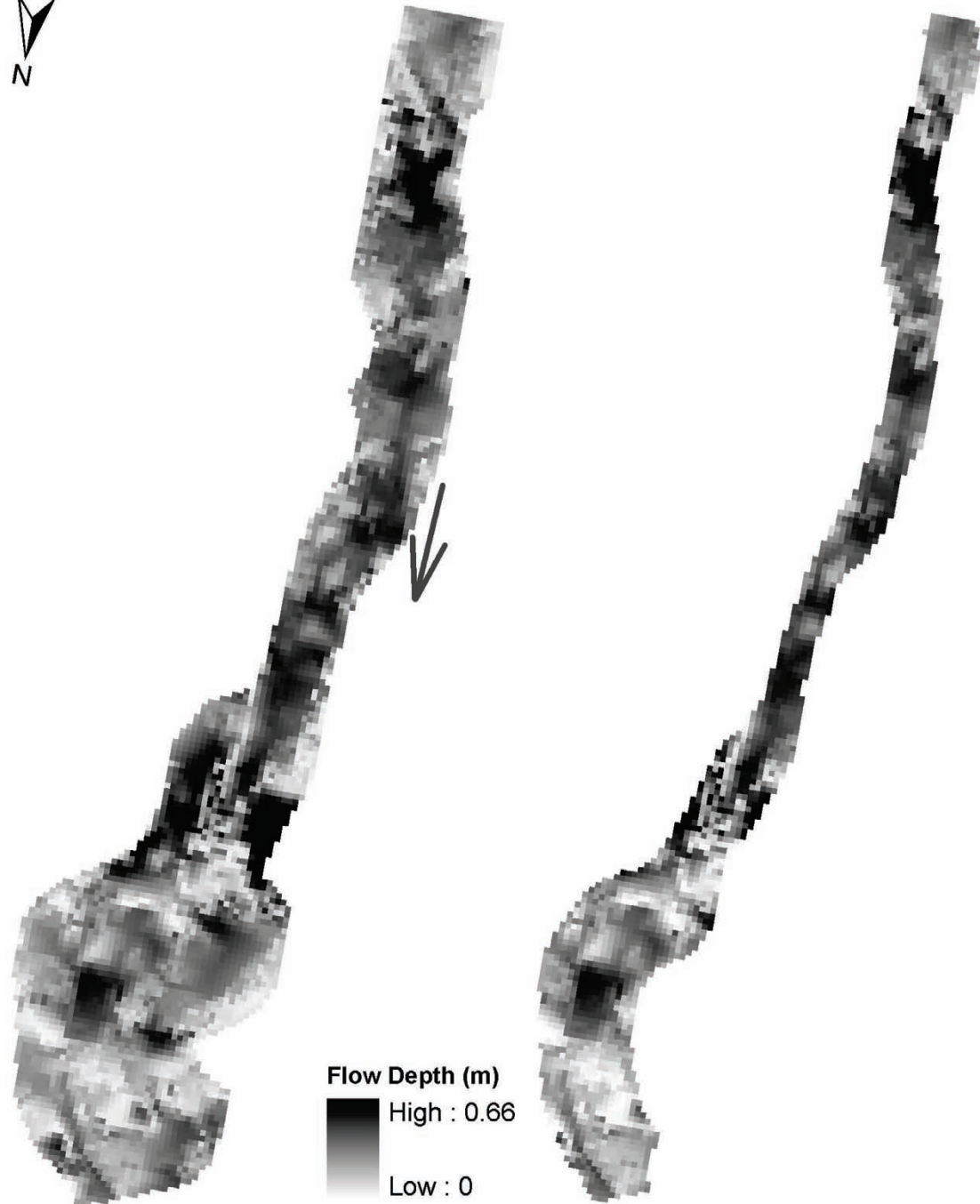


Figure D-40: Depth variability for ~bankfull flow, reach FC-5 (6/25/2008).

FC-5
mid flow
7/17/2008



Full Width
0 1 2 Meters
1:60

50% Width

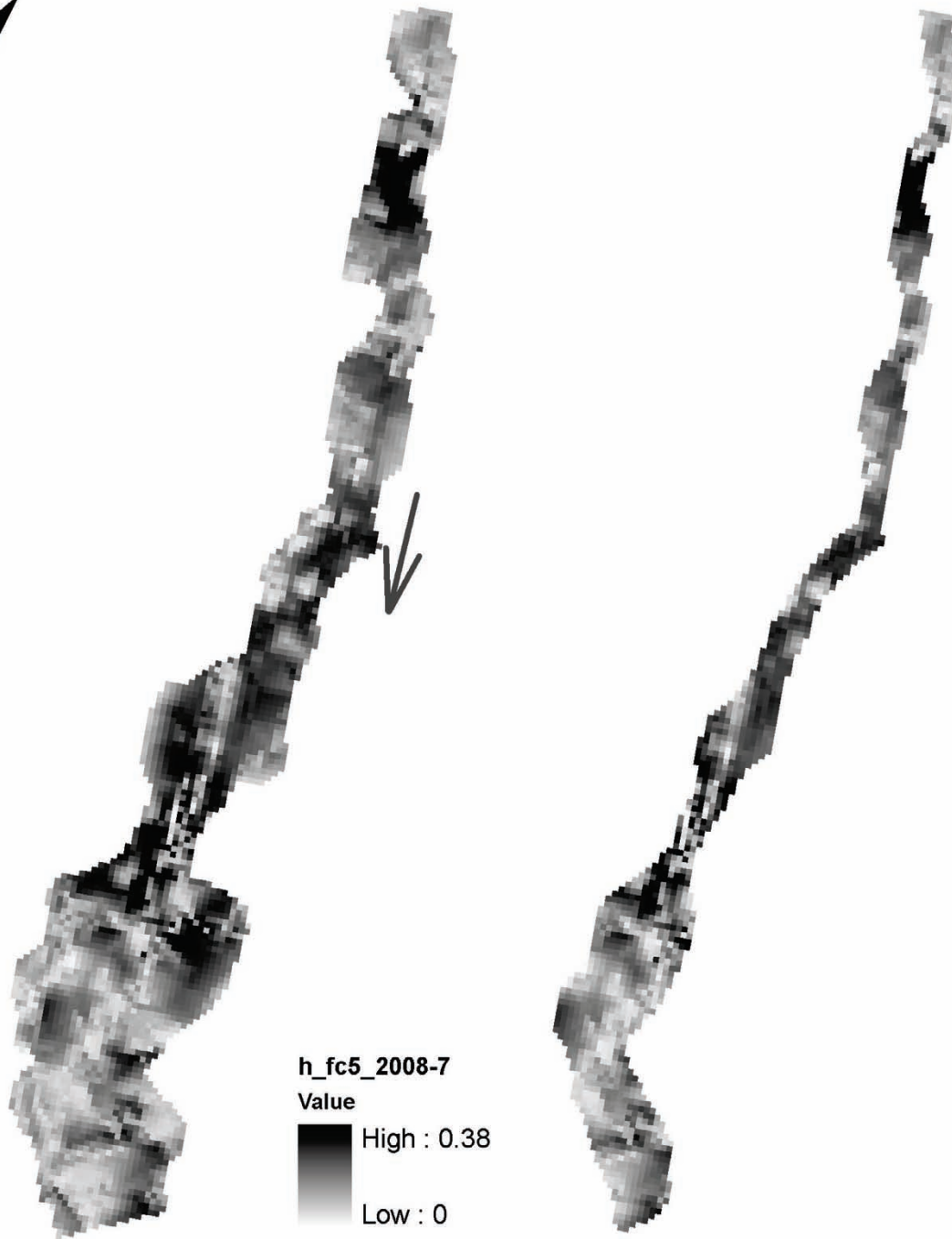


Figure D-41: Depth variability for mid flow, reach FC-5 (7/17/2008).

FC-6
mid flow
7/8/2007



0 1 2 Meters
1:90

Full Width

50% Width

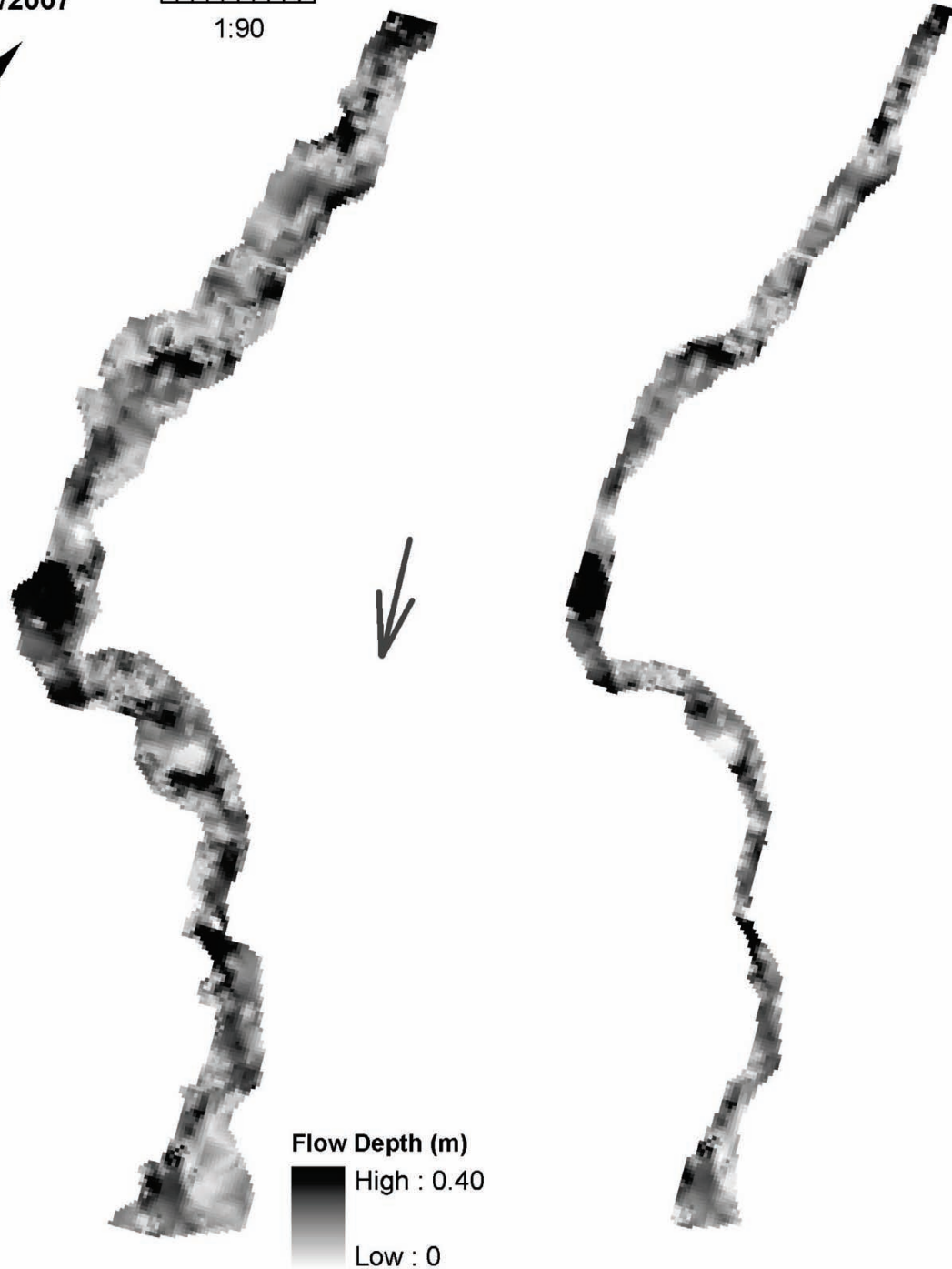


Figure D-42: Depth variability for mid flow, reach FC-6 (7/8/2007).



Figure D-43: Depth variability for ~bankfull flow, reach FC-8 (6/25/2008).

FC-6
mid flow
7/17/2008



0 1 2 Meters
1:90

Full Width

50% Width

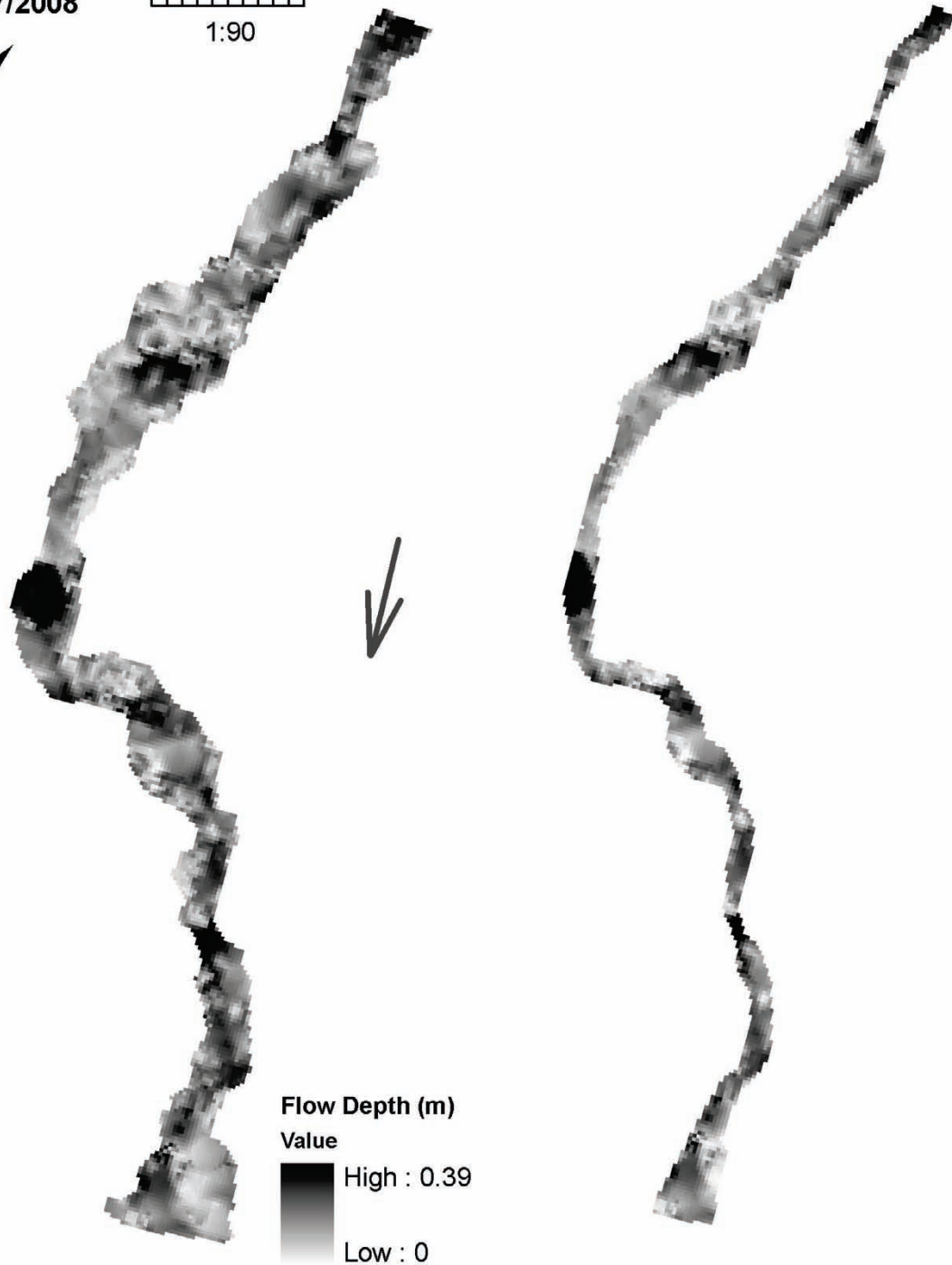


Figure D-44: Depth variability for mid flow, reach FC-6 (7/17/2008).